Non-destructive investigation of surface and sub-surface road pavement profiles

Michael Oliver Gordon
BEng (Hons)

PhD
The University of Edinburgh
November 2000

To Esther

Declaration

I hereby declare that this thesis and the work discussed was carried out solely by Michael Gordon under the supervision of Dr Mike Hardy, unless otherwise stated within the text.

Michael Gordon

November 2000

Abstract

There are currently over 16 million kilometres of roads in the world, of which 365,000 kilometres make up the UK road network. In 1997/98 the Highway Agency in England spent £530 million on road maintenance. As traffic loads are continually increasing, the associated costs to maintain the road network are also increasing. The incorporation of non-destructive investigations in pavement maintenance plays an important role in helping to reduce this overall cost.

Simulations of the whole life performance of pavements have been developed to help to optimise the maintenance cycle. One of the key assumptions of such models is that there is no connection between the asphalt layer thickness profile and the surface profile of a road. As it is known that heavy vehicles can change the profile and surfacing thickness, and that their wheel loads do tend to peak at particular points along the road surface, there is a possibility that this assumption is incorrect.

The purpose of this thesis is to develop a method to investigate the correlation between road surface and sub-surface profiles.

Ground Penetrating Radar is one of the few techniques that can determine pavement layer thicknesses. A commercial radar system has been integrated with a custom-built trailer to find both the surface and sub-surface profiles along sections of pavement. It is necessary to determine the radar speed through pavement layers in order to use this system and a new semi-intrusive technique has been developed to replace the need for coring.

Acknowledgements

This project was inspired and supervised by Dr Mike Hardy to whom I am gratefully indebted for his direction and insight. His constant encouragement and helpfulness have been deeply appreciated.

I would like to thank Professor Mike Forde and all the members of the NDT Research Group for their continued support throughout my years of study. Special mention has to made of Kevin Broughton for his technical expertises and assistance.

I am very grateful to Dr Andrew Collop from The University of Nottingham for his inspiration and valued input to this research.

I also wish to express my thanks to the following individuals and organisations:

EPSRC for the funding that made this study possible.

Ian Fowler and Peter Lehany for helping to build the radar trailer.

Norman Bell and the team at Allied Associates for their technical support.

FLAC for granting us access to conduct road surveys on the A720 and M8.

Scott Wilson Ltd. (Edinburgh) for supplying the required information on the A720.

The fourth years who helped me with the experiments in Chapter 5.

Finally, I am especially thankful for friends like Hywel who painstakingly proof read my work in the final days.

Contents

Chapter 3: GPR and Impact Testing of pavements

List of Figures

List of Tables

List of abbreviations

AASHO	American Society of State Highway Officials
ABAQUS	Finite element package
APPARE	Automated Pavement Profile Analysis and Roughness Evaluation system
BACMI	British Aggregates Construction Materials Industries
CDP	Common depth-point method
CMP	Common mid-Point method
CRIM	Complex Refractive Index Method
CSD	Cross Spectral Density
DBFO	Design, Build, Finance and Operate
DBM	Dense Bitumen Macadam
DCP	Dynamic Cone Pentrometer
DFT	Discrete Fourier Transform
E	Electric Field
EM	Electromagnetic
FDTD	Finite-Difference Time-Domain
FFT	Fast Fourier Transform
FLAC	Forth Local Authority Consortium
FWD	Falling Weight Deflectometer
GMC	General Motors Corporation

GPR	Ground Penetrating Radar
GSSI	Geophysical Survey Systems Inc.
H	Magnetic Field
HDM	Heavy Duty Macadam
HGV	Heavy Goods Lorry
HRA	Hot Rolled Asphalt
HRM	High speed Road Monitor
IE	Impact-Echo
IFT	Inverse Fourier Transform
IR	Impulse response method
IRI	International Roughness Index
IRRE	international Road Roughness Experiment
IRT	Infrared Thermography
LPC	Laboratories des Ponts et Chausées
NAT	Nottingham Asphalt Tester
NDT	Non-Destructive Testing
NIST	National Institute of Standards and Technology
OS	Ordnance Survey
PA	Porous Asphalt
PCC	Portland Cement Concrete
PSD	Power Spectral Density
PSPA	Portable Seismic Pavement Analyzer

RTRRMs	Response-Type Road Roughness Measuring Systems
SASW	Spectral Analysis of Surface Waves
SMA	Stone Mastic Asphalt
SPA	Seismic Pavement Analyzer
TRL	Transport Research Laboratory
TRRL	Transport and Road Research Laboratory (Former name of TRL)
UCW	Ultrasonic Compression Wave
USW	Ultrasonic Surface Wave
UT	Ultrasonic Transducer
WARR	Wide Angle Reflection and Refraction

Chapter 1

Introduction

There are currently over 16 million kilometres of roads in the world, of which 365,000 kilometres make up the UK road network. In 1997/98 the Highway Agency in England spent £530 million on road maintenance (Anon, 1999A). As traffic loads are continually increasing, the associated costs to maintain the road network are also increasing.

In January 1999 the UK Government increased the maximum weight of 5-axle lorries from 38 tonnes to 40 tonnes due to new EC directives (Anon, 1997A). This increase in loading will inevitably result in increased wear on the roads, therefore increasing the associated costs of maintaining the road network. A report by the National Audit Office (NAO) 'Department of Transport: Regulation of Heavy Lorries' (Anon, 1987) stated that damage caused to roads and bridges in the UK by heavy lorries cost £580 million per year (1986-87). The incorporation of non-destructive investigations in pavement maintenance plays an important role and can help reduce this overall cost.

Simulations of the whole life performance of pavements have been developed to help to optimise the maintenance cycle. One of the key assumptions of such models is that there is no connection between the asphalt layer thickness profile and the surface profile of a road. As it is known that heavy vehicles can change the profile and surfacing thickness, and that their wheel loads do tend to peak at particular points along the road surface, there is a possibility that this assumption is incorrect.

The purpose of this thesis is to develop a method to investigate the correlation between road surface and sub-surface profiles.

Ground Penetrating Radar is one of the few techniques that can determine pavement layer thicknesses. A commercial radar system has been integrated with a custom-built trailer to find both the surface and sub-surface profiles along sections of pavement. It is necessary to

determine the radar speed through pavement layers in order to use this system. In addition, a new semi-intrusive technique has been developed to replace the need for coring.

Chapter 2 reviews current literature concerning the design and maintenance of flexible pavements. Chapter 3 introduces Ground Penetrating Radar (GPR) and Impact Testing, reviewing their use in the maintenance of highway pavements. Chapter 4 describes tests on a thin pavement using GPR and Impact Testing. The accuracy of the techniques and the difficulties associated with interpreting the recorded signal are discussed. Chapter 5 introduces a new semi-intrusive technique used to determine radar velocities within different materials, thus replacing the need for coring. The design and testing of a radar trailer to measure profiles on the surface and sub-surface is presented in chapter 6, with further experiments on a motorway, 'A' road and minor road presented in chapter 7. Conclusions and recommendations for further work are presented in chapter 8.

Chapter 2

An introduction to flexible pavements: Design and maintenance

2. Introduction

The Romans were the first to construct roads in a scientific manner. These consisted of several different layers which increased in strength from the bottom upwards (Figure 2.1). These roads were built as straight as possible to enable troops to be moved quickly between settlements. The main characteristics of these roads were their linearity and durability.

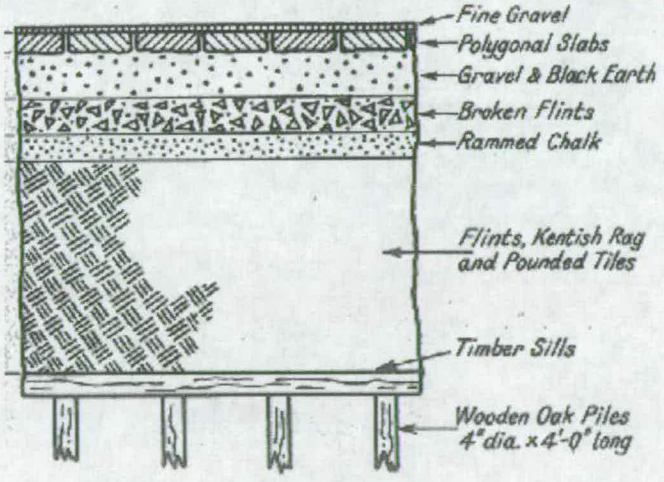

Figure 2.1: An example of a section through a Roman road (Collins and Hart, 1936)

The fall of the Roman Empire resulted in the roads falling into disrepair, with very little road-building activity over the next 1,500 years. It wasn't until the 18th and 19th century that engineers focused more on improving roads due to their importance in everyday life. The main thrust of their work was to concentrate more on using the subgrade to support the

load with the surface being used as a wearing course and a "roof" to shed water. People like McAdam, Telford and Metcalf brought about this pioneering approach.

2.1 Types of pavements

A pavement is described in BS 6100 as the road structure above the subgrade. It is the whole construction of a road or airstrip including stabilised soil and the surface, whether of asphalt, concrete, wood or stone blocks. There are two basic types of pavements, flexible and rigid.

2.1.1 Flexible Pavements

The term flexible describes the ability of the pavement to flex or move under applied loads. It is believed that the first use of a binder product to produce a flexible pavement was in America in 1870, where the binder was a powdered natural rock asphalt (Atkinson (ed), 1997). Since these times there has been a wide variety of binders available to the engineer to use in flexible road construction.

A flexible pavement is made up of several different layers as shown in Figure 2.2. The surface of the pavement is the area which most immediately effects the traffic. It must be sufficiently uniform to allow traffic to pass in comfort and safety at a reasonable speed, however, not so smooth that the cars will skid. There must be good drainage to remove pools of water forming on the road in wet conditions.

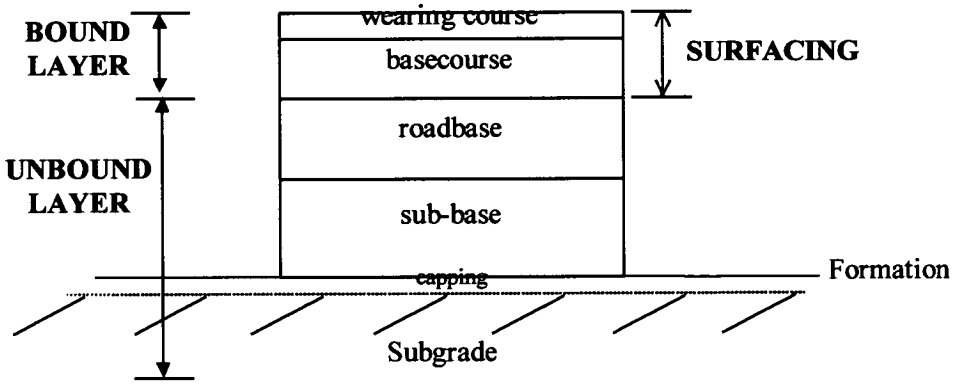

Figure 2.2: The structure of a flexible pavement

Subgrade: This is the soil on which the pavement is built. If properties of the foundation are not very good, then a subgrade improvement layer or *capping* is used. The capping is usually a cheap material made up of granular or treated material. The *formation* is the surface of the subgrade.

Sub-base: This is the layer immediately above the formation layer which acts as the foundation or load-bearing layer as well as preventing damage to the subgrade while work is going on.

Roadbase: This is the main structural part of the pavement so it must resist being permanently deformed or cracking due to fatigue.

Basecourse: This is the lower layer of the *surfacing* on which the *wearing course* is placed. The basecourse distributes some of the load and helps to provide a level surface on which to place the wearing course. This layer will provide both water and skid resistance as well as providing an evening surface for the traffic. When the pavement is only experiencing light loading, a wearing course is only used.

The roadbase, basecourse and the wearing courses use a bituminous mix made up of aggregates and a hydrocarbon binder. It is the thermoplastic properties of the binder which make it ideal for road use. Thermoplastic materials become viscous when heated. This property makes the material easy to be mixed with aggregate when it is hot, whereas, cooling produces a strong and relatively stiff material.

McAdam's roads did not have any binder and relied on the interlocking abilities of the stone for load carrying capacity.

2.1.2 Rigid Pavements

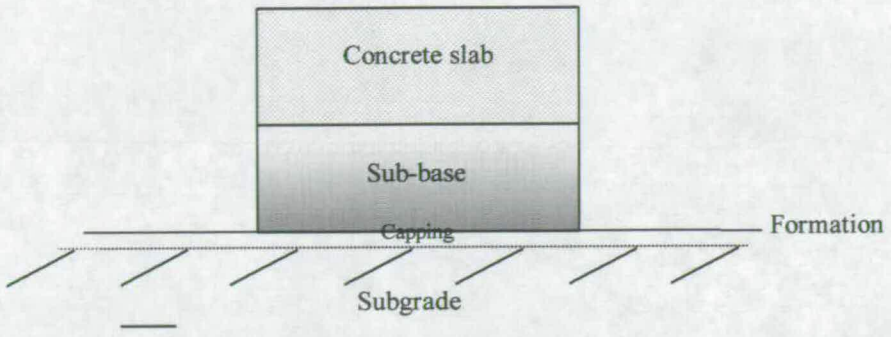

Figure 2.3: The structure of a rigid pavement

These type of pavements consist of portland cement concrete surfacing placed on a sub-base course or basecourse. The concrete slab will function in the same way as the roadbase and surfacing of the flexible pavement.

There are variations in these two basic types of roads:

Flexible composite: This is a flexible pavement in which the roadbase material is cement bound.

Rigid composite: These roads have a concrete main structure overlaid with a bituminous surfacing.

However, it should be noted that this research project will deal solely with flexible pavements.

2.2 Pavement deterioration

Pavements deteriorate in two main ways; surfacing failure and failure below the surfacing. Surfacing failure can be caused by a loss in surface texture, loss of impermeability and/or surface regularity. Remedial measures involve replacement or repair of only the surface. As a result a large emphasis is placed by the highway engineer on the material used on the surface.

Failure beneath the surfacing layers is more difficult to diagnose. In flexible pavements, horizontal and vertical strains are the main modes of failure. Horizontal strain will result in

deformation in both the unbound and bound layers, possibly causing surface deformation. These methods of failure are discussed further in section 2.3.

The reason for these failures is mainly due to repetitive loading of the structure, which weakens its ability to withstand these strains, eventually failing due to material fatigue. This introduces the need for the designer to determine the design life of the pavement. At the end of the design life, the pavement's structure will rapidly deteriorate, resulting in major works being required to restore the road to a sound condition. A survey was carried out by TRL (Lister, 1972), which correlated the structural condition of a flexible pavement with the apparent defects at the surface. The critical stage generally consisted of 10mm rutting or cracking along the wheel path, which was later defined as the *design life* of the pavement. It is measured in terms of the number of equivalent standard (80kN) axle passes the pavement can sustain.

Prevention of these failures may be achieved by increasing the thickness of the bound material, thus containing the resultant horizontal stresses, or by using a material that is strong enough to resist these stresses.

Trying to identify the type of deterioration and the main cause of it is an important aspect in carrying out maintenance. Below is a list of common types:

- Ageing and weathering
- Pot holes
- Rutting
- Pushing
- Deformation
- Fretting
- Cracking
- Polishing
- Plucking
- Embedment

Several of these common types of deterioration are described in the following sections.

2.2.1 Rutting

Rutting is the formation of depressions or tracks in the surface of the pavement caused by permanent plastic flow of the surface course and, in extreme cases, binder in the wheel path.

It is the result of a combination of carriageway design, high temperatures and wheel loads. The tendency to rut increases with greater imposed wheel load, slower load rate and higher temperature. It is usually found in approaches to traffic lights, bus lanes and slow lanes on trunk roads.

In hot climates, where pavements are prone to rutting, the rolled asphalt is replaced with asphaltic concrete (AC), which uses the grading of aggregate to form an interlocking structure to provide the pavement strength. However, the drawback in using these materials is that in cold weather the material can become brittle and result in cracking.

Smith and Jones (Smith and Jones, 1998) reported that the use of AC, designed using the Marshall method, is not appropriate in areas of high traffic stresses and high pavement temperatures. Their work showed that the 75-blow Marshall compaction method did not simulate the effect of years of secondary compaction under traffic loading. They noted that maintaining a voids in mix not less than 3%, after secondary compaction, would minimise the risk of plastic deformation.

They proposed a new methodology for designing the bituminous surfacing in developing countries with tropical climates and where mixing equipment is limited. This involved a combination of the Marshall test method and reference refusal density, using a vibration hammer in accordance with the percentage refusal density test. The authors indicated that future improvements in this methodology would be expected due to further laboratory mix tests being produced.

2.2.2 Cracking

It is important for the highway engineer to ascertain the reason for cracks occurring on the pavement, thus enabling the correct repair method to be used.

There are several different reasons for cracking occurring, some of these are given below:

- Poor laying conditions: The rapid chilling of the surface layer during rolling whilst the remainder of the layer is quite mobile will lead to "hair-line" cracks forming. These are not a serious form of cracking and will usually close up under trafficking. However, wider and deeper

cracks can occur during laying due to severe dragging of the material by the Paver. These types of cracks must be rectified as they can penetrate the full depth of the layer.

- Structural weakness: Excessive deflections in a weak pavement can lead to "alligator" cracks forming on the surface due to this inadequate structural strength. Using unsuitable materials in the pavement, poor drainage, inadequate design of the loading conditions or normal deterioration can all result in weakening of the structure.

- Shrinkage of clay subgrade: Drying out of the subgrade due to severe drought conditions or building near deep-rooted trees which seep up any moisture in the ground lead to longitudinal cracks occurring on or below the surface. However, this form of cracking is very uncommon.

Laying asphalt over old concrete and some cement-bound materials can also cause cracking. Thermal movements or structural instability of old concrete can lead to "reflective" cracking. The thermal movement of the concrete, due to temperature changes, causes cracks to develop above the joints and cracks in the concrete. Cracking caused by instability of the structure is dependent on the amount of traffic moving the individual slabs under the vehicle roads. In cement-bound materials, such as lean-mix, "reflective" cracking can develop in the early life of the laid material.

2.2.3 Pushing and plucking

In high stressed areas pushing and plucking can occur. Pushing is the folding of wearing course materials on itself and can be a result of soft binder or, in rare cases, fuel/oil spillage which softens the material locally.

Plucking is the loss of aggregate under trafficking, especially in areas where chipping from a chipped asphalt surface have not been properly embedded in the asphalt.

2.2.4 Deformation

Deformation applies to general distortion on the pavement surface due to a variety of cases such as rutting, as described earlier. Another is frost heave, which is the freezing of water in the pavement structure causing it to deform.

2.2.5 Fretting and embedment

Fretting is the ageing and hardening of the binder resulting in the loss of aggregate particles. A severe form of fretting occurs when large and small aggregate is removed causing potholes to form in the pavement.

Fretting is caused by several different factors including low binder content in the mix, poor compaction, poor weather conditions during laying and inadequate layer thickness.

Embedment is the loss of surface texture when chippings are applied and compacted to a HRA wearing course. Too thick a binder layer, using inappropriate size of chipping or letting the traffic use the road too soon after laying, are some of the reasons for embedment occurring.

2.3 Highway maintenance

The progressive deterioration of the pavement with time means that routine maintenance is vital if the pavement is to perform satisfactorily for as long as possible.

Maintenance of pavements is one of the most important factors for the proper functioning of the road system. Unfortunately, poor maintenance usually results in a gradual failing of the pavement; this has resulted in the allocation of funds to the areas which are in most immediate need of it. With a limited amount of money available for road maintenance, the engineer must decide which area of the road network most badly needs the funds. Snaith and Kerali (Snaith and Kerali, 1986) suggested that between 2% and 4% of the maintenance budget should go to collecting data and managing the highway-maintenance systems. These systems are used to record information about the highway's condition at regular intervals, (annually), and placed into a database.

Atkinson (Atkinson (ed), 1997) has delineated all aspects of highway maintenance, including grass cutting, lighting, sign cleaning and repair and drainage maintenance. However, this chapter will only focus on maintenance of the structure and surface condition of the pavement.

There are two main areas of maintenance required on road pavements:

1. Maintenance of the pavement structure to ensure the road can carry future loadings
2. Maintenance of the surface of the pavement to preserve its skid-resistance, prolonging the durability of the surfacing, seal cracking and retaining a good ride quality.

Before carrying out any maintenance on the pavement, the engineer must first assess the structural strength and the surface condition of the pavement.

2.3.1 Assessment of the pavement structure

Once a pavement has been designed, it will have a certain structural design life before needing repair. Engineers realised that many of the roads built in the 1950s and 60s were now coming to the end of their design life and therefore methods had to be developed to analyse the pavements. Determining which areas along the pavement need to be repaired is mainly achieved using non-destructive techniques. Further examinations of these areas, located in the initial surveys, may result in the need for coring.

The next section will summarise different non-destructive techniques used to analyse the pavement. Non-destructive testing describes the ability to analyse a material without physically disturbing the structure, which is ideal when examining pavements.

2.3.1.1 Cores and trial holes

Cores can be taken along the pavement to obtain information on the thickness of each layer, the depth of any cracks, delaminations, and various physical parameters, i.e. density, void content and binder/aggregate affinity.

Digging trial holes or trenches enables *in situ* density measurements, particularly in unbound layers. These can help the engineer compare the relative differences between wheel paths

and other areas. Careful removal of each of the layers can also enable the upper surface of each layer to be examined for cracking, deformations and in some cases faulty workmanship. Brown (Brown, 1996) discusses the use of testing apparatus such as the Nottingham Asphalt Tester (NAT) and Dynamic Cone Penetrometer (DCP) to examine different properties of the pavement material once they have been removed from cores or trial holes.

2.3.1.2 Deflection measurements

The structural condition of a pavement can be obtained by measuring the amount it deflects under a standard load. The amount it deflects by is dependent on:

- Size of applied load
- Thickness of the layers
- Structural properties of the material used in the pavement
- Nature of the subgrade

Therefore, weak areas within the pavement will result in high deflections. The deflectograph and the Benkelman beam are the two methods used to achieve these measurements.

The deflectograph

The deflectograph is a lorry-mounted, mechanised system which places a measuring beam onto the surface of the pavement. While the vehicle moves forward at a steady speed (≈ 2km/h), the measuring beam, attached to the lorry by a cable, is released to the position where the wheel is applying the load. Once a measurement has been taken, the system is drawn forward to its previous position relative to the vehicle. Measurements are usually taken at intervals of 3.8m. Figure 2.4 shows the deflectograph in use.

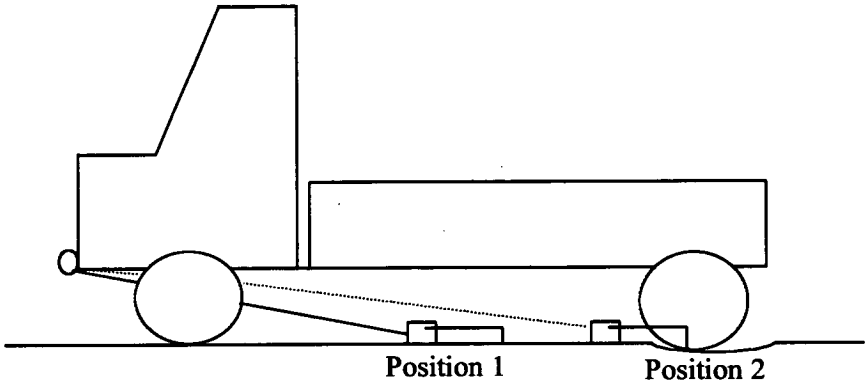

Figure 2.4: The deflectograph

The disadvantages of this method are that the applied load acts more gradually on the pavement compared to the loads produced by vehicles moving at normal speed. The deflection measurement does not necessarily give the full picture of the way the pavement responds to the applied loads as no consideration is given to the shape of the "deflection bowl" around the load. The deflectometer cannot be applied to rigid pavements or pavements which have little research information available on them.

Benkelman Beam

The Benkelman beam operates on the same principle as the deflectograph, but differs in some important aspects. Deflections are measured using dial gauges rather than electronic transducers. Only a single measurement is made whereas the deflectograph measures in pairs, with one in each wheel track

A two-axle lorry, with two pairs of rear wheels, is loaded symmetrically to a total load of 62kN. The deflection when the wheels are at position A is measured, shown in Figure 2.5. The lorry is then driven forward, past the tip of the beam, at a speed so that in 10secs the wheels are about 3m from the end of the beam. The deflection is continually monitored over this period, enabling a maximum to be obtained. The deflection 3m from the beam is also recorded and is known as the recovery deflection. As these tests are temperature dependent, the temperature of the pavement is measured in a predrilled hole, bored to a depth of 40mm below the surface, and filled with glycerol. Allowances should be made for variations in temperature above and below 20 degrees.

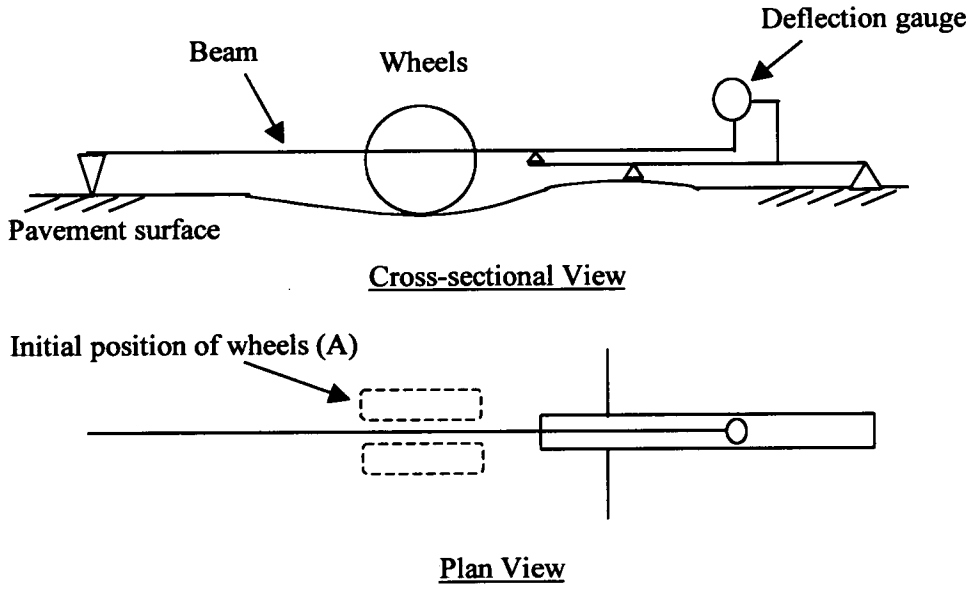

Figure 2.5: The Benkelman beam

The pavement deflection is half the sum of the maximum and recovery deflection and is expressed in hundredths of a millimetre. It can be seen that this is a less attractive method, taking a team of engineers one day to analyse 1km. However, the beam results are taken to be the standard. Further discussion of the Benkelman beam can be found in Salter (Salter, 1988)

Falling Weight Deflectometer

The Falling Weight Deflectometer (FWD) was designed in the early 1970s to examine certain characteristics of a flexible pavement. Since then it has gained widespread acceptance as one of the most effective methods for evaluating the flexible pavement. It has also been used in detecting deterioration in cement-treated layers and determining the condition of the joints in concrete pavements (Armitage, 1989; Brunton *et al.*, 1989; Chan and Evans, 1994).

A metal baseplate, on the surface of a pavement, is connected to a footplate with springs of a certain stiffness. A weight is dropped onto the footplate, which exerts a force into the baseplate and thus into the ground. A diagram of the set-up is shown on Figure 2.6(a).

Varying the height the mass is dropped, changing the spring stiffness or mass of the weight will change the peak force imposed on the pavement. Geophones are used to take measurements below the falling weight and at standard distances away from the applied load. These geophones measure the deflected shape of the loaded surface, known as the deflection bowl (Figure 2.6(b)). These deflection measurements, along with layer thickness values obtained from coring information, are used to provide estimates on the strength of each layer, including the subgrade, and the strain and stress distribution in each layer (Watson, 1994). The FWD test has also been used to determine the depth to the bedrock (Roesset *et al.*,1995).

Several FWD vehicles have been designed, the main difference being the size of weight which is dropped. Heavier weights are used to test heavier pavements such as airfields.

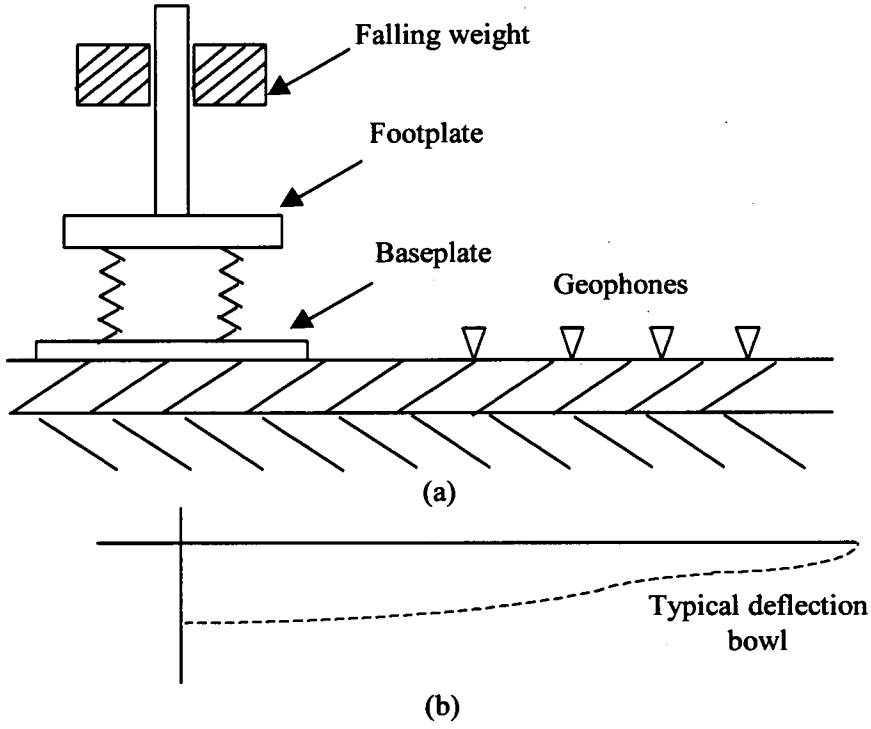

Figure 2.6: (a) The principle of the Falling weight deflectometer (FWD) (b) A typical deflection bowl produced by the FWD

2.3.1.3 Ground penetrating radar

Ground penetrating radar (GPR) can be used instead of cores and trial holes to obtain the layer thickness measurements (see Chapter 3). There are several methods available to the

operator, each will be discussed in Chapter 5. A new semi-intrusive method for determining radar wave velocities will also be discussed.

2.3.2 Assessment of the pavement surface

The assessment of the surface of the pavement is another important area in highway maintenance. The simplest technique used by the engineer is to carry out visual inspection of the pavement for crack distribution and propagation, surface distress and deformations. Skid-resistance tests are carried out using SCRIM (Sideways force Coefficient Routine Investigation Machine). This device measures the force exerted on a loaded wheel which is set at an angle of 20° to the direction of the vehicle. These measurements are usually combined with the visual inspection results by a computer program known as CHART (Computerised Highway Assessment and Rating Technique) and MARCH (Maintenance, Assessment, Rating, Costing of Highways).

2.3.2.1 Texture measurements

There are a multitude of methods used to measure the texture of a pavement. These include the "patch" method, where a measured quantity of sand or grease is smeared onto the pavement in the shape of a circle and the resulting diameter is measured. Another method is to take a plaster cast of the pavement surface, then smear paint onto it and the area that received paint is measured. Rose *et al.* (Rose *et al.*, 1973) reviewed these different methods for measuring the pavement texture.

Elton and Harr (Elton and Harr, 1988) also reviewed common methods used to measure the texture. These included skid-resistance tests, measuring the variation in the reflected light which was shone onto the pavement, and the use of lasers and charge coupled devices to measure the variations in pavement asperity height. Elton and Harr proposed the use of a laser system to perform rapid distance measurements from a moving vehicle. The variation of these measurements, over time or distance travelled, was correlated to the texture measures.

2.3.2.2 Crack measurements

Laurent *et al.* (Laurent *et al.*, 1997) used a laser system to perform 3D mapping of the pavement in order to map rutting and crack detection. This was done using an auto-

synchronised laser-scanning device which used triangulation. They noted that the classical approach of using laser triangulation was limited, as the collection optics of the camera must have a short focal length to enable the entire width of the road to be scanned, thus reducing the vertical resolution. The proposed auto-synchronised triangulation method uses a doubled sided mirror, with one side scanning the laser unto the pavement surface and the other side used to orient the reflected beam into the collection optics. The large field of view is achieved due to the rotating polygonal mirror (Figure 2.7). Curved projection mirrors were used to enable the necessary operating range to be minimised.

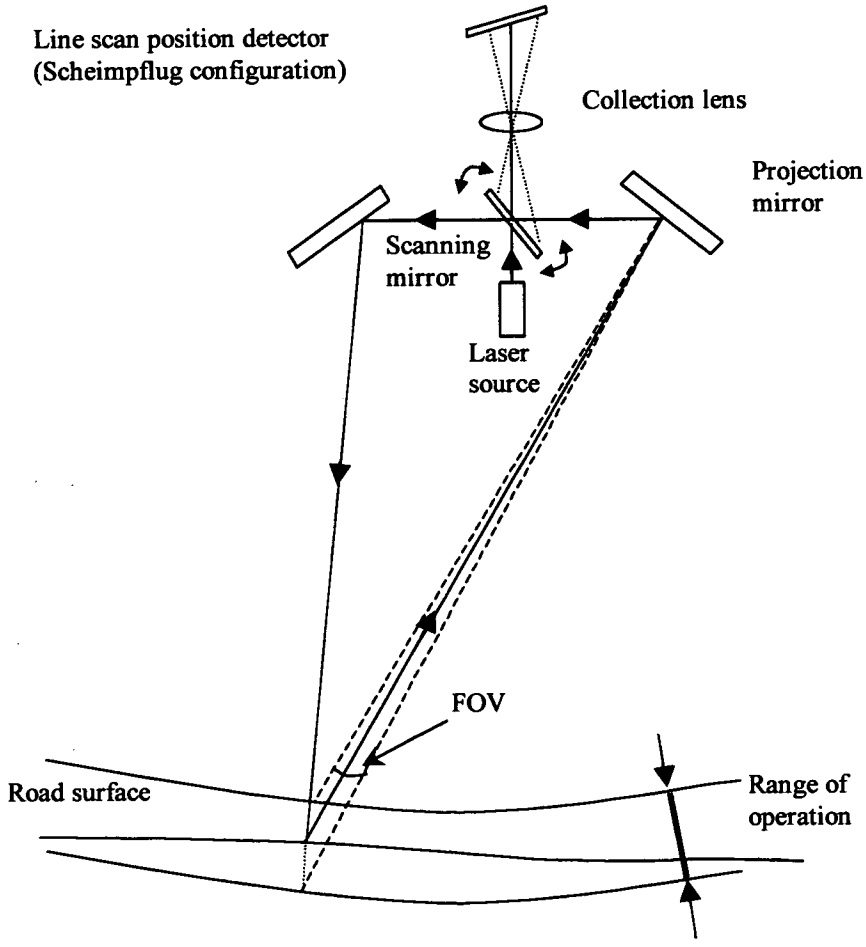

Figure 2.7: Increased field of view (FOV) due to the rotational polygonal mirror (Laurent *et al.*, 1997)

The laser system had a vertical resolution <0.5mm, and was able to fire 300 lines/sec, with each line made up of 1024 points. Preliminary experiments produced good results.

Simulated trials of calculating the rut depth showed that the system can obtain reliable measurements with a noise to signal ratio as low as 7dB. Future work on detecting the roughness of the pavement and locating potholes is planned.

Huang *et al.* (Huang *et al.*, 1998) have developed an automatic way of determining the extent of cracking on the pavement surface using a video camera and parallel computing technology. Their aim was to process the length, width and orientation of the cracks in real time and at traffic speeds, without producing overlaps or gaps in the images. This could only be achieved by using very powerful parallel computer processors.

The computer programs they used to detect the cracks had to be able to distinguish the black cracks against a background that varied from white to black. They also had to deal with noisy backgrounds due to the pronounced surface texture.

The accuracy of this system was compared to the results obtained using eight observers who classified the same stretch of road. They found that the success rate was about 80% compared with a majority of the observers. However, they did indicate that the program could only classify single images which meant that a single crack, spanning two adjacent images, would be counted as two separate cracks. The system also requires images to be collected with no overlaps or gaps, which therefore requires the driver to go at a constant speed, knowing the time taken to produce one frame a second by the camera. Alternatively the continuous speed of the vehicle would have to be monitored and taken into consideration in the computer program.

2.3.2.3 Roughness measurements

The roughness of the pavement is another surface measurement. Sayers *et al.* (Sayers *et al.*, 1986B) stated that road roughness is:

> *"The variation in surface elevation that induces vibrations in traversing vehicles"*

The measurement of road roughness is achieved using two measuring devices:

- The profilometer measures the longitudinal elevations along the road. This information is then analysed to obtain one or more roughness indices (see section 2.4).

- The Response-Type Road Roughness Measuring systems (RTRRMs) measure the vehicle response to roughness.

Engineers realised that there was no similarity between the multitude of methods used to measure road roughness. In the 80s the World Bank and Government of Brazil proposed an International Road Roughness Experiment (IRRE) to find a standard index appropriate for all the different roughness measuring systems in use. The index would be used to enable comparisons to be made between different devices (Sayers et al., 1986A).

In 1982 a total of 49 road test sites were measured in Brasilia, Brazil. Research teams from the United States, Belgium, France and the UK measured the roughness with different RTRRMs type machines and profilometers. This work eventually led to an International Roughness Index (IRI) being established.

Sayers (Sayers, 1995) brings together all the information, spread over many different references, to define the IRI. He was one of the original researchers who prepared instructions on using various machines to measure the IRI. He defines the IRI as:

"IRI is calculated from a measured longitudinal road profile by accumulating the output from a quarter-car model and dividing by the profile length to yield a summary roughness index with units of slope"

The quarter-car simulations were developed shortly after General Motors developed their profilometer. Sayers noted that the quarter-car was used in the IRI as it could be used with all profiling methods that were in use at the time of creating the index.

The following is based on Sayers summary of the IRI. Further information on the background to algorithms used to calculate the IRI can be found in his paper.

1. A single longitudinal profile with sampling intervals no longer than 300mm should be used.

2. A vertical resolution of 0.5mm is suitable for all types of roads. He noted that the required resolution is dependent upon the degree of roughness on the road.

3. A constant slope is assumed between adjacent sampled points.

4. A moving average is used to smooth the profile.

5. Filtering of the "smoothed" profile is performed using a quarter-car simulation with specific parameter values based on the Golden car (vehicle simulation with a set of parameter values). The simulated speed should be 80km/h.

6. The IRI value is obtained by dividing the simulated suspension motion (linearly accumulated) by the length of the profile resulting in IRI units of slope (metres/km).

Perera *et al.* (Perera *et al.*, 1996) compared laser, ultrasonic and optical profilometers from different companies. The IRI was used to perform the comparison between the different devices. Calibration centres were set up in different states across America, with a total of thirty eight different road profilers used. The profile information measured by each machine was compared to that measured by a hand-held dipstick device, and sand patch tests to measure the surface macrotexture depth (texture of pavement). Using different states and different road surfaces (asphalt-surfaced and concrete pavements) enabled a varied test platform to be set-up.

They found that there was a varied agreement between the dipstick IRI values and the profiler IRI values between different sites. The presence of the aggregate seal coat on the asphalt-surfaced pavement affected the data collected by the ultrasonic measuring systems. They concluded that the ultrasonic systems may be affected by varying macrotexture depth and materials used in the construction of the seal coat. However, they found that no clear conclusion could be reached concerning the concrete sites on the effect of the macrotexture on the different types of profilometer.

Responses-Type Road Roughness Measuring system (RTRRMs)

The RTRRMs are used to measure the roughness of the pavement relative to the motion of a vehicle as it moves along. A review on several of these devices can be found in Yoder and Witczak (Yoder and Witczak, 1975). The roadmeter, developed by Yoder (Yoder, 1973), measured the displacement of the vehicle's axle relative to its body as its traverses the pavement. The roadmeter statistic could be calculated from the weighted displacement and correlated to the road condition. The roughometer is a similar system; a heavy trailer suspends a wheel over the pavement. When it strikes a bump, the displacement relative to the trailer can be measured. It is assumed that the large inertial mass of the trailer provides a relative datum to measure these bumps. Elton and Harr (Elton and Harr, 1988) noted that

the information from the roadmeter and roughometer only applies to the entire length of the tested pavement and not to a specific location on the pavement.

2.4 Longitudinal Profilometers

To measure the true longitudinal profile of a pavement requires a level survey to be carried out. These surveys are very accurate, providing absolute height variations measured from a global datum, i.e. one that never changes. These measurements are used to determine the wavelengths along the pavement and thus predict the vehicle response. However, this technique is time-consuming and requires major disruption to the traffic. Therefore, engineers saw the need for a fast and more efficient way of measuring the profile while causing limited interruptions to the traffic flow.

In the 60s, the General Motor Corporation (GMC) built a profilometer which accurately measured the true profile over a range of wavelengths, Spangler and Kelly (Spangler and Kelly, 1964). The GMC profilometer used a series of accelerometers to compute the longitudinal profile of the road using a small feeler wheel positioned at the centre of the test vehicle. This machine could be operated at speeds between 40 and 50mph.

Dickerson and Mace (Dickerson and Mace, 1976) describe the use of a trailer-mounted laser profilometer which could rapidly calculate the road elevations relative to an absolute datum. The profilometer was a rigid beam, 5m long, on which four pulsed semiconductor lasers were mounted and used to determine the longitudinal profile. It could be towed at speeds of up to 80km/h and measure features from 0.2 to more than 100m long with a vertical resolution of approximately 1mm accuracy.

The paper discusses the use of 3 and 4 sensor profilometers at different positions along the beam. Certain assumptions were made when using 3 sensors:

- The centre and rear sensors are started on a flat horizontal surface.
- The beam is completely rigid (no vertical movement).
- The sensors make measurements at precisely the same points along the profile.

However, it was impossible to accurately measure the same points along the profile due to the road texture, step size and transverse movement of the beam. The actual profiles were

obtained by taking levels along the test sections. This enabled the error measurements to be calculated by comparing the difference in the curvature between the measured profile and that of the actual profile. The major error was the road texture, which was reduced by taking 2000 scans/s. Dickerson and Mace found that when using 4 sensors the error in curvature was about $0.3km^{-1}$ for distances of 100m.

Elton and Harr (Elton and Harr, 1988) reviewed different devices used to measure the longitudinal profile. They noted that the straight-edge profilometers only calculate variations within the wheel bases of the straight edge, resulting in no absolute measurement of the pavement profile being obtained. They also discussed the development of a device which measures the longitudinal pavement profile, texture and deflection at the same time. A load vehicle is used with 4 lasers placed on a rigid beam which is hung over the side of lorry. An algorithm was used to calculate the deflected and undeflected profiles along the road. The difference between these values is a measurement of the deflection of the pavement due to the load wheel. The texture measurement was obtained by calculating the standard deviation of several position measurements. A large value indicated a rough pavement, whilst a small value meant the road was smooth.

The front three sensors measured the undeflected profile of the pavement with the 4th laser, located beside the load wheel, to measure the deflected shape.

The authors found it difficult to get the laser to take measurements at the same position read by the previous laser. Misalignment of the lasers, temperature changes and shaking of the beam (due to motion of the vehicle) all added to the errors.

Noss (Noss, 1990) discusses the development of a Norwegian device used to measure road roughness. Noss's roughness meter qualified as a class 1: precision profiler (Sayers *et al.*, 1986), which is the highest degree of accuracy when measuring the IRI of a pavement. Noss's system used a total of 18 ultrasonic sensors, 17 of which were placed in a straight line along an aluminium bar fitted to a trailer (sensors 25cm apart). The 18^{th} sensor measured a fixed distance and corrected for velocity changes caused by the effects of air humidity, air temperature and air density.

The readings were taken in such a way that an overlap occurred between different readings from two successive loggings. The maximum speed was dependable on the spacing between each reading, but Noss noted that the machine had been tested up to speeds of 80km/h

(recommended speed for IRI measurements). The elevation readings had an accuracy of about 0.25 to 0.4mm for a 100m long "smooth" pavement. He found that this accuracy was dependable on the texture of the pavement and the spacing between the successive loggings.

Zhu *et al.* (Zhu *et al.*, 1996) described an Automated Pavement Profile Analysis and Roughness Evaluation system (APPARE). The system analyses the statistical properties of the road pavement profiles and uses the IRI and the profile index to describe the roughness of the road.

Several field studies were carried out using APPARE and have resulted in this system being adopted by the Louisiana Transport division as a standard profilograph test procedure and quality control for the acceptance of newly constructed pavements.

Jordan and Cooper (Jordan and Cooper, 1989) discussed the use of the longitudinal profilers to indicate the structural condition of the pavement. The trends in the profile were compared to the assessment of the structural condition using visual inspection and deflection measurements. The High-speed road monitor (HRM) described by Still and Jordan (Still and Jordan, 1980) was used to measure the longitudinal profile and rut depth. They found that the change in unevenness of a road is a more important indicator of the deterioration of the pavement than the absolute level of the unevenness.

2.5 Maintenance methods

The next section gives a brief explanation of some of the various types of maintenace procedures carried out by the highway engineers.

2.5.1 Retexturing

Poor skid-resistance and smooth (polished) road surfaces are mainly due to the polishing action of the traffic or excess binder rising to the surface. These problems require the road to be retextured in a number of different ways:

- Blasting of hot compressed air/grit or shot-blasting
- Diamond saw grooving

- Applying an overlay of asphalt

It should be noted that the surfaces to be overlaid require hot or cold planning in order to roughen up the texture to remove the excess binder and correct any irregularities.

2.5.2 Overbanding to seal cracking

If cracks are not sealed then ingress of water will lead to weakening of the pavement, freezing of this water will increase the damage.

Overbanding is a very effective method used to seal pavements with a bitumen compound, which have occasional cracks. The overbanding must be able to accommodate any movement in the surface and have the same skid-resistance as the rest of the pavement. It should be noted that this type of sealant is not beneficial in surfacing which has multiple cracks in a small area.

2.5.3 Localised Patching

Filling in pot holes, repairing or laying of services along the pavement requires localised patching. Over the years this work has come under a lot of criticism from the general public due to the unsatisfactory results of this work. In 1992 (Anon, 1992A) the government brought out new legalisation to improve this reinstatement work. The contractors were required to:

1. Prevent subsequent failure of adjacent material to the patched area by sufficiently cutting back to the sound material.

2. Fully compact all layers of a reinstatement to avoid subsequent settlement or they need to leave a surcharge to accommodate such settlement.

The main need for localised patching is on carriageway edges which do not have any edge support (kerbs) and no positive drainage. Without the kerbs, the vehicles can encroach on the road verge, which is the weakest point on the road. With no positive drainage water gets into the pavement and leads to rapid deterioration. However, localised patching in pavements which have suffered failure on edges with no kerbs, has not improved the

problem. These patches are laid down without adequate pavement foundation, thus failing much quicker than anticipated.

2.5.4 Surface Sealing

Surface sealants such as slurry sealing or surface dressing can be applied to pavements which have minor cracking or surface abrasion.

- Slurry sealant is applied as a thin veneer and is only suitable for low speed and lightly trafficked situations due to its poor skid resistance.

- Surface dressing provides good texture depth resulting in high speed skid-resistance, however, special binders may be required to enable its use in heavily trafficked (high stress) areas.

Surface dressing is constructed by applying a film of bituminous adhesive to the pavement and chippings are added and rolled into it.

These sealants do not have any significant structural strength, although, they will seal the cracks and prevent the ingress of water. Choosing the right sealant depends on how heavily trafficked the pavement is and the speed at which vehicles traverse it.

2.5.5 Resurfacing or overlay of pavements

Resurfacing of a pavement is carried out to strengthen an existing pavement in order to increase its design life or to correct the surface profiling. This improves the drainage of surface water, the ride quality and skid-resistance.

The British Aggregates Construction Materials Industries (BACMI) have produced a book called "Bituminous mixes and flexible pavements: An introduction " (Anon, 1992B). The book examines all the maintenance procedures used in the UK. The BACMI suggest that the highway engineer should consider several different things before resurfacing a pavement. These include:

- Is the strength of the pavement adequate for the future increase in loads?

- Does the shape of the road construction ensure satisfactory riding quality and surface water drainage?

- What level of skid-resistance is required?

2.5.6 Reconstruction of pavement

Reconstruction of the pavement entails removal of the full construction depth and replacement of a newly designed alternative construction thickness. This new design may be of flexible, rigid or composite construction type.

2.6 Whole-life road performance models

Whole-life road models are increasingly being used to predict the degradation of a pavement over time when subject to realistic traffic and environmental loads. Validation of these models is achieved by examining how in-service roads perform over a period of time. These performance measurements usually include calculating changes in the surface profile and structural integrity of these roads, which are then included in the model.

These models are designed to enable the highway engineer to predict when and where pavement damage will occur, thus minimising the cost and inconvenience of the repairs. This next section will mainly focus on work carried out by Collop (Collop, 1994), who has developed and validated one of these whole-life road performance models.

Collop reviewed three whole-life models:

- Brademeyer model (Brademeyer *et al.*, 1986, Brademeyer, 1988)

- Ullidtz model (Ullidtz and Larsen, 1983)

- Papagiannakis model (Papagiannakis *et al*, 1988)

Each author used the ASSHO road tests to validate their models.

2.6.1 AASHO road test

Several road life monitoring experiments have been carried out over the years. One of these was conducted by the American Association of State Highway Officials (AASHO) (Anon, 1962A, 1962B). These tests were carried out in Ottawa, Illinois over a two-year period. The main aim of these tests was to determine the relationship between road performance and structural design and loading.

Multiple lanes were built, with each lane made of a particular construction type. Loads ranging from a 2000lb lorry with a single axle to 48,000lb lorry with a tandem axle were used in the tests. Different factors such as "Present Serviceability Index" (PSI) and number of "standard" axle loads required to cause damage were determined from these tests. PSI is related to the road condition by:

$$PSI = 5.03 - 1.91\log(1+SV) - 1.28RD^2 - 0.01\sqrt{(C+P)} \quad (2.1)$$

(Numbers range from 0-5)

where:
SV is the mean slope variance of the surface profile,
C is the linear cracking per 1000 ft^2,
P is the bituminous patching in ft^2 per 1000 ft^2, and
RD is the mean rut depth for both wheel tracks.

A value of 5 represents a "perfect road" and 0 represents a very poor road. A value of 2.5 is described as "acceptable for a primary road system".

The main criticism of the ASSHO road tests is that the same vehicle was used in each lane, and all the sections were built on top of the same subgrade and subject to the same weather conditions. Therefore, any performance relationship could only be applied to roads of similar operating conditions.

2.6.2 Brademeyer whole-life model

This model used a non-linear vehicle model to generate a digitised load history. Combining this with an influence function for each road response variable enabled the response of the

road at points along it to be found. The mean and variance of each road response was used in a computer program to simulate 23 sections of the ASSHO tests.

This model assumed that the environment was constant, however, the severe freeze-thaw cycles, seen in the ASSHO tests, had not been accounted for in the model simulations. This was achieved by applying weekly and seasonal weighting factors to the model. These values were obtained from deflection measurements taken from the unused control loop in AASHO test.

The response of the road to a number of moving loads and dynamic axle loads was modelled, but the contribution to the dynamic axle loads caused by vehicle roll was ignored.

The model's predictions of damage and serviceability compared quite well to the AASHO tests, although, for a twin axle, the predicted rutting results were much higher. This was put down to over predicting of the rutting occurring in the subgrade. Adjustment in the model to calculate rutting based on the maximum compressive strain instead of subgrade deflections improved the results.

2.6.3 Ullidtz whole-life Model

Ullidtz and Larsen recognised that permanent deformation and crack propagation are not only related to the dynamic forces, but to the thickness of the layer and the material parameters. Their road model was divided into 0.3m length sub-sections, consisting of 4 layers (asphalt, base, sub-base and subgrade layers). Using the weekly climate conditions experienced during the ASSHO tests and a regressive process they were able to find the variations in material parameters.

Correction factors were applied to model the severe freeze-thaw effects, however, no consideration was given to the direct effects of the environment on fundamental material properties.

A linear quarter-car model was used to calculate the dynamic loading produced by a heavy vehicle.

The model produced a good correlation between the measured rut depth from the ASSHO tests and the simulated values.

2.6.4 Papagiannakis whole-life model

Ten sections of the ASSHO test were simulated, six which developed severe roughness, and four that remained fairly smooth. A spatial mean value and a coefficient of variation were used to describe the distribution of the material parameters.

The applied axle load on the four smooth roads was assumed to be static, whereas the rough road sections were modelled dynamically with short load lengths (5.2m) experiencing one complete load cycle. It should be noted that this length was obtained by assuming the predominate frequency of the load variation is 3Hz for a vehicle speed of 58 km/h. These 5.2m lengths were divided into 6 intervals and a load segment was assigned to each of these divided intervals.

The effect of the deteriorating road roughness on the dynamic axle loads was modelled empirically, assuming Gaussian or Trapezoidal frequency distribution on road roughness. Collop noted that this method does not take account for vehicle-road interaction therefore it can not be easily applied to different sections.

The authors of this model concluded that the model produced fairly accurate predictions of distress and performance for the smooth road sections from the ASSHO test sections. For the rough roads, they found that the dynamic loads could be modelled well on four out of the six ASSHO road sections.

2.6.5 Collop whole-life model

Collop concluded that each of the above models could not be easily applied to situations of mixed traffic flow unless serious changes to the models were undertaken to fit the parameters to the observed results. None of the models investigated the relationship between damage propagation due to "weak spots" in the pavement structure (e.g. due to variations in asphalt layer thickness) and "hot" spots on the pavement surface produced by peak dynamic loading.

Collop's WLPPM was broken into several different models in order to account for most of the important aspects of vehicle/pavement interaction. These are listed below:

- Environmental model

- Pavement surface profile model
- Dynamic vehicle model
- Pavement primary-response model
- Fatigue cracking model
- Permanent deformation model
- Asphalt modulus-degradation model

He validated the model using in-service UK roads. The selected test sections (total length 100m) were relatively flat and straight. Strain gauges were placed at the bottom of the asphalt layer in order to measure the horizontal tensile strain.

Four key areas of the test section were instrumented

1. Traffic monitoring: Use of a CUED/Golden River weighing sensor enabled the axle weight to be found for each vehicle. Vehicle classification, speed, time of day and lateral location of wheel path were also found.
2. Environmental Monitoring: Thermocouples and moisture monitors were placed at several depths to continuously monitor temperature and moisture levels respectively.
3. Road profile monitoring: The TRRL High Speed profilometer (Still & Jordan, 1980) was used to measure the longitudinal profile of the road.
4. Road strength monitoring: The TRRL deflectograph and FWD were used to measure the static and dynamic surface deflection bowl of the pavement section.

An instrumented hammer was used to carry out impulse response tests on the section. The exerted force is measured using a transducer located at the hammer face. Corrections are made for the outbound inertial forces, associated with the mass of the hammer, using an accelerometer located on the back of the hammer head.

The spatial repeatability of the dynamic tyre forces was measured, as well as wheel forces and road response.

Some of the conclusions from Collop's research are listed below

- Short wavelength surface-roughness components are smoothed out, whereas long wavelengths components increase in amplitude due to traffic loading.
- In thick pavements (250mm of asphalt), asphalt layer thickness variations tend to dominate the profile-degradation process
- In thinner pavements (125mm asphalt), the surface-roughness induced loads are dominant.

Several assumptions were made when using the model to predict pavement performances. One of these was that there was no correlation between the asphalt-layer thickness profile and pavement-surface profile. This was made because no research had been carried out in this field. Collop noted that validation of this assumption requires a large number of flexible pavements to be analysed.

The aim of this research project is to design and build a trailer to carry out analysis using ground penetrating radar to examine whether or not there is any correlation between the surface and sub-surface profiles.

2.7 Conclusions

Brown (Brown, 1998) discussed how future pavement design and maintenance will need to place more emphasis on economic and innovative solutions. He believes this is possible due to experience and research gained over the past 20 years as well as the governments implementation of DBFO (Design, Build, Finance and Operate) in their privatisation policy.

Brown indicated the need for improved development in non-destructive testing techniques to evaluate the structural ability of the pavements, especially in measuring the surface deflection bowl at reasonable speed, while still obtaining the accuracy of the FWD. There is also a need for effective design of overlays which do not experience reflective cracking.

New developments in surfacing materials such as porous asphalt (PA), formerly known as pervious macadam, and stone mastic asphalt (SMA) are replacing the traditional hot rolled asphalt. The use of PA enables better drainage of water through the layer by dispersing it at the edge, so reducing spraying of water. This is achieved by having a designed void content

in the range 20-25% and laid on top of impermeable mixtures. SMA has a good resistance to rutting and provides a reduction in noise compared to chipped rolled asphalt.

Chapter 3

GPR and Impact Testing of pavements

3. Introduction

Ground Penetrating Radar (GPR) is a non-destructive technique for investigating objects hidden by optically opaque barriers. It detects changes in the electromagnetic properties of materials, principally the permittivity, and is capable of producing cross-sectional representations of what is beneath surfaces. The main applications of GPR for highway pavement investigation are detection of moisture, air voids, delaminations and layer thicknesses. If used correctly, it can provide accurate information on the condition of the pavement resulting in major savings in road maintenance.

This chapter presents an introduction to the technique and a review of its application to the investigation of highway pavements. Problems associated with the technique are also discussed. It then looks forward to the developments currently underway in the field including what might be possible in the near future with advances in hardware and signal processing capability. Suggestions for the future direction of the research in this field to enhance the data collection and interpretation are also made.

When impact techniques are applied to a pavement they result in stress waves (compression and shear) being produced. There are two basic techniques used to produce these stress waves: ultrasonic transducers and impact sources. The remainder of this chapter will discuss these techniques in more detail as well as looking at new non-contact technology which could be used in the future to analysis pavements.

3.1 What is radar?

Radar is an acronym for "Radio Detection and Ranging" which implies the use of radio waves, transmitted from an antenna, to detect an object as well as determine the distance to the object. The radio wave in GPR testing is a short pulse of electromagnetic energy. Detection of an object or interface is achieved by detecting reflections of the pulses by a receiving antenna.

Ground penetrating radar (GPR), surface penetrating radar and ground probing radar are some of the names used to describe this technique to investigate shallow subsurface objects that have electrical properties that are different to the surrounding host.

GPR operates in a similar way to conventional radar but with several important differences:

- Conventional radar operates in ranges up to hundreds of kilometres whereas GPR operates in ranges from several centimetres to tens of metres.
- Doppler effect is used by conventional radar but not in GPR, i.e. the changing frequency of the wave motion observed when the target is moving.
- The resolution of conventional radar can be tens of metres whereas GPR is as small as several millimetres.
- GPR can be transmitted through lossy media, whereas conventional radar is only used through air or a vacuum (space).

3.1.1 History of GPR

GPR has been used to detect objects within an optically opaque surface for many years. The work of Hulsenbeck (Hulsenbeck, 1926) appears to be the first known use of pulsed techniques to detect reflections produced by dielectric variations which did not necessary involve conductivity.

Pulsed radar techniques were used extensively in the 70s to map geographical structures in the ground such as rock formations as well as determining the depth of ice. Presently GPR systems have been used in archaeology, road and tunnel investigations, location of voids, detecting ground water, locating mineshafts and pipe and cable detection.

3.2 Introduction to electromagnetic waves

GPR uses electromagnetic (EM) fields, consisting of coupled electric (E) and magnetic (M) fields, to examine structures or objects. The electrical properties tend to be the dominating factor controlling the response of GPR. The variation of magnetic properties are small for common geological materials of interest.

3.2.1 Radar Antennas

A simplified explanation of how radar antennas work will now be given. More sophisticated explanations can be found in Kraus (Kraus, 1991) and Paul and Nasar (Paul and Nasar, 1987).

3.2.2 Antennas pattern

Two types of ground probing radar antenna are generally used on pavements, i.e. "bowtie" and "horn" antennas (Figure 3.1 and Figure 3.2). The horn antenna produces a more focused beam though the general pattern of radiation is similar. These types of antenna are typically found in most commercial GPR systems. They are preferred because of their linear phase response over a wide frequency range and convenient size.

On placing an antenna on a surface, the frequency content of the emitted pulse changes relative to that emitted in air. The antenna is said to be coupled or loaded to the surface. The peak frequency of the radiated signal generally becomes lower on coupling (Sellmann *et al.*, 1993).

The pattern of the electrical and magnetic field of a particular radar system tells us in which direction the antenna will be most sensitive, i.e. the best orientation of the antenna to obtain the strongest reflections from an object or structure. Figure 3.3 shows the direction of the magnetic (H) and electric (E) plane inside the 900MHz antenna.

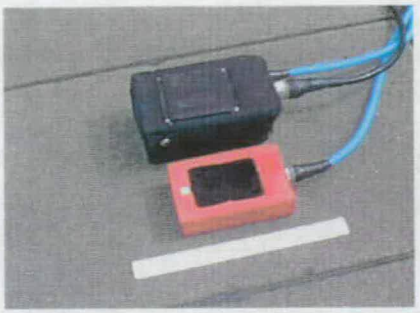

(a)

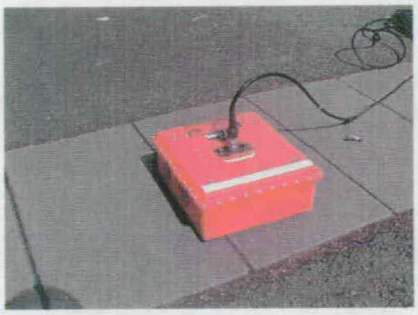

(b)

(c)

Figure 3.1: GSSI bow-tie antenna (a)1.5 GHz (b) 500 MHz (c) 900MHz

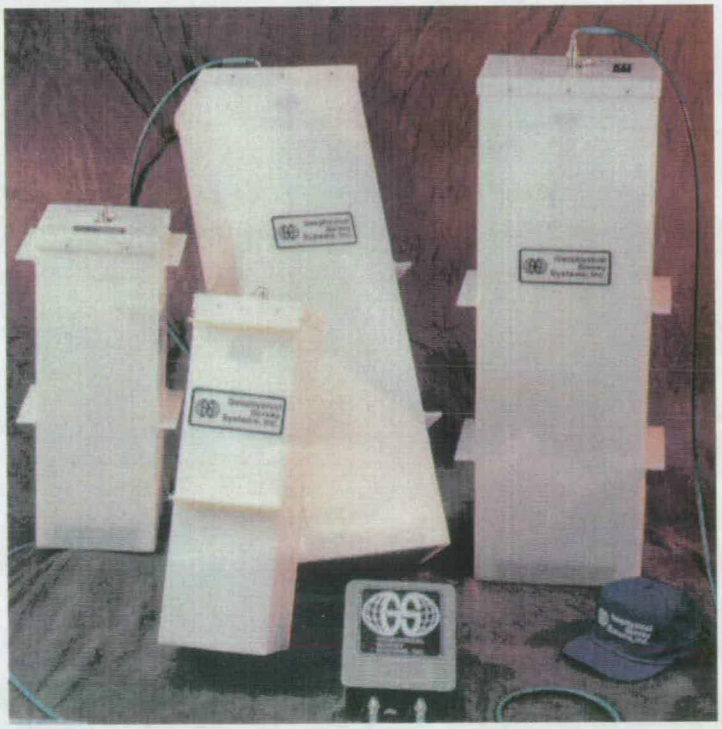

Figure 3.2: GSSI horn antennas

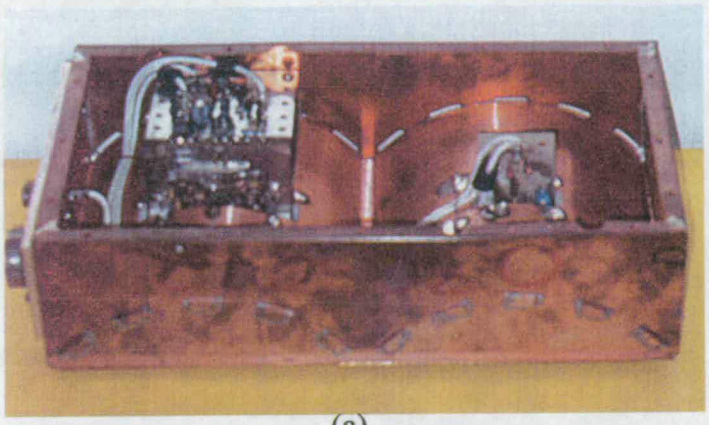

(a)

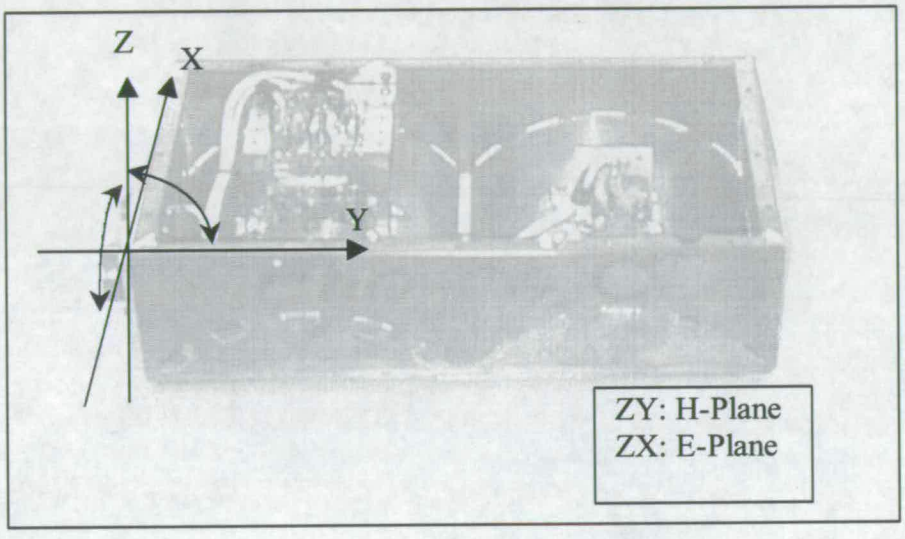

(b)

Figure 3.3: (a) Inside the 900MHz antenna (b) The direction of the electric (E) and magnetic (H) fields

Estimation of the beam width for different frequency antennas over water is provided by Davidson and Forde (Davidson and Forde, 1996), which indicates the generalised response for sub-surface interfaces in homogenous layered materials.

The spreading radar beam also leads to some geometrical distortion of the sub-surface layer profiles. On passing over an inclined layer the signal returned to the receiver is that from the point on the sub-surface interface, perpendicular to the emerging signals rather than the point directly below the antenna. Figure 3.4 illustrates this principle for the use of GPR to locate river beds. This causes a shift in the depth and angle of inclination which is

significant beyond slope angles of $\alpha = 25°$. Such angles are only encountered in pavements where there are significant changes in the structures.

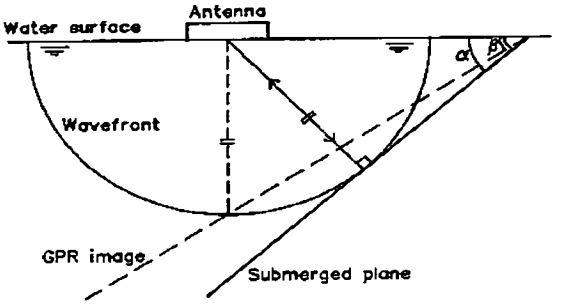

Figure 3.4: Ground-penetrating radar image of a sloping plane (Davidson and Forde, 1996)

A further factor to consider is the influence of signals 'ringing' back and forth between two good reflectors. This is apparent when GPR is used over water as the interface is shown repeatedly in time down the profile. These reflections are known as 'multiples' and should not be confused with reflections from true structures.

3.3 General Principles

The basic principle underlying GPR is that electromagnetic signals transmitted into the medium of interest are partially reflected on encountering a change in the electrical properties. The reflected signal is recorded at a receiver while the transmitted part continues through the new material. This process is continued when further electrically-different media are met by the transmitted signal. The series of reflections recorded at the receiver allow an image of the interior structure to be built up. An explanation of GPR is also provided in the HMSO document (Anon, 1994) which concerns the technique's usage for the investigation of pavement defects. The depth of a layer of material is determined from the time it takes the reflected wave to be detected at the receiver. Knowing the velocity of the wave through the relevant media, the depth is calculated as:

$$d = v\left(\frac{t}{2}\right) \tag{3.1}$$

where: d = thickness of layer (m)

v = velocity of electromagnetic wave through the layer (m/ns)

t = time between reflections (ns)

In the determination of layer thicknesses the above equation is employed using the time between the observed reflections and the relevant velocity, estimated from Table 3.1.

Material	Relative permittivity	Velocity (m/ns)*
Fresh water	81	0.033
Saturated clays	5 - 40	0.05 - 0.13
Saturated silts	5 - 30	0.06 - 0.13
Saturated sand	20 - 30	0.06 - 0.07
Wet bedrock	5 - 20	0.05 - 0.13
Dry asphalt	2 - 4	0.15 - 0.21
Wet asphalt	6 - 12	0.09 - 0.12
Dry concrete	4 - 10	0.09 - 0.15
Wet concrete	10 - 20	0.07 - 0.09

*For GPR data nanoseconds (ns), i.e. 10^{-9} seconds, is an appropriate unit of time.

Table 3.1: Relative permittivity and velocity values for some materials

3.4 Material Properties

The electrical properties that govern the propagation of electromagnetic waves through materials are electrical conductivity, magnetic permeability and relative permittivity. The value of the magnetic permeability for common geological materials is weak and is not considered. These properties, and corresponding radar velocities, are presented in Table 3.1 for the materials of interest in a pavement survey. In general the conductivity determines how far through a material the signal penetrates while contrasts in relative permittivity govern the proportion of energy transmitted and reflected at material boundaries.

The velocity of the electromagnetic wave decreases with an increase in relative permittivity. The speed of electromagnetic waves through low-loss non-magnetic materials such as water or soils is approximately:

$$v = \frac{c}{\sqrt{\varepsilon_r}} \tag{3.2}$$

where: v = signal velocity (m/ns),

c = velocity of light ($\approx$ 0.3 m/ns),

ε_r = relative dielectric constant. (see Appendix A):

Attenuation describes how energy is lost or dissipated. As the signal propagates into the material it will experience losses. The most significant loss mechanism is associated with material loss which causes the electrical energy to be converted into heat energy.

The attenuation of the signal, α, due to material loss is:

$$\alpha = 12.86x10^{-8}\omega\sqrt{\varepsilon_r}\left(\left[\sqrt{\left(1+\tan^2\delta\right)}-1\right]^{\frac{1}{2}}\right)(\text{dB/m}) \qquad (3.3)$$

where: $\tan\delta = 1.8x10^{10}\dfrac{\sigma}{\omega\varepsilon_r}$

σ = Material conductivity (S/m)

ε_r = Relative permittivity

ω = Frequency (Rad/s)

The electrical conductivity has the greatest bearing on the degree of signal attenuation, i.e. on the extent to which the signals penetrate. The higher the conductivity, the greater the attenuation and less the depth of penetration. Conductivities of paving materials can vary greatly due to the presence of salt in any water that is present in the pores. The attenuation also increases with the frequency of the wave that is propagating through the medium so high frequency surveys will not be able to penetrate wet materials that have salt dissolved in them.

The power of emitted radiation is also a factor and as lower frequency antennas produce more powerful signals they therefore allow greater depths to be probed. However, there is a trade off, since the lower the frequency, the poorer the vertical (depth) resolution.

For slightly conducting materials $\tan\delta << 1$, which is typical of geological and building materials. Therefore the attenuation can be simplified as:

$$\alpha = 1.64\times10^{3}\frac{\sigma}{\sqrt{\varepsilon_r}}\ (\text{dB/m}) \qquad (3.4)$$

The derivation of attenuation from Maxwell's equations can be found in many books such as Daniels (Daniels, 1996B) or Kraus (Kraus, 1991).

A description of all the losses experienced when a signal travels from a transmitter to the target and back to the receiver is given by Daniels (Daniels, 1996B). He describes the loss mechanism as.

$$L_t = L_e + L_m + L_{t1} + L_{t2} + L_s + L_a + L_{sc}$$

where:

L_t = total path loss (dB)

L_e = antenna efficiency loss (dB)

L_m = antenna mismatch losses (dB)

L_{t1} = transmission loss from material to air (dB)

L_{t2} = retransmission loss from material to air (dB)

L_s = antenna spreading losses (dB)

L_a = attenuation loss of material (dB)

L_{sc} = target scattering loss (dB)

Daniels stated that the typical depth of penetration of an antenna rarely exceeds 20 wavelengths, except in very low-attenuation dielectric media (lossless media).

3.4.1 Conduction and displacement currents

Conduction and displacement currents, within the material being examined, are produced when an electric field is applied to a material.

A conduction current will be produced when an electric field is applied to a conductor causing the charge to move at a constant velocity. The movement of charge within the material causes the dissipation of energy in the form of heat due to collisions with non-moving objects.

In Figure 3.5(a), a constant voltage across the resistor (R) will produce a constant current known as a conduction current:

$$i_1 = \frac{V}{R}$$

Whereas, the current through the capacitor (C) is known as a displacement current:

$$i_2 = \frac{dQ}{dt} = C\frac{dV}{dt} \tag{3.5}$$

where: Q = charge (coulomb)

V = voltage (volt)

C = capacitance (Farad)

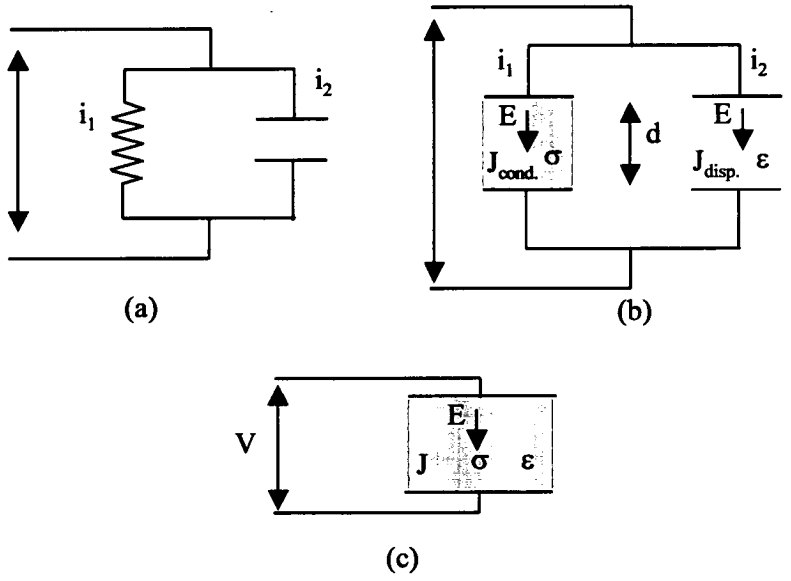

Figure 3.5: (a) and (b) Conduction current through a resistor (R) and displacement current through a capacitor (C) (c) Conduction and displacement current through a dielectric medium that is also conducting (adapted from Kraus, 1991)

No actual current flows through the capacitor, however, the same amount of charge flows onto opposite plates of the capacitor so that this external effect is as though it did.

If the resistor is viewed as a capacitor filled with a conducting medium (Figure 3.5(b)) the electric field (E) is:

$$E = \frac{V}{d} \tag{3.6}$$

where: d = distance between the capacitor's plates

The conduction current density within the resistor is:

$$J_{cond} = \frac{i_1}{A} = \frac{V}{RA} = \frac{\sigma V}{d} = E\sigma \qquad (3.7)$$

where: J_{cond} = Conduction current density (Amperes/m^2)

R = Resistance (ohms)

σ = Conductivity (S/m)

A = Cross-sectional area (m^2)

The displacement current density within the capacitor can be worked out by substituting equation (3.6) and C=εA/d, where A is the area of the plates and ε is the permittivity and d is the spacing between the plates, into equation (3.5).

$$i_2 = \frac{\varepsilon A d}{d}\frac{dE}{dt} = \varepsilon A \frac{dE}{dt}$$

$$J_{disp} = \frac{i_2}{A} = \varepsilon \frac{dE}{dt}$$

Substitute D = εE

$$J_{disp} = \frac{dD}{dt} \qquad (3.8)$$

where: D = Electric flux density (coulombs/m^2)

$J_{disp.}$ = Displacement current density (Amperes/m^2)

ε = permittivity (Farads/m)

E = electric field (Volts/m)

A combination of displacement and conduction current are found in any natural materials, therefore, instead of having two separate elements in parallel, only one is present which has both capacitance and resistance (Figure 3.5(c)).

$$J_{total} = J_{cond} + J_{disp} \qquad (3.9)$$

Figure 3.6 shows the relationship between the total current and displacement and conduction current. If we assume the conductivity and permittivity to be constant, then at a transition frequency (ω_t), the displacement and conduction current will be equal. Below this frequency, conduction currents dominate, causing dissipation of the EM wave in the material. Above this frequency, displacement current dominates and the EM wave propagates into the material as a wave with little or no dispersion. This simplified

explanation is for idealised materials, however, real materials have some frequency variations in their electrical properties.

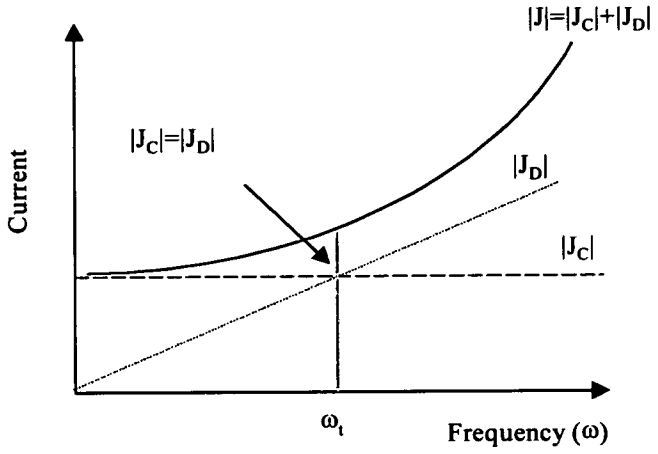

Figure 3.6: Conduction, displacement and total current against frequency (Annan, 1997)

The velocity and attenuation can be related to the permittivity and conductivity when the antenna operates above the transition frequency.

3.4.2 Effective use of GPR

Choosing the correct antenna frequency and orientation depends on several factors:

- Depth of target
- Geometry of target
- Electrical properties of target
- Electrical properties of host material
- Geography of the surroundings in which the survey is carried out

Answering each one of these questions will enable the operator to decide which type of antenna(s) to use in a particular investigation and result in the most accurate detection of the target.

The range of GPR depends on the frequency of the antenna, low frequencies (≤ 500MHz) will result in deeper penetration of the radar wave, but, the downside is that the resolution of the image is reduced. High frequency antennas enable better resolution of the image but have poorer penetration. This results in a compromise being found between the depth and resolution. Another factor which affects the range is attenuation of the signal, discussed earlier.

3.4.3 Reflection coefficient

The electromagnetic waves, propagating into the target, will be reflected back to the surface due to changes in the electrical impedance. Electrical impedance is the opposition to the flow of current. Changes in the relative permittivity of the ground are the controlling factor in the electrical impedance resulting in reflections of the signal at the boundaries of the electrically dissimilar materials (Figure 3.7).

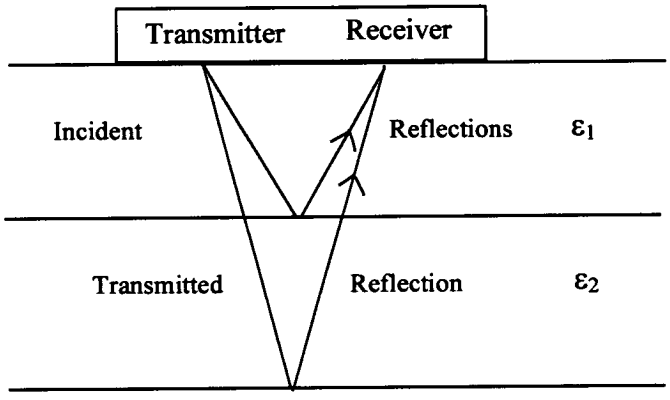

Figure 3.7: Reflection and transmission effects within a layer material

The incident wave propagates from the transmitter through the material until it encounters a change in the relative permittivity causing part of the wave to be reflected back to the receiver. The rest of the wave will propagate through to the second layer. This process will continue until all the energy has been attenuated.

$$\text{Reflection coefficient} = \frac{\sqrt{\varepsilon_1} - \sqrt{\varepsilon_2}}{\sqrt{\varepsilon_1} + \sqrt{\varepsilon_2}} \qquad (3.10)$$

$$\text{Transmission coefficient} = \frac{2\sqrt{\varepsilon_2}}{\sqrt{\varepsilon_1} + \sqrt{\varepsilon_2}} \qquad (3.11)$$

3.5 GPR terminology

Certain terminology is used when describing the use of GPR. Some of these will be defined below in order to understand its use in subsequent chapters.

Scan Line and Sample points

A scan line is shown on Figure 3.8. It is made up of a number of samples (128, 256, 512 or 1024). The rate at which these scan lines are produced is dependent on the radar system, in the GSSI Sir10A+ system, (GSSI, 1996), this can be anything from 2 to 200 scans per second (scans/s), but, this value is dependent on the number of antennas being used by the system and the type of filter used to clean the data.

The rate of producing scan lines can also be controlled using a survey wheel (odometer). The user can obtain a fixed number of scans over a unit distance even though the antenna movement may vary. The scan rate will then be measured in scans per meter (scans/m) and will produce a uniform horizontal scale for an entire survey. Further discussion on the limitations of using a survey wheel will be found in Chapter 6.

Transmit rate

The transmit rate or transmit pulse repetition rate limits the speed at which the GSSI radar system can produce scan lines or traces. The Sir10A+ radar system can have a transmit rate between 2 and 78kHz whereas, in the Sir10H system values can be anything between 10 and 225kHz.

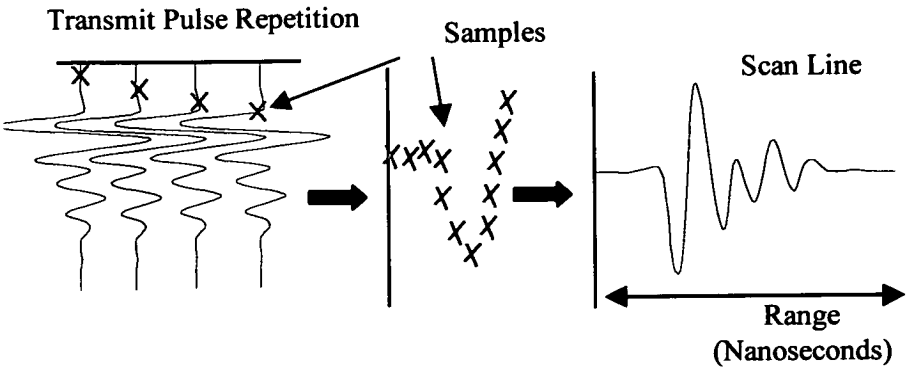

Figure 3.8: Diagram showing how a scan line is produced

If a transmit rate of 52kHz is chosen then 52,000 transmitted pulses will be produced in one second. In order for one scan line to be produced, it must sample equally spaced points along the transmitted pulse as it propagates through the object or structure under investigation (Figure 3.8). Due to current technology limitations a transmit pulse is required for every sample point recorded.

Time range

The time range is an adjustable time window enabling the user to vary the amount of the scan line recorded. Its units are nanoseconds (ns). Adjusting the range gives the user the ability to zoom in and out on sections of the scan line. However, too small a range may cut off some important information, too large a range may make it difficult to see important features. Therefore, choosing the correct range value is extremely important when carrying out GPR surveys.

The desired range is dependent on the frequency of the radar antenna and the radar velocity within the medium under investigation. The calculations below give an example of how the range can be decided (Table 3.2). It should be noted that the time range should be increased by at least 30% to account for uncertainties in velocity and depth variations (Annan, 1997).

	Example 1	Example 2
Distance to interface D (m)	10	0.6
Velocity (m/ns) V	0.3	0.1
Time delay (ns) $T=2D/V$	67	6
Time range setting (ns)	90	8

Table 3.2: Example of working out the time range

Time Gain

When a radar signal propagates through different media it will experience attenuation. The amount of attenuation is dependent on the conductivity of the materials (see section 3.4). This attenuation results in the signal reflected from large depths being much smaller compared to ones from shallow depths (Figure 3.9).

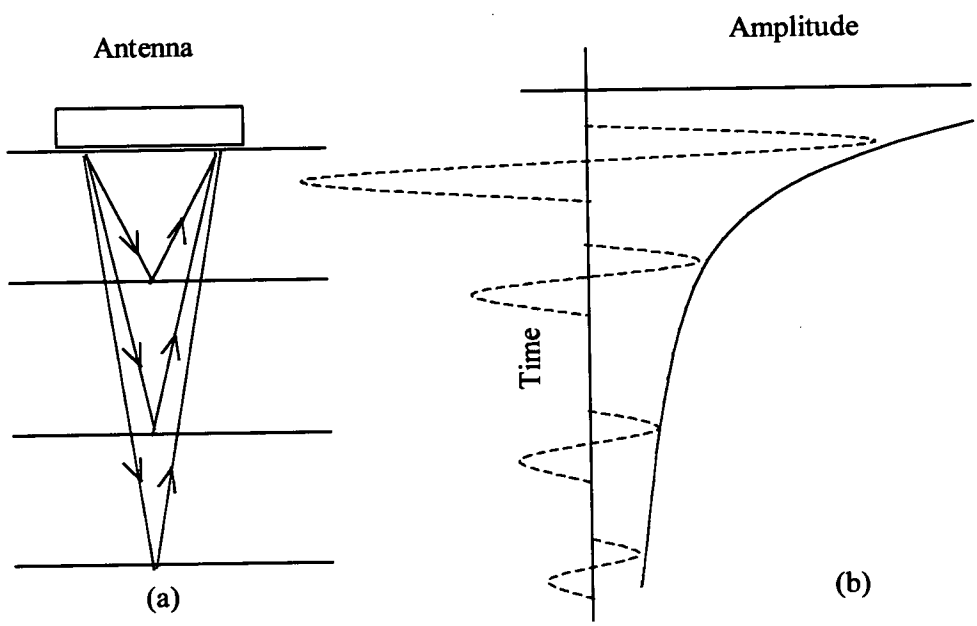

Figure 3.9: (a) An ideal model of a pavement with each layer having equal reflective horizons and impulse responses (b) The envelope of the reflection amplitude against time

In order to compensate for this a *time gain* is applied to the signal, which compensates for attenuation using a time dependent gain function. Various forms of time gain can be used to enhance the signal (Figure 3.10). It should be noted that the type of display device used will also play a factor in the amount of time gain applied.

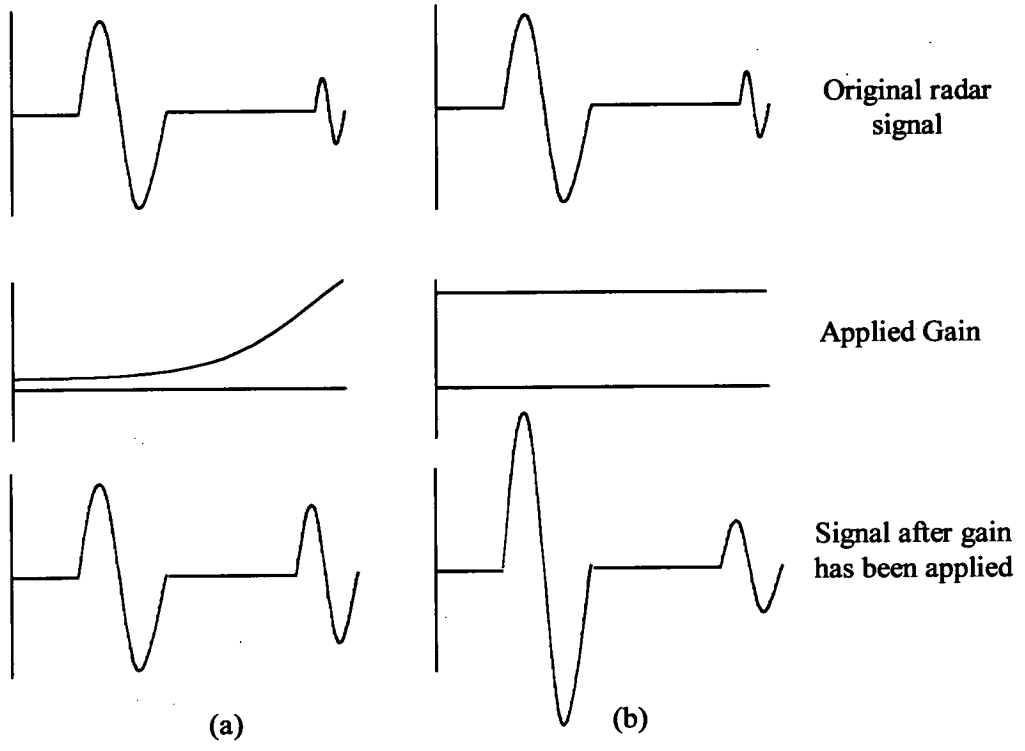

Figure 3.10: (a) Time varying gain where signal amplification varies with gain (b) Same gain applied across the whole signal

3.6 Graphical presentation of radar signals

There are three main formats used to present radar results. Deciding on which one to use is largely dependent on user preference.

3.6.1 O-scope

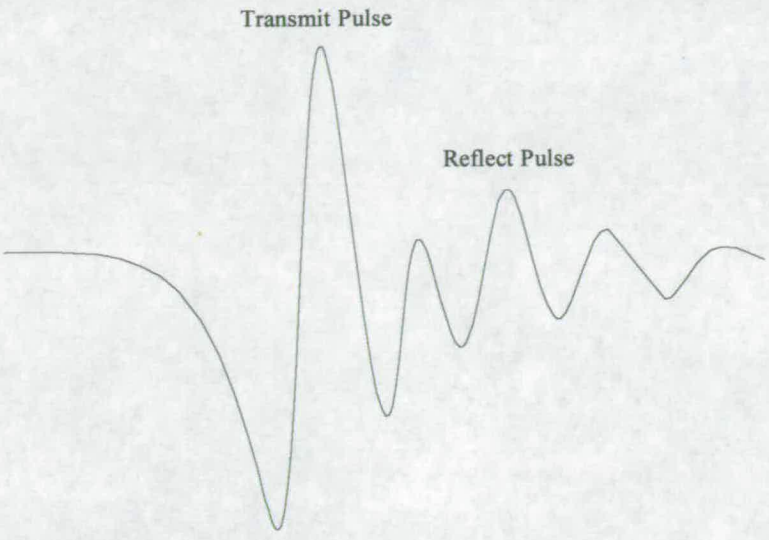

Figure 3.11: A typical radar O-scope plot

The oscilloscope or o-scope plot (Figure 3.11) shows a single scan line which contains the transmit pulse and reflection signals from the structure or object under investigation.

3.6.2 Wiggle plot

The wiggle plot is a sequence of radar o-scope plots, each plotted adjacent to the previous one. The space between them is defined by the user (Figure 3.12).

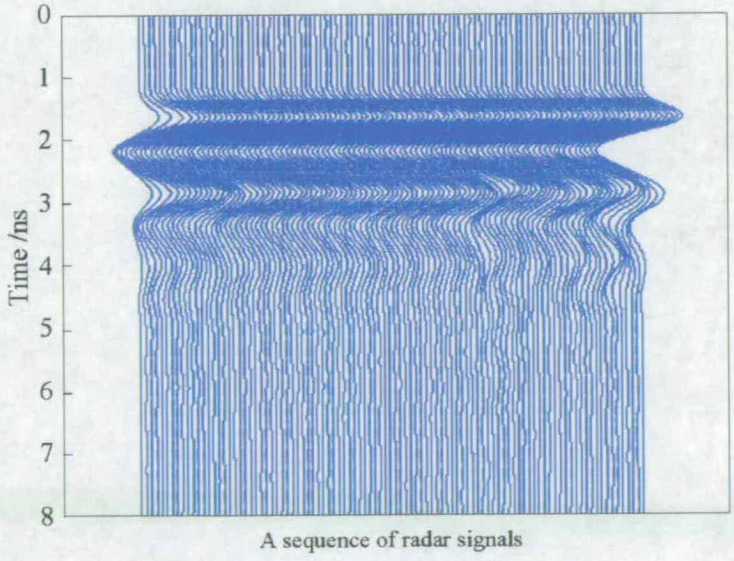

Figure 3.12: Wiggle plot

3.6.3 Radargram

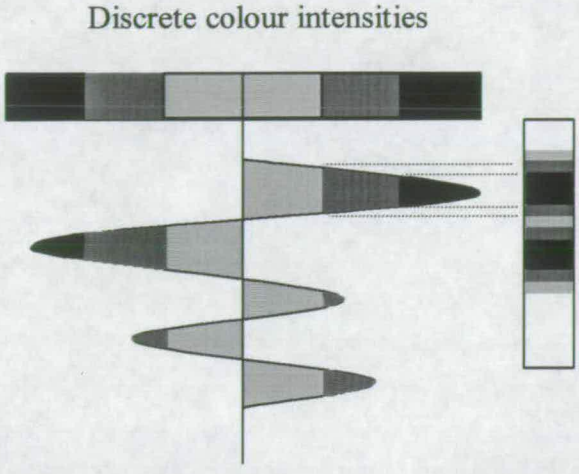

Figure 3.13: Grey scale presentation of radar signal (adapted from Bungey and Millard, 1993)

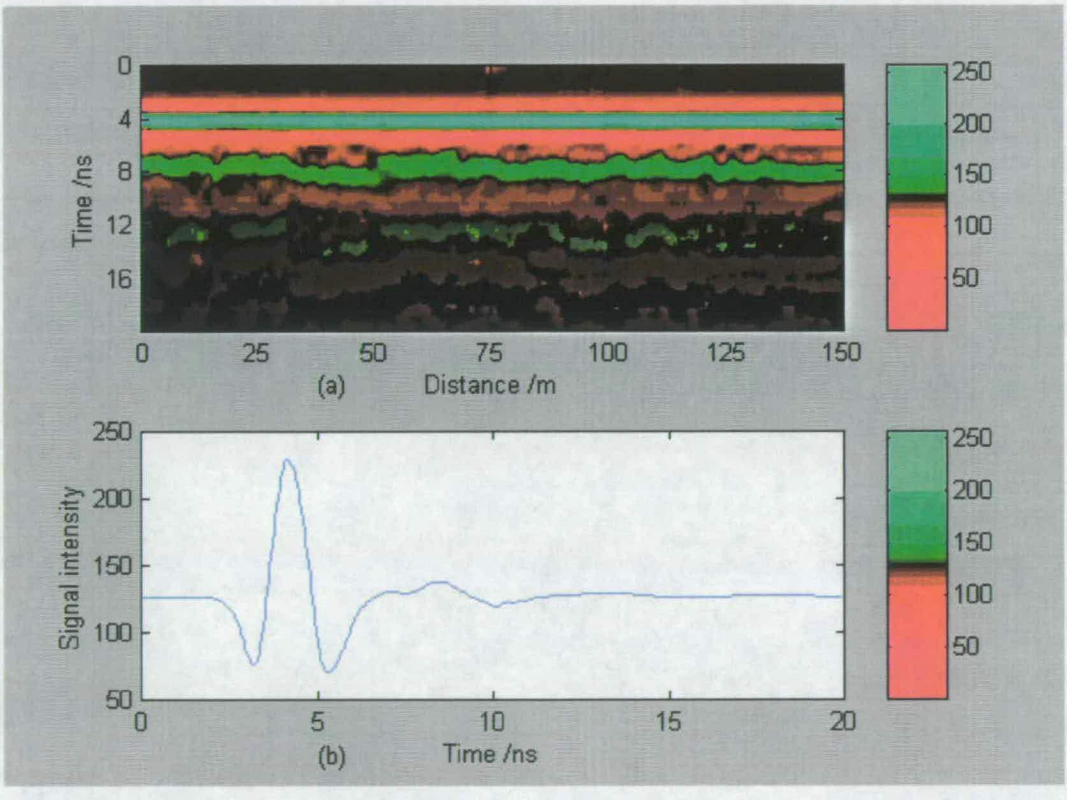

Figure 3.14: (a) Radargram format (b) O-scope format

The most common method used to display the radar signals is known as the radargram. This involves dividing each o-scope signal into discrete regions and assigning a certain colour intensity to each region, this is shown in Figure 3.13. Grey or colour scales can be used to display the image. Each successive o-scope plot is assigned colours until a composite colour plot is produced (Figure 3.14(a)). Further discussion of radargram plots can be found in Bungey and Millard (Bungey & Millard, 1993).

3.7 Enhancement of radar signal

The displayed information can be processed to help improve the interpretation of the results. Migration, event picking, gain enhancement and filtering are some of the many techniques available. Further information can be found in "Surface Penetrating radar" by Daniels, (Daniels, 1996B).

3.7.1 Signal processing

Signal processing is a very strong tool enabling information to be pulled out of a signal which is not apparent when viewing it in its original format. Two important techniques used in processing are Fast Fourier Transforms (FFT) and filtering. The mathematics used in FFT analysis can be found in Appendix B. A more detailed description can be found in many books such as Oppenheim (Oppenheim, 1978).

3.7.1.1 Filtering

Filtering of a signal is used to remove unwanted frequencies within a waveform. There are four main types of filters:

- *High pass filters* only allow frequencies above a given value to remain in the signal.
- *Low pass filters* only allow frequencies below a given value to remain in the signal.
- *Band pass filters* allow frequencies in a given range to remain, removing all outside that range.
- *Band stop filters* remove frequencies in a given range, allowing all outside that range to remain.

There are many different designs of filters within each of these groups, each having their own unique ability to clean the signal.

3.7.1.2 Problems in interpreting the signal

Signal Sampling

The rate at which a signal is sampled will determine how closely the discrete signal matches the original analogue one.

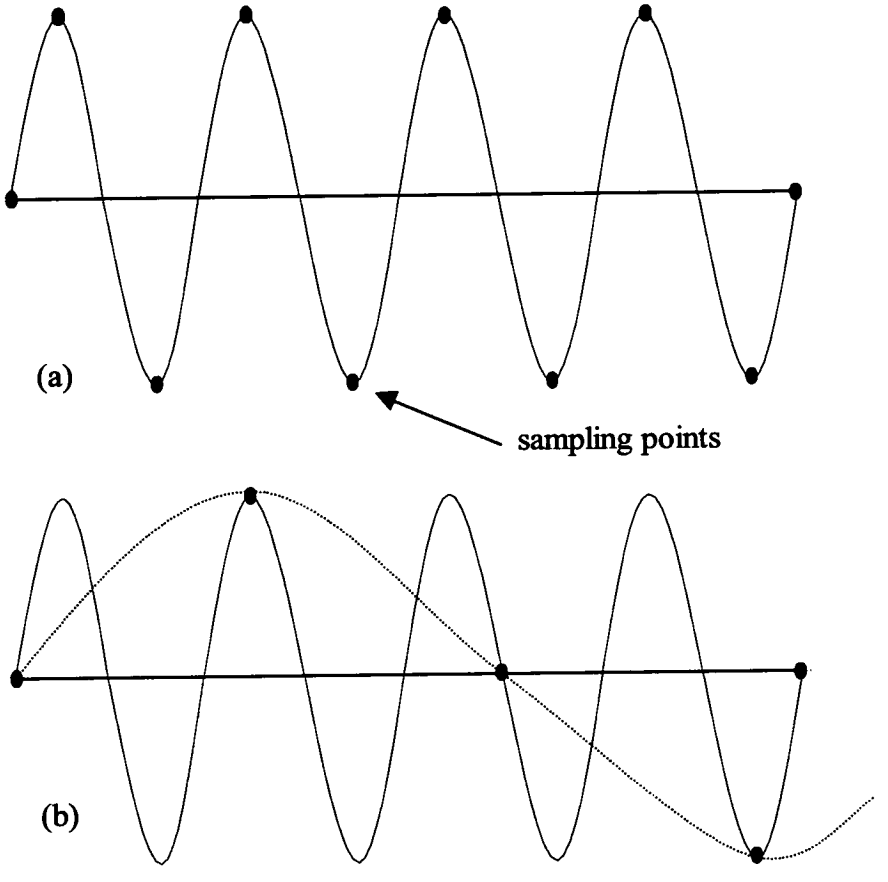

Figure 3.15: (a) Sufficient sampling of a high frequency signal (b) Insufficient sampling of a high frequency signal resulting in a low frequency alias

In order to prevent poor sampling of the signal the Nyquist sampling theorem is used. The definition of the Nyquist frequency is:

"The sampling rate must be at least twice the frequency of the highest frequency component of the waveform being sampled" (Ramirez, 1985).

Figure 3.15(b) shows the result of insufficient sampling of a high frequency signal, resulting in a low frequency alias.

Noise

Background noise can be another problem in interpreting the signal. Although it is a constant physical phenomenon caused by a multitude of sources, it can in some cases cause problems in analysing the signal (Figure 3.16). The use of some sort of digital filter can play an important role in eliminating these problems.

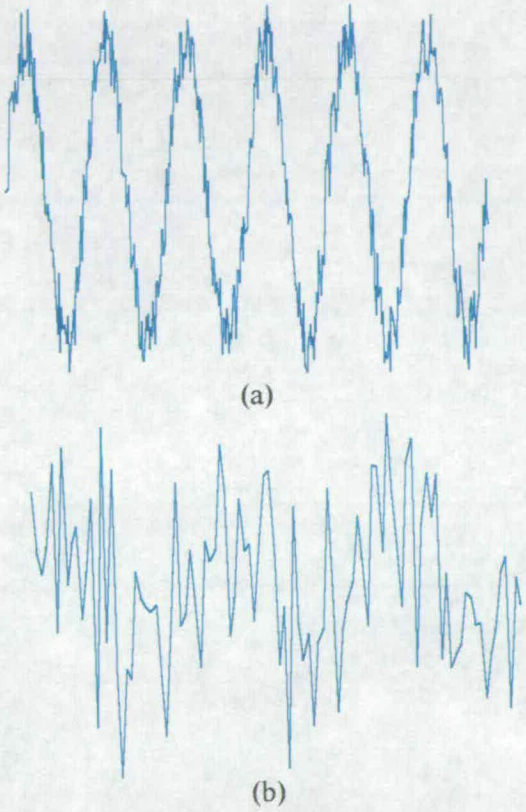

Figure 3.16: (a) Tolerable noise level (b) Intolerable noise level

Noise can also be caused by the conversion of an analogue signal to a digital signal. There are two major noise sources associated with this conversion process:

- Time jitter caused by the acquisition of the signal
- Quantising noise during digitising

Time jitter can occur when an analogue waveform activates a level trigger to gate the acquisition window. Noise on the signal can cause subsequent windows of this waveform, being triggered at a different point, resulting in horizontal instability of the waveform, which in turn can produce a rocking of the waveform on the screen. Prevention of this will only be achieved with careful design of the digitiser.

Quantising noise is caused by the error of approximation when signals are converted from analogue to digital. An example of this would be in using a converter which could resolve 100 levels along the range. Therefore, a 10 volt range will only be resolved to the nearest tenth of a volt. A voltage of 8.245volts will be rounded to 8.2volts by the computer, thus producing quantisation of the signal and effective noise of 0.045volts.

3.8 Review of recent GPR investigations on pavements

Weil (Weil, 1991, 1992A, 1992B, 1993A, 1993B, 1995) reports widely on the experience of using Infrared Thermography (IRT) and GPR to assess highway and airport pavements. IRT uses an infrared camera to detect changes in surface temperature that can be related to the presence of voids beneath the pavement, or delaminations within the pavement itself. The limitations of IRT are that whilst large areas can be covered quickly, it is not possible to gain accurate pictures of the depths or exact extents of voiding beneath, or cracking within, pavements. Whilst GPR is a slower technique to apply, as pavements must be scanned in many parallel lines, he does recognise its value in pinpointing problems and finding the true depth of voiding.

Weil recommends that IRT is used to direct the GPR surveys to particular areas where it can be used more efficiently to get a detailed picture of damaged areas.

Adcock *et al.* (Adcock *et al.*, 1995) report the use of GPR by the USA Air Force to detect significant variations in pavement thickness, voiding and water ingress as well as the thicknesses of surfaces on airfield pavements of both Portland Cement Concrete (PCC) and Asphalt Concrete (AC).

They developed a sophisticated vehicle with GSSI 2.5GHz horn antennas mounted at the front and 900MHz "bowtie" antennas at the rear. The aim was to use the 2.5GHz antennas to give accurate information about the dielectric constant of the surface material. This was

calculated by measuring the amplitude of the reflected pulse from the pavement and comparing with the amplitude of the pulse reflected from a steel plate. As the reflected field strength is related to the incident strength by the reflection coefficient

$$r = \frac{\sqrt{\varepsilon_2} - \sqrt{\varepsilon_1}}{\sqrt{\varepsilon_2} + \sqrt{\varepsilon_1}} \quad \text{(equation 3.10)}$$

where ε_1 is the permittivity of the medium through which the pulse is travelling when it meets an interface with a material of permittivity ε_2.

The high frequency pulse was not suitable for penetrating through the PCC or AC top layer, so the 900MHz antennas were used to measure the time for the reflection from the bottom of these layers. The knowledge of the permittivity of the material from the reflection coefficient allows the travel times for the 900MHz pulse to be translated back into a layer depth. Their system was intended to be fully automated, but they found it difficult to ensure that an automated system could find all the correct peaks in the signals for the data analysis and therefore some manual intervention was required. However, with this intervention, layer depths could be found with accuracies of ±5%.

Heiler *et al.* (Heiler *et al.*, 1995) have tackled the problem of automatic detection of asphalt thickness and depth to reinforcement in composite pavements using neural networks. The networks were trained to recognise the quality of the data presented to them and to locate the reflections from the three features required. Different networks were used for the quality testing and the location, but the location network has 124 input points and 3 analogue outputs with one per feature required.

The results were quite promising with the networks identifying the rogue data sets, but also identifying between 5 and 20% of the correct data sets as defective. It is pointed out by the authors that this conservatism by the networks is at least on the safe side.

For good data sets the location of the features was very accurate. It is clear that huge amounts of accurate data are required to train the networks before they can be of any use and that accurate and good quality radar data is required if there are to be consistent, good results.

The use of neural networks in this context is quite encouraging if characteristic responses within the radar signal are easily identifiable. Unfortunately, what is being looked for in the radar trace is often quite difficult to predict in advance of seeing it, and there is a long way to go before such networks can replace the eye of an experienced operator.

Daniels' book, "Surface Penetrating Radar" (Daniels, 1996B), contains many case studies including reports from Wilkinson, of Durham County Council, UK and Caiou, Côte and Derobert of the *Laboratoires des Ponts et Chausées* (LPC) in France on the application of GPR to pavement investigation.

Wilkinson reports that GPR can be used to determine thicknesses of bituminous or concrete pavements, spacing and location of reinforcement and dowels, cracking and, if there is not too much reinforcement in concrete pavements, the position of cracks and voids beneath the pavements. This can be carried out more efficiently than by the traditional methods of coring. Surveys can even be carried out at highway speed with sufficient accuracy. He does report that a survey of operators in the UK were not able to agree on the materials of construction of older roads where the pavement had been developed in a piecemeal fashion. As perhaps 80% of the UK's roads fall into this category this is one area where there may be room for development.

The team from the LPC report on their experience of using a 700MHz centre-frequency system and confirm that it can only resolve layers of 5cm or greater, and that the accuracy is approximately 8%. This work was carried out in the '80s and since then they have investigated the use of synthetic-pulse radar. They are encouraged by their initial findings and suggest that it can penetrate further into the road than the amplitude modulated pulse system by a factor of 1.5 or more.

Mesher *et al.* (Mesher *et al.*, 1995) have developed the Road Radar with the specific objective of identifying and quantifying pavement layer thicknesses. Rather than use the amplitude of reflected waves to determine the permittivity of layers, they use a multiple antenna array to evaluate it. This is because the amplitude of a pulse reflected by a material interface is prone to changes in its amplitude due to other factors apart from the reflectivity of the interface. These factors include the height of the antenna above the road, which is difficult to maintain constant at high speed, and the rough surface of the pavement scatters

the incident pulse rather than reflecting it neatly. The set-up of their multiple antenna array is shown in Figure 3.17.

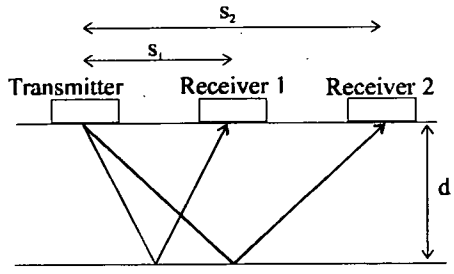

Figure 3.17: Multiple receiver bistatic antenna array

The change in the travel time as the pulse travels along different path lengths can be used to determine the layer thicknesses.

Along with this system, they have developed sophisticated software incorporating artificial intelligence, time-domain signal processing, neural networks and pattern recognition techniques. The software will still defer to the operator if it encounters changes in construction which it is not happy to analyse. Once the operator has intervened the software can take over once more.

They present several field studies and the results are very encouraging for resolving layer thicknesses from 50mm to 2m. They suggest, however, that the precise determination of the velocity in the material might be strongly correlated to the pavement density or water content.

As the water content is probably the most influential factor influencing the wave speed through the material it is likely that this might be determined from the velocity. The dielectric constant of water is 81 and for most dry material, it is less than 10. The effective dielectric constant of a wet material is considerably higher than in its dry state, even when the water content is only a small percentage by volume.

The velocities measured on three pavements varied between 120 and 148 mm/ns although the average values at the three pavements were 126, 129 and 130 mm/ns. These velocities match those in Table 3.1 well, but the spread of velocities at each site was 120-143, 125-133 and 121-148mm/ns which indicates that using a single core at a site as a calibration for the radar survey is likely to lead to errors of the order of 10% or so.

Maser (Maser, 1996) presents a review of the use of GPR for evaluation of pavements, bridge decks, bridge piers and geotechnical applications. He compares contact bowtie antenna technology and non-contact horn antennas. He also suggests that the amplitude of the reflection of the pulse can be used to determine the permittivity, and hence wave-speed of each layer in a pavement, and that it is possible to make suitable measurements at highway speed. Asphalt layers as thin as 5cm can be detected with a 1GHz horn antenna. The accuracy achieved for asphalt layer thicknesses has been ±7.5% and for the base layers is ±12%. Success with concrete pavements has not been so good due to the poor penetration of the pulse through the concrete because:

- Similar dielectric properties of concrete with the granular base material it is placed on making it more difficult to pick up the reflection from the concrete/base layer interface.
- The water and dissolved salts content of the concrete cause more electromagnetic attenuation compared to asphalt.

A hybrid horn/coupled antenna system is suggested to improve the penetration whilst maintaining the calculation of the wave speed by examination of the reflection of the pulse from the concrete surface.

Maser (Maser, 1986, 1991, 1993, 1994), Maser and Roddis (Maser and Roddis, 1990) and Maser *et al.* (Maser *et al.*, 1995) present field studies from New Hampshire, Germany, Texas and Kansas on which Maser bases his paper discussed above.

Maser and Kande (Maser and Kande, 1999) discuss the use of GPR for detecting damage under airfield pavements. Two airfields were surveyed using 1GHz horn antennas in order to detect delaminations, the presence of large air voids and stripping within the asphalt layers.

A series of longitudinal passes, typically 1m apart, were carried out along certain areas prone to damage. The calibration of the GPR results was achieved by examining the dielectric contrast between surface and sub-surface areas where damage is known to have occurred. These results were represented on a colour plan view (colour levels were used to represent the amount of dielectric contrast), with more intense colour indicating a higher probability of sub-surface damage. Subsequent cores taken from areas on the maps which showed a high probability of damage were found to have some sort of damage.

Failure to carry out surveys on the sub-surface layers within airfields can lead to catastrophic results due to the high volume of traffic experienced by airports.

Ballard has investigated some experimental sections of road that have been cored for comparison (Ballard, 1993). He identifies significant variations in pavement thickness along the length of each pavement investigated (up to 30mm or 10% of the pavement thickness) and suggests that these might have a significant effect on the life of the pavements involved. As the pavement stiffness is, to a first order according to simple plate bending theory, proportional to the thickness to the third power, he is undoubtedly correct. GPR provides a much better tool for investigating the quality of new pavements or overlays than other methods as it can give spatial resolution along the road much more precisely than even the most extensive, and hence destructive, coring surveys.

Hobbs *et al.* (Hobbs *et al.*, 1993) review the advantages of the GPR technique for surveying structures in general and the specific costs of maintaining the highway infrastructure in the UK and USA. They cite the difficult-to-interpret nature of GPR traces as one reason why GPR is not more widely used and suggest that the techniques used for ultrasonic signal analysis might be useful for reduction of GPR images. It is also shown by illustration that GPR images can be more amenable than their ultrasonic counterparts in certain circumstances. Ultrasonic testing of road pavements has not met with much success as the short wavelengths involved are diffracted by all the small inhomogeneities of the materials involved. This leads to rapid attenuation of the travelling wave and significant "clutter" of the received signal.

Uddin and Hudson (Uddin and Hudson, 1994) are interested in detecting voids beneath concrete pavements. They state that half of these can be found by visual inspection when looking for pumped material. Deflection measurements have been tried but are not reliable indicators because of variable slab-to-slab joint conditions and lifting of slab edges due to temperature effects.

They report the use of two different GPR systems. RODAR is a vehicle-mounted, non-contact system that can carry out surveys at 10mph. Donahue's Remote Sensing Van uses a combination of IRT and GPR. High frequency transducers are used to give good resolution although the paper does not give much detail of the systems involved.

Several case studies are taken from the literature and it is concluded that GPR is a promising tool for this purpose, but that improvements need to be made to the analysis of the results and presentation to the end user.

Hugenschmidt *et al.* (Hugenschmidt *et al.*, 1998) carried out radar surveys in Switzerland. GPR was used to investigate delaminations occurring between the layers, and to detect porous zones (mainly filled with water) and surface cracking. Coring and a visual survey had been carried out before the survey was undertaken, this would be used to help calibrate the radar results. A pair of 2.5GHz and one 900MHz antenna were used with a GSSI Sir10a. Using the cores enabled the radar wave velocity through the asphalt pavement to be calculated, which was used to convert the time values on the radar plots to depth measurements (It was assumed that the wearing course and basecourse had the same velocity value).

Low intensity reflections from the asphalt pavement base were observed on certain parts along the pavement where road surface damage was visible. They believed the reason for the change in the signal intensity was due to saline water getting into the cracks. This was backed up by the de-icing program that had been applied to the stretch of road during the months before the survey. However, in certain other parts of the pavement, the change in the reflection pattern was due to actual changes in the construction of the pavement. Hugenschmidt noted the importance of co-operation between the geophysicists and road engineers in interpreting the data. Additional resources like structural and material data resulted in the correct interpretation being achieved in this project.

Attoh-Okine (Attoh-Okine, 1996) compares the cost of a GPR survey from a vehicle in the traffic stream with a traditional coring survey, with cores at either 20 per mile or 2 per mile depending on the purpose of the survey. He developed a cost model for each method and then compared them. This study showed that the GPR survey would be between 2 and 3.5 times cheaper than coring, although there is very little data to back these figures up.

This brief survey of recent literature highlights the possible benefits of using GPR for pavement thickness evaluation, such as rapid and cheap surveys with more detail than is possible by other methods, but also reveals the engineer's frustration at the amount of manual intervention that is required to analyse the masses of data that can be collected. The use of advanced processing systems has not yet alleviated this problem.

Two methods for determining the permittivity of the pavement materials are found. Either the amplitude of the reflected pulse can be used or a multiple antenna bistatic array can be used. Both methods appear to have been successful.

3.9 Current and future developments

Maser (Maser, 1996) looks at future developments including the stepped frequency and synthetic aperture radar.

Stepped frequency radar can be explained by examining the Fourier decomposition of the desired pulse that is transmitted by the antenna. As the pulse is sent repeatedly, at a pulse repetition rate, T, then the pulse can be synthesised by the summation of a set of scaled and appropriately phased sine waves with frequencies i/T Hz, where i=1,2,3... . If each of these component sine waves is transmitted in turn, the response to the pulse can be determined by the inverse Fourier transform (IFT) of the scaled and phase-corrected responses.

This method gives great control over the effective shape of the transmitted pulse and an increase in the power that can be transmitted, hence improving the penetration. The cost of this is that the signals take longer to transmit as many frequencies must be transmitted and the results must be recombined before a picture is produced.

The synthetic aperture radar involves use of an array of antennas (or a single moving one) that can together provide data that resolves the shape and depth of targets with much greater accuracy than a single antenna can on its own. Again, there is a cost in the data processing associated with this method.

Both of these methods are explained in more detail by Daniels (Daniels, 1996A,1996B). Further signal processing developments are also discussed including the possibility of Wavelet analysis to enhance images.

Weedon *et al.* (Weedon *et al.*, 1994) explain the development of a stepped frequency radar system with a switched antenna array designed specifically to resolve images at a range of 40cm. A 2D Finite Difference Time Domain simulation is used to try to reconstruct the true image from the radar image by iteratively modifying the simulation model until its output matches the measured image. They meet with some success, but are limited to locating 2D images such as straight bars and only attempted the procedure with the bars in the optimum

position for the antenna array. These limitations mean that this technique cannot be applied directly to highway pavements, but the extension to 3D and the use of planar, rather than focused arrays would not seem to be insurmountable extensions to this work.

Langman and Inggs (Langman and Inggs, 1994) describe the theory and development of a stepped frequency radar system and describe the Extended Prony Method as an alternative to the IFT for getting enhanced spatial resolution. The results are convincing both in simulation and experiment but there is no mention of the processing time cost which would appear to be considerable.

Warhus *et al.* (Warhus *et al.*, 1994) describe in detail the design requirements for a GPR system with a single transmitter, but an array of receivers spanning the pavement surface particularly for RC bridge decks. Images of the deck are reconstructed using the techniques for synthetic aperture radar processing as described by Daniels (Daniels, 1996B).

Mast and Johansson (Mast and Johansson, 1994) explain their 3-dimensional reconstruction of a test specimen of reinforced concrete using a synthesised aperture technique. Their antenna had a bandwidth from 0.5-3.5GHz and the 3D rendered image is very impressive. The downside of this is the quantity of data that has to be collected to produce the images, but with the cost of the hardware reducing all the time it may well be possible to produce a similar technique for scanning highways in the future using arrays of antennas in parallel, or maybe as described by Warhus *et al.* (Warhus *et al.*, 1994).

Johansson and Mast (Johansson and Mast, 1994) present an alternative method for producing 3D images. The data acquisition required is the same but the analysis procedure is very different and is more akin to a deconvolution and migration of the data in three dimensions. Whilst the results of this analysis do not look as good as those from the previous technique (Mast and Johansson, 1994), the authors point out that the computational effort is much reduced and that this method will become more attractive as the number of strata involved in the analysis increase.

Nelson (Nelson, 1994) reports on the 3D modelling efforts for simulating GPR with Finite Difference Time Domain simulation at the Lawrence Livermore National Laboratory.

The concrete is modelled as a 2-phase random mixture with the aggregate having different electromagnetic properties to the cement matrix. The simulations are compared with real

measurements under fairly ideal conditions in an anechoic laboratory. These prove to be a good match. The conclusions are that the precise modelling of the aggregate-cement mix is important if the simulation is to work as the scattering, diffracting and shadowing effects of the particles are significant.

Gros *et al.* (Gros, *et al.*, 1994, 1995A, 1995B) and Edwards *et al.*(Edwards *et al.*, 1993) have brought the concept of data fusion into NDT. Data fusion is the simultaneous analysis of the results of different sensors, not necessarily even the same type of sensor, to give an improved image of the object under investigation. A simple example is the fusion of many readings of a GPR record by averaging in order to reduce background noise effects and improve the image. More sophisticated techniques are illustrated by different sensors that detect aircraft by scanning the skies in a crude and rough way. A second set of sensors can identify the aircraft, and a third set will give its speed and direction.

There are several mathematical techniques available for bringing together the information from different sensors, such as IRT and GPR data with different antenna. These include statistical ensemble averaging, Baysian inference methods, the Dempster-Shafer theory of evidence, fuzzy logic and neural networks.

Gros (Gros, 1997) implements Baysian and Dempster-Shafer fusion theory to bring together eddy current surveys (which give a surface profile of defects), ultrasonic surveys (which give cross-sectional profiles of defects), and X-ray radiographic surveys (giving through depth images) of weld cracks. He concludes that the Dempster-Shafer extension of the Baysian theory gives better answers.

3.10 Sonic testing of pavements

3.10.1 Impact-echo applied to thin pavements

Impact-echo is an acoustic, non-destructive method used to evaluate the conditions of a wide range of structures. The principal inventors of impact-echo were Sansalone and Carino (Sansalone, 1997), who developed the technique in the 80s to test concrete and masonry structures for structural damage like delaminations, voids and cracks (Sansalone and Carino, 1988,1989).

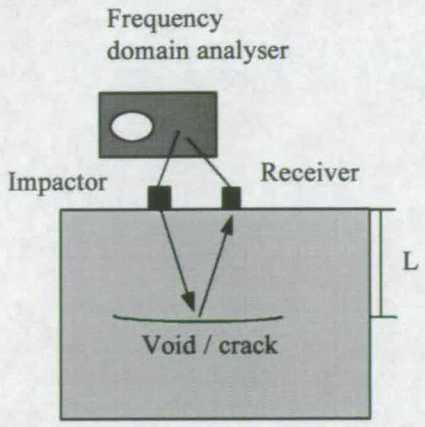

Figure 3.18: Impact echo test method

The theory behind impact-echo is that when a test object is tapped with a small steel ball (impactor), a transient stress wave is produced which propagates through the medium (Figure 3.18). This stress pulse, which propagates into the material as a spherical wave front, is made up of primary/pressure (P-waves) and secondary/shear (S-waves) waves. The faster P-waves move under compression (longitudinal) motion, whereas the slower S-waves move under shear (transverse) motion perpendicular to the direction the wave is travelling. It should be noted that a Raleigh wave (R-wave) travels along the surface of the material, away from the impact source.

Reflections of these P and S-waves occur at the bottom of the material or at a crack within the material, i.e. where there is a sudden change in acoustic properties. When the reflected waves reach the surface, they experience a major acoustic change, due to the air/material interface, so that the wave will be reflected back into the material. This will occur several times until all the energy has been dissipated. These oscillations produce displacements at the surface of the material, which will be detected by a receiver (accelerometer) several centimetres away from the impact point.

The major advantage of this non-destructive test method is that only one surface needs to be accessible for the impactor and receiver attachment.

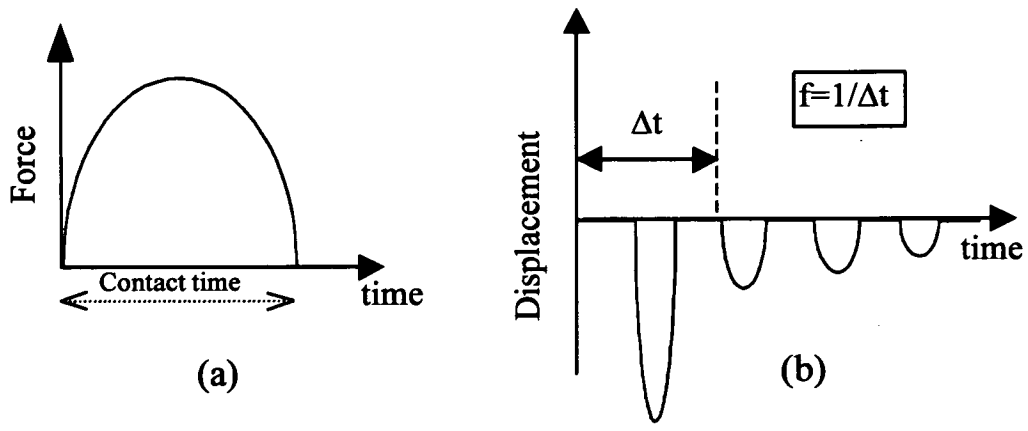

Figure 3.19: (a) Force-time graph showing the contact time of the impact (b) Ideal displacement response obtained by the receiver

The impact on the surface of the material is approximated to a half sine wave as shown on the force vs. time diagram in Figure 3.19 (a). The duration of this wave is known as the *contact time*, reduction of this time results in smaller defects being detected, although, the energy and the penetration capability of the waves are reduced. Therefore, the selection of the impact source is very important when carrying out these tests.

When the stress wave encounters an interface, at depth L, it is reflected and gives rise to surface excitation frequency, which is detected by a receiver (displacement transducer or accelerometer). Figure 3.19(b) shows the idealised response of this surface excitation.

The surface excitation frequency is related to the velocity of the wave, V_P, by:

$$f = \frac{V_P}{2L} \qquad (3.12)$$

The travel path, L, is the thickness of the material or the distance to the anomaly, as shown in Figure 3.18.

A laser vibrometer can be used instead of an accelerometer due to its ability to operate without any contact on the material being tested, however, these devices are very expensive. A laser light is shone onto the material and measures the displacement of the surface caused by the impactor.

Koehler *et al.* (Koehler *et al.*, 1997) have used a scanning laser vibrometers to detect the response from concrete specimens which were being examined by ultrasound. The researchers had to overcome the high signal to noise ratio due to the roughness of the concrete, this was achieved by using a random speckle modulation technique. This technique changes the focus of the laser by a small amount while observing the interferometer signal amplitude. The ultrasonic measurement can be taken when the interferometer noise is low. Further developments are continuing in this area to increase the processing speed of this technique.

3.10.2 Ultrasonic analysis of pavements

The same theory used to explain how waves travel through material using the impact-echo method is applied to ultrasonic theory. The measurement of ultrasonic velocities depends upon generating a dynamic pressure wave (pulse) into a material of known thickness and measuring the transit time of the emerging acoustic pressure wave.

The whole object can be scanned to produce A-scans, B-scans and C-scans. A-scans shows the signal amplitude on the y-axis and the time of the signal on the x-axis. It is similar to the 0-scope plots shown in section 3.6.1. The depth to anomalies can be determined directly from this information. B-scans are like the radargram plots shown in section 3.6.3, where the depth information is obtained by associating colour or grey scales to the associated amplitude of the received signals in a two dimensional plot. C-scans are two dimensional images which show a particular depth range as a plan view of the object being examined (Figure 3.20).

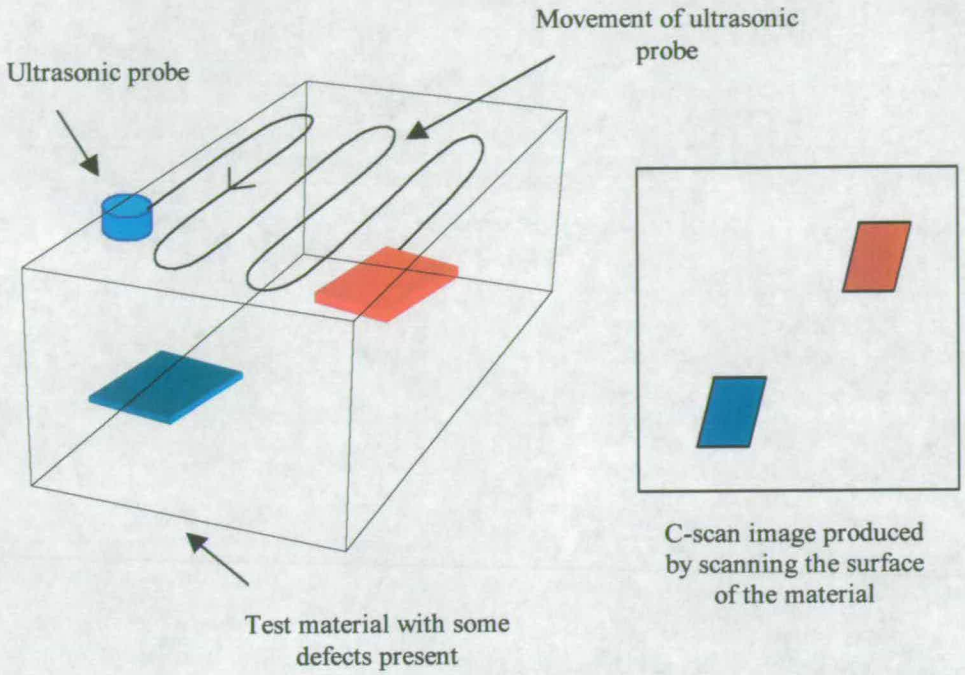

Figure 3.20: Example showing how a C-scan is produced

The generation and detection of an acoustic wave is usually accomplished by a piezoelectric transducer. This piezoelectric ceramic material, within the transducer, can convert electrical into acoustic energy, and vice versa. Therefore, electrical signals, which are converted into mechanical vibrations and transmitted into the element, can be detected by a receiver which converts the mechanical vibrations back into an electrical signal. The orientation of the piezoelectric transducer with respect to the surface of the material is important. The angular tolerance is usually a few degrees so good coupling is essential in these circumstances. In certain strongly curved surfaces, acoustic lenses are used to insure proper coupling.

The behaviour of the transducer is governed by several factors:

- Piezoelectric material used in the transducer
- Mechanical and electrical construction
- External mechanical and electrical load conditions

Excessive ringing of the piezoelectric element after the initial excitation can be a major problem, however, significant improvements in using mechanically coupled damping materials has reduced this factor.

An impedance matching coupling medium (water, oil or grease) is essentially to enable the transducer to be acoustically bonded to the material being tested. Djordjevic and Green (Djordjevic and Green, 1994) noted that the coupling medium can cause large transmit time errors due to the partial transmission and reflection of the ultrasonic energy causing changes in the shape of the transmitted waveform. These result in errors in thickness and velocity calculations.

Djordjevic and Green (Djordjevic and Green, 1994) reviewed non-contact ultrasonic transducers used in examining composite fabrics. There are several non-contact methods for generation and detection of ultrasound. These include:

- Capacitive pick-ups
- Electromagnetic acoustic transducers (EMAT's)
- Laser beam optical generators and detector
- Air-couple ultrasonic systems

The laser ultrasonic system has a marked improvement over the others. The general principle behind the laser ultrasonic system is that a laser pulse strikes the surface of the material being tested. Vaporisation or ablation of the surface occurs, causing a longitudinal wave to propagate, perpendicular to the surface, into the material. Reflections will be produced at the bottom of the material or from flaws within it; these propagate back to the surface and cause a small amount of displacement (ranging from one tenth of a nanometer to a few nanometers). A second laser illuminates this area where the motion has occurred. The pulse duration of this laser should be at least 10μs.

The ultrasonic surface motion causes a small phase shift or frequency shift in the scattered light (Doppler effect), which can be detected using a interferometric system. These systems use wave interference to make precise measurements of length of displacements in terms of wavelengths.

3.10.3 Calculating the velocity of the ultrasonic wave

The velocity of the ultrasonic wave, travelling through a material, is dependent on the density and elastic properties of that material. The longitudinal velocity (V_L) can be found from:

$$V_L = \sqrt{\frac{E}{\rho}} \tag{3.13}$$

where: E = Young's modulus (N/m^2)

ρ = Mass density (kg/m^3)

The frequency range of ultrasonic transducers can vary between 20kHz and 400MHz. However, the typical frequencies range from 50kHz to 300kHz when investigating homogenous materials.

3.10.4 Seismic pavement analyser

Researchers in Texas have produced a portable device which can apply impact-echo and ultrasonic methods to pavements. Yuan *et al.* (Yuan *et al.*, 1997, 1998) have designed a seismic pavement analyser (SPA) at the University of Texas, El Paso. The SPA is a trailer-mounted device used to measure different pavement properties to a depth of 2m. Using the variation in moduli as a function of the deterioration of a pavement they have used the trailer to monitor the condition of pavements.

This device carries out five different non-destructive tests:

- Impulse response method (IR)
- Ultrasonic compression wave velocity measurement (UCW)
- Impact echo measurements (IE)
- Spectral analysis of surface waves (SASW)
- Ultrasonic surface wave method (USW)

A computer is used to lower transducers and sources to the pavement when the trailer is stationary. These devices measure the response induced by a large and small pneumatic

hammer which produce low and high frequencies respectively. A complete testing cycle takes about one minute, enabling the modulus and thickness of each layer to be found as well as Poisson's ratio and the temperature of the top layer.

The researchers compared their measured values to those obtained from direct seismic measurements made on the top of each layer to evaluate the accuracy of the device. They found that their results correlated well with the direct tests. They did indicate that further developments to optimise the location and spacing of the sensors should be implemented so that the variation in modulus can be further exaggerated. They suggested that this could be achieved by placing the sensors closer together or perpendicular to the traffic flow. They also suggest looking at the quantitative relationship between the FWD and the SPA.

A portable version of the SPA has also been developed known as the PSPA (Anon, 1999B). This is a hand-held device which provides measurements on the top layer due to it having only a high frequency source and two accelerometers.

Further discussion of sonic testing for evaluating the in-situ properties of pavements can be found in Popovics and Popovics, (Popovics and Popovics, 1998).

3.11 Conclusions

The range of techniques available to highway engineers for the assessment of pavement condition are many and varied. The simultaneous analysis of the information from different systems would greatly enhance the reliability of the interpretation, and even extend interpretation into areas not yet envisaged.

The developments of new radar hardware such as stepped-frequency radar, improved horn and array antennas, signal processing techniques such as synthetic aperture radar, the accurate three-dimensional simulation of these techniques for improved understanding and training of neural networks. Also the techniques of data fusion to bring together many sources of information in a rational and quantifiable way seem to spell an exciting and rapidly developing improvement in the use of GPR in many fields, including highway pavement assessment.

The use of laser technology to acquire information on the elastic properties of the pavement material as well as its layer thicknesses is a potential area for development in Impact Testing of pavements.

Chapter 4

Preliminary non-destructive testing experiments on thin flexible pavements

4. Introduction

This chapter investigates the advances that can be made in the use of existing GPR technology in the field of thin pavement investigation. The accuracy of the technique and the difficulties in trying to interpret the recorded signals are discussed. The "impulse echo" method, which uses sonic rather than electromagnetic waves to detect the interfaces of materials and locate voids or delaminations within the pavement, is also discussed.

The first set of experiments examines how effectively GPR can be used to measure thin pavements (thickness < 0.2m) and whether changing the material beneath the thin layer has any effect on the initial response from the surface. The final experiments look at the use of sonic techniques in detecting layer thicknesses.

4.1 Impulse radar of thin pavements

Thin pavements (thicknesses < 200mm) create particular problems for GPR as the wavelength of a 1GHz radar pulse is in the range 90-210mm depending on the velocity (see Table 3.1). In the radar image, the response from the underside of the pavement can not be seen clearly. This is due to difficulty in resolving the individual constituents of the radar signal, which can include the initial impulse, signal leakage from the transmitter to the receiver, reflections from the pavement surface itself and then reflections from the first interface. This is illustrated in Figure 4.1, which shows a GPR survey over a section of pavement.

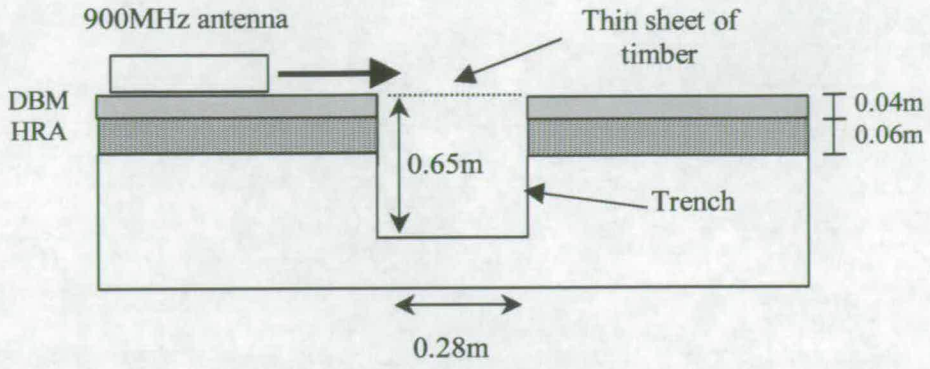

(a)

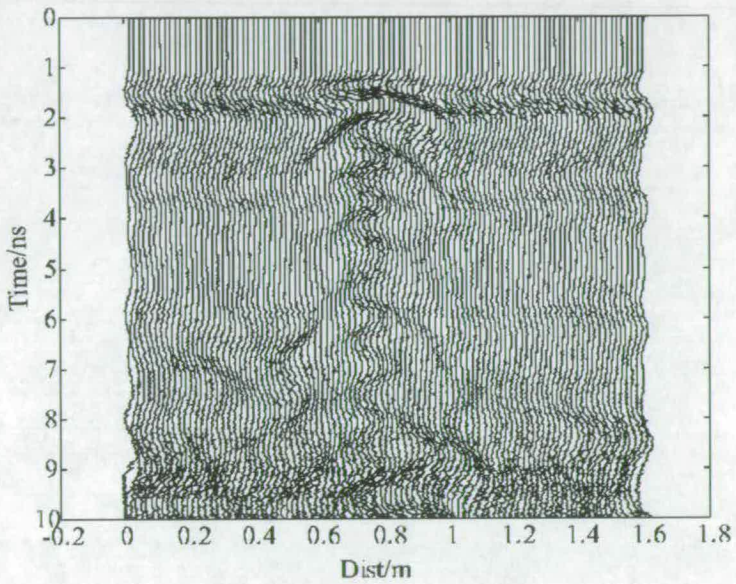

(b)

Figure 4.1: (a) Cross-sectional view of pavement (b) A wiggle plot showing the response from a 900MHz antennas as it is pulled over a thin pavement with the surface removed at the middle section

The radar registered the air-gap in the pavement when the antenna was drawn across it (Figure 4.1). The radar response changes at this point because the pulse travels faster through air than the pavement materials. The antenna will detect the closest point to it as it travels over the trench. Therefore when the antenna is over the middle of the trench, the

reflection centred around 3ns is from the sides of the trench which are 0.14m away from the antenna and not the base of the trench, which is 0.65m from the antenna.

The radar data on either side of the trench shows a reflection centred about 4ns (Figure 4.2), i.e. approximately 1.8ns from the transmit pulse (2ns reflection). The radar velocity in asphalt can vary between 0.09 and 0.21m/ns (see Table 3.10). The reflection at the bottom of the Hot Rolled Asphalt (HRA) layer should appear between 1.0 and 2.2 ns from the start of the transmit pulse (depending on the velocity value). However, the antenna is unable to distinguish the bottom of the Dense Bitumen Macadam (DBM) layer which would appear between approximately 0.9 and 0.4ns (depending on the velocity) from the start of the transmit pulse. This time range is within the initial surface reflection/direct transmission time of this antenna. A higher frequency antenna could detect this thin layer but this was not available to the researcher at the time. However, a higher frequency antenna would run into the same problems if applied to even thinner pavements. Chapter 7 examines this area in more detail in order to determine the minimum pavement thicknesses that different frequency antennas can measure.

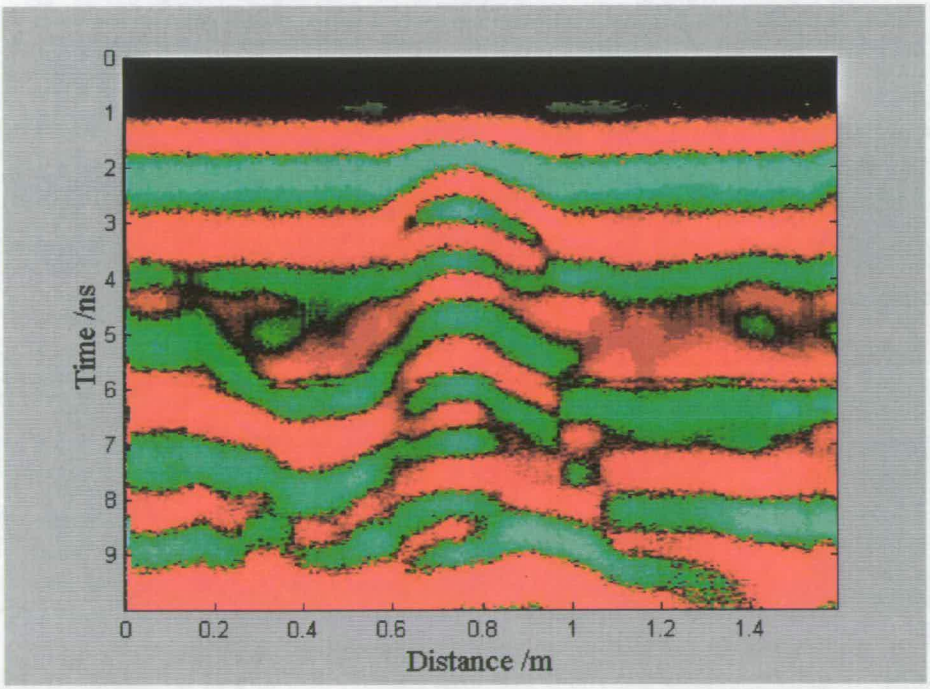

Figure 4.2: This is the same as Figure 4.1, however, it is displayed as a radargram

4.1.1 GPR investigation of thin asphalt slabs

The surface slab that had been removed from the road scan was removed to the laboratory for further investigation. Details of the slab geometry are shown in Figure 4.3.

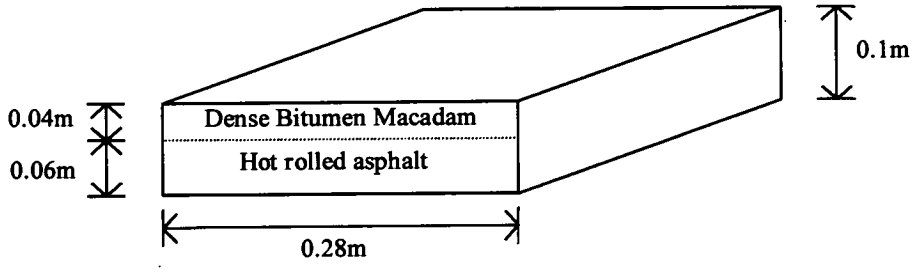

Figure 4.3: Thickness detail of the pavement slab

An initial investigation was carried out to find the precise speed of the radar pulse through the slab. The pavement slab was placed on its side and passed between two 900 MHz antennas, which were also on their sides. The antennas were 0.105m apart, in order for the piece of pavement to fit between them. The velocity of the radar pulse through the slab is given by:

$$\text{Velocity of radar pulse (v)} = \frac{c}{\sqrt{\varepsilon_r}} \text{ m/ns} \qquad (4.1)$$

where: c = velocity of light in a vacuum ($\approx$ 0.3m/ns)

ε_r = relative permittivity

Pulses were transmitted from one antenna to the other with the slab in position, and also with the slab removed so that the pulse only travelled through the air. The received pulses are shown in Figure 4.4.

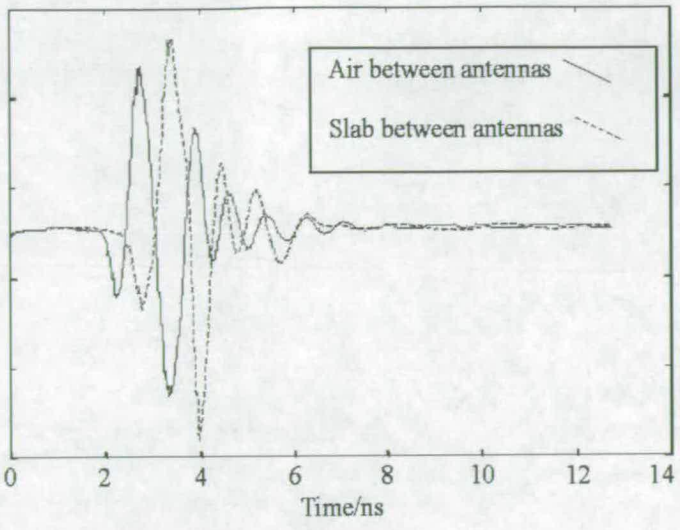

Figure 4.4: Delay of radar pulse through the slab

The transmit time between antennas is extended because of the slower speed through the slab. Closer inspection shows that this time increase is 0.40ns. With the slab in position the time between the transmission and reception is T_S. This includes:

1. Travel time from the transmitting antenna (some distance inside the box in which it is mounted) through to the front of the box.
2. Through the small air gap between the antenna and the slab.
3. Through the slab and out of the other side.
4. Through the clearance gap and into the box of the receiving antenna.

Let T_a be the travel time when the slab is replaced by an air gap. Then:

$$T_s = \frac{d}{v_s} + T_0$$
$$\text{and } T_a = \frac{d}{v_a} + T_0 \qquad (4.2)$$

where d is the thickness of the slab, v_s is the speed through the slab, v_a is the speed through air and T_0 is the time to travel through everything except the slab or the air that has replaced it.

Simply taking the difference of these gives the observed delay, Δ as:

$$\Delta = T_s - T_a = \frac{d}{v_s} - \frac{d}{v_a} = \frac{d}{c}\left(\sqrt{\varepsilon_r} - 1\right) \qquad (4.3)$$

As Δ, d and c are known it is simple to find the relative permittivity of the slab material and hence the velocity through the slab (it is assumed that the velocity through the air is 0.3m/ns). It turns out that the velocity of the radar pulse through the slab is 0.14m/ns and its relative permittivity is 4.8. This value is low in the range for bituminous paving materials and indicates a dry material which is consistent with the slab having been kept indoors for several days after removal from the road.

4.1.2 Testing of slab on artificial sub-base

The next part of the experiment was to set the 900 MHz antenna on top of a container filled with different materials, as shown in Figure 4.5.

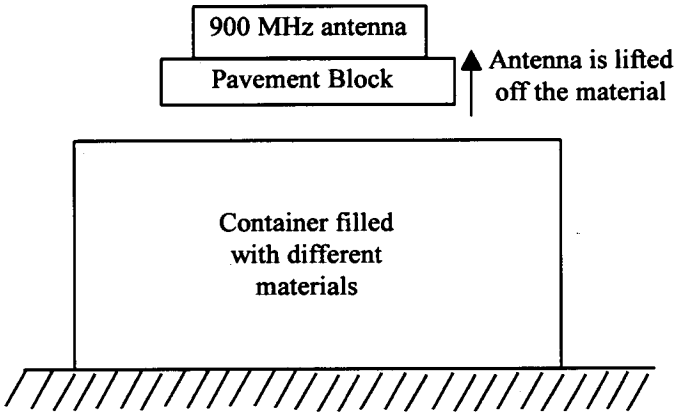

Figure 4.5: Set-up used to examine whether there is any effect on the signal if the material beneath the slab is changed

Figure 4.6(a) shows three scans with the 900MHz antenna on the top surface of the slab as it rests on a bed of coarse "concrete" sand. The reflection from the bottom of the slab is expected at 1.4ns after the initial pulse, this can be seen at about 6ns on Figure 4.6(a). The large reflections between 12 and 16ns are from the bottom of the sand bed. The three scans are almost indistinguishable showing the repeatability of the radar scans, and it is this property that will be used to try to distinguish the slab thickness from the initial pulse.

As well as using coarse "concrete" sand as a sub-base material, single-graded silica sand and gravel with stone sizes up to 10mm were also used. The results from the radar scans with

these three different sub-bases are shown in Figure 4.6(b). It is clear from this figure that the direct transmission and reflection from the asphalt slab top surface are not changed by the sub-base material. However, by 6ns the pulses are diverging as the reflections from the bottom of the slab are now being received and these will be modified by the different materials with which the slab is in contact. The pulses diverge at approximately 1.5ns after the initial pulse is received which is consistent with this observation.

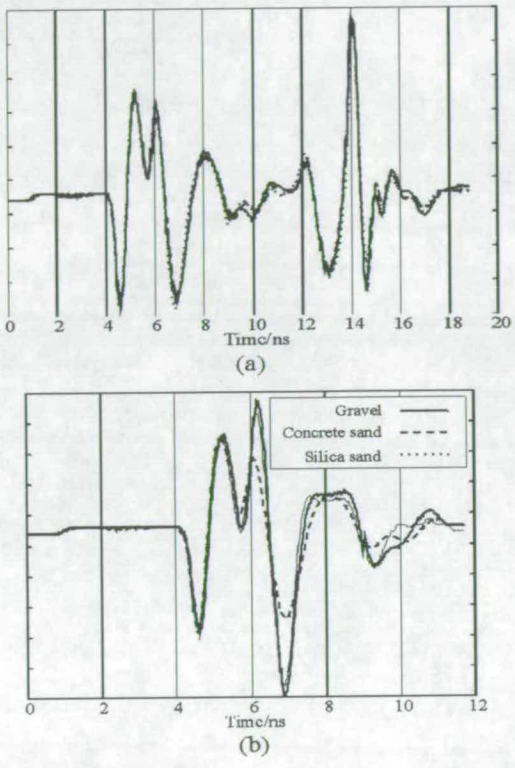

Figure 4.6 (a) Repeatability of the radar scans; (b) Scans with different sub-base materials

Figure 4.7(a)-(c) are the responses when the slab is raised above the sub-base. The introduction of this air gap between the top of the sub-base and the slab is observed to change the reflection from the bottom of the slab in each case only when the initial clearance of 0.1m is introduced. After this clearance the reflection from the bottom of the slab does not change but there is an additional reflection from the surface of the sub-base material. The expected delay after the reflection off the slab base is 0.667ns for every 0.1m that the slab is raised. This is consistent with the delays observed on the graphs.

In order to emphasise this effect Figure 4.7 (d)-(f) show the same results but the response of the slab in contact with the sub-base (zero height) has been subtracted off all the other

responses. The original response with the slab not raised is also included so that the time delay between the slab surface and base reflections can be identified. This is labelled as "0m" on the graphs.

This can be seen more clearly on Figure 4.8, which shows the response of the slab in contact with the "concrete" sand sub-base. The response of the slab in contact with the sub-base (zero height) is subtracted off all the other responses, with the lines separated to increase the clarity. The response from the bottom of the pavement slab is shown. The 0.4 and 0.3m response lines, shown in the upper part of the diagram, are exactly the same up to 0.3m, but, the 0.4m line represents the pavement block being lifted a further 0.1m, therefore the lines will separate at the 0.3m marking. This same observation is found when looking at the 0.1 and 0.2m response lines, shown in the lower part of the diagram (Figure 4.8).

When this technique was used to remove the initial pulse from the scan on the actual road it did not meet with any success. This is thought to be due to the fact that the slab had dried between its existence in the field and testing in the laboratory. The effect of moisture in pavement materials has a great effect on their testing with GPR due to the high permittivity of water.

Gravel sub-base

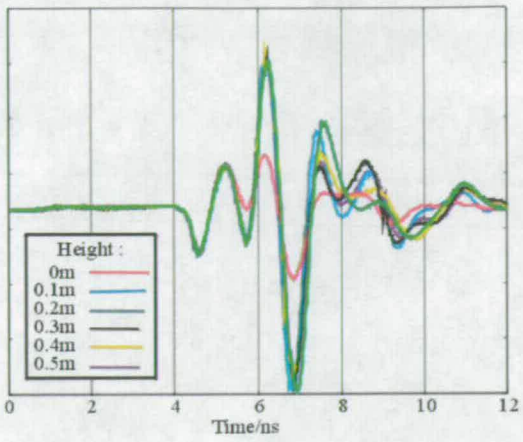

(a)

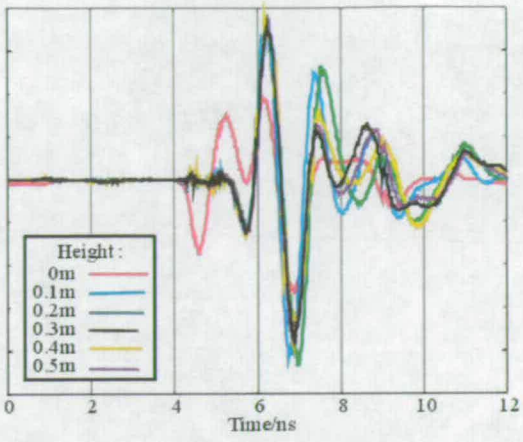

(d)

Concrete sand sub-base

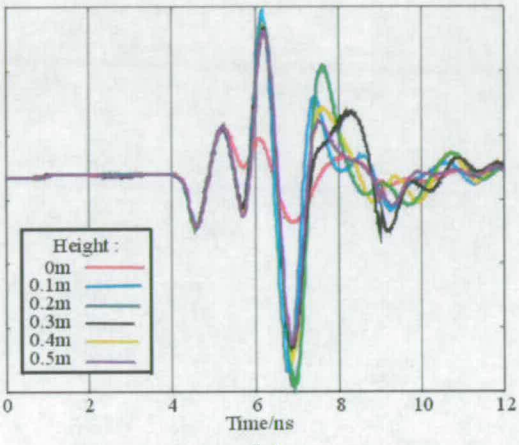

(b)

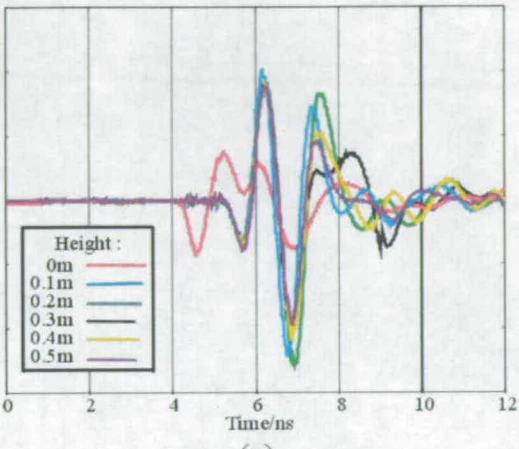

(e)

Silica sand sub-base

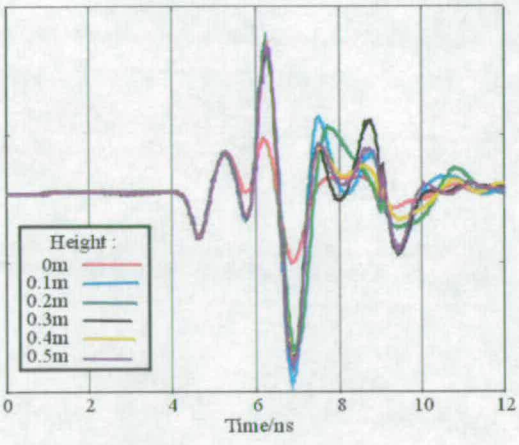

(c)

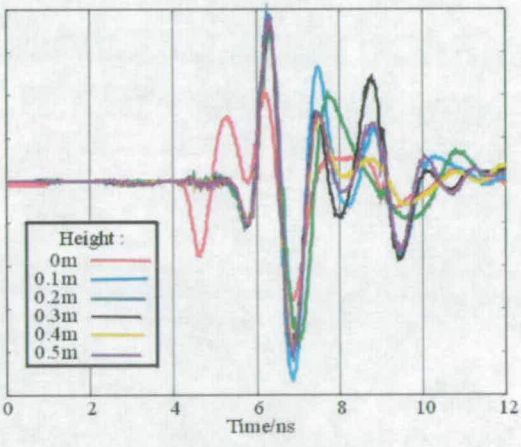

(f)

Figure 4.7: (a)-(c) Effect of lifting slab off different sub-bases (d)-(f) Deviation as slab is raised off different sub-bases

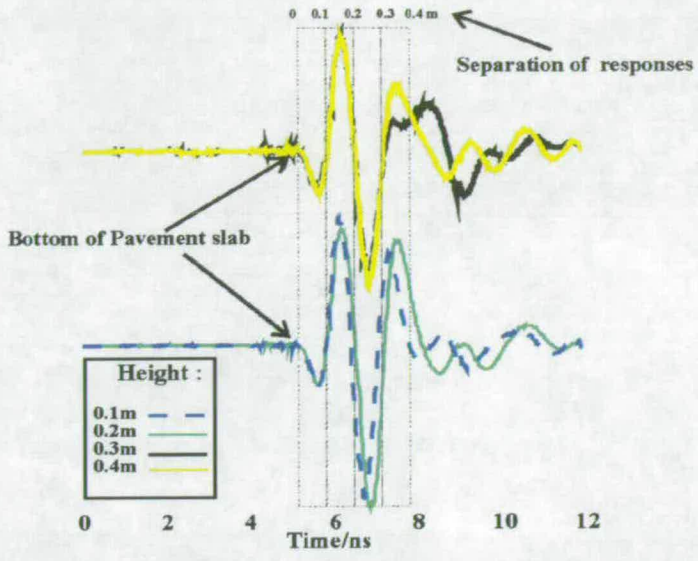

Figure 4.8: Shows the separation of the responses when the concrete sand sub-base is tested

4.2 Impact-echo and sonic testing applied to thin pavements

The impact-echo technique, discussed in chapter 3, was used on the pavement slab to investigate its use in detecting thin layers. Figure 4.9 shows the experimental set-up used to carry out these tests.

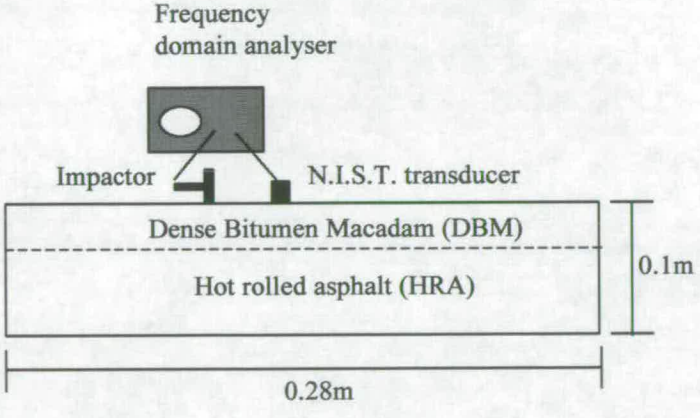

Figure 4.9: Impact echo set-up used to test the thin pavement

The compressive velocity of the pavement block was found by using two ultrasonic transducers and a Pundit ultrasonic non-destructive digital indicating tester, produced by C.N.S Instruments Ltd.

The transmitter was placed on one end of the pavement block and the receiver on the other end (Figure 4.10).

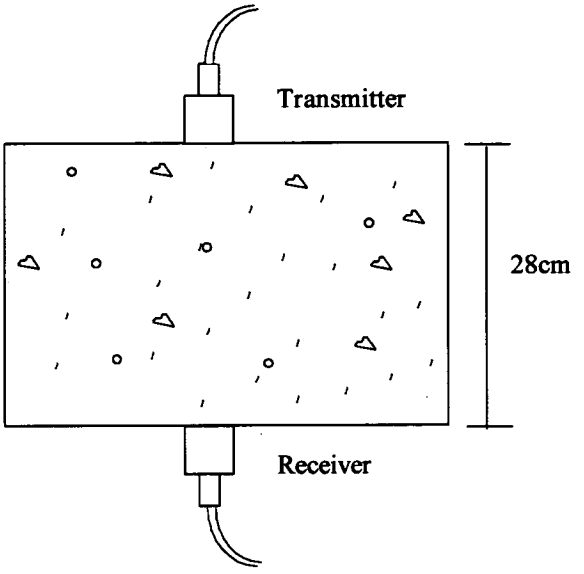

Figure 4.10: Direct transmission set-up used to propagate ultrasonic pulses through the pavement block

This set-up enabled the transmit time through the pavement slab to be accurately measured. Knowing the distance the pulses travel in the material will enable the velocity to be determined from the equation below:

$$\text{Pulse velocity} = \frac{\text{Path length}}{\text{Transmission time}} \qquad (3.4)$$

It is stated in the Pundit manual that the transmission time and path length should be measured to an accuracy of about (+/-) 1%.

The velocity through the two layers of the pavement block are shown in Table 4.1.

	Fine Layer	Course layer
Transmission Time (μs)	99 =98+1%	97 =98-1%
Path Length (L) (m)	0.28	0.28
Velocity (V) (m/s)	2828	2828

Table 4.1: Compressive velocity through pavement layers

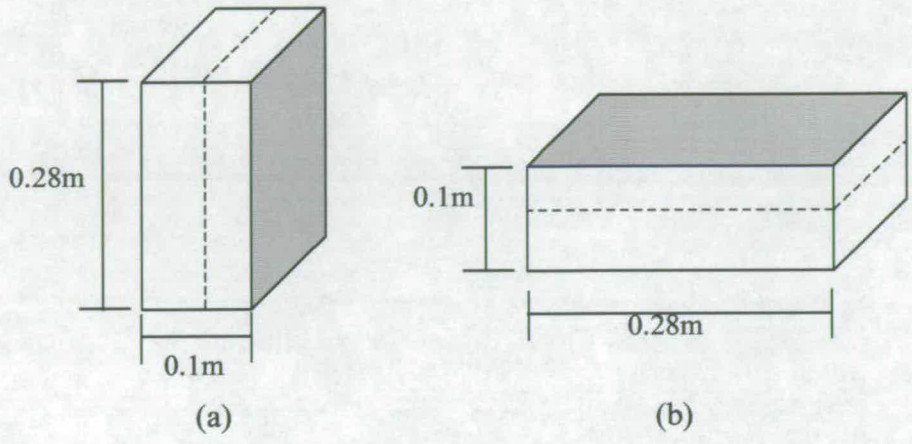

Figure 4.11: (a) Slab on its side (b) Slab flat

	Slab on its side	Slab flat
2-way Path length (L)	0.56m	0.2m
Theoretical Frequency ($f = V/L$)	≈5kHz	≈14kHz

Table 4.2: Theoretical frequency values (V ≈ 2800m/s (see Table 4.1))

The slab was then placed flat on the workbench for impulse-echo testing. A NBS conical reference transducer, produced by the National Institute of Standards and Technology (NIST), was used to receive the reflected waves. A piece of foam was placed underneath the slab, during each experiment, to prevent pulses travelling through the workbench. The transducer, which was connected to a frequency analyser, was placed on the surface of the pavement slab. The NIST transducer has a larger frequency range, 0 to 1MHz, and good

coupling with the surface. A PCB type 086 C80 hammer was used to apply impacts to the surface of the slab.

The impact point was initially 2cm away from the receiving transducer. This distance was increased in steps of 2cm up to and including 6cm. A total of five different impacts were recorded by the frequency analyser so that the background noise could be reduced when the responses were averaged.

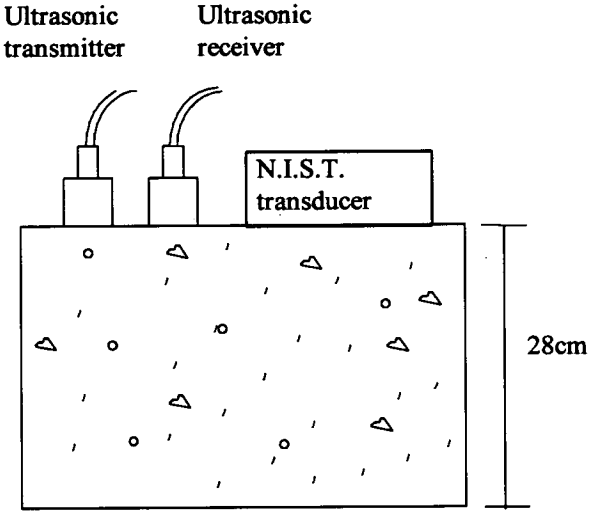

Figure 4.12: Ultrasonic indirect transmission method used to analyse the pavement block on its side

The next part of the experiment was to use two sets of ultrasonic transducers (UTs), a 54kHz and 82kHz, in place of the PCB hammer as shown in Figure 4.12. One of the transducers was connected to the Pundit with the other one connected to the frequency analyser. The main problem with the UT was that the actual input waveform was not known. Even though one of them was connected to the analyser, its waveform was not the correct input wave as it had travelled through the pavement prior to being recorded. In order to overcome this obstacle a 26μs reference bar was used, with an accelerometer at one end and one of the UTs at the other end. The response through the bar was recorded and from this it was possible to find the input waveform as the force is proportional to the displacement. The input response for the 54kHz and 82kHz transducers were calculated. The UTs were positioned at different distances from the NIST transducer and measurements were taken. The position of the ultrasonic transmitter and receiver were reversed and the experiment was repeated. The transmitter was initially 7cm from the NIST, and moved to positions 9 and 11cm away. A

total of ten responses were recorded and the average of the absolute value of the Fourier transform was found. These experiments were repeated with the slab placed flat on the workbench.

4.2.1 Analysis of Impact echo responses

The frequency range of interest, calculated from the velocity, were found earlier to be 5-14kHz. With the PCB hammer it was found that the input frequency range was too small, this can be seen in Figure 4.13. The pavement response when using the 82kHz transducer is shown on Figure 4.14. Whilst it is not clear on initial inspection of these figures, comparison with the responses from the 54kHz transducer reveal that the 82kHz transducer gave less energy in the important frequency range.

Calculating the transfer function between the input and output of the 54kHz responses produced good correlation with the theoretical values. Figure 4.15 and Figure 4.16 show the responses when the 54kHz transducer is used. It was noted that when the side of the pavement block was being analysed the NIST transducer picked up many high frequency responses between 3 and 5cm, however, as the input gets further away the high frequency responses disappear. The reason for this is due to the transmitter being so close to the NIST transducer and the surface area is very small so the surface vibrations will be concentrated in a small area thus causing the receiver to respond to the input 54kHz pulse directly. This effect did not occur when the pavement block was flat due to the larger surface area being analysed so dissipating the vibrations.

The 82kHz responses show that a frequency of 7.5kHz is being continually picked up as the highest frequency. This frequency is also evident to a lesser extent when the 54kHz transducer is used. It can be concluded that this is either a spurious resonance of the measurement system, or a resonance of the specimen that is not connected with the thickness that was being examined. In the field, such resonances would not occur and it is therefore not considered important here.

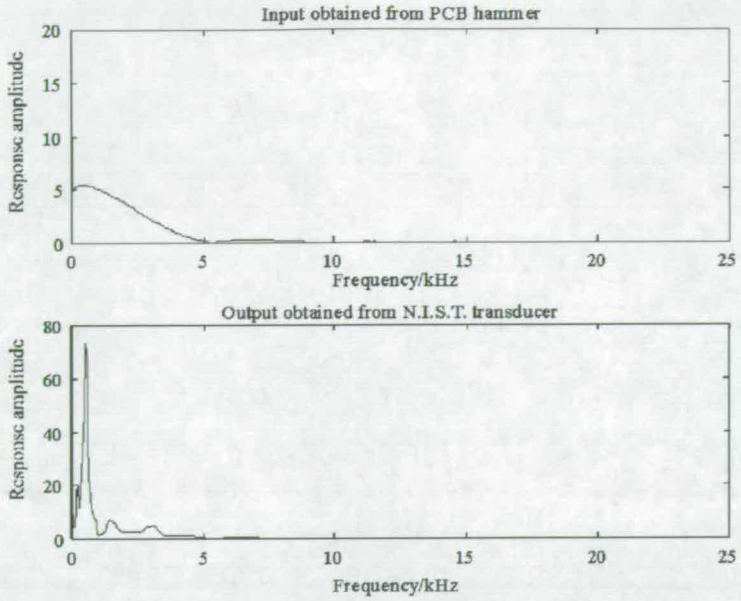

Figure 4.13: Response obtained from N.I.S.T. transducer when using the PCB hammer

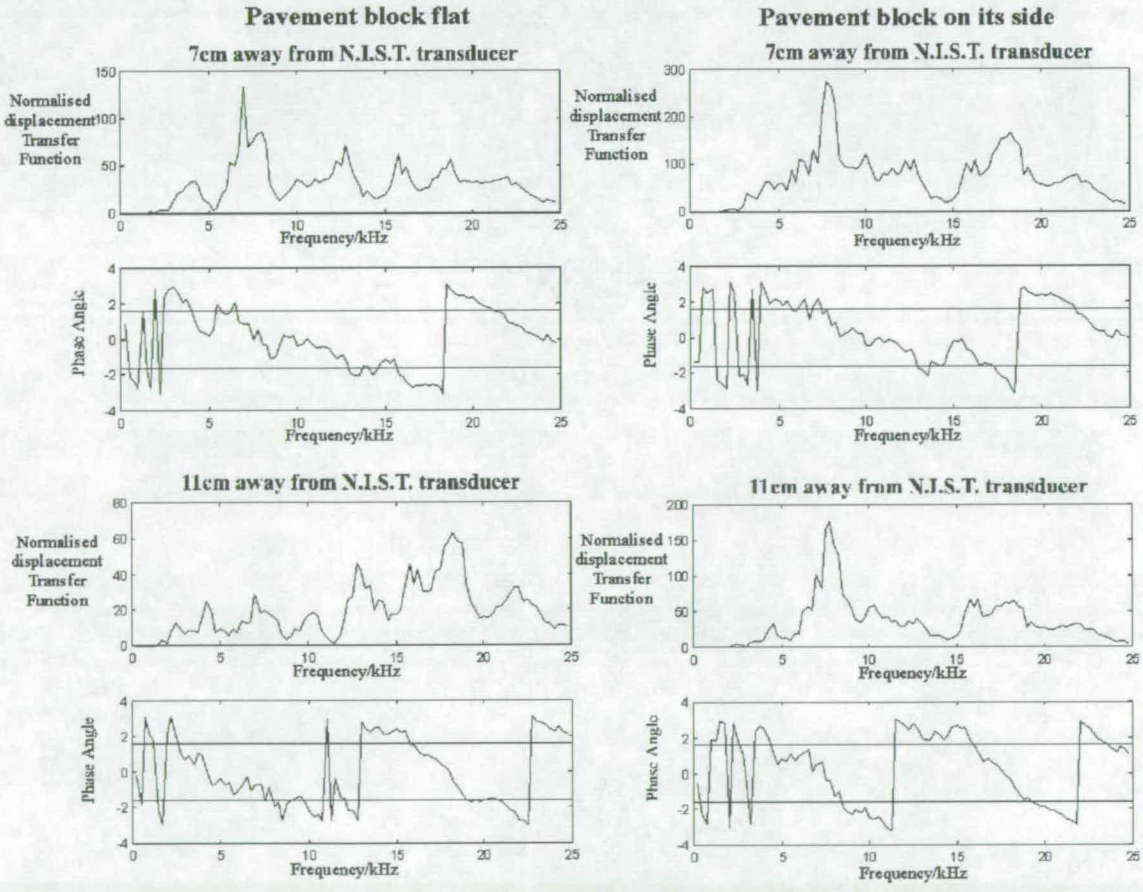

Figure 4.14: Responses obtained when using the 82kHz transducer

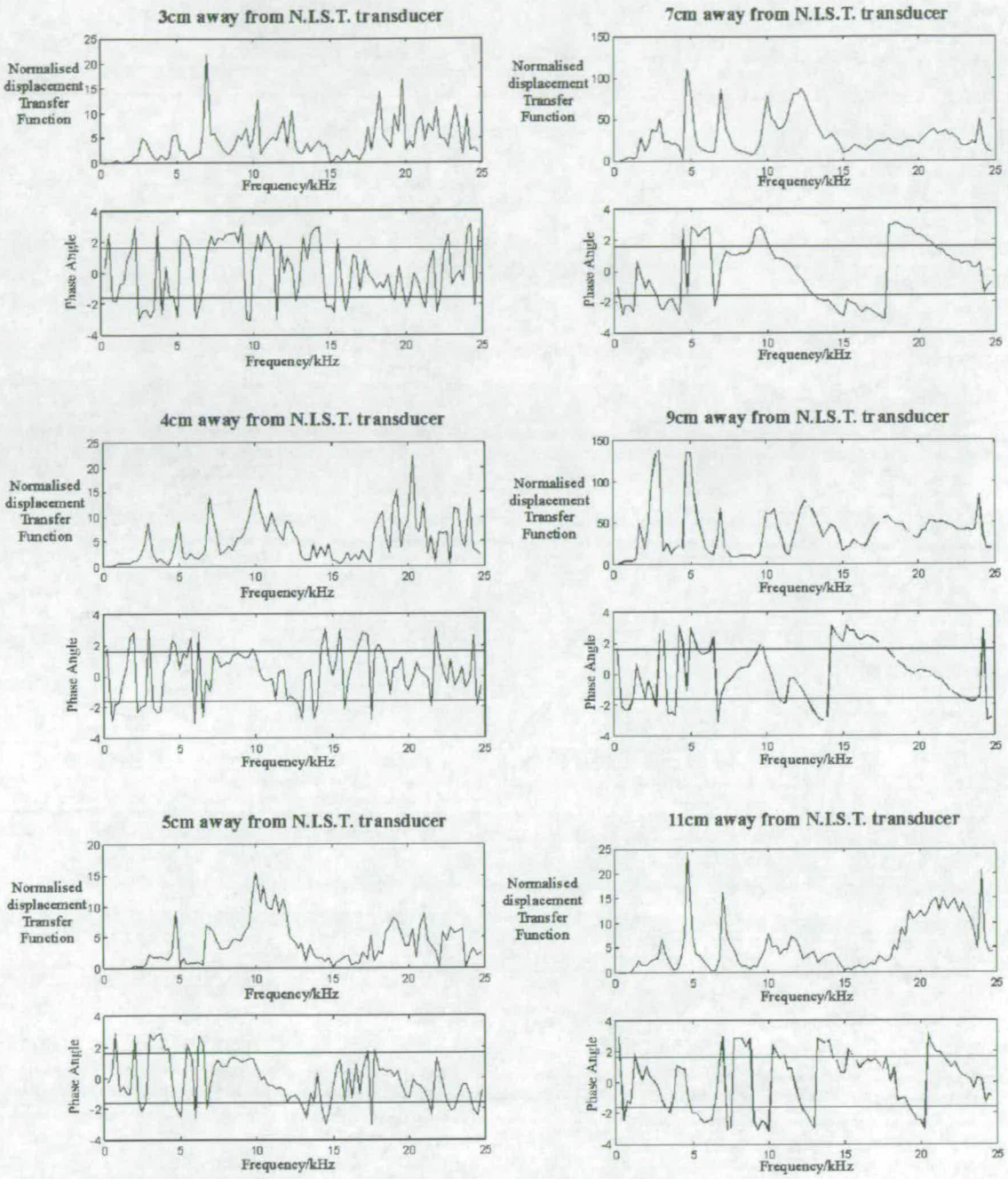

Figure 4.15: Responses obtained from 54kHz transducer when the pavement block is flat

Theoretical value of the frequency = 5kHz(side)

Theoretical value of the frequency = 14kHz (flat)

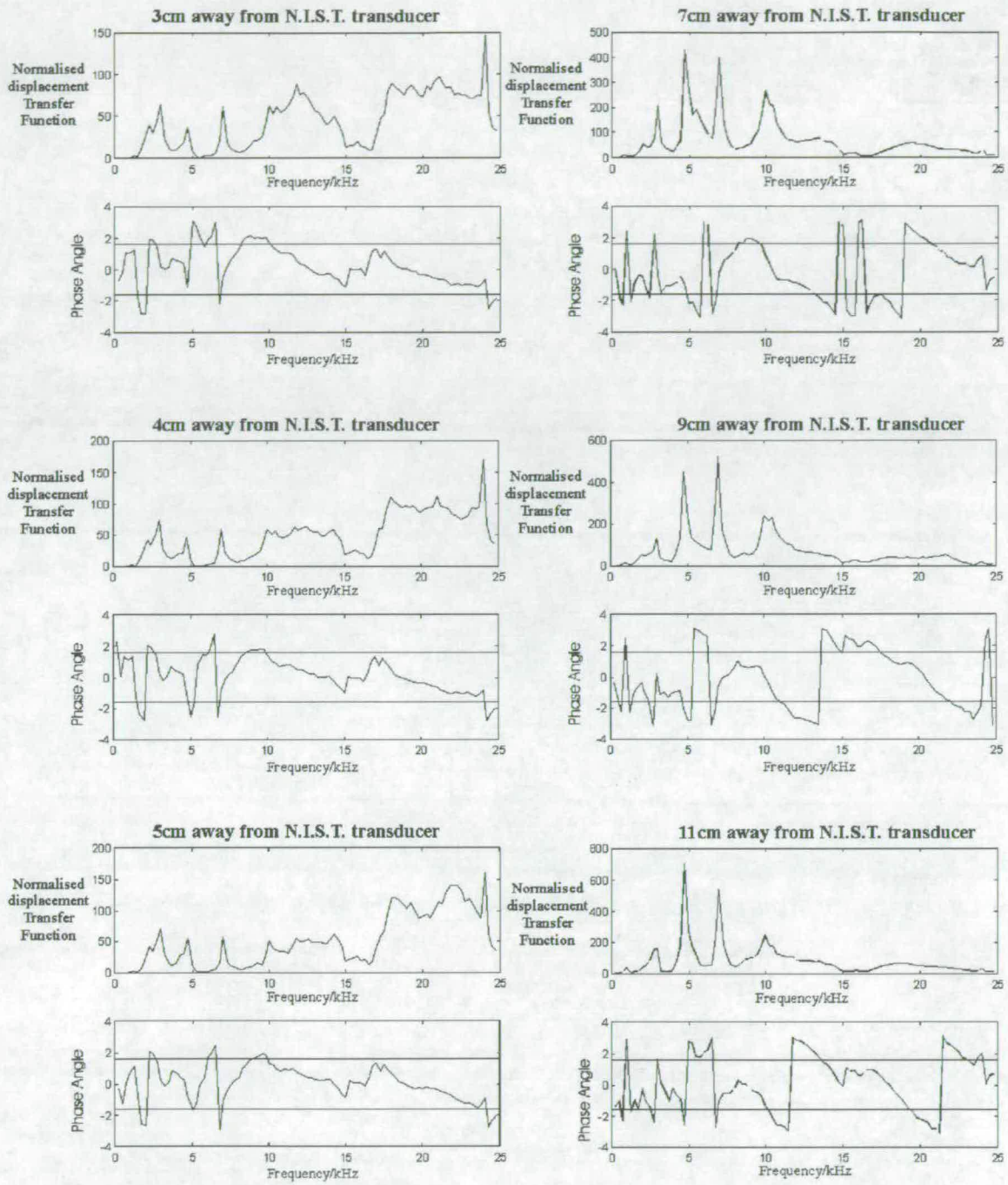

Figure 4.16: Responses obtained from 54kHz transducer when the pavement block is on its side

Theoretical value of the frequency = 5kHz (side)

Theoretical value of the frequency = 14kHz (flat)

4.3 Conclusions

The GPR responses of thin pavements can be impossible to interpret directly due to confusion of initial pulse reflections from the bottom of the thin layers, whether from the bottom of the bituminous layers of the pavement or interfaces between different bituminous materials.

The effect of the material beneath the thin layer (and hence the thickness of the layer itself) has no effect on the initial response from the surface and this can therefore be eliminated to reveal the response from the bottom layer.

To accurately analyse thin pavements using sonic techniques requires high frequency waves to be inputted into the pavement, however, the drawback is that the energy and penetration capability of the waves are reduced.

When applying sonics to the pavement slab some interesting results were found. The PCB hammer's input frequency range was too small. A good correlation with the theoretical values was found when using the 54kHz transducer. In comparison, the 82kHz transducer gave less energy in the important frequency range. The set-up of the equipment could explain some of the responses.

The sonic technique requires analysis of the actual material through which the waves are propagating. In the field this method has many obstacles which must be overcome before it can be successfully applied.

Chapter 5

Semi-intrusive determination of radar wave velocity

5. Introduction

The use of Ground Penetrating Radar (GPR) in civil engineering is becoming increasingly common. GPR, discussed in earlier chapters, is a non-destructive technique for investigating objects hidden by optically opaque barriers. High frequency radio wave pulses are transmitted from an antenna through the host material. Changes in dielectric properties of the material result in partial reflections of the pulses. These are picked up by a sensitive receiving antenna. Knowing the velocities of the radar wave through the different materials and the time of the pulses between transmission and reception enables the engineer to obtain the distance to the reflecting object or interface. There are several well-established techniques used to find the velocity of propagation.

This chapter looks at the theory behind refraction and reflection of electromagnetic waves. A review of established techniques used to determine radar wave velocities within materials is given and finally, it introduces a new, semi-intrusive method developed to determine velocities. This new method provides an additional, quick, readily interpreted and practical tool for GPR operators to use.

5.1 Refraction and reflection of electromagnetic waves

When electromagnetic waves, travelling through a homogenous medium, are incident on a second homogenous medium, part of their energy will be reflected, part may be absorbed and the rest will be transmitted into the second medium. If the wave is not normally incident on the interface it will be refracted (bent). If the angle of incidence is increased, at some point the wave will no longer enter the second medium but travel along the surface of

the medium, this occurs at the *critical angle* of incidence. Further increasing of the incident angle will result in total internal reflection (Figure 5.1).

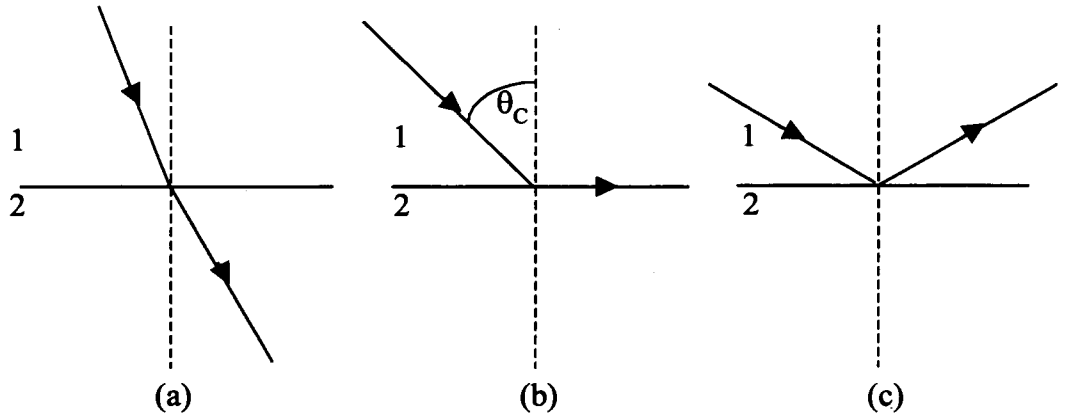

Medium 1 (velocity) :V_1
Medium 2 (velocity) :V_2 (Assume $V_2 > V_1$)
θ_C : Critical angle

Figure 5.1: (a) Ordinary refraction (b) Refraction at critical angle (c) Total internal reflection

5.1.1 Snell's law

This law, named after the Dutch mathematician Willebord van Roijen Snell, states that the ratio of the sines of the angles of incidence and refraction of a wave are constant when it passes between two given media (Paul & Nasar, 1987).

$$\frac{\sin\theta_2}{\sin\theta_1} = \frac{v_2}{v_1} \qquad (5.1)$$

where: θ_1 and θ_2 = angles of incidence and refraction respectively

v_1 and v_2 = speed of light in mediums 1 and 2 (Figure 5.2)

The incident ray, the refracted ray and the normal to the boundary at the point of incidence all lie in the same plane.

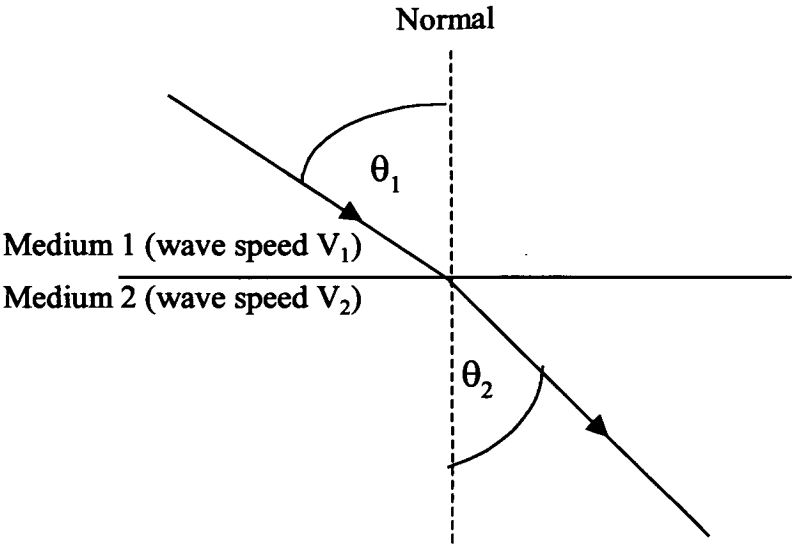

Figure 5.2: Definition sketch for Snell's Law

An incident ray entering a medium of higher velocity will result in the refracted ray being bent away from the normal; a lower velocity will cause the ray to bend towards the normal. A ray incident along the medium will be reflected along the normal.

These above principles were used in developing a new semi-intrusive method for determining radar wave velocities in different medium.

5.2 Methods used to determine radar wave velocity

The method chosen to determine radar pulse velocity in practice will depend on the accessibility over/around the object under investigation, its geometry, the required accuracy, the time and manpower available, and the amount of physical interference with the structure that is acceptable. It is well known that the radar pulse velocities depend on the electrical properties of the media under investigation (Daniels, 1996B). All media are assumed to be of low loss and therefore the radar pulse velocity is well approximated as being only a function of the electrical permittivity. Such an assumption is commonly made in GPR fieldwork.

5.2.1 Transmission method

This method can only be used if two sides of a structure or object are available to the user. By placing a transmitter and a receiver on different sides of the structure, the time taken for the radar wave to travel directly from one antenna, through the structure and into the second antenna can be obtained. The velocity can be calculated by dividing the separation distance of the antennas, d, by the time taken for the signal to travel through the structure, T_1.

$$v = \frac{d}{T_1} \qquad (5.2)$$

Gordon *et al.* (Gordon et al, 1998) discussed the experimental set-up of this method in more detail. The method can be very accurate, but it only gives an average velocity between the transmitter and receiver. If there are changes in the velocity along the path from transmitter to receiver then the pulse will be refracted, its path length will not be straight (unless the path happens to be perpendicular to the interfaces where the velocity changes), and this will lead to errors in using equation 5.2, even if the average velocity is required.

This method is the basis for impulse radar tomography which is a sophisticated and time-consuming method by which the pulse velocity can be found at any point in the structure (assuming that sufficient access is available to implement the transmission method many times), (Colla *et al.*, 1997).

5.2.2 Common-mid Point method (CMP)

The Common mid-point (CMP) or Common depth-point (CDP) method can be used to determine the radar signal velocity when only one side of the structure is accessible. Daniels (Daniels, 1996B) discusses this method in more detail. A transmitter and receiver are placed next to each other on the same surface of the material and they are then moved in incremental steps away to equal distances from a common point. A series of one-way travel times between the receiver and transmitter is recorded.

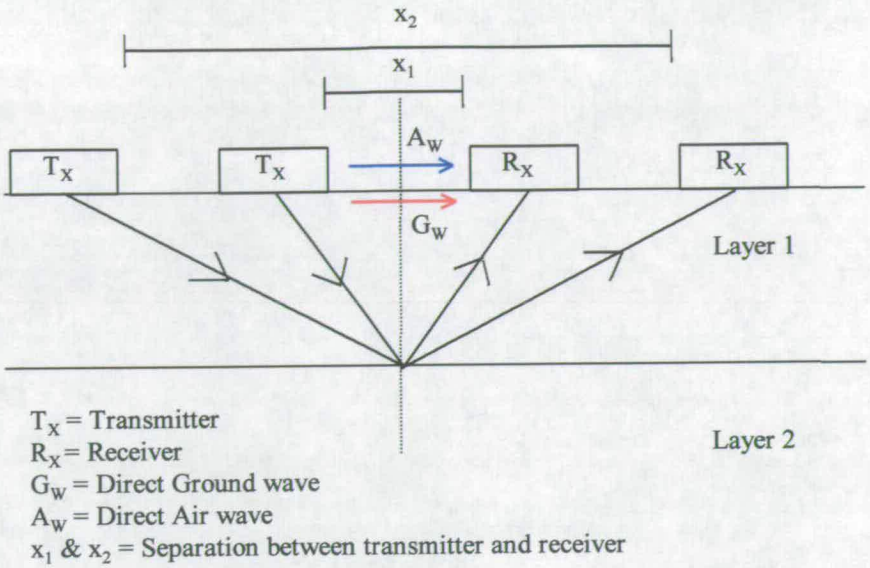

Figure 5.3: Common mid-point method (CMP)

If the travel times are t_1 and t_2 for antenna separations of x_1 and x_2, then the velocity is given by:

$$v = \sqrt{\frac{x_1^2 - x_2^2}{t_1^2 - t_2^2}} \qquad (5.3)$$

The Wide Angle Reflection and Refraction (WARR) method is very similar to the CMP method however one antenna is held fixed while the other one is moved incrementally away along a straight line, Annan (Annan, 1997). Figure 5.5 shows a typical radargram when carrying out a WARR survey.

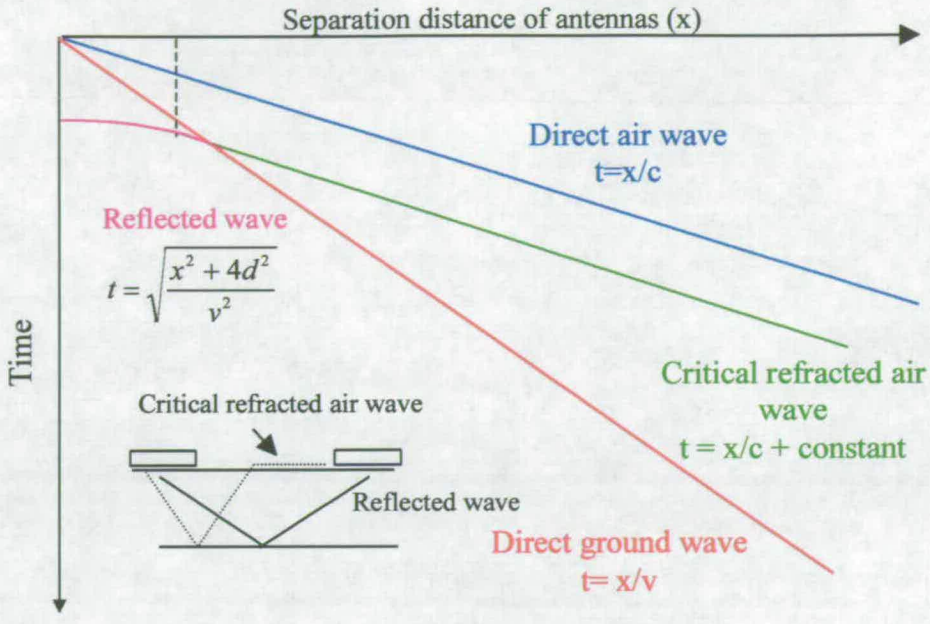

Figure 5.4: The idealised event arrivals of the different electromagnetic waves (Adapted from Annan, 1997)

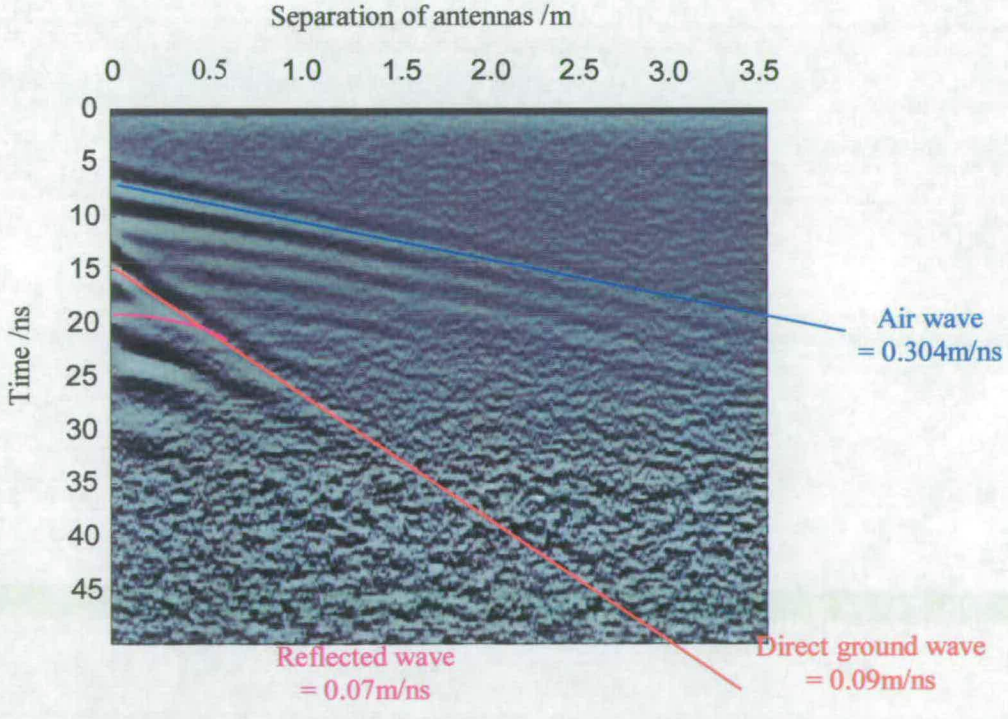

Figure 5.5: Radargram obtained from a WARR survey

5.2.3 Reflection coefficient method

An antenna is placed at a height from the surface of the material such that a clear reflected signal is observed. Let the reflected signal have an amplitude of A_S. A metal plate is then placed below the antenna which results in 100% reflection of the radar pulse. This fully reflected amplitude is A_P. Figure 5.6 shows a diagrammatic set-up of this method.

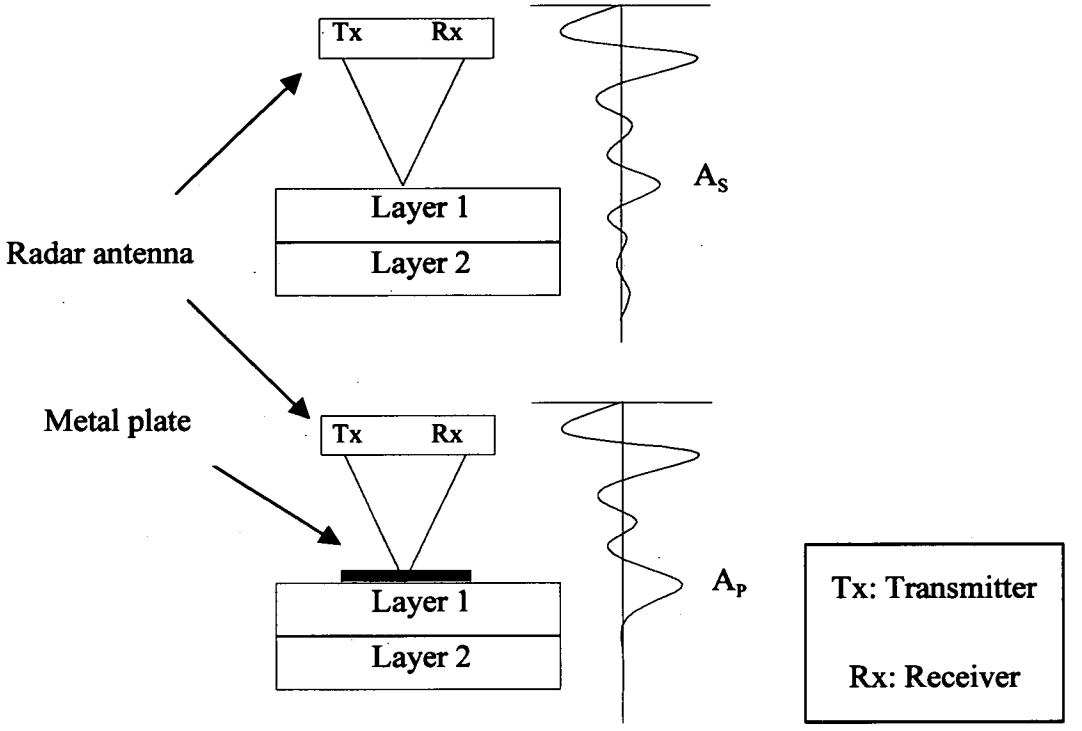

Figure 5.6: The reflection coefficient method

The radar velocity through the material can be calculated from:

$$v = \left(\frac{A_P - A_S}{A_P + A_S} \right) c \qquad (5.4)$$

where c is the speed of light in free space.

Once the radar velocity has been calculated in the top layer, the velocities in subsequent layers can be calculated as long as a reflection is obtained from these layers. The mathematics are shown below.

$$\varepsilon_1 = \frac{v^2}{c^2}$$

$$\varepsilon_2 = \varepsilon_1 \left[\frac{R_1 - R_2}{R_1 + R_2} \right]^2$$

$$\therefore v_2 = \frac{c}{\sqrt{\varepsilon_2}} \text{ (layer 2 velocity)}$$

where

$$R_1 = \frac{4\sqrt{\varepsilon_1}}{1 - \varepsilon_1}$$

$$\text{and } R_2 = \frac{\text{Ratio of reflected amplitude of layer 2}}{\text{Ratio of reflected amplitude of surface layer}}$$

These equations can be applied to multiple layers as long as R_2 is known for that layer. Further discussion of this method can be found in Maser (Maser, 1993).

5.2.4 Trenching and coring

Perhaps the most commonly used methods for determining the velocity of the impulse radar through civil engineering materials is to take cores out of the object under investigation, or cut a trench though a section of it in order to determine the target depth, and therefore the impulse radar velocity.

5.3 Summary of existing methods

Each of the existing methods has its place and is favoured by certain practitioners. The main advantage of the transmission and reflection coefficient methods is the simplicity of implementing them. However, the applicability of the transmission method is limited by the need to have access to opposite sides of the structure under investigation. Further, only an average value of the velocity is obtained although more than one layer can be present. The main disadvantage of the reflection coefficient method is the variation in the accuracy of the results. The amplitude of the pulse reflected by the material interface is prone to changes due to the roughness of the surface causing scattering of the incident pulse rather than reflecting it neatly. There is also propagating errors when calculating the velocity in multiple layers. The CMP method can provide accurate estimations of the GPR velocities. However, post-processing of the data is required which is time consuming. To implement

this method, physically separated transmitting and receiving antennas are required, but, in some commercial GPR systems both the transmitter and the receiver are located within the same unit and cannot easily be separated.

A new semi-intrusive method is proposed which is easy to implement using any commercial radar system and the interpretation can be done with relative accuracy in the field. The obvious disadvantage of this method is its intrusive nature.

5.4 A new semi-intrusive method.

A direct method of GPR pulse velocity determination which involves less intrusion than coring or trenching, is proposed. The method can be easily employed and used directly in the field investigation of stratified materials producing reasonably accurate results. For example GPR surveys of masonry walls, road pavements and geological sites.

A metal bar is inserted into the object under investigation at a known angle and this is then observed using radar. As a pencil sticking out of a glass of water appears to bend due to the different speeds of light through air and water, so the straight metal bar will appear to bend due to changes in the velocity through different materials.

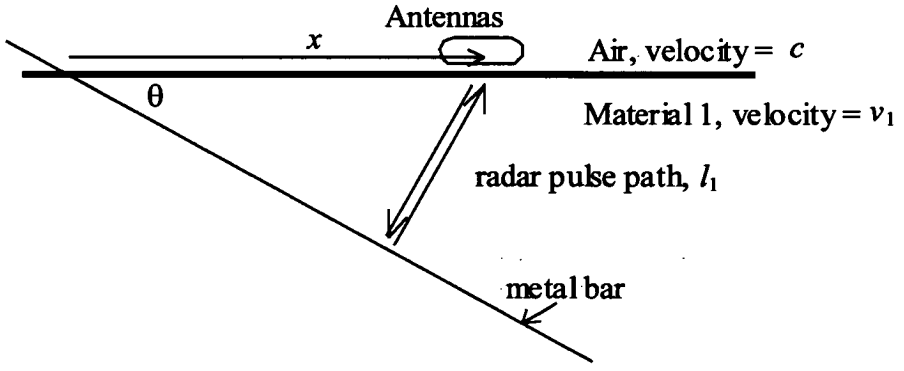

Figure 5.7: Locating a metal bar with impulse radar

Figure 5.7 shows an investigation of a metal bar at an angle θ to the ground. When the antenna is a distance x from the point of insertion of the bar then the path length for a reflection from the bar is:

$$l_1 = 2x\sin\theta \qquad (5.5)$$

and the time taken to travel this distance in this material is:

$$T = \frac{l_1}{v_1} = \frac{2x\sin\theta}{v_1} \qquad (5.6)$$

Therefore, if a graph is plotted of T against x, a straight line with gradient $2\sin\theta/v_1$ will result.

If material 1 comprises a layer of thickness H_1 over the top of a different material, which has a radar pulse velocity of v_2, then the path followed by the pulse to the bar and back is complicated by refraction at the layer interface as shown in Figure 5.8.

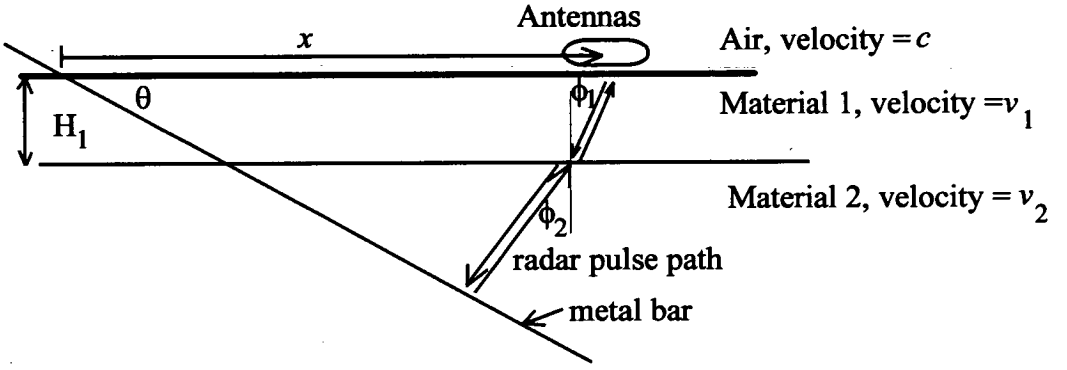

Figure 5.8: Locating a metal bar through an overlying layer

Snell's law gives us:

$$\frac{\sin\phi_1}{\sin\phi_2} = \frac{v_1}{v_2} \qquad (5.7)$$

and because the first reflection from the bar is at right angles to the bar:

$$\phi_2 = \theta \Rightarrow \sin\phi_1 = \frac{v_1}{v_2}\sin\theta$$

$$\Rightarrow \cos\phi_1 = \sqrt{1-\left(\frac{v_1}{v_2}\right)^2 \sin^2\theta}$$

$$\Rightarrow \tan\phi_1 = \frac{\frac{v_1}{v_2}\sin\theta}{\sqrt{1-\left(\frac{v_1}{v_2}\right)^2 \sin^2\theta}}$$

Therefore the total time for the pulse to travel from the transmitting antenna to the bar and back to the receiver is now:

$$T_2 = 2\left(\frac{H_1}{v_1\cos\phi_1} + \left\{x - \frac{H_1}{\tan\theta} - H_1\tan\phi_1\right\}\frac{\sin\theta}{v_2}\right)$$

$$= 2H_1\left\{\frac{v_2^2 - v_1^2\sin^2\theta}{v_1 v_2^2\sqrt{1-\left(\frac{v_1}{v_2}\right)^2\sin^2\theta}} - \frac{\cos\theta}{v_2}\right\} + \frac{2\sin\theta}{v_2}x \qquad (5.8)$$

Therefore, if a graph is plotted of T against x, a straight line with gradient $2\sin\theta/v_2$ will result. Therefore the speed of radar signals at any point on the radar trace is most easily estimated by measuring the gradient and using:

$$v_2 = 2\sin\theta\frac{\Delta x}{\Delta T} \qquad (5.9)$$

where $\frac{\Delta x}{\Delta T}$ is the best estimate for the rate of change of x with T (reciprocal of the slope determined above) at the required position.

In fact the gradient of the line will always be $2\sin\theta/v$ no matter how many layers are passed through. The change in velocity with depth can therefore be reconstructed by investigation of the tangent to the T against x curve.

5.5 Computer simulation

In order to test the effectiveness of this technique a series of GPR simulations were carried out in two and three dimensions using a Finite-Difference Time-Domain (FDTD) based GPR model, developed by Giannopoulos (Giannopoulos, 1997). Figure 5.9 shows the result of a two dimensional simulation of a three-layer system. The top layer has a radar speed of 0.130m/ns, the middle layer a speed of 0.110m/ns, and the underlying layer has a speed of 0.075m/ns. A metal bar is penetrating the layers at an angle of 26° to the horizontal. The reflection from this bar can be clearly seen, as can the reflections from each layer interface. When equation 5.9 is used to determine the speeds in each layer, the speeds are recalculated as 0.140m/ns, 0.107m/ns and 0.082m/ns. The errors in these estimations are less than 10%.

The expected error is directly attributable to the accuracy with which the slopes can be determined from the graph. In this case measurements were made using pencil and ruler, as they might be if used out in the field. More sophisticated methods of regression analysis are available for more accurate velocity determination, although they have not been used in this investigation.

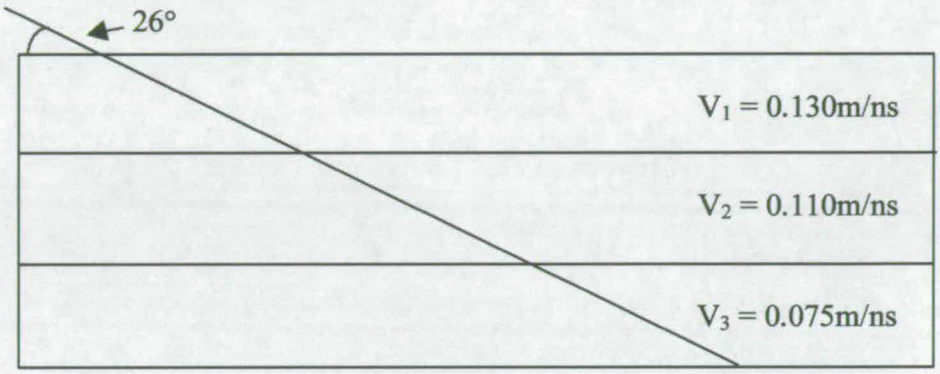

(a)

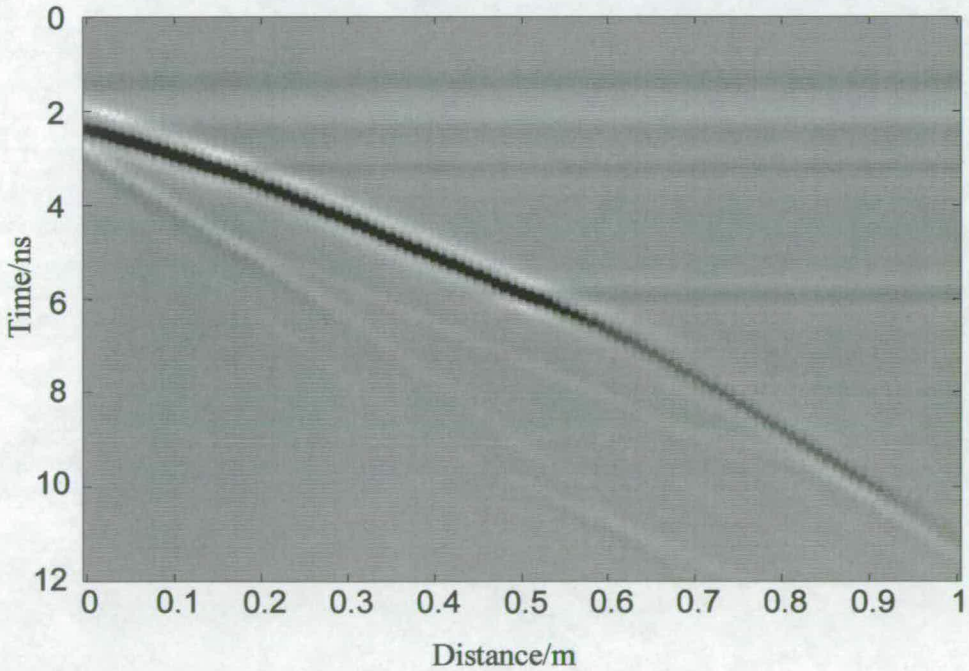

(b)

Figure 5.9: (a) Schematic drawing showing the three distinct layers in the two dimensional simulation (b) Simulated radar data

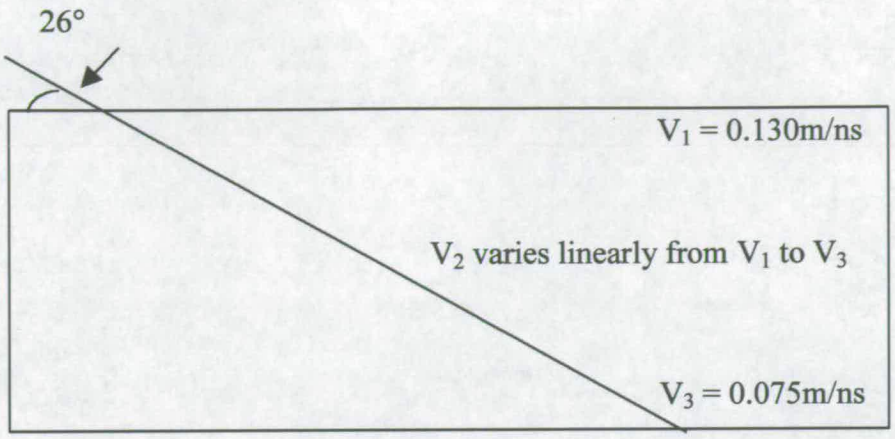

(a)

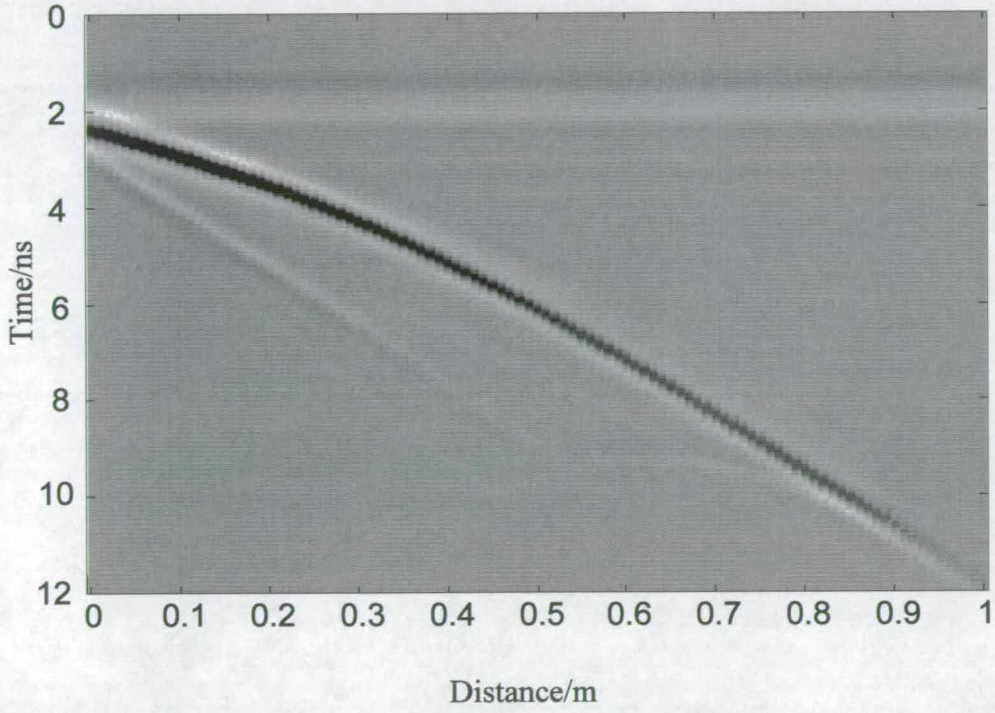

(b)

Figure 5.10: (a) Schematic drawing showing the gradated layers used in the two dimensional simulation (b) Simulated radar data

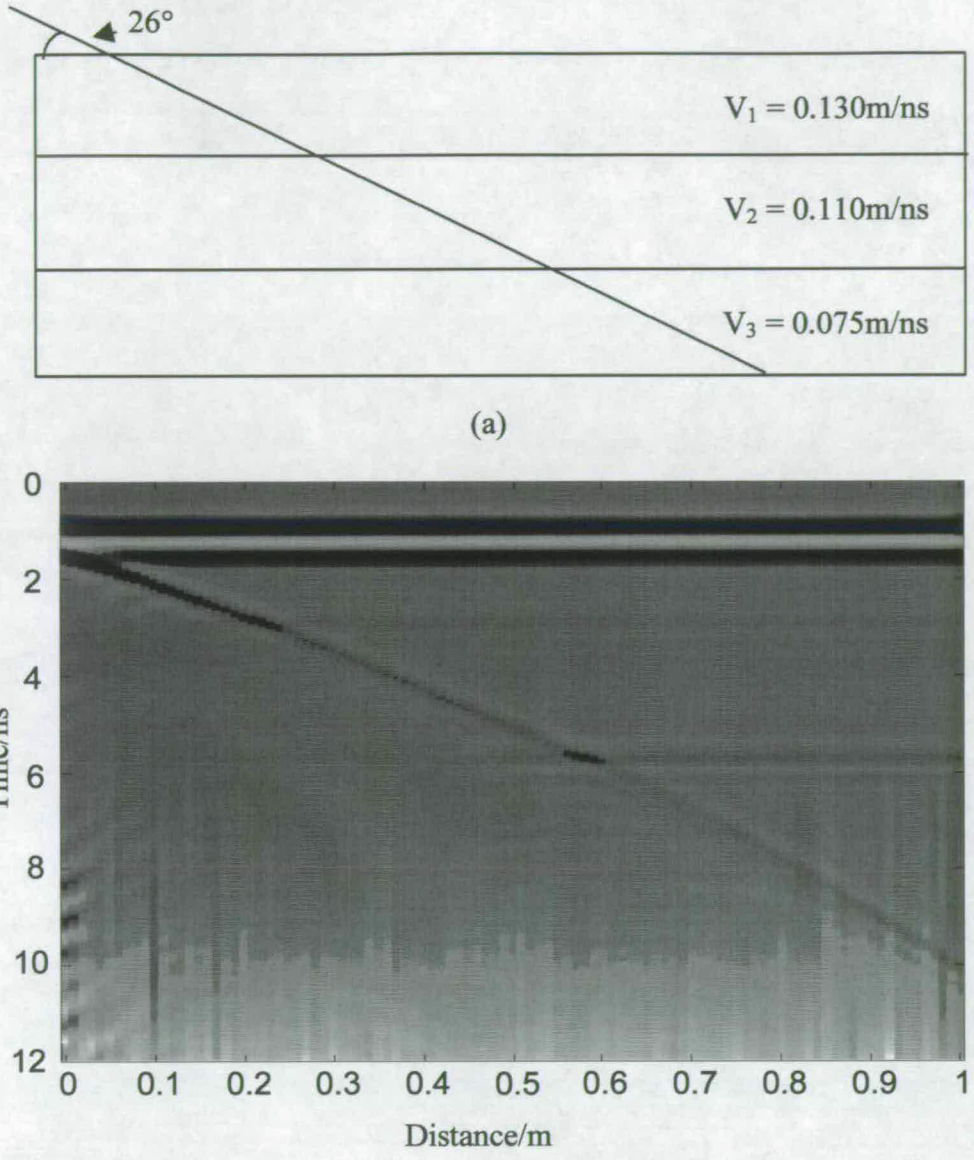

Figure 5.11: (a) Schematic drawing showing the three distinct layers in the three dimensional simulation (b) Simulated radar data

Figure 5.10 shows the simulation of a similar system, but with the radar pulse velocity of the middle layer varying linearly with depth, ranging between the velocity values of the top and bottom layers. The effect of a layer like this is to greatly reduce the reflections from any interface which could lead to a false assumption that there are no layers present and therefore that the bottom (third) layer has the same properties as the top layer. With this configuration, the metal bar is observed to bend gradually through the depth of the second

layer. Equation 5.9 can be used to determine the radar speed at any point on this radargram. None of the conventional means of determining radar velocity could have determined this gradual change in material properties.

Finally, in Figure 5.11, a three dimensional simulation of the first experiment is presented. The reflections from the bar are now not as strong due to the increased geometric attenuation of the radar pulse. This was expected because contrary to the two dimensional models, where the simulated GPR source produces a cylindrical propagating wave, the GPR pulse is simulated as a propagating spherical wave (Giannopoulos, 1997). However, the reflections from the bar are still clearly visible and equation 5.9 can still be used to determine the impulse radar velocities. The derived velocities are identical to those for the two dimensional simulation.

5.6 Laboratory experiments

Before implementing the technique in the field some initial experiments were carried out in the laboratory. A plastic tank was filled with layers of saturated sand (100% moisture content), damp gravel (2.2% moisture content), and saturated gravel.

The laboratory experiments were carried out in a plastic tank in order to model an ideal soil structure (Figure 5.12). Due to the size of the tank (dimensions shown in Figure 5.13) it was decided to use only the smallest antenna available to the researchers, this was a GSSI 1.5GHz bow-tie antenna.

Figure 5.12: Showing the metal bar (inclinometer attached to it) inserted into plastic tank

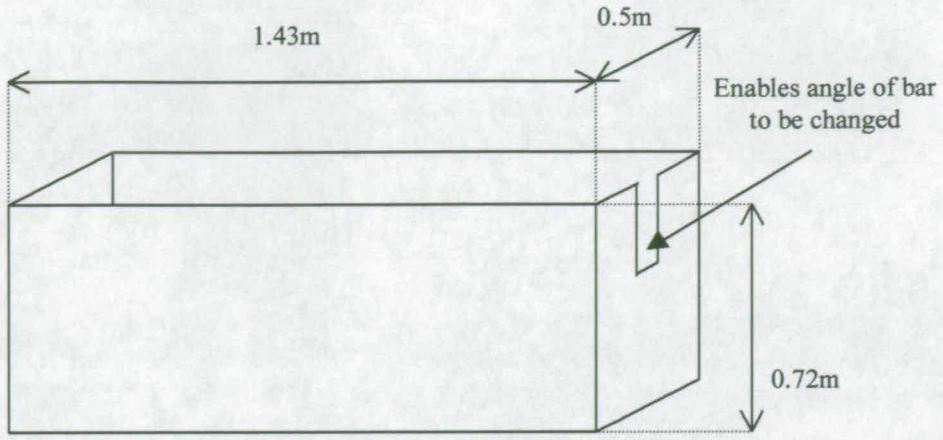

Figure 5.13: Dimensions of plastic tank

The tank rested on a wooden frame, enabling a piece of metal to be placed underneath the tank, this plate can be used to set the correct time range of the radar plot. The metal plate produced a large reflection, indicating the position of the base of the tank within the signal, which in turn was used to adjust the size of the time range, Figure 5.14.

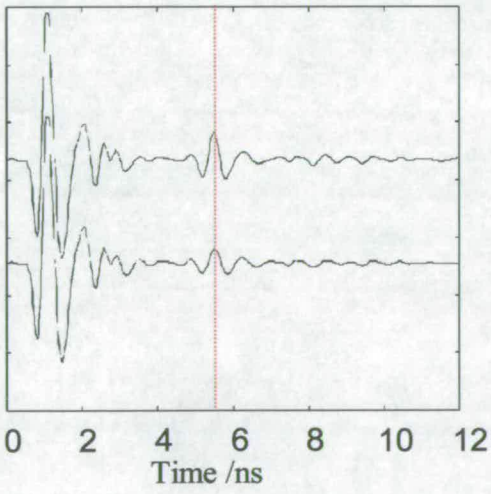

Figure 5.14: The plot shows the normal radar signal obtained from the plastic tank (lower plot) compared to the signal response when the metal plate is placed on the base (red line) of the tank

The transmission method, described earlier, was used to determine the velocities through each individual layer. Two antennas were placed on each side of a wooden box and a

reading was taken. A second reading was then taken when the material was placed in the box, enabling the difference in the time, Δ, between the two signal responses to be found (Figure 5.15).

From Figure 5.15 (equation 4.3)

$$\Delta = \frac{d}{v_s} - \frac{d}{v_a} = 7.7ns$$

$$v_s = \frac{0.5}{7.7 + \frac{0.5}{0.3}}$$

$$v_s = 0.05m/ns$$

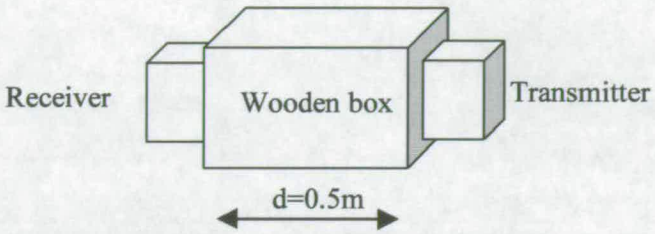

The velocities were 0.07, 0.16 and 0.05 m/ns for the saturated sand, damp gravel and saturated gravel respectively.

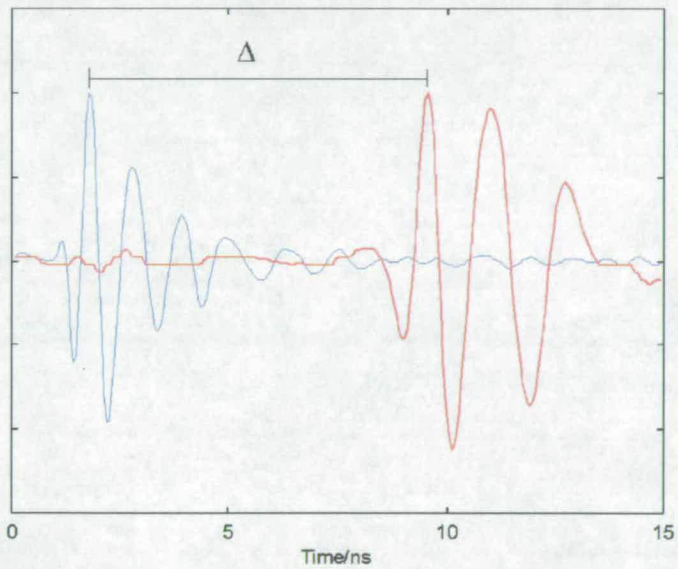

Figure 5.15: Normalised o-scope plots showing the effect of adding the saturated gravel to the box (red)

Initial experiments were carried out to determine the optimum angle for inserting the metal bar. Angles greater than 30° gave weak reflections because the main energy in the radar is directed downward into the soil and the energy radiated at angles greater than 30° are small. Angles less than 20° gave good reflections, but require large horizontal distances if significant depth penetration into the ground is required. Therefore shallow angles should

be avoided. In practice angles between 22° and 26° were used, as these gave a good compromise between the requirements.

Once the layers of material had been placed into the tank (Figure 5.16) the 1.5GHz antenna was positioned in such a way that the survey wheel could be run along the side of the tank (Figure 5.17).

Figure 5.16: Levelling the different materials in the tank

Figure 5.17: How the survey wheel was positioned in each survey

Two typical results are shown in Figure 5.18 and Figure 5.19. These show radargram plots of the time against the horizontal distance along which the antenna has been moved. Figure 5.18 shows a layer of saturated sand over saturated gravel. The top layer has the faster velocity and the velocities were determined using equation 5.9 as 0.07m/ns and 0.05m/ns which correlated with the values determined using the transmission method.

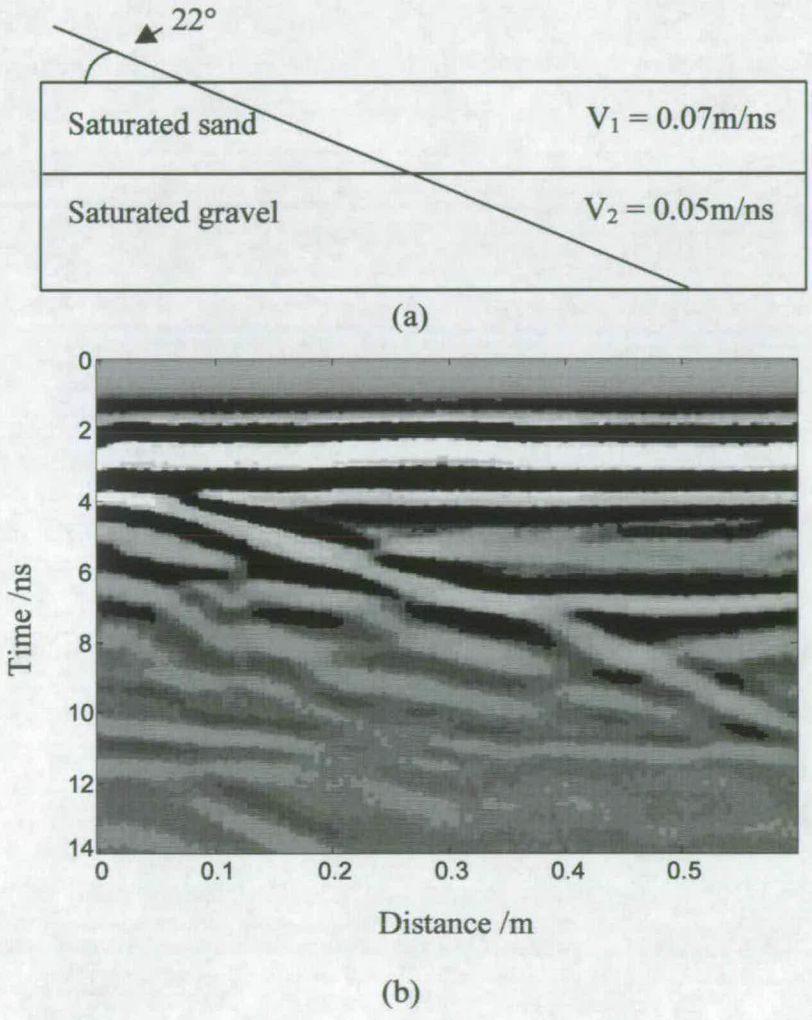

Figure 5.18: (a) Cross-sectional view of the saturated sand over saturated gravel (b) Radargram from the GPR survey of the layers

In Figure 5.19 a three-layer example with layers of damp gravel, saturated sand and saturated gravel is presented. The slopes of the graph give velocities of 0.13m/ns, 0.07m/ns and 0.06m/ns respectively. These laboratory experiments proved that the method could be used to determine impulse radar velocities through different strata

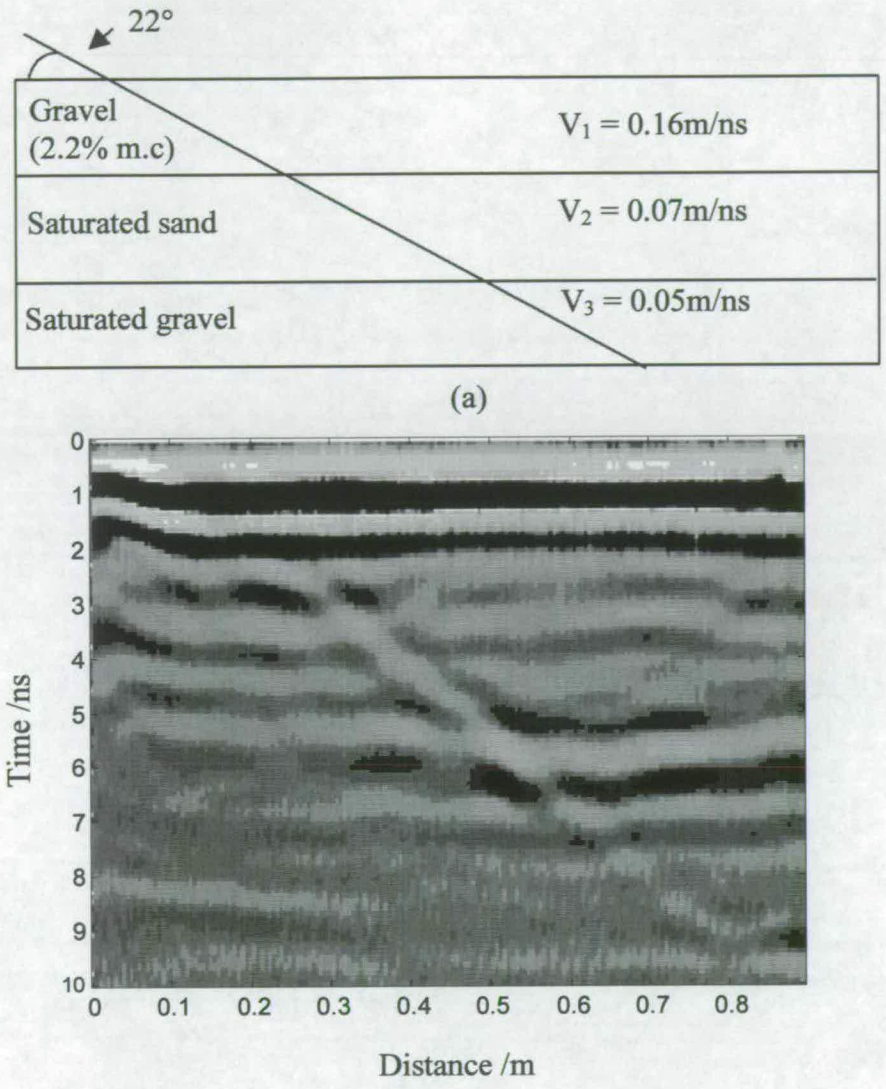

Figure 5.19: (a) Cross-sectional view of the gravel; (2.2% m.c.) over saturated sand over saturated gravel (b) Radargram from the GPR survey of the layers

5.7 Case study

A radar survey of the beach at Gullane in East Lothian (Scotland), shown in Figure 5.20, was carried out to determine how many different layers of sand can be identified using this method. A metal bar was inserted into the sand and a radar survey was carried out above it

(Figure 5.21). The result can be seen in Figure 5.22. This radargram clearly shows two different layers each with a distinct velocity. The top layer of sand has an impulse radar velocity of 0.23m/ns as determined by equation 5.9. The next layer, which is the least distinct due to the steep angle, has a velocity of 0.11m/ns. As one would expect, the top layer velocity indicates that the sand layer is very dry and the bottom layer velocity shows that this sand layer is damp.

Figure 5.20: The beach at Gullane in East Lothian (Scotland) where the field trial was carried out

Figure 5.21: Taking measurements on the beach

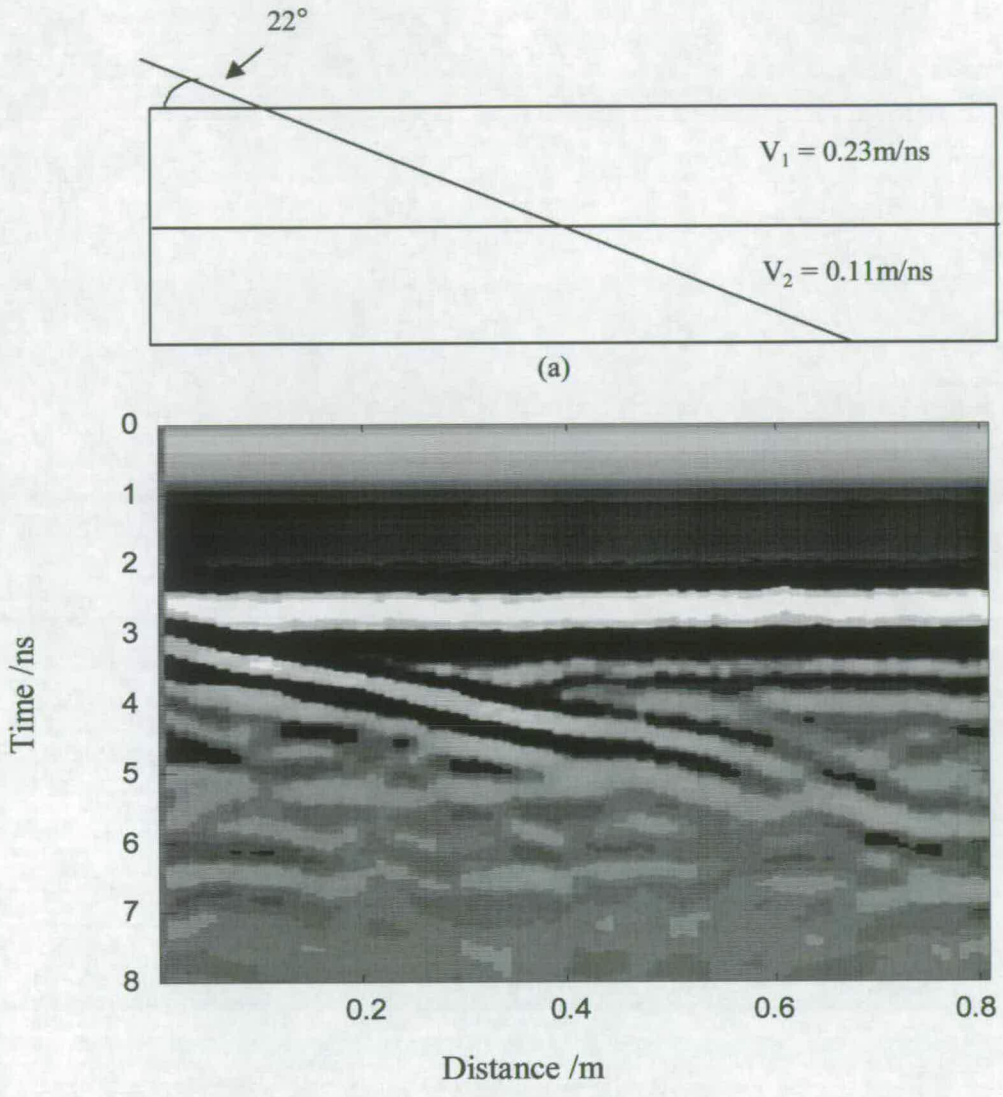

Figure 5.22: (a) Derived velocities from the radargram (b) Radargram from the GPR survey of the beach

5.8 Conclusions

The chapter reviewed several established techniques used to determine radar wave velocity within various materials. Each technique has its advantages and disadvantages and usage will depend on the accessibility around the object under investigation, its geometry, the

required accuracy, the time and manpower available, and the amount of physical interference with the structure that is acceptable.

A new semi-intrusive method is proposed which involves the insertion of a metal bar into the object under investigation, thus enabling the impulse radar velocity of the material under investigation to be readily interpreted from the radargram. The series of GPR simulations carried out in two and three dimensions using an FDTD GPR model produced results with errors of less than 10%. However, it was noted that these errors could be reduced if more sophisticated methods of regression analysis were used.

Several experiments were carried out in the laboratory. Initial experiments were carried out to find the optimum insertion angle of the bar, this was found to be between 22° and 26°. Additional experiments investigated how accurately the radar velocities could be determined when two and three-layer models were used. It was found that there was a good correlation between the velocities determined using the transmission method and those using the new method.

Finally, the new method was tested in the field. The aim was to determine how many different layers of sand could be identified. A metal bar was inserted into the sand and it could be seen from the radargram that there were two distinct velocities. The top layer had a velocity of 0.23m/ns, indicating a very dry layer of sand, and the bottom layer was 0.11m/ns, indicating damp sand.

This new method provides a quick, readily interpreted and practical tool for GPR operators to use. However, it is confined to shallow depths due to the limited depth of penetration of the metal bar.

Chapter 6

Design and testing of a radar trailer

6. Introduction

The longitudinal profile of a pavement is an important measurement which provides information on the ride quality for vehicles. There are several techniques available for carrying out this measurement, varying from high-speed vehicle-based profilers, using ultrasonic, laser or optical measuring systems, to a hand-held dipstick. The aim of this project was to use GPR to measure the longitudinal profile of the surface and subsurface layers on pavements. A trailer was designed and built to carry four GPR antennas; three to calculate the surface profile with the fourth to examine the sub-layers of the road. Surface profile measurements with GPR show good comparisons to the actual profile determined by traditional surveying techniques.

6.1 Aims of research

This research project is designed to supplement work carried out by Collop (Collop, 1994) on whole-life pavement performance model (WLPPM). Several assumptions were used in producing his model (see section 2.5.7) one of these assumptions stated that:

"The asphalt layer thickness profile is uncorrelated with the pavement surface profile."

The main aim of this research is to test whether or not this assumption is correct.

A trailer was proposed to carry out longitudinal profiling of the surface and subsurface layers on the near side of pavements using GPR. A GSSI Sir 10A+ radar system was used to measure the profiles of the surface and sub-surface layers. This is a digital system capable of real time measurements from four separate radar antennas. Tests were carried out on in-service roads around Edinburgh enabling the correlation between the surface and sub-

surface layers to be obtained. These tests examined whether or not the profile on the surface of the road propagates through to other layers or is localised effecting only the top layer (Figure 6.1).

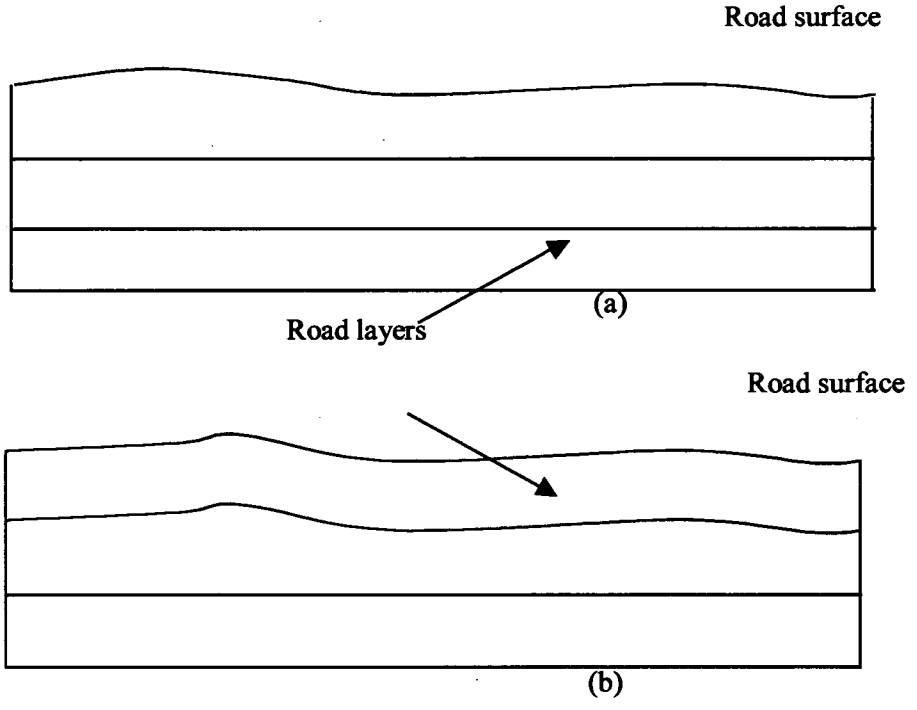

Figure 6.1: Diagrammatic presentation of flexible pavements showing (a) Localised profile only effecting the top layer (b) Profile effecting two layers

6.2 Design Concept

Calculating the surface profile of a pavement using GPR antennas requires them to be suspended over the pavement surface, whereas the sub-surface layer determination requires antennas to be coupled to the surface. Ideally the more antennas that can be used to take measurements the more accurate the results, but, due to the limitations of the equipment a maximum of four antennas can be used. These antennas must be placed in a straight line to enable accurate correlation of the measured profiles.

Three antennas were used to calculate the surface profile with the fourth antenna being used to measure the profile of a layer beneath the surface.

6.3 Initial experiments

There are several techniques available for measuring longitudinal profiles; the most sophisticated use lasers. Laser profilers are usually mounted onto a vehicle. Measurements are then taken of the actual profile of the roadway in each wheel path. The profile of the road is obtained by analysing the data supplied by the lasers using a computer inside the vehicle (see chapter 2). Patterson (Patterson, 1986) found that the unevenness of a pavement was due to four main factors:

- Traffic loading
- Surface distress
- Structural conditions
- Climate conditions

The majority of the unevenness found in the UK is due to traffic loads, especially Heavy Goods Vehicles (HGVs). Theoretical and experimental investigations of dynamic axle loads (Cole, 1990) have shown that two different frequency ranges can be identified on HGVs:

- 1.5-4 Hz: Sprung mass rigid body vibration (Vibration of main vehicle body).
- 8-15 Hz: Unsprung mass rigid body vibration (Vibration of the axles and wheels, sometimes referred to as "wheel hop").

The pavement is subjected to the varying force due to the vehicle bouncing at a certain frequency. Therefore, over time the pavement may start to replicate the frequency of the vehicles.

If we know the bounce frequency and velocity of the vehicle then the wavelengths can be found by using the equation:

$$v = \lambda f \qquad (6.1)$$

where: v = Vehicle speed (m/s)

f = Vehicle bounce frequency (Hz)

λ = Wavelength (m)

Lowest frequency of HGV: $f \approx 2$Hz	*Highest frequency* of HGV: $f \approx 15$Hz
Fastest speed of 70mph = 31.1m/s	Lowest speed of 35mph = 15.6m/s
Longest wavelength $\lambda = 31.1/2 \approx$ **15m**	Smallest wavelength $\lambda = 15.6/15 \approx$ **1m**

Table 6.1: Wavelengths of interest along a pavement surface

Using equation 6.1 the profile wavelengths of interest along the surface of the pavement are approximately between 1m and 15m as derived in Table 6.1.

Several initial experiments were carried out to optimise the use of GPR in analysing the surface and sub-surface layers.

6.3.1 Determination of layer thicknesses

The first experiment was designed to determine how easily the thickness of layers within the pavement could be detected using GPR (Gordon *et al.*, 1998). These tests are discussed in chapter 4. The results from these tests showed that some difficulties are encountered when interpreting the recorded signals. The received signal is made up of several different pulses which must be taken into consideration when interpreting the results (Figure 6.2).

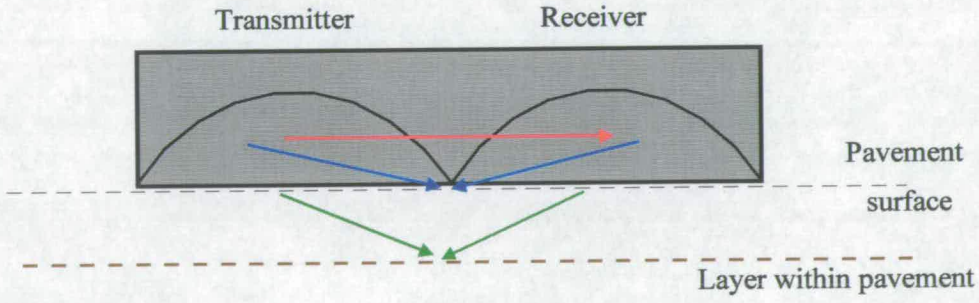

Figure 6.2: Different signals which are detected by a antenna when it is coupled with the ground

The different signals are:

- Signal leakage from the transmitter to the receiver.
- The reflected pulse from the surface of the pavement.

- The reflected pulses from the layers within the pavement layer.

Antennas which have a higher central frequency will have an improved vertical resolution, resulting in thinner pavement layers being identified. However, the downside of this is the reduction of the depth of penetration.

6.3.2 Optimum height of radar from pavement surface

The next experiment was designed to determine the optimum height an antenna could be suspended from the pavement in order to receive a clear reflection signal. Figure 6.3 shows the experimental apparatus used to find this optimum height. A GSSI 900MHz antenna was used to pick up the reflection signals from the pavement surface. It should be noted that the height of the radar antenna from the pavement block is approximately half the radar path length.

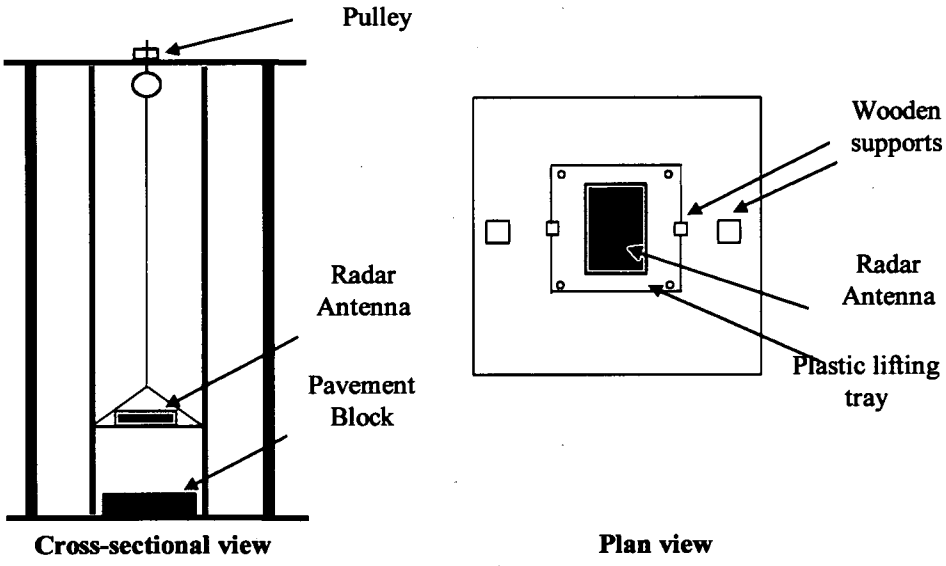

Figure 6.3: Lifting rig used to determine the optimum height

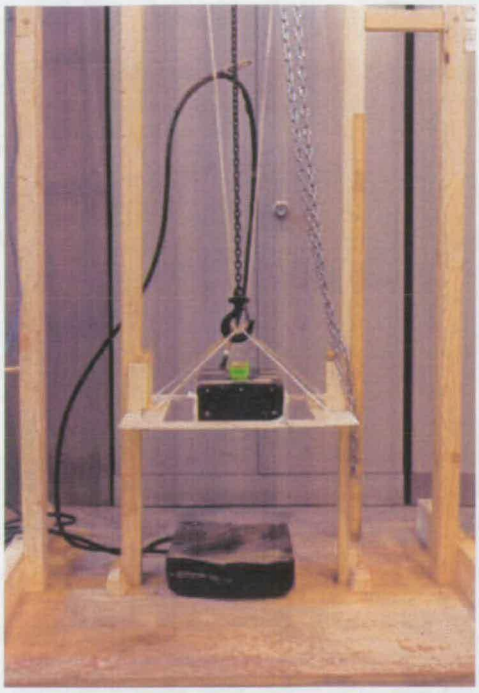

Figure 6.4: Photograph of lifting rig

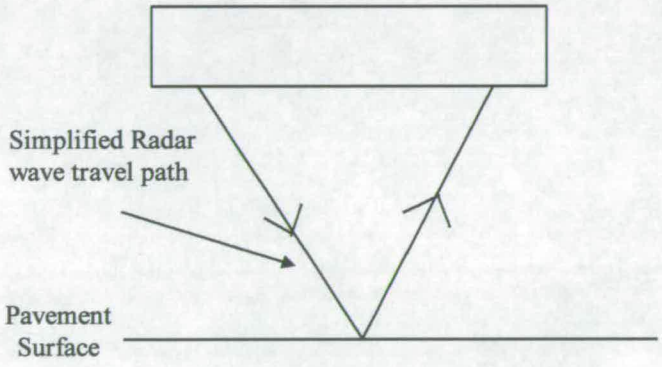

Figure 6.5: Simplified radar wave travel path

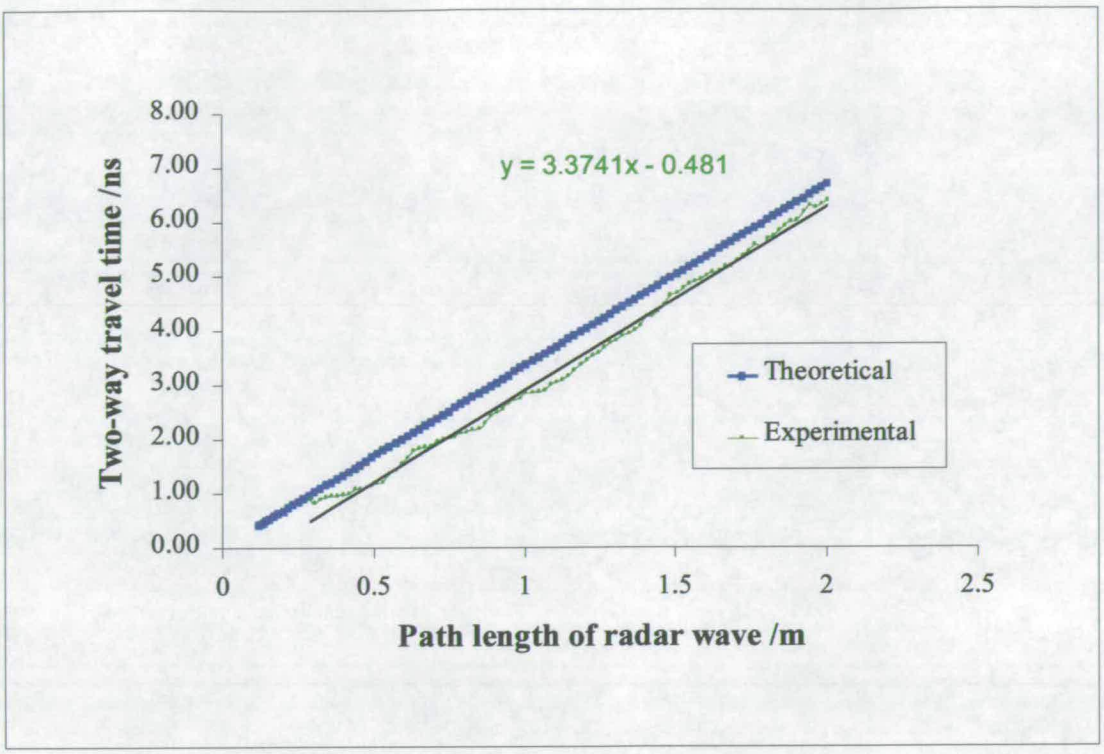

Figure 6.6: A graph showing the two-way travel time obtained from a 900MHz antenna

The results on Figure 6.6 show that the two-way travel times in this experiment are less than the theoretical values. The reason for this is that a time constant is added onto the reflection signal by the manufacturers to compensate for the time loss caused by the signal travelling through the cables. However, this added value has overcompensated for the loss in time.

In order to determine the amount of time that has been overcompensated, a least squares fit is used on the experimental results. The reciprocal of the gradient of the best-fit line should be equal to the speed of light in a vacuum. This was found to be approximately 0.3m/ns which is correct. The intercept of this line represents the overcompensated time. Figure 6.7 shows the result of adding on the compensated time.

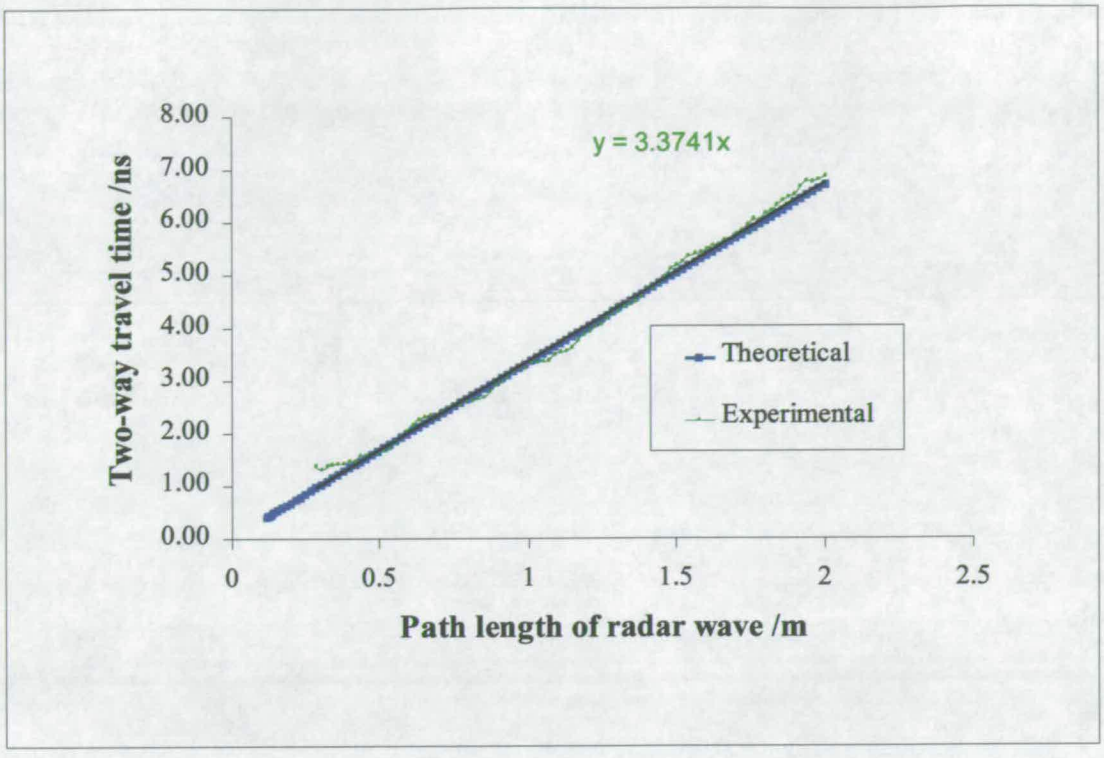

Figure 6.7: A graph showing the adjusted two-way travel time obtained from a 900MHz antenna

The result from this experiment showed that a clear reflection from the surface of the pavement sample could be obtained when the radar antenna was at a height of between 13cm and 38cm. This is approximately half the path length of the radar wave. A height between 25 and 30cm gave the best result. Below 13cm, the reflected signal was mixed up with the transmit pulse and the reflected pulse from the layers within the pavement block (see section 6.3.1). Above 38cm, the reflected pulse has a small amplitude, making it difficult to identify. This information was used in the design of a truss, attached to a trailer, which would suspend three 900MHz antennas over the wheel path, on the near side of the road.

6.3.3 Calculating the spacing between each antenna

Calculating the ideal spacing between the antennas will depend on the method used to calculate the profile of the surface of the pavement. Figure 6.8 shows one of the preliminary proposals for obtaining the profile.

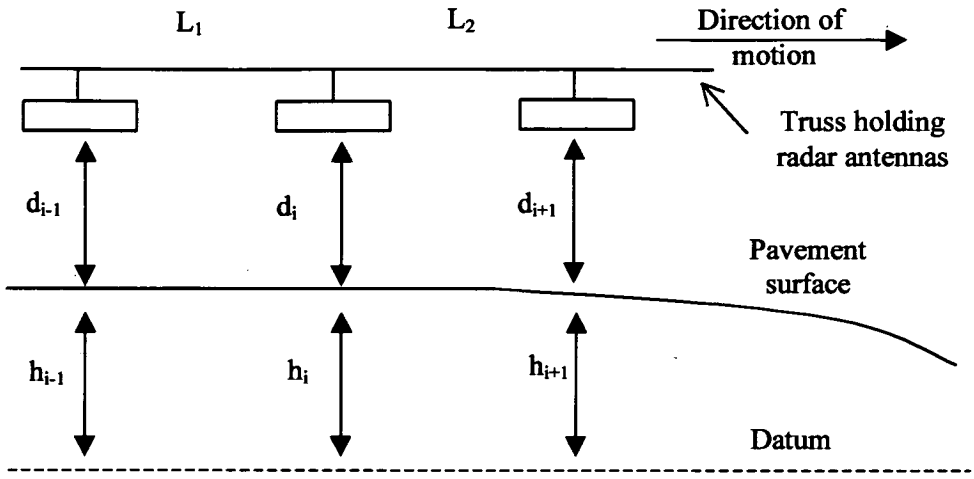

$$(d_{i-1}+h_{i-1})+(d_{i+1}+h_{i+1})=2(d_i+h_i)$$
$$\therefore h_{i+1}=2d_i-d_{i-1}+2h_i-h_{i-1}-d_{i+1}$$

Figure 6.8: Preliminary proposal for obtaining the surface profile

The following assumptions would have to be made to use this method:

- The beam is completely rigid (no vertical movement).
- The sensors make measurements at precisely the same points along the profile.

The main problem with this method is that it is very difficult to ensure that the radar antennas take measurements at exactly the same position read by the previous one. If this was not achieved the method was found to produce large errors in the recreated profile. This same problem was encountered when using lasers (see section 2.4).

The method which was chosen uses the height of the antennas to obtain curvature readings along the pavement. These are then used to recreate the surface profile.

Curvature theory

The amount a curve "bends" at each point is a measure of its curvature at that point, i.e. the rate of change of direction of a curve with respect to distance along the curve. A straight line has zero curvature whereas a circle has a uniform curvature (which will increase with a decreasing radius).

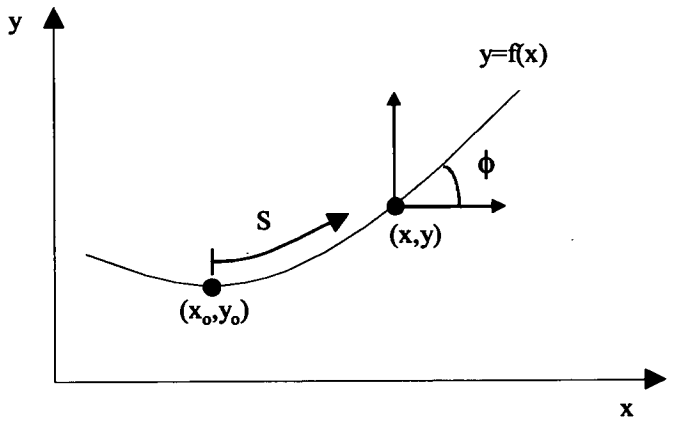

Figure 6.9: The rate a curve bends at (x,y) is $\kappa = \frac{d\phi}{ds}$

Arc length between x_o and x is

$$s = \int_{x_o}^{x} \sqrt{1 + f'(x)^2}\, dx$$

$\tan\phi = \frac{dy}{dx} = f'(x)$, at any point (x, y)

$\therefore \quad \phi = b + \tan^{-1} f'(x)$

where the constant *b* is included to take into consideration the fact that ϕ may not fall in the principal value range of the inverse tangent function.

$$\text{Curvature} = \frac{d\phi}{ds} = \frac{d\phi}{dx} \bullet \frac{dx}{ds}$$

$$\frac{d\phi}{dx} = \frac{1}{1 + (f'(x))^2} \cdot f''(x)$$

and

$$\frac{ds}{dx} = \sqrt{1 + (f'(x))^2}$$

$$\text{Curvature}(\kappa) = \left|\frac{d\phi}{ds}\right| = \left|\frac{f''(x)}{\left[1 + (f'(x))^2\right]^{\frac{3}{2}}}\right| = \left|\frac{\frac{d^2y}{dx^2}}{\left[1 + \left(\frac{dy}{dx}\right)^2\right]^{\frac{3}{2}}}\right| \qquad (6.2)$$

The value of $d\phi/ds$ will be positive when the curve is bending to the left while travelling along the increasing s direction and is negative when it is bending to the right. The value of the curvature, κ, will be zero for a straight line as ϕ remains constant.

The reciprocal of the curvature has units of length and is called the *radius of curvature.* If a curve has curvature $\kappa \neq 0$ at a certain point, then the radius of curvature of the curve at this point is $\rho=1/\kappa$. This theory can be found in many mathematic books such as "Calculus with Analytic Geometry" by Fraleigh (Fraleigh, 1985).

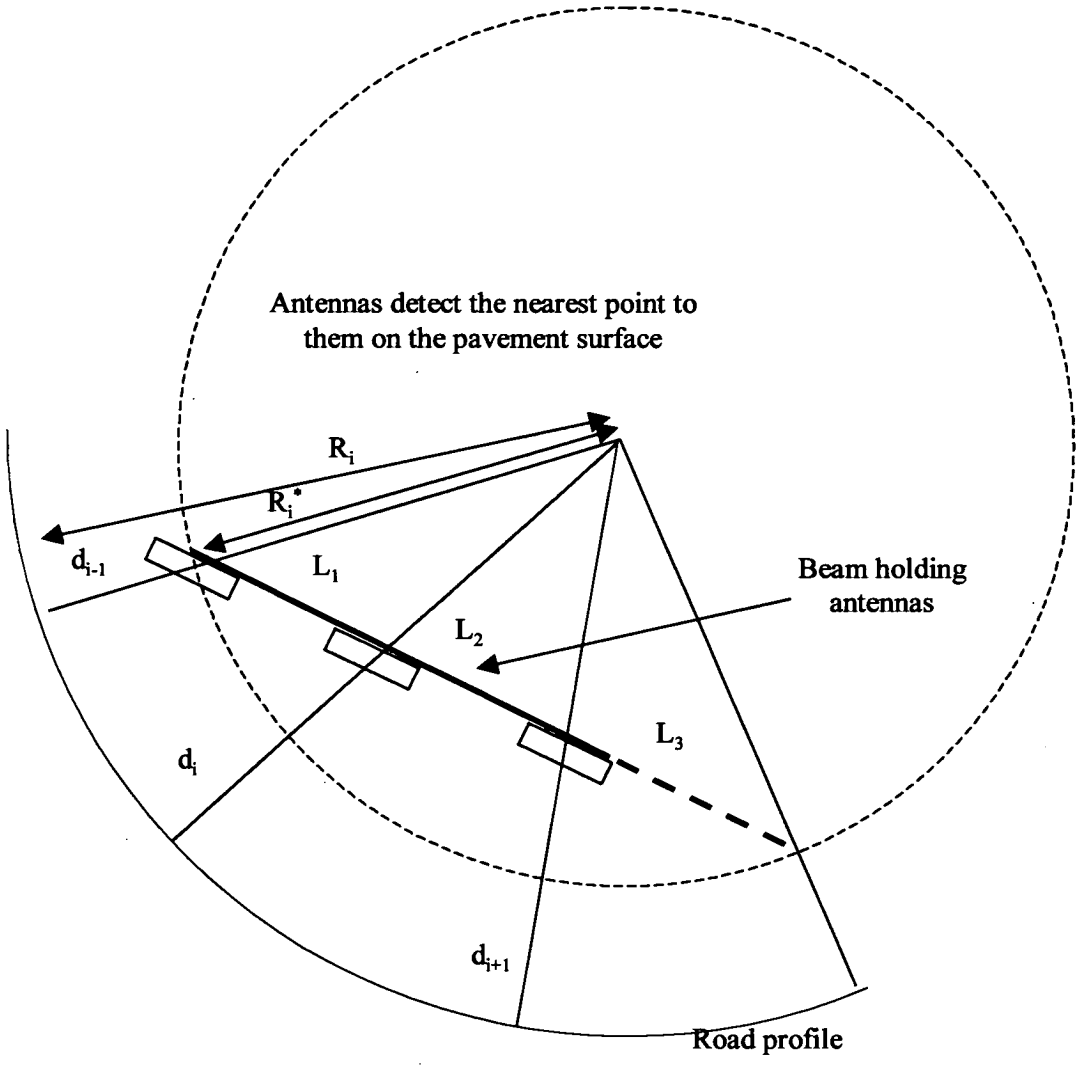

Figure 6.10: Radius of curvature calculation

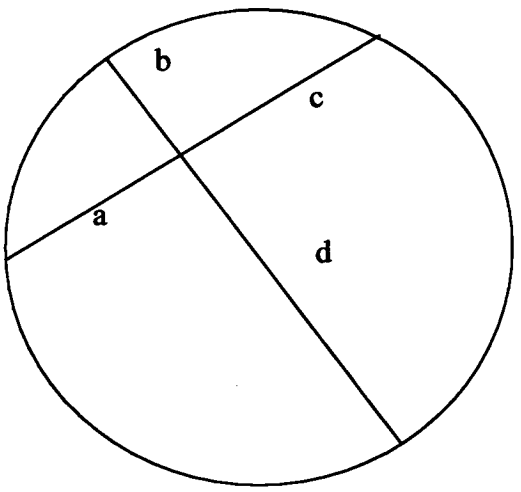

Figure 6.11: Circle geometry, a well known Euclidean theorem

From Figure 6.10:

$$d_i^* = d_i - d_{i-1}$$
$$d_{i+1}^* = d_{i+1} - d_{i-1}$$
$$R_i^* = R_i - d_{i-1}$$

From circle geometry (Figure 6.11):

$$d_i^*\left(2R_i^* - d_i^*\right) = L_1(L_2 + L_3) \qquad (1)$$
$$d_{i+1}^*\left(2R_i^* - d_{i+1}^*\right) = L_3(L_1 + L_2) \qquad (2)$$
$$\text{From (2) } L_3 = \frac{d_{i+1}^*\left(2R_i^* - d_{i+1}^*\right)}{(L_2 + L_3)} \qquad (3)$$

subst.(3) into (1)

$$d_i^*\left(2R_i^* - d_i^*\right) = L_1\left(L_2 + \frac{d_{i+1}^*\left(2R^* - d_{i+1}^*\right)}{(L_2 + L_3)}\right) \qquad (4)$$

$$2R_i = \frac{L_1L_2(L_1 + L_2) + (d_i - d_{i-1})^2(L_1 + L_2) - (d_{i+1} + d_{i-1})^2 L_1}{(d_i - d_{i-1})(L_1 + L_2) - L_1(d_{i+1} - d_{i-1})} + 2d_{i-1}$$

Radius of curvature:

$$R = \frac{1}{2}\left(\frac{L_1 L_2 (L_1 + L_2) + d_i^2 L_1 + d_i^2 L_2 - d_{i+1}{}^2 L_1 - d_{i-1}{}^2 L_2}{d_i L_1 + d_i L_2 - d_{i-1} L_2 - d_{i+1} L_1} \right) \qquad (6.3)$$

$$\therefore \kappa = \left. \frac{d\phi}{ds} \right|_i = \frac{1}{R_i}$$

$$\phi_i = \int \frac{1}{R_i} ds + \text{constant} \qquad (6.4)$$

Note: The constant will be the gradient of the pavement at the start of the survey.

However,

$$\tan \phi_i = \left. \frac{dy}{dx} \right|_{X_i}$$

$$y = \int \tan\phi \, dx \qquad (6.5)$$

The arc length :

$$ds = \sqrt{1 + \tan^2 \phi} \; dx$$

$$\frac{ds}{dx} = \sqrt{1 + \tan^2 \phi}$$

$$x = \int \frac{1}{\sqrt{1 + \tan^2 \phi}} ds + \text{constant} \qquad (6.6)$$

The height of the radar antennas from the road surface (d_{i-1},di and d_{i+1},) and the spacing between the antennas (L_1 and L_2) are fed into equation 6.3 to find the values of the radius of curvature along the pavement. Equations 6.4, 6.5 and 6.6 are evaluated using Simpson's rule. A graph of y against x can be plotted; this is the radar trailer's attempt to plot the surface profile of the pavement.

Mapping the profile of a road using the curvature technique described above requires calculations to be carried out to find which spacing values of the antennas can most accurately map the profile. The spacing must ensure that wavelengths between 1m and 15m can be mapped. The value of L_1 and L_2 must be determined in order to cover this range of wavelengths.

In order to find the correct spacing values, two simulations were carried out. The first simulation used a sine wave to represent an ideal road surface. An analytical method was used to calculate the curvature along this road. Noise was then introduced along the sine wave and a computer approximation calculated the curvature.

Analytical method

$y = \sin(\gamma x)$

where: γ = wavenumber (radians/m)

$$\frac{dy}{dx} = \gamma \cos \gamma x$$

$$\frac{d^2y}{dx^2} = -\gamma^2 \sin \gamma x$$

$$\therefore \text{(From equation 6.2)}\ k_1 = \frac{-\gamma^2 \sin \gamma x}{\left[1 + \gamma^2 \cos^2 \gamma x\right]^{\frac{3}{2}}}$$

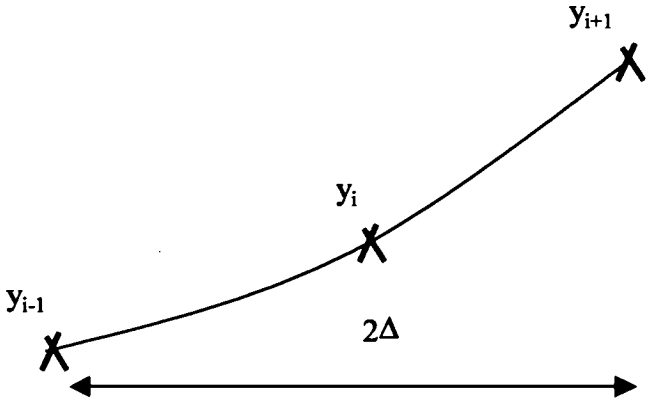

Figure 6.12: Points on a simulated noisy sine wave

Δ = spacing intervals along the road

$$\frac{dy}{dx} = \frac{y_{i+1} - y_{i-1}}{2\Delta}$$

$$\frac{d^2y}{dx^2} = \frac{\frac{y_{i+1} - y_i}{\Delta} - \frac{y_i - y_{i-1}}{\Delta}}{\Delta}$$

$$\therefore \frac{d^2y}{dx^2} = \frac{y_{i+1} - 2y_i + y_{i-1}}{\Delta^2}$$

(From equation 6.2) $$k_2 = \frac{\frac{y_{i+1} - 2y_i + y_{i-1}}{\Delta^2}}{\left[1 + \left(\frac{y_{i+1} - y_{i-1}}{2\Delta}\right)^2\right]^{\frac{3}{2}}}$$

The average percentage error between k_1 and k_2 is calculated using the equation below:

$$\text{Average percentage error} = \frac{\int (k_1 - k_2)^2}{\int k_1^2} \times 100\% \qquad (6.7)$$

Figure 6.13 shows how the percentage error between k_1 and k_2 is effected as the value of Δ/λ (antenna spacing/wavelength) is increased for different noise ratios. The spacing of the antennas can be found by choosing the minimum value on one of the noise ratio lines on

(Figure 6.13). The correct line was chosen by calculating the noise ratio for 1 and 15m wavelengths on a simulated "good" road.

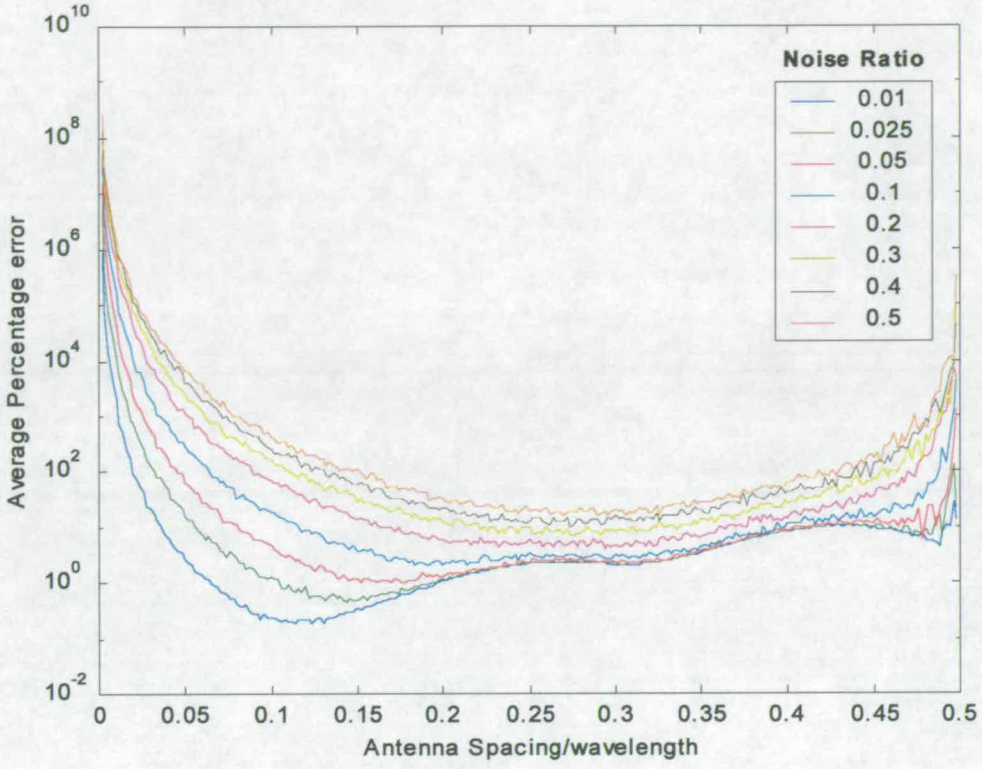

Figure 6.13: A graph showing how the percentage error varies with increased antenna spacing/wavelength for different noise ratios

A simulated "good" road

The simulation of a one-dimensional random "good" road profile was generated from a series of coefficients derived from spectral density values (Dodds and Robson, 1973). Dodds and Robson proposed that if a road was considered a homogenous, isotropic random process with a Gaussian distribution, a single track PSD estimate could be used to generate a complete description of that road. The slope of the PSD was a function of the root-mean-square (RMS) (roughness) of the road. This analysis involved surveying several different types of road surfaces for which surface undulations were measured.

A set of random phase angles, uniformly distributed between 0 and 2π were applied to the coefficients of the spectral density. In order to obtain the equally-spaced spot heights, z_r,

along the profile, the inverse discrete Fourier transform of the spectral coefficients must be worked out (see Cebon and Newland, 1983; Cebon, 1985; Newland, 1993).

$$z_r = \sum_{k=0}^{N-1} \sqrt{s_k} e^{i\left[\theta_k + \frac{2\pi kr}{N}\right]} \quad r = 0,1,2,\ldots,(N-1) \qquad (6.8)$$

where $s_k = \frac{2\pi}{N\delta} S(\gamma_k)$

N = Number of samples

$S(\gamma_k)$ = Desired spectral density

$\gamma_k = \frac{k}{N\delta}$ = the spatial spectral frequency (wavenumber (cycles/m))

δ = the distance interval between successive ordinates along the surface profile

θ_k = a set of independent random phase angles uniformly distributed between 0 and 2π

$$S(\gamma_k) = S(\gamma_0)\left|\frac{\gamma}{\gamma_0}\right|^{-n_1} \text{ for } |\gamma| \le \gamma_0$$

$$S(\gamma_k) = S(\gamma_0)\left|\frac{\gamma}{\gamma_0}\right|^{-n_2} \text{ for } |\gamma| \ge \gamma_0$$

$n_1 = 2.0$ (constant)

$n_2 = 1.5$ (constant)

$S(\gamma_0)$: A constant dependent on roughness category

	Road Class	**$S(\gamma_o)$ x10^{-6} m^3/cycle**
(i)	Very good	2-8
(ii)	good	8-32
(iii)	average	32-128
(iv)	poor	128-512
(v)	very poor	512-2048

Table 6.2: Values of S(γo) dependent on roughness category

(note: γ_o is $1/2\pi$ cycles/m)

Dodds and Robson gave different road types a different values of $S(\gamma_0)$, shown in Table 6.2. Type (i) or (ii) are generally motorways, (iii) or (iv) are principal roads and (iv) or (v) are minor roads.

Robson (Robson, 1979) revised the values of n_1 and n_2 and said they should be 50% larger. He also suggested that a road could be represented by a single spectrum of the form:

$$S(\gamma) = C\left|\frac{\gamma}{\gamma_o}\right|^{-w} \qquad (6.9)$$

where: w = 2.5, and values of C as shown in Table 6.3.

Road Class	**C x10^{-8} m$^{0.5}$cycle$^{1.5}$**
Motorway	3-50
Principal Road	3-800
Minor Road	3-3000

Table 6.3: Values of 'C' for a single slope spectrum

Equation 6.9 was used to simulate the "good" road with the original values of n_1 and n_2, as the revised values had not been found by the author until after the design of the trailer.

The amplitude for wavelengths between 1 and 15m along the simulated road were found. The ratio of the accuracy of an antenna to the amplitude was found for different wavelengths.

$$\text{Noise ratio} = \frac{\text{Accuracy of antenna}}{\text{Amplitude at a certain wavelength}} \qquad (6.10)$$

	Amplitude	Accuracy of antenna	Noise ratio
1m wavelengths	0.01m	0.005m	0.5
15m wavelengths	0.04m	0.005m	0.125

Table 6.4: Noise ratio calculated from simulation of "good" road

- *The spacing value for mapping 15m wavelengths ≈ 3m.*

However, the antenna spacing values used in the trailer were 1.4m and 3m (Figure 6.14) due to the position of the axle and limits on the maximum size that a trailer can be by law (section 6.4).

The minimum spacing between the antennas was 0.5m due to the interference of the cables.

Δ/λ =0.28 (This value represents the position of minimum value on the 0.5 noise ratio line (Figure 6.13))

$\Delta = 0.5$m

$\therefore$ The minimum wavelength (λ) = 0.5/0.28 ≈ 1.8m

- *Therefore the smallest wavelengths that could be physically measured ≈1.8m.*

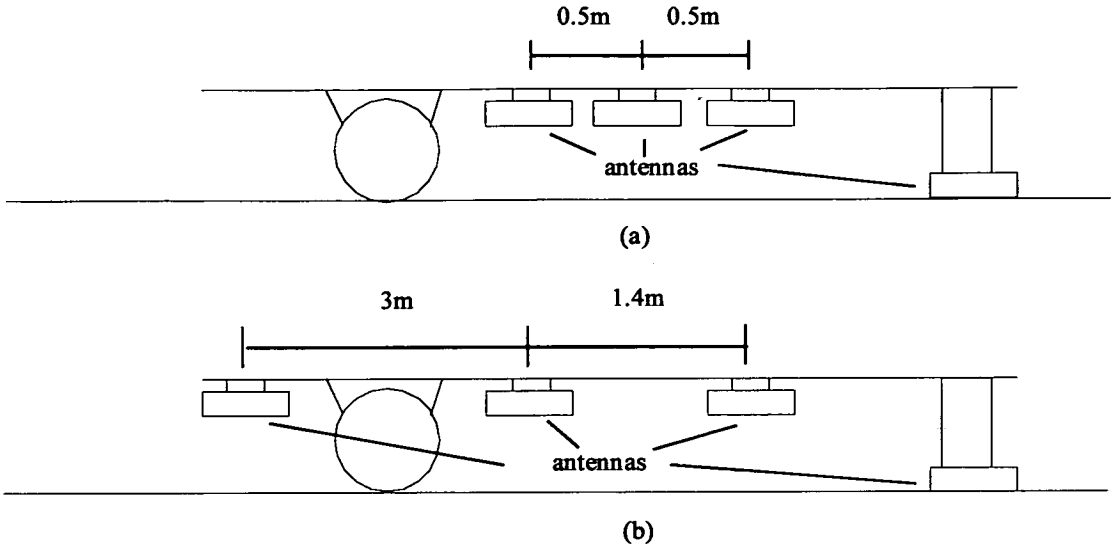

Figure 6.14: The spacing of the antennas for (a) Short wavelengths (b) Long wavelengths

6.4 Truss and trailer design

The trailer would carry four antennas along the pavement; three suspended in the air with the fourth one coupled to the ground.

In order to design and build a trailer which was road-worthy the following regulations had to be followed. These are based on the current laws in Great Britain which can be found in "The complete towing guide for trailer and caravan owners nationwide" (Anon, 1997). The following laws are based on a trailer having two wheels and being towed by a vehicle (private):

- The maximum length should not exceed 7m (excluding the drawbar).
- The maximum width should not exceed 2.3m (this includes mudguards).
- Maximum load for unbraked trailers is 750kg.
- Secondary coupling must be used on unbraked trailers (usually a wire connecting the car to the trailer).
- The maximum weight of an unbraked trailer which can be towed by a vehicle (private) should be 50% of the vehicles kerb weight or 750kg, whichever is less.

A steel truss would be used to carry the radar antennas, it would be suspended on the near side of a long single-axle trailer. Below is a list of specifications which had to be met by the truss:

- The bottom of the antennas need to be between 25 and 30cm off the ground in order to pick up a clear reflection from the surface of the pavement (section 6.3.2).
- The steel frame of the truss must be above the antennas so that no reflections from the steel frame are picked up.
- The antennas must be placed far enough apart so that no reflections are obtained from other antenna cases (the minimum distance that the antennas could be apart was found to be 0.5m due to cable interference).
- The bars in the base of the truss need to be 30cm apart to fit the antennas between the sections.
- The height of the truss was 50cm as this would result in less deflection in the truss due to the increased cross-section, i.e. keeping it more rigid.
- The maximum allowed deflection of the truss was +/- 0.5mm.

The steel truss was designed using ABAQUS (finite element program), making sure each of the above design specifications were achieved. Two different loadcases would be carried by the truss, representing the position of the antennas to measure short and long wavelengths (see section 6.3.3). The steel radar truss, with the two loadcases, is shown on Figure 6.15. Figure 6.16 shows an example of how the truss deforms with loadcase 1.

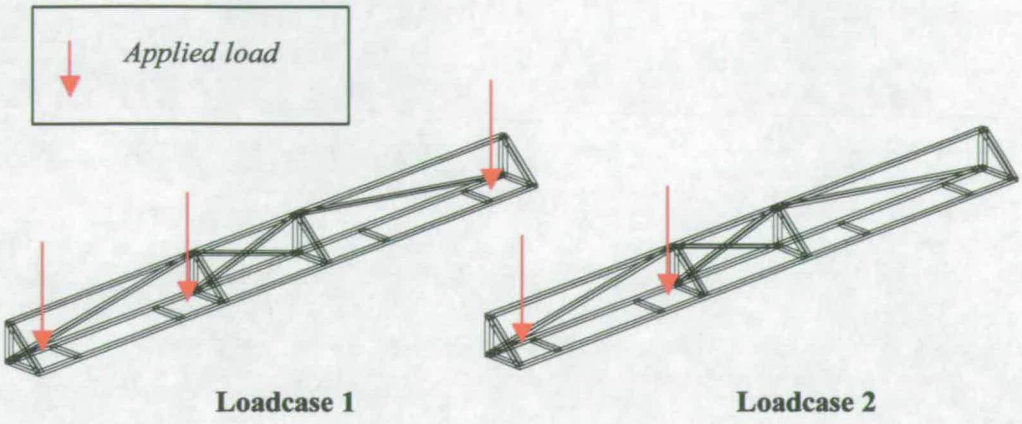

Figure 6.15: The two loadcases used by the truss

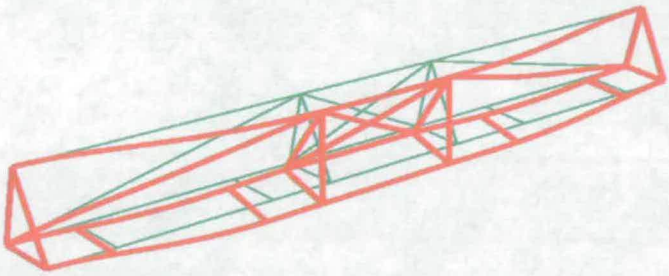

Figure 6.16: Deformation (red) of truss when loadcase 1 is applied (note: deformation has been magnified by 500)

The dynamic loading of the radar truss had to be considered in order to design a frame which was rigid enough to deflect by less than 0.5mm. Larger deflections than this would result in large errors in the curvature calculations. ABAQUS was programmed to work out the natural frequency of the truss. If the natural frequency was too low, i.e. could be reached by the trailer as it travelled along the pavement, then the truss would be redesigned. It should be noted that when the forced frequency, produced by the trailer interaction with the pavement roughness, equals the natural frequency of the truss, then resonance will occur. At the resonant frequency, the truss will produce its maximum deflection.

	Load case 1	Load case 2
Maximum displacement	0.34 mm	0.38 mm
Natural frequency (eigen mode 1)	15.38 Hz	15.38 Hz

Table 6.5: Natural frequency of truss produced by each loadcase

The frequency values indicate that the trailer would have to travel over 15 cycles (of the same period length) per second in order for its natural frequency to be reached. Therefore, a truss with these values is acceptable.

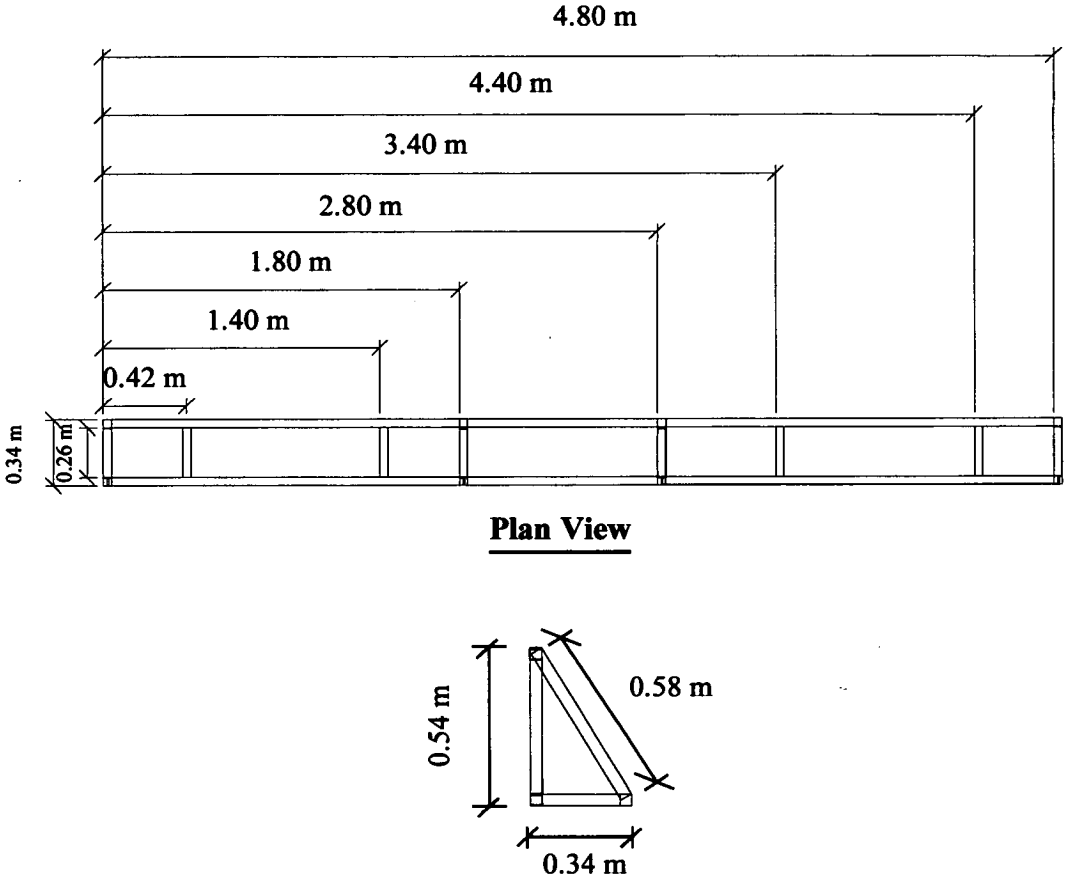

Figure 6.17: Dimensions of truss

Due to the small budget and the time limit it was decided that using the chassis of an old caravan would be the quickest way of building a trailer. A second-hand caravan was obtained and the top half was removed, leaving the bare chassis (Figure 6.18). The chassis was extended by cutting it into two parts and fitting it with new steel sections. A steel frame was welded to the chassis and planks of plywood were placed along it to stiffen up the frame (Figure 6.21). Steel straps were then placed at equal intervals along the top to prevent the wooden panels from flexing. The tow bar was reinforced and a new jockey wheel was attached.

Figure 6.18: Removal of the top half of the caravan

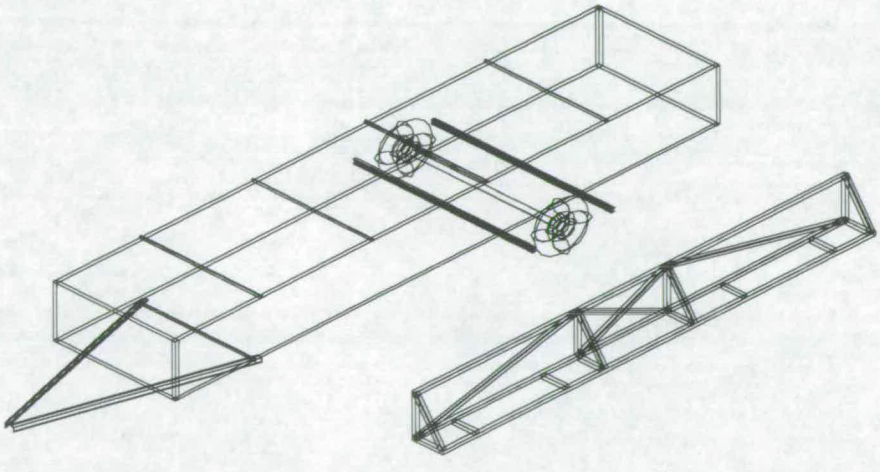

Figure 6.19: Sketch of how the trailer will look along side the truss

Figure 6.20: Chassis is cut and extended

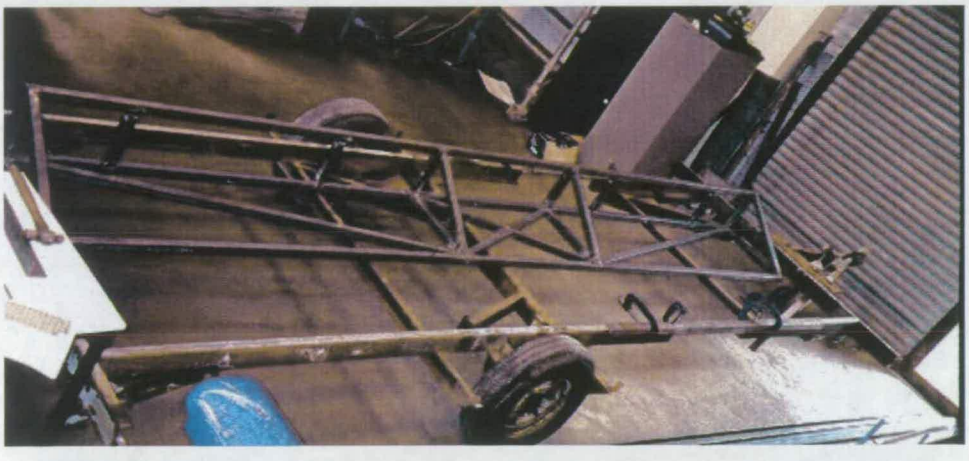

Figure 6.21: Photographs showing the chassis extended and new steel sections and sides fitted

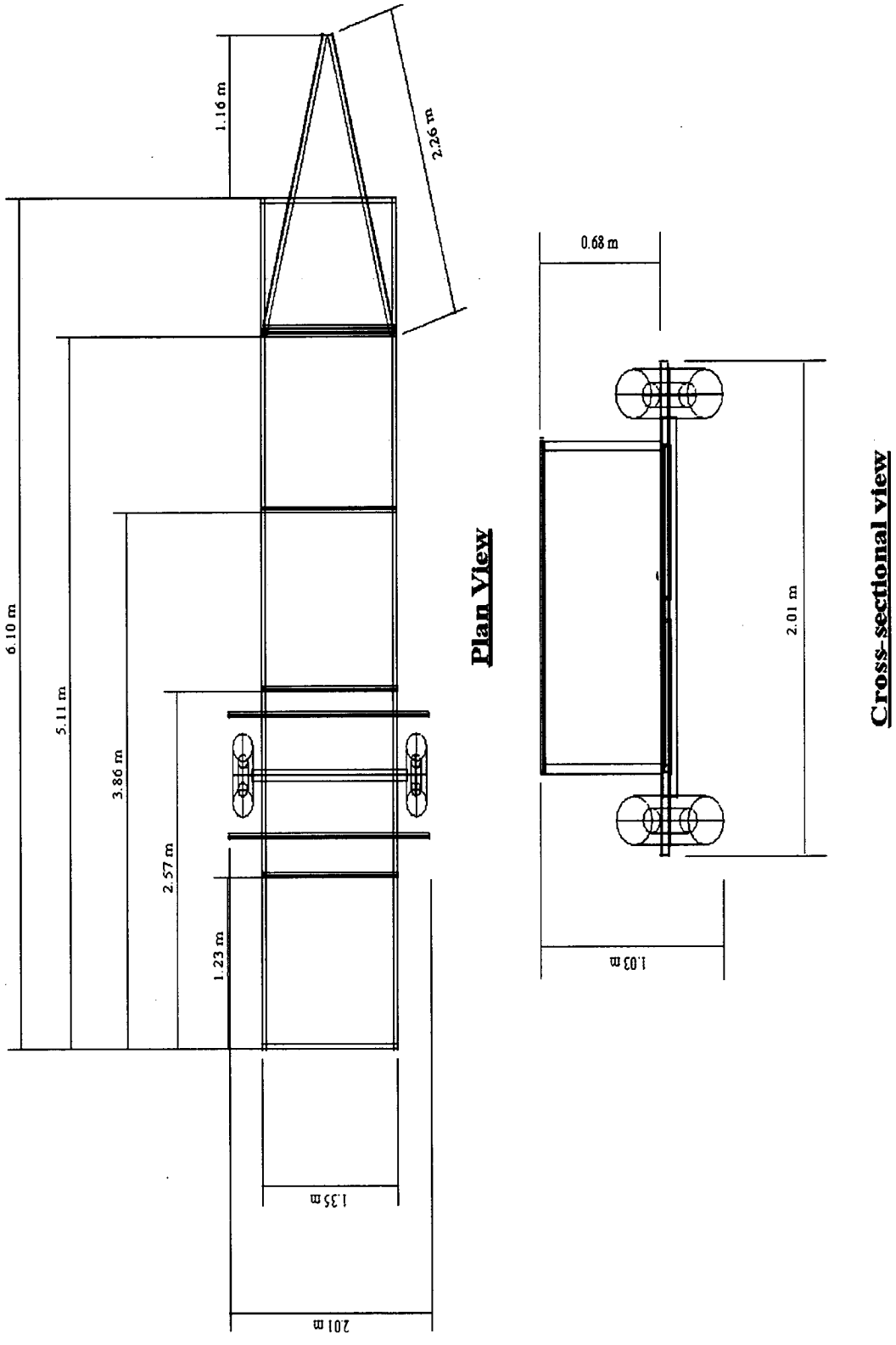

Figure 6.22: Trailer dimensions

The trailer was partially floored behind the axle, which has two purposes:

1. To enable sand bags to be placed on the right side of the trailer which counteracts the weight of the steel radar truss hanging on the left side of the trailer.

2. To reduce the weight load being applied to the towing vehicle through the tow bar.

All the wiring of the trailer was placed in conduits in order to keep all the electronics together in a waterproof casing.

Figure 6.23: Finished trailer

Wooden holders had to be designed and built to carry the radar antennas on the truss. Wood was used as it has little or no interference on the radar signal. Two types of holders were built. The 900MHz antennas were fitted to the truss using a holder which allowed only the vertical height of the antennas to be adjusted while keeping the antenna parallel to the truss (Figure 6.24(c)). The 1.5GHz antenna was placed in the front holder as shown in Figure 6.24(b). Figure 6.25 shows how this holder works. All the antennas were kept in a straight line.

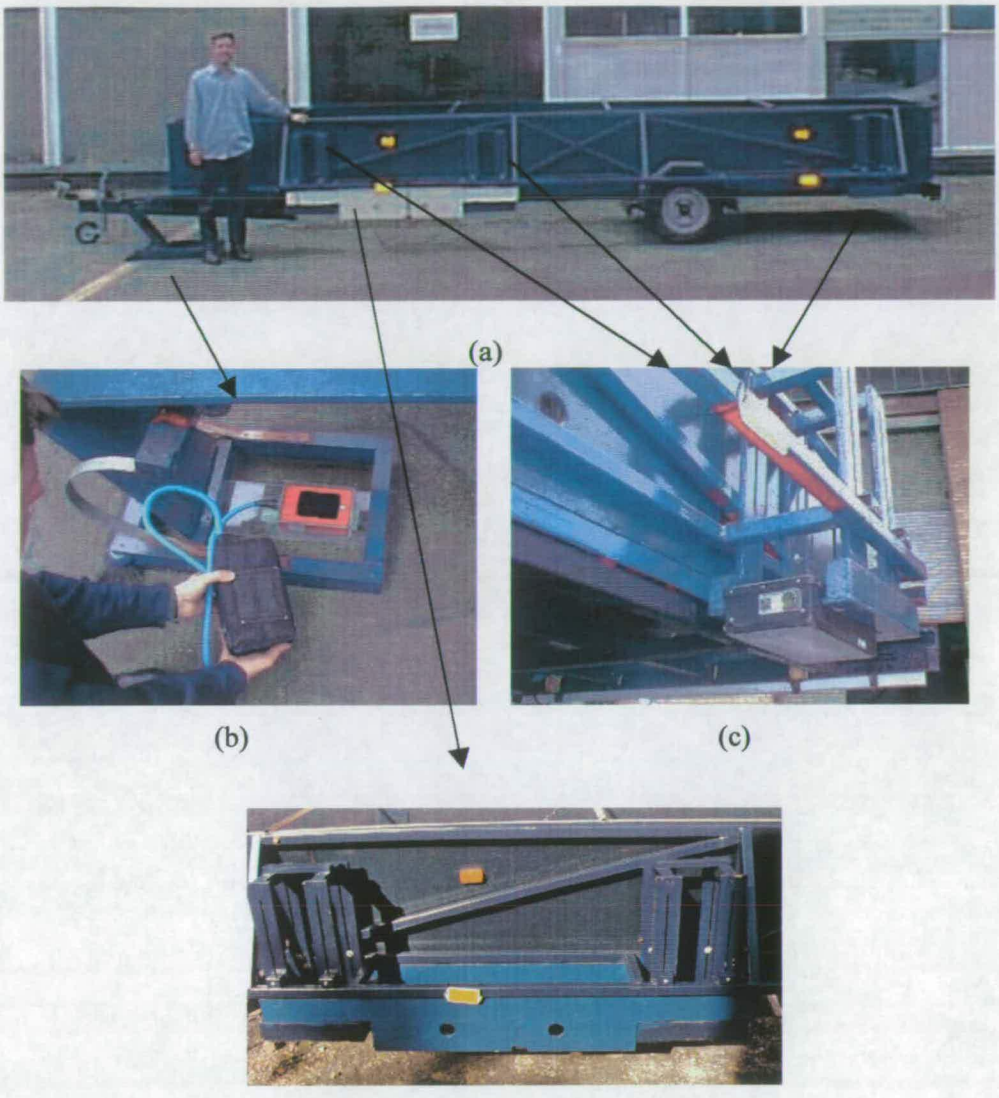

Figure 6.24: (a) The truss is fitted on the left side of the trailer (b)Wooden holder used to carry 1.5GHz antennas (c) Wooden holders used to fix the 900MHz antennas to the truss (d) Wooden holder used to position the antennas 0.5m apart (short wavelength set-up)

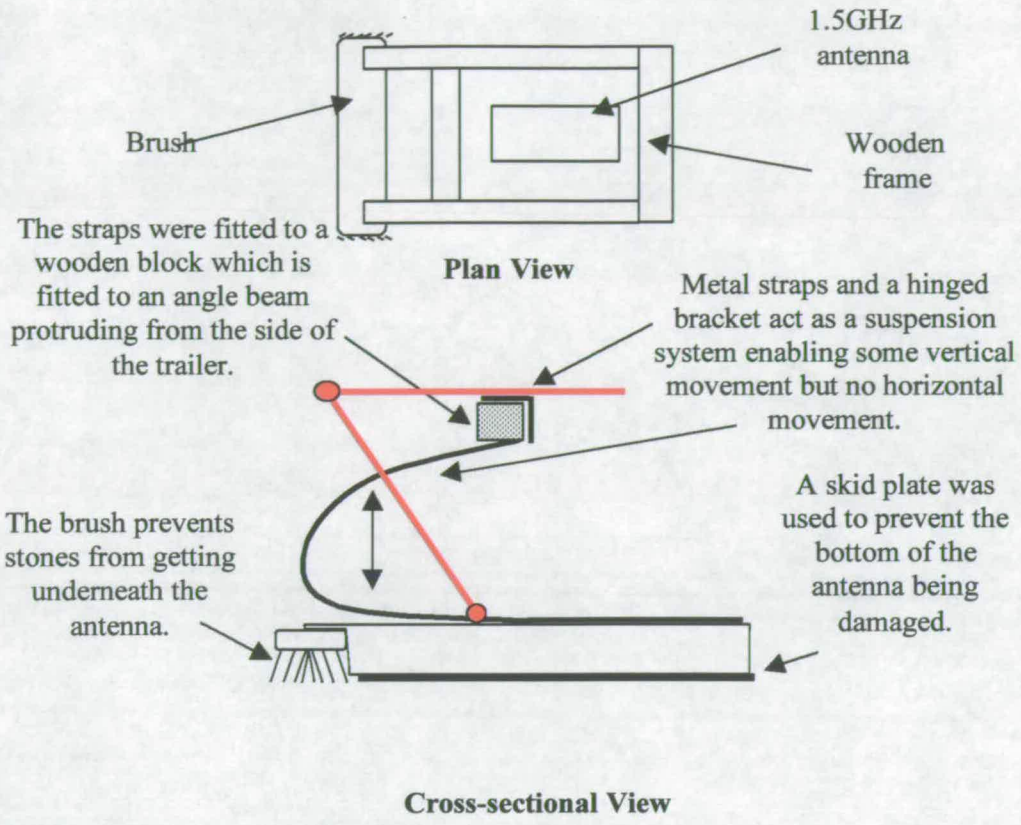

Figure 6.25: Sketch of the front holder

6.5 Radar system set-up

6.5.1 Survey wheel set-up

The rate at which scan lines are produced is controlled by a survey wheel. Several things must be taken into consideration when using a survey wheel in order to achieve accurate measurements and obtain the correct horizontal resolution.

The following criteria must be met when using the survey wheel (see Figure 6.26):

- Scans/sec > Scans/m * velocity of traverse
- Scans/m < spatial survey rate

The spatial survey rate is the number of scan lines emitted by the antennas in one metre if it is moved at a constant velocity. The main factors that controls the spatial survey rate are the ability of the radar system to transmit these scan lines (transmit rate) and the speed at which the antenna will move along the surface of the material.

6.5.2 Sampling interval

The time interval between sample points along a scan line is known as the temporal sampling interval, whereas the spacing between discrete radar scan lines is known as the spatial sampling interval.

Annan (Annan, 1997) noted that the temporal sampling interval should be at least six times the central frequency of the antennas to obtain a good survey.

$$t = \frac{1000}{6 f_c} \tag{6.11}$$

where: t = Maximum sampling interval (ns)

f_c = Central frequency of antenna (MHz)

The spatial sampling interval is dependent on the wavelengths of interest along the survey. The spatial sampling interval should be at most half the smallest wavelength, i.e. the Nyquist frequency. In the radar system this is controlled by setting the scans per meter (scans/m), however, as discussed in section 6.5.1, this is controlled by several factors.

Criteria 1: Scans/sec>scans/unit * velocity of traverse

Velocity of trailer (mph) =	30
Velocity of trailer (km/h) =	48
Velocity of trailer (m/s) =	13.33
Max scans/sec =	28

Criteria 2: Scans/unit <spatial survey rate

Transmit Rate =	100	kHz
Period(Time taken to do one sample per scan) =	0.00001	sec
Samples per scan =	512	
Time taken for 1 scan	0.0051	sec
Wt 4 antennas	0.0205	sec
Processing time (ms) =	5.1200	wt 1 antenna
Processing time (ms) =	20.4800	wt 4 antenna
Spatial survey (m/scan) =	0.0683	wt 1 antenna
Spatial survey (m/scan) =	0.2731	wt 4 antenna
Spatial survey rate (scans/m) =	3.6621	wt 4 antenna

A	B	A*B			
Scans/unit	**velocity of traverse**			**Does it meet criteria 1?**	**Does it meet criteria 2?**
scans/m	*m/s*	*scans/s*	*Scans/sec*		
1	13.33	13.33	28	yes	yes
2	13.33	26.67	28	yes	yes
3	13.33	40.00	28	no	yes
4	13.33	53.33	28	no	no
5	13.33	66.67	28	no	no
6	13.33	80.00	28	no	no
7	13.33	93.33	28	no	no
8	13.33	106.67	28	no	no
9	13.33	120.00	28	no	no
10	13.33	133.33	28	no	no
11	13.33	146.67	28	no	no
12	13.33	160.00	28	no	no
13	13.33	173.33	28	no	no
14	13.33	186.67	28	no	no
15	13.33	200.00	28	no	no
16	13.33	213.33	28	no	no
17	13.33	226.67	28	no	no
18	13.33	240.00	28	no	no
19	13.33	253.33	28	no	no
20	13.33	266.67	28	no	no

Figure 6.26: Spreadsheet used to check the setting used by the radar system when using the survey wheel

6.6 Computer program

The analysis of pavement profiles and thicknesses requires repetitive calculations to be carried out on the radar results. Every scan line, representing a different position along a pavement, has to be analysed to find out the distance from the pavement surface or layer to each antenna.

The computer program had to be able to read the output information from four radar antennas, three of them used to produce a profile plot of the surface of the pavement, with the fourth antenna's information used to detect a layer thickness. The surface profile would then be compared to the layer detected within the pavement.

The scan line on Figure 6.27 shows a very clear transmit and reflect pulse, the difference between these is the two-way travel time, which is the time taken for the radar pulse to travel from the antenna to the pavement and back again (see chapter 3). The first part of the program had to be able to obtain the two-way travel time from each scan line. The distance travelled is determined from the time it takes the reflected wave to be detected at the receiver. Knowing the velocity of the wave through the relevant media the depth is calculated from Equation 3.1.

$$d = v\left(\frac{t}{2}\right)$$

where: d = thickness of layer

v = velocity of electromagnetic wave through the layer

t = time between reflections.

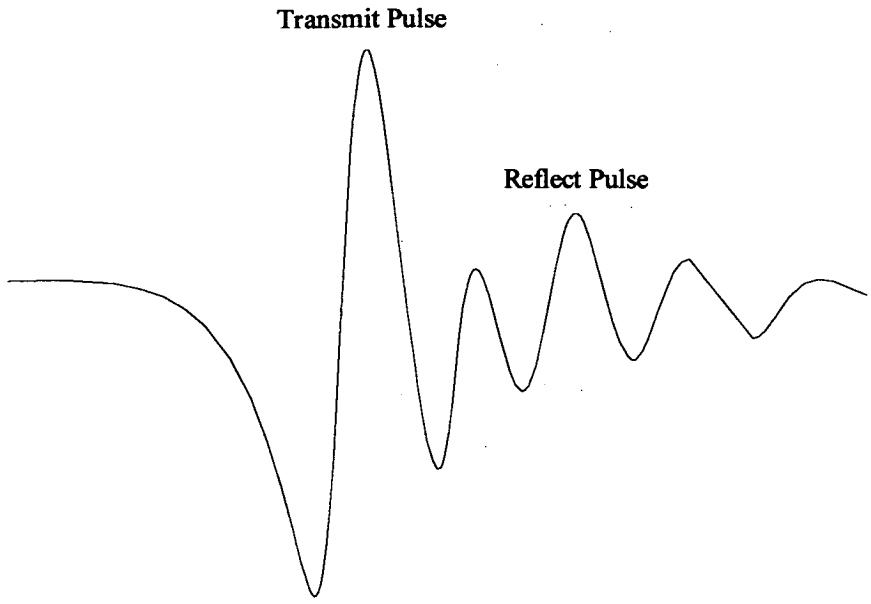

Figure 6.27: A typical radar scan line

The readings obtained at set intervals along the pavement will be converted into x and y coordinates of the pavement surface using equations 6.5 and 6.6 , which was discussed earlier.

6.6.1 Surface reflection picking

The program chose the reflection from the pavement surface automatically by using a method of locating the position of maximum and minimum values along the scan line. Once this reflection had been found, upper and lower limits were produced around this point, thus a window area was created. The size and position of the window would be used in the next scan line. The position of the maximum within this window was obtained, enabling the new height of the radar antenna from the pavement surface to be calculated. This window position was automatically adjusted if the maximum value moved outside this area. This was achieved by calculating the maximum within two different window sizes (Figure 6.28).

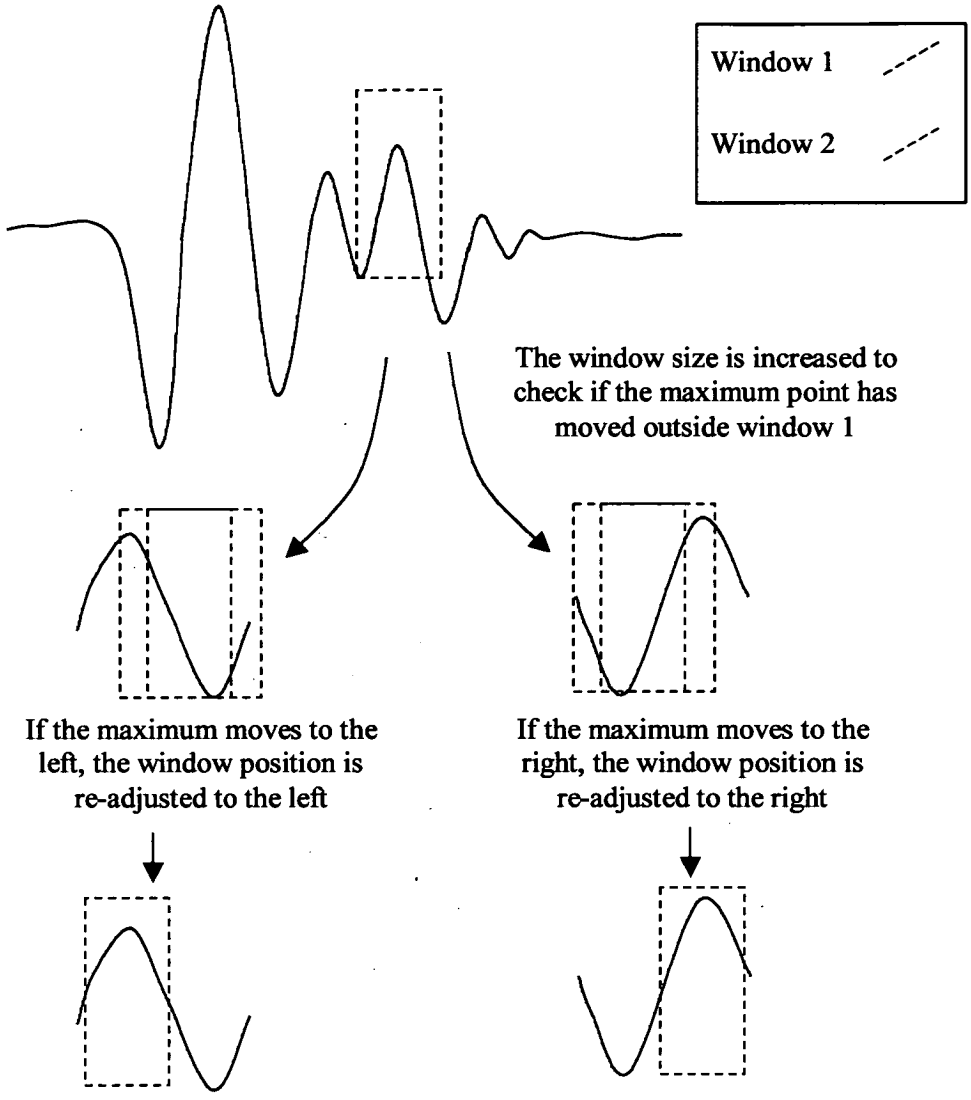

Figure 6.28: Locating the maximum value from each scan line

If the maximum moved to the right or left the program repositions the window. Using this new location it commenced calculating the maximum in the next scan line. This process would continue until all the radar scan lines had been analysed. The first preliminary experiment detailed in section 6.7 uses this method.

This surface-mapping program was ideal for obtaining measurements along short road sections (<40m), but, longer than this requires more modifications to this program. Figure 6.13 can be used to explain the shortcoming in the original program. It can be seen from

this graph that the error becomes very large when analysing very long or very small wavelengths.

This problem was overcome by obtaining spot height information along the road, either from Ordnance Survey maps (OS), level survey or from the original design drawing. The spot height on OS maps are usually taken at 50m intervals, therefore, cubic spline interpolation is applied to them in order to increase the number of sample points.

The height information, obtained from the radar antennas, is broken into smaller sized sections which partially overlap (see Figure 6.30). Each section is calculated the same way described above, however, a best-fit line is then fitted to them in order to calculate the gradient. This is compared to the original gradient obtained from the spot height information. The program automatically adjusts the gradient to match the original value if there is any difference (Figure 6.29).

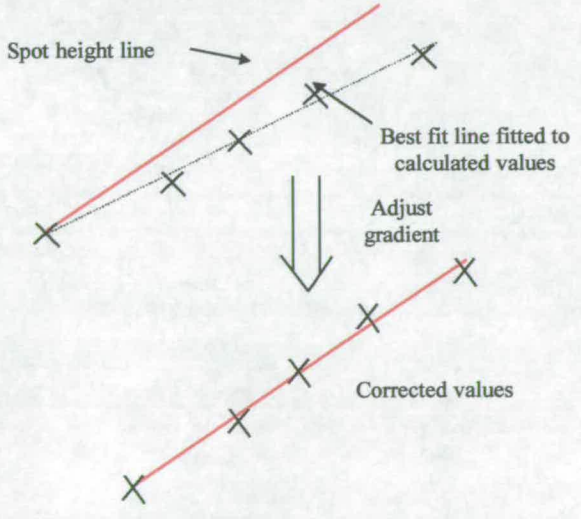

Figure 6.29: Correction of the gradient of the calculated values using the spot height information

Weighted averaging was applied to the overlapped sections to obtain new height values. Once this had been carried out, all the new height information was reconstructed back into the relative height of the pavement. This is summarised in the figure below.

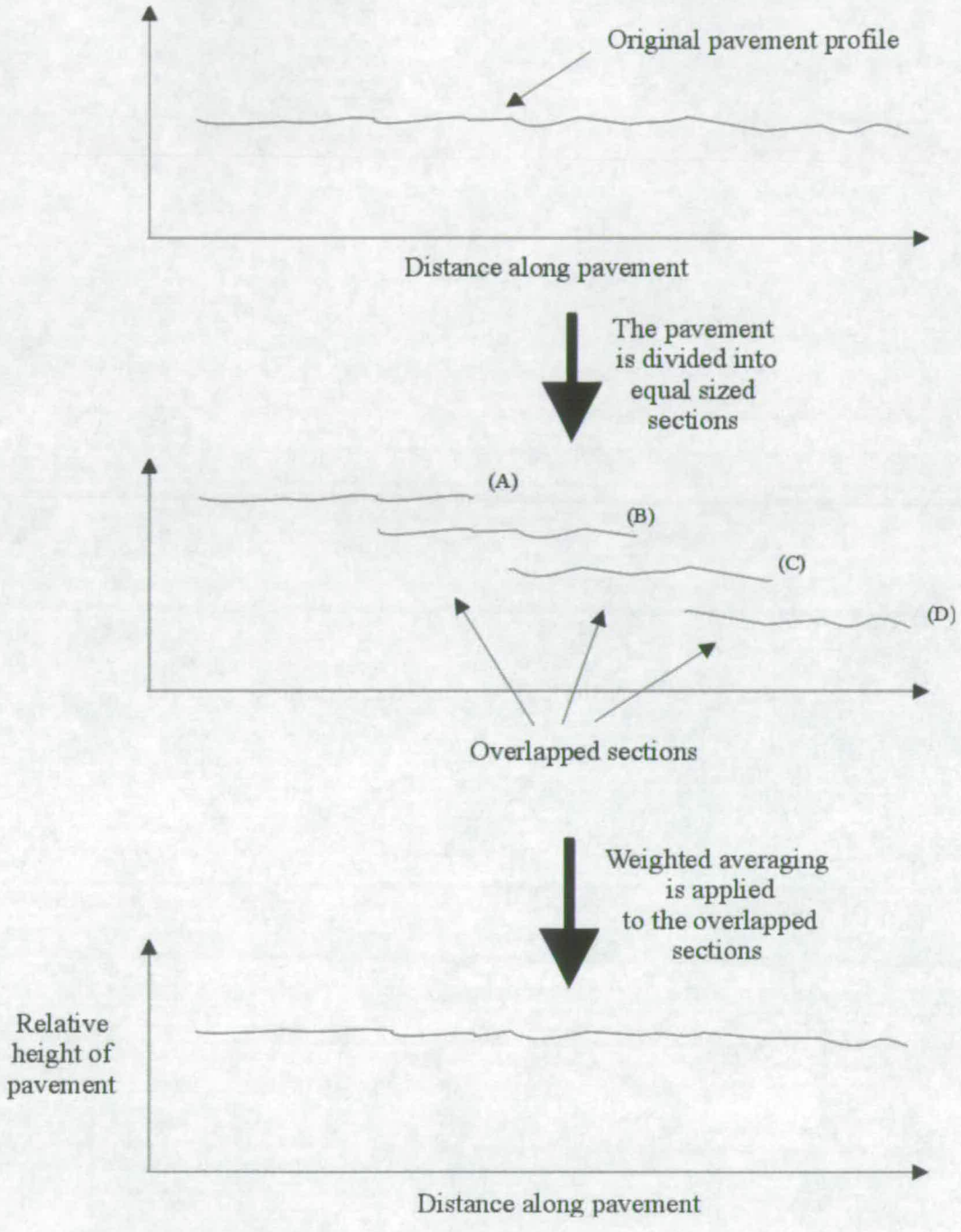

Figure 6.30: Method used to reconstruct the surface profile of the pavement

6.6.2 Sub-surface layer picking program

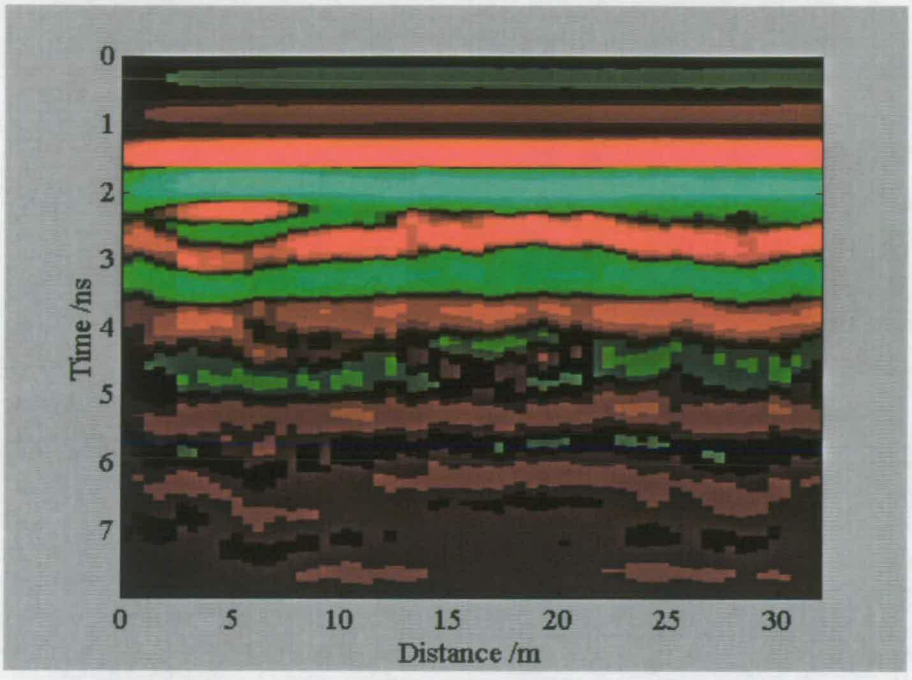

Figure 6.31: Radargram plot obtained from a pavement

Placing a radar antenna on the ground and moving it along the surface will produce a series of reflection signals, due to changes in the electrical properties of the material, which can be displayed in various formats (see section 3.5). Figure 6.31 shows a radargram plot obtained from a pavement of known layer thicknesses. The bright green line, at about 2ns, shows the position of the transmit pulse, the main reflection from a layer occurs between 3ns and 4ns.

This reflection information, from different layers, needs to be picked out from the radargram in order to determine the layer thicknesses. An initial program, similar to the one used to obtain surface reflections was used. The only difference in this program was that the user could determine the position of the window around the layer reflection; the depth of this layer could then be worked out from the velocity and time information. The user input was only required with the first scan line, and the program would automatically check the other scan lines using the same technique, described in the surface picking program (section 6.6.1). The main problem with using this method is that the window can move to a position were the transmit pulse information is present, resulting in the wrong peak being followed by the program (Figure 6.32). This same problem was found when using commercially produced software.

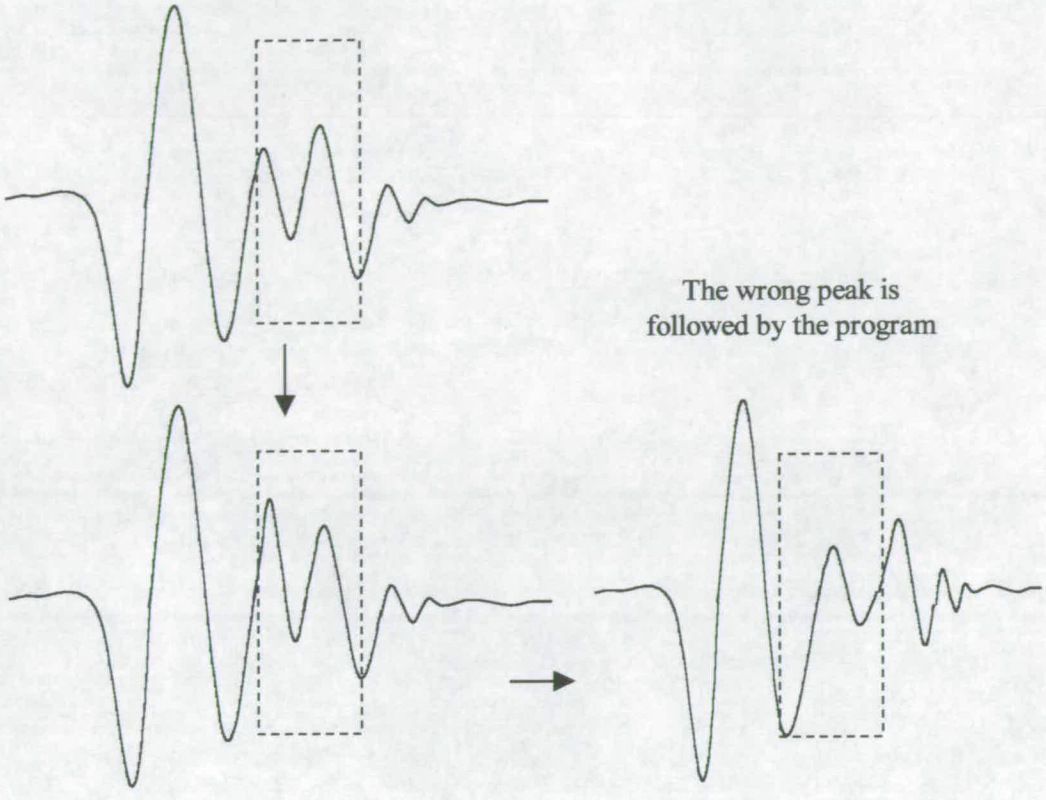

Figure 6.32: Choosing the wrong peak from the scan line

To get around this problem a semi-automatic approach is required. This involves displaying the radar information, obtained from the pavement, as a radargram plot. The area of interest, relating to the reflection from one of the layers, was chosen by clicking points along this line. The program creates straight lines between these points and with predefined thresholds calculates the position of the maximum values (Figure 6.33).

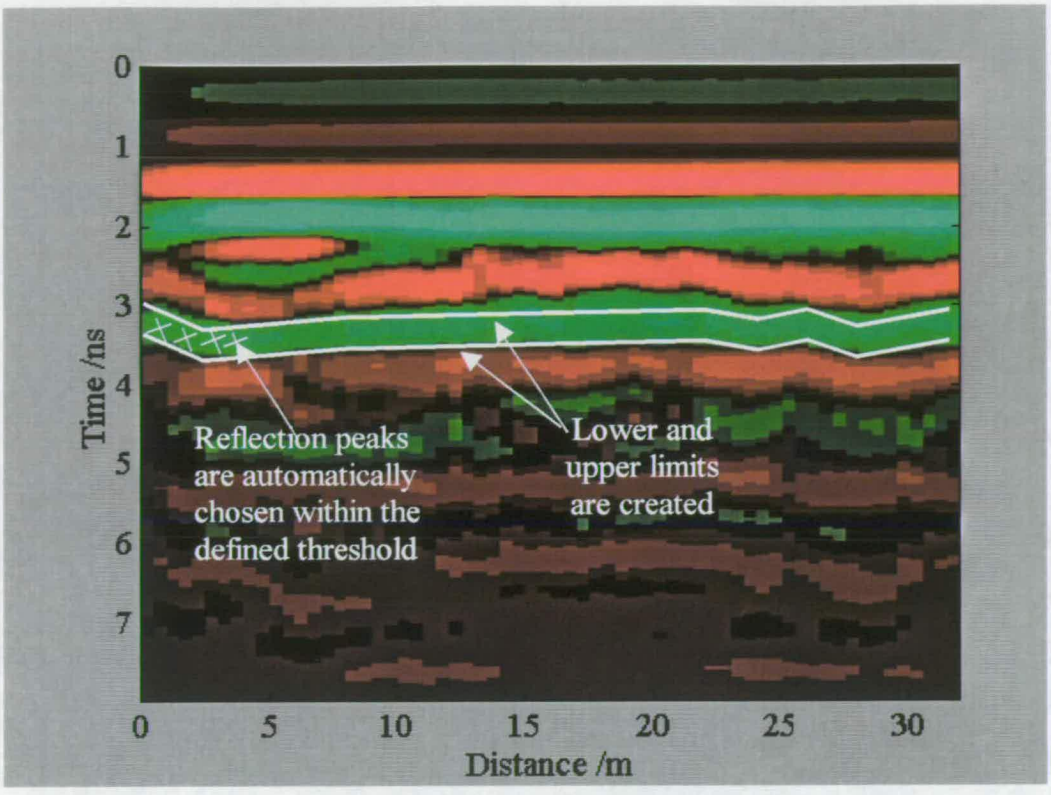

Thresholds are created once points have been chosen along the radargram

Figure 6.33: How the sub-surface program chooses reflections

Therefore, the program will operate the same way the surface reflection picking program worked, but, instead of automatically changing the window position, the position of the window will be predefined by the user.

6.7 Preliminary experiments

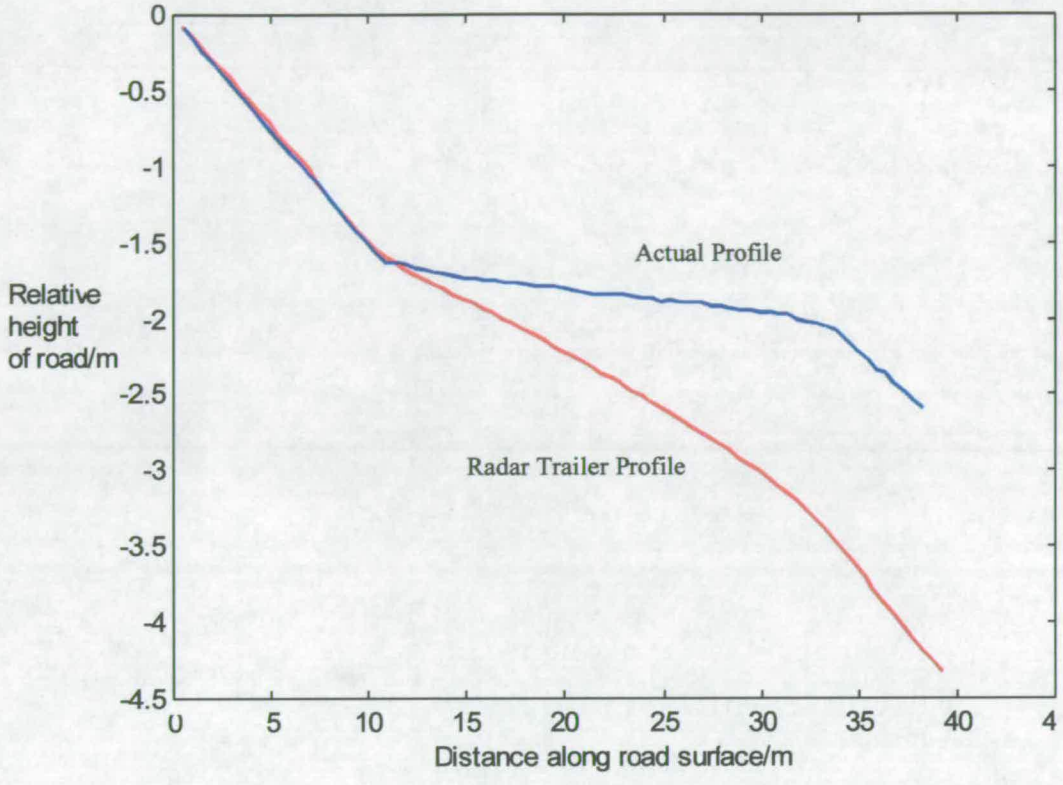

Figure 6.34: A graph showing the actual road profile and the profile calculated by the radar trailer

An experiment was carried out to compare the profile measured using the radar antennas to the actual profile of the road which is determined using a total station. The program used to create the surface profile did not use any spot height or level survey information. The test road had an initial gradient of 7 degrees which flattened out to a slope angle of 2 degrees before reverting to 5 degrees. The antenna spacing values for mapping the long wavelengths, i.e. 3m and 1.4m spacing, were used in this experiment, the results are shown on Figure 6.34.

The radar signals in the Sir10A+ system, used in this experiment, were experiencing time jitter (see section 3.7.1.2). This was causing parts of the scan lines to wobble, therefore causing inaccuracy in the distant measurements. The system was sent back to the manufacturer, but, they were unable to fix the problem. To overcome this setback the antennas recorded 50 scan lines at each 0.5m increment on the pavement. The 50 scan lines were averaged in order to obtain one scan line at each increment along the pavement. This

process was very timely and produced a large radar file, therefore, it was decided that only the long wavelength set-up would be used on this pavement.

A graph of the curvature along the road was plotted (Figure 6.35). A good correlation between the radar trailer and the actual values, obtained by the total station, was found, however, the antennas had difficulty in mapping large changes in road gradient. This in turn caused the calculated profile plot to be unable to map the profile as accurately (see Appendix C). Using a 0.5m spacing, i.e. the small wavelength set-up, would have reduced this error.

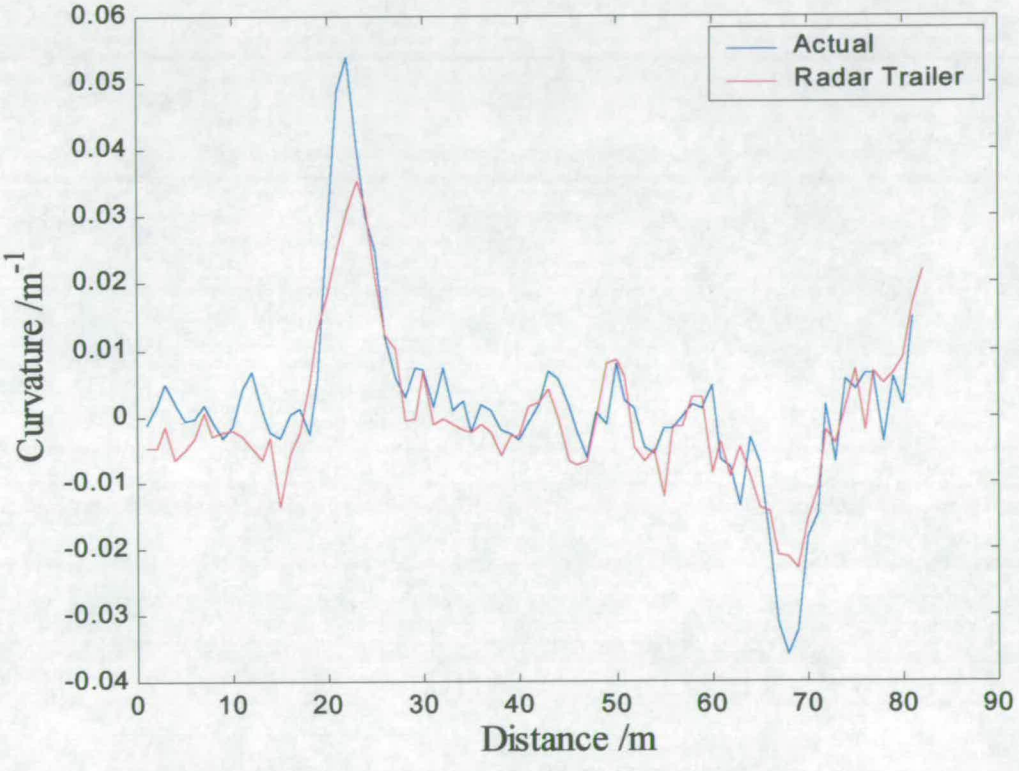

Figure 6.35: Comparing the actual and radar trailer curvature values

It was felt that this road was not very representative of a motorway, although, it did highlight a shortcoming of the equipment.

A second road was analysed and this experiment used information obtained from a level survey to recreate the surface profile, (Figure 6.36). Only the long wavelength set-up was used due to the reasons explained above. The results show that this method improves the ability of the program to recreate the actual profile.

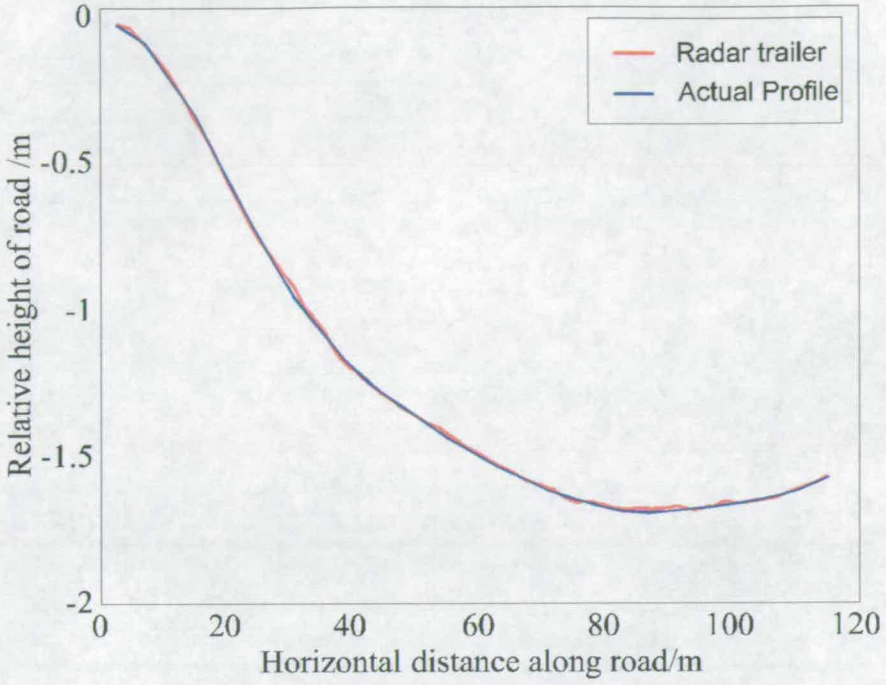

(a)

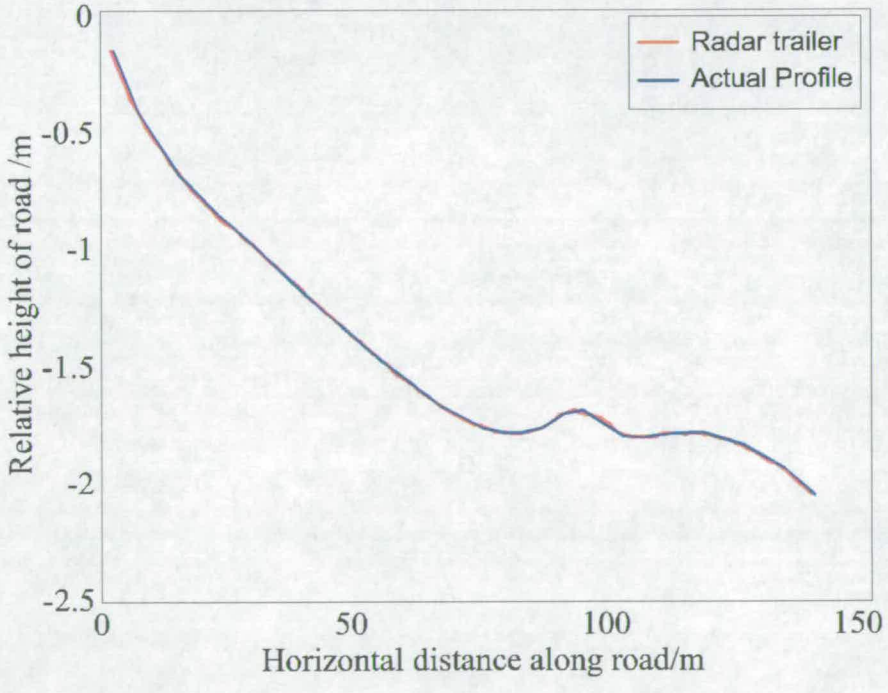

(b)

Figure 6.36: Graphs showing the actual profile and the profile recreated with the radar trailer

6.8 Conclusions

A method for comparing the longitudinal profile of the surface and subsurface layers on pavements using GPR is proposed. Several specifications had to be met in order to achieve these aims.

- Three radar antennas were to be used to detect the surface profile, with a fourth antenna detecting the sub-surface layers on pavements.
- Wavelengths of interest are between 1m and 15m.

Three sets of experiments were carried out:

- To determine how effectively GPR can detect layers within the pavement.
- To determine Optimum height range of radar from pavement surface.
- To determine the spacing of the antennas.

The optimum height was found to be between 25 and 30cm. In order to map the long wavelengths it was calculated that the three surface antennas needed to be 3m apart. However, due to the position of the axle and limits on the maximum size that a trailer can be by law, the spacing between each antennas was 1.4m and 3m respectively. The smallest spacing between the antennas was 0.5m due to the interference from the cables. It was found that with this spacing, the smallest wavelengths that could be measured were 1.8m.

A preliminary experiment was carried out on the profile mapping of the pavement surface. The results showed that the antennas operated well except with large changes in the road's gradient. It was, however, concluded that this road did not simulate the conditions of a motorway.

The second set of experiments show that using spot heights or level information improves the ability of the program to recreate the actual profile.

Chapter 7

Wavelength analysis of road layers

7. Introduction

The main aim of this chapter is to determine whether any relationship exists between the surface and sub-surface longitudinal profiles. GPR was used to map the surface and sub-surface layers. The relationship between these layers was extracted using correlation techniques.

The chapter commences by looking at the ability of different antennas to measure thin pavements. The 1.5GHz antenna was chosen to analyse the sub-surface profile due to its accuracy in mapping thin layer pavements and the success of high frequency GPR as used and verified commercially (see chapter 3).

The main experiments examined actual road data obtained from a motorway, 'A' road (bypass) and minor road. These experiments investigated the correlation of surface profile and asphalt layer thickness profile over a wide range of pavement constructions, and also to verify the method evolved here over the full range of pavement constructions that occur in UK roads.

7.1 Theoretical analysis of antennas

The use of high frequency radar to detect pavement layers has proven to be very successful (see chapter 3) with radar results accurately matching cores taken along the road. Improvements in radar electronics has also enabled high-speed surveys to be undertaken with low-speed surveys still being used when more detail is required.

Using radar to analyse pavement layers requires the user to choose the most suitable antenna to carry out the task. The following section looks at the theory behind making this decision.

The surface layer of a flexible pavement can be as thin as 40mm. To measure layers of this thickness requires the wavelength of the antenna, within the medium, to be of this magnitude. The following section will examine the wavelengths that can be measured by three commonly used antennas, these being 400MHz, 500MHz and 1.5GHz.

The velocity of the radar wave can be related to the frequency and wavelength by:

$v = \lambda f$ (Equation 6.1)

where: v = Velocity of electromagnetic wave within medium (m/ns)

λ = Wavelength (m)

f = Central frequency of antenna (Hz)

In Air		
400MHz	**500MHz**	**1.5GHz**
$\lambda = \frac{0.3 \times 10^{-9}}{0.4 \times 10^{9}} = 0.75m$	$\lambda = \frac{0.3 \times 10^{-9}}{0.5 \times 10^{9}} = 0.6m$	$\lambda = \frac{0.3 \times 10^{-9}}{1.5 \times 10^{9}} = 0.2m$

Table 7.1: Wavelengths in air of different frequency antennas

The surface layer of a flexible pavement is made of asphalt. The velocity of the electromagnetic wave within the asphalt layer is dependent on whether or not the layer is wet or dry. The velocity values can vary from 0.09m/ns (wet layer) to 0.21m/ns (dry layer) (Table 3.1). The wavelength values in Table 7.2 are obtained by assuming that the asphalt layer is both homogenous and isotropic.

In asphalt (surface layer)			
	400MHz	**500MHz**	**1.5GHz**
Min vel. (0.09m/s)	$\lambda = \frac{0.09 \times 10^{-9}}{0.4 \times 10^{9}} = 0.225m$	$\lambda = \frac{0.09 \times 10^{-9}}{0.5 \times 10^{9}} = 0.18m$	$\lambda = \frac{0.09 \times 10^{-9}}{1.5 \times 10^{9}} = 0.06m$
Max vel. (0.21m/s)	$\lambda = \frac{0.21 \times 10^{-9}}{0.4 \times 10^{9}} = 0.525m$	$\lambda = \frac{0.21 \times 10^{-9}}{0.5 \times 10^{9}} = 0.42m$	$\lambda = \frac{0.21 \times 10^{-9}}{1.5 \times 10^{9}} = 0.14m$

Table 7.2: Maximum and minimum wavelengths in asphalt of different frequency antennas

The minimum vertical (depth) resolution that can be obtained by an antenna is one quarter the antenna's wavelength in the medium (λ/4). This is a theoretical value so a safety factor of two should be used, i.e. one half wavelength (λ/2) (Annan, 1997; Daniels, 1996B). Therefore, interfaces which are spaced closer than one half wavelength result in the reflected signal from one interface being mixed up with that from the other interface, making it impossible to distinguish the two interfaces without further processing of the signal. This was discussed in section 6.3.1, where it was noted that the received radar signal from thin layered pavements is made up of several different signals.

Assuming that the relative permittivity of the surface layer is 9, then the values shown in Table 7.3 for the velocity and wavelength of the radar wave within this layer would be found.

Table 7.3 shows that the 400MHz and 500MHz can detect layers of 0.125m and 0.1m respectively. These results demonstrate that the 500MHz antenna will only be able to detect thickness values along the surface layer which are ≥0.1m whereas, the 400MHz antenna will detect values which are ≥0.125m. However, the 1.5GHz antenna can detect layers as thin as 0.035m. Therefore the 1.5GHz antenna is the best antenna to use for detecting the 0.04m surface layer. This antenna was used in the main road experiments.

	400MHz	500MHz	1.5GHz
Velocity $\left(v=\frac{c}{\sqrt{\varepsilon_r}}\right)$	$\frac{0.3\times10^{-9}}{\sqrt{9}}$ $=0.1m/ns$	$\frac{0.3\times10^{-9}}{\sqrt{9}}$ $=0.1m/ns$	$\frac{0.3\times10^{-9}}{\sqrt{9}}$ $=0.1m/ns$
Wavelength $\left(\lambda=\frac{v}{f}\right)$	$\frac{0.1\times10^{-9}}{0.4\times10^{9}}=0.25m$	$\frac{0.1\times10^{-9}}{0.5\times10^{9}}=0.2m$	$\frac{0.1\times10^{-9}}{1.5\times10^{9}}=0.07m$
Minimum vertical resolution $\left(\frac{\lambda}{2}\right)$	0.125m	0.1m	0.035m

Table 7.3: Wavelength values for surface layer in test road

7.2 Main experiments

The relationship between the surface and sub-surface profiles were analysed for three different types of roads. Two of them were flexible pavements and the third road was a flexible composite pavement. The following sections give details of each road, describing the tests carried out and the subsequent results obtained.

7.2.1 M8 extension

The information on the M8 extension was supplied by the Forth Local Authority Consortium (FLAC). Figure 7.1 shows the position of the M8 extension in relation to Edinburgh city centre. The starting position of the survey was located 80m from Hermiston Gait roundabout. The construction details are shown on Figure 7.2, which is a flexible pavement design.

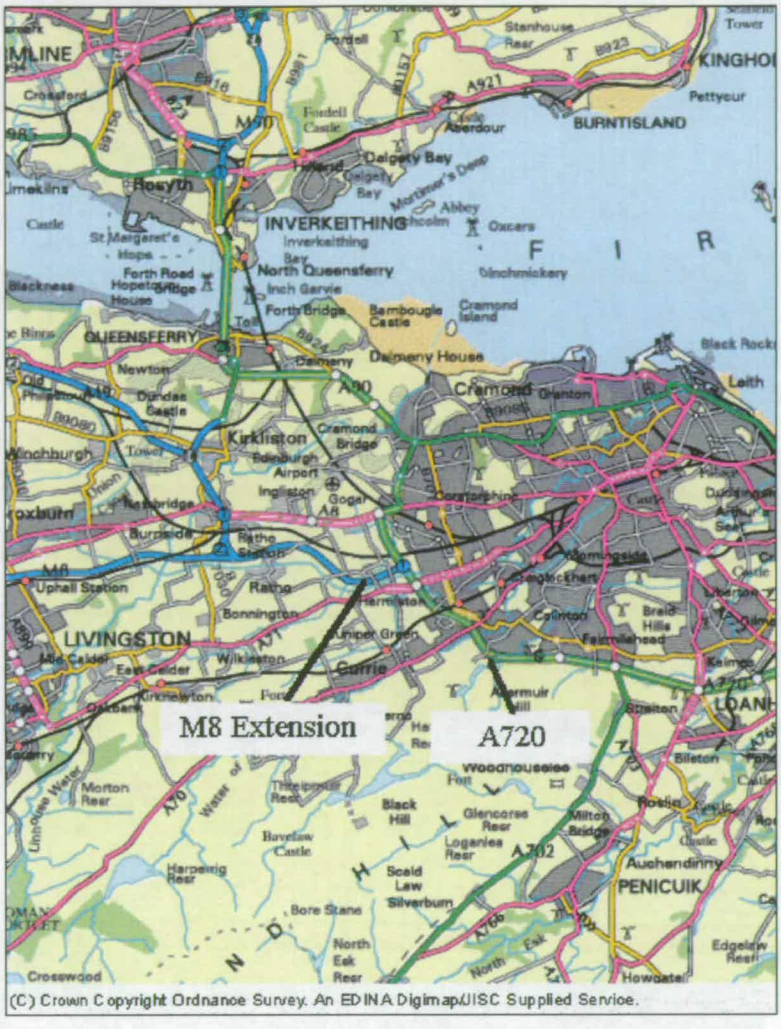

Figure 7.1: Map showing the position of the M8 extension and A720 in relation to Edinburgh city centre (Reproduced from Ordnance Survey maps with the permission of The Controller of Her Majesty's Stationery Office. © Crown Copyright ED NC/99/246.)

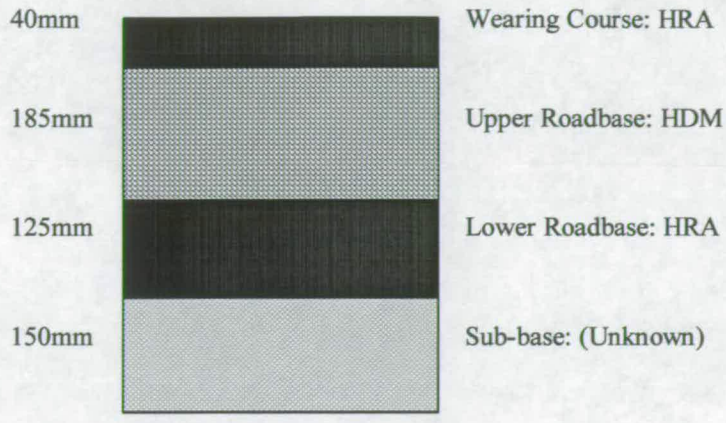

Figure 7.2: Average layer thicknesses along the M8 extension

7.2.2 The A720 (Edinburgh Bypass)

The test section was a dual carriageway located between Dreghorn and Baberton junctions on the A720 (Figure 7.1). Scott Wilson Ltd. supplied the construction information on this road. They were due to start work on upgrading the road from a flexible composite road to a flexible road. A detailed investigation of the road structure had been undertaken by WDM Ltd. Eight 150mm diameter cores were taken along each lane on both directions of the road. A summary of the core information was supplied to the author, but, only the structural condition of two cores was supplied. The author was unable to tie this core information in with the radar scans as their positions in relation to any known reference points were not supplied. However, in general the road construction consisted of 140mm of bituminous bound material and 220mm of cement bound material, over 220mm of sub-base material, shown in Figure 7.3.

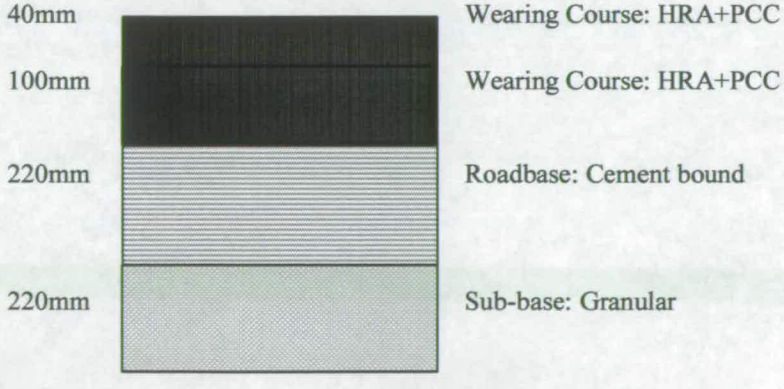

Figure 7.3: Average layer thicknesses along the A720

7.2.3 The A199

The main road from Tranent to Wallyford (A199) is a minor road which has come to the end of its design life (Figure 7.4). This road is of flexible pavement construction. Unfortunately the author could not obtain any coring records for this pavement.

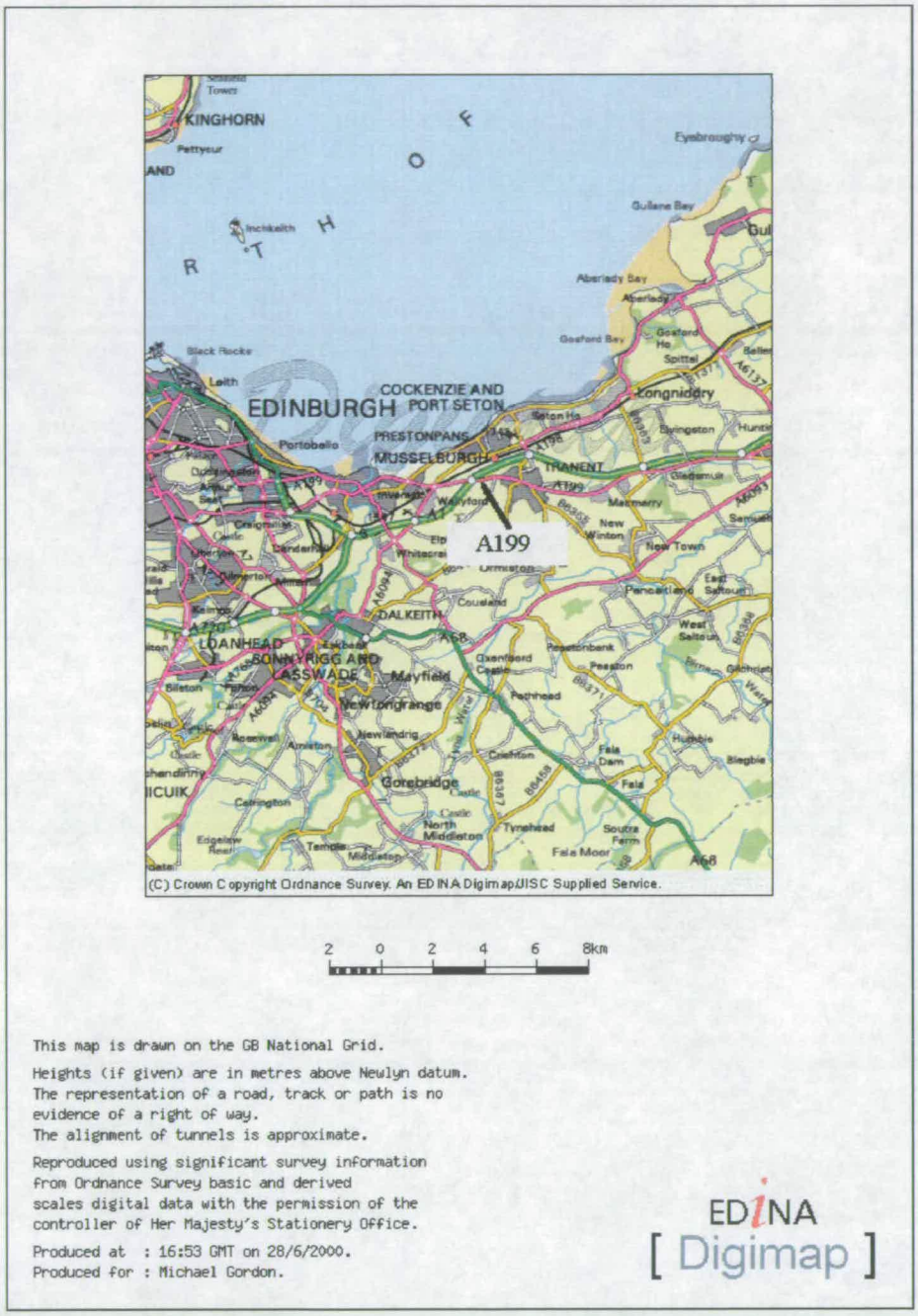

Figure 7.4: Map showing the A199 on the east side of Edinburgh (Reproduced from Ordnance Survey maps with the permission of The Controller of Her Majesty's Stationery Office. © Crown Copyright ED NC/99/246.)

7.2.4 Experimental set-up

The long and short wavelength surveys started at the same point on the road. The minimum wavelengths of particular interest were 1m, however, due to the interference of the cables the smallest possible wavelength that could be measured were found to be 1.8m or 0.56cycles/m (section 6.3.3). Calculating wavelengths of this magnitude requires the sampling frequency (Nyquist frequency) to be at least twice the highest frequency present in the signal, in this case it will be 1.12cycles/m. The higher the Nyquist frequency the more accurately these wavelengths will be calculated (see section 3.7.1.2). In these experiments, 0.5m and 0.2m intervals were used to calculate the long and short wavelengths respectively.

The vehicle speed was determined using a spreadsheet which checked to see if certain criteria were met (see Figure 6.26). This information was used to obtain the maximum speed possible for measuring the long and short wavelengths.

	Transmit rate (kHz)	Scans/sec	Scans/m	Maximum Vehicle velocity
Long wavelength	100	28	2	30mph
Short wavelength	100	28	5	10mph

Table 7.4: Based on the spreadsheet information on figure 6.26

The survey was carried out after 9pm to minimise the disruption to the traffic flow. All necessary road safety measures were implemented including flashing lights fitted to the back of the trailer and front of the car and all occupants wore reflective yellow clothing. Figure 7.5 shows the vehicle used to tow the trailer. The car was an ideal size to store all the radar equipment and cables whilst enabling an operator to sit in the back and operate the equipment.

Figure 7.5 Vehicle used to tow trailer

The trailer set-up consisted of three 900MHz antennas suspended from the radar bar, used to measure the surface profile; a fourth antenna (1.5GHz) was coupled to the road surface to measure the sub-surface profile. Figure 7.6 to Figure 7.8 show the set-up of the trailer and subsequent surveying at different sites.

Figure 7.6 Setting up equipment before carrying out road survey

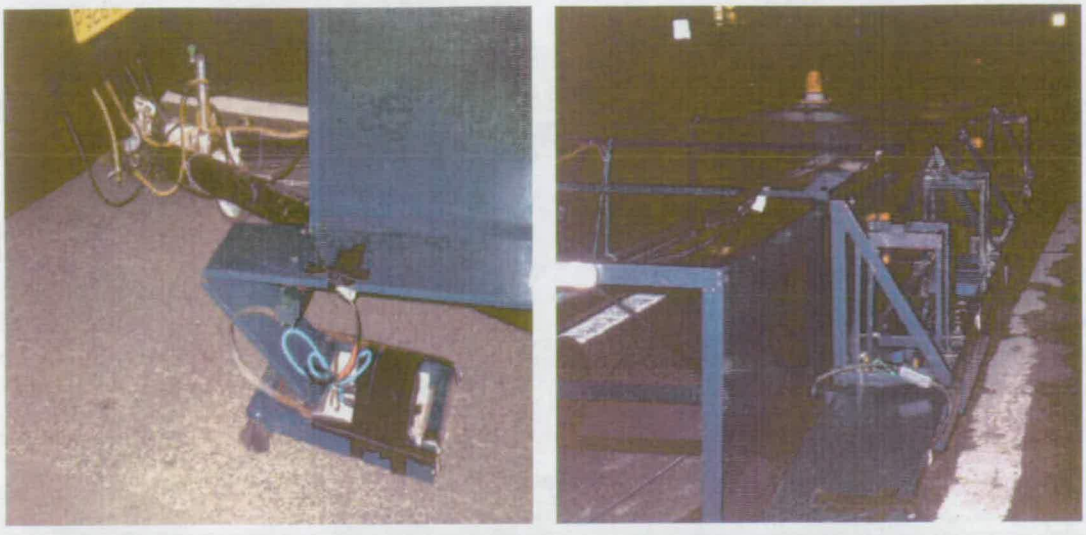

(a) (b)

Figure 7.7: (a) Antenna detecting the sub-surface (b) Surface mapping antennas

(a) (b)

Figure 7.8 (a) Surveying the M8 (b) Surveying the A199

7.3 Results

The profile of the surface was correlated with the bottom of the surface layer. The reason for choosing this layer was that the value of the velocity for this layer could be obtained from the reflection coefficient method (see section 5.2.4), assuming that the layer is homogenous and isotropic. Using this method to determine the velocity in subsequent layers requires the velocity in the previous layer to be known. Mesher *et al.* (Mesher *et al.*, 1995) noted that the cumulative errors in the velocity estimation, using the reflection coefficient method, causes this technique to be inappropriate for multiple layers. Therefore, it was decided to only use the profile information from the bottom of the surface layer.

The radar information from the 1.5GHz antenna had to be analysed further to check whether or not this antenna could obtain the reflection information from the bottom of the surface layer. The wearing course thickness of the M8 extension and the A720 was 40mm, which is a standard thickness to use in this type of road design. Layers this thin should be visible to the 1.5GHz antenna (see section 7.1). However, if the relative permittivity of the layer below the surface layer is such that they are electrically similar then a reflection pulse will not be produced at the interface of these layers. Using the information from Table 7.5 it was proven empirically that a reflection could be produced between these layers (see Appendix D).

Figure 7.9: Carrying out the reflection coefficient method

	Relative permittivity	Velocity of radar wave (m/ns)
M8 extension	5.4	0.1291
A720	5.7	0.1257
A199	4.5	0.1414

Table 7.5: Relative permittivity and velocity values obtained from each road

The following section uses spectral analysis to compare the surface and sub-surface profiles. A Hamming windowing function was used in each case to produce the power spectral density (PSD) and cross spectral density (CSD) plots of the data. Different sizes of windowing functions can help rule out the effect of window leakage. To test if this is occurring in the road data two different window sizes (128 and 256 samples) were used on the long wavelength analysis of the M8 section.

All wavenumbers above 0.56cycles/m, i.e. wavelengths below 1.8m, are ignored as these are the shortest wavelengths that the antenna set-up can identify (see section 6.3.3). The short wavelength set-up refers to the antennas spaced 0.5m apart, whereas they are spaced 3m and 1.4m apart in the long wavelength set-up (see section 6.3.3 for more details).

It should also be noted that the short and long wavelength surveys start at the same point unless otherwise stated. The short wavelength surveys will show more detail than the long wavelength surveys as more scan lines are being emitted per meter.

7.3.1 M8 extension wavelength analysis

7.3.1.1 Long wavelength analysis

Figure 7.10(a) represents the radargram produced by the antenna coupled to the pavement surface. The reflection centred around 3ns is from the base of the surface layer. The sub-surface layer picking program (section 6.6.2) was used to calculate the thickness of this layer. The thickness value is then subtracted from the surface profile in order to produce the profile of the sub-surface layer. The surface and sub-surface layer profiles are shown in Figure 7.10(b).

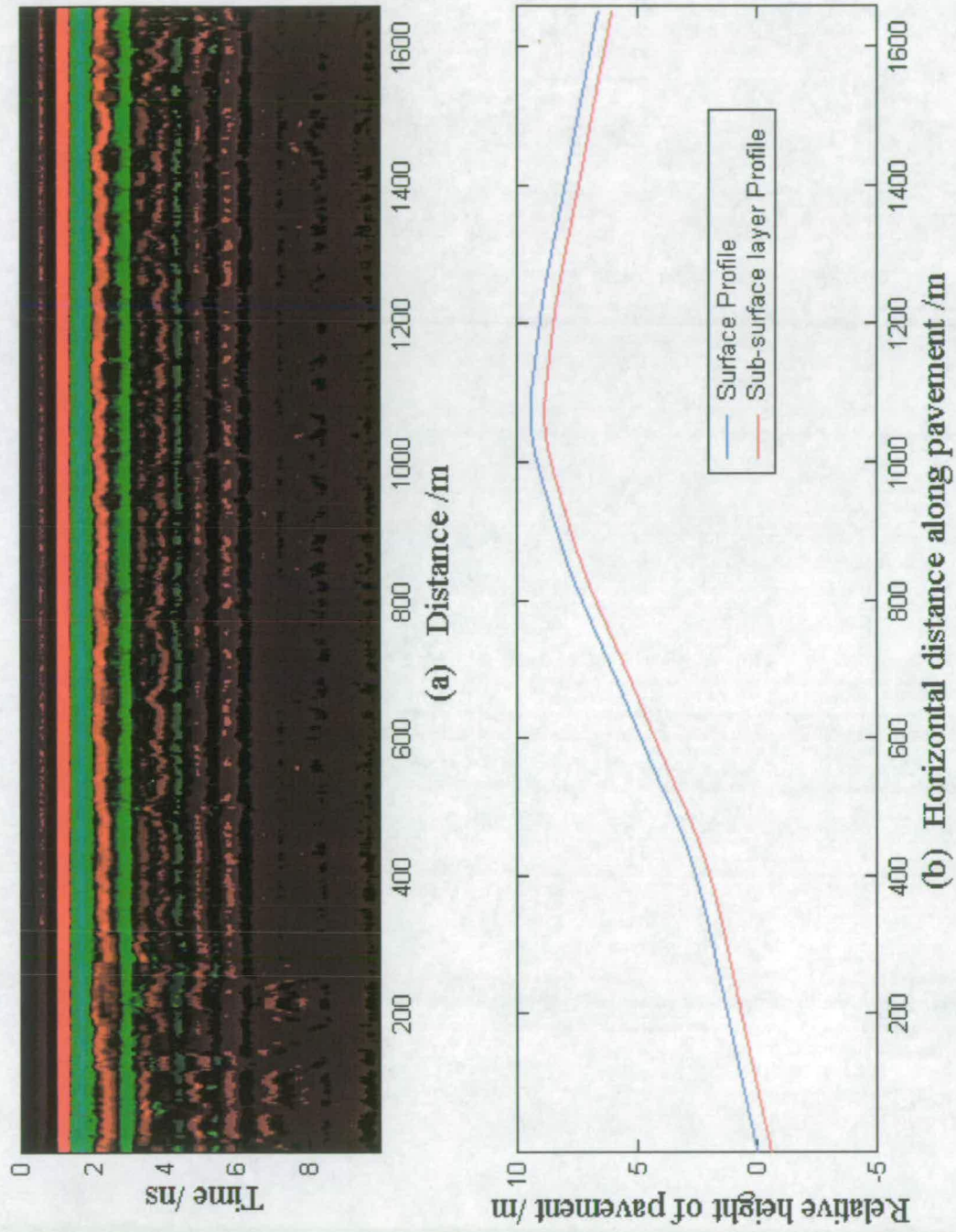

Figure 7.10: (a) Radargram of M8 pavement layers (b) Pavement elevation (Long wavelength survey)

A magnified section of this plot is shown in Figure 7.11. The average distance to the layer interface from the surface is about 0.08m (using the velocity value of 0.1291m/ns (Table 7.5)), whereas, it is known that the layer is 0.04m thick. This difference in thickness can be caused by a dry road surface over a moist sub-surface. The relative permittivity value calculated using the reflection coefficient method only gives a value for the surface of the pavement and not an average value of the layer. By back-calculating, using the desired thickness of the layer and the travel time, it was found that the relative permittivity would need to be 21.3 to get a thickness value of 0.04m. Alternatively, if a lower velocity value of 0.07m/ns is used then the correct thickness can be obtained. However, it should be noted that the profile of the pavement is unchanged regardless of the velocity used.

The spectral analysis of the data, shown on Figure 7.12, shows that two prominent wavenumbers occur in the PSD plots when using 128 samples, i.e. 0.12 cycles/m and 0.19 cycles/m. These correspond to wavelengths of 8.3m and 5.3m respectively. The coherence values at these points were about 0.5 for each case using 128 samples. It is more difficult to see any prominent peaks, in the spectral graphs, when using 256 samples.

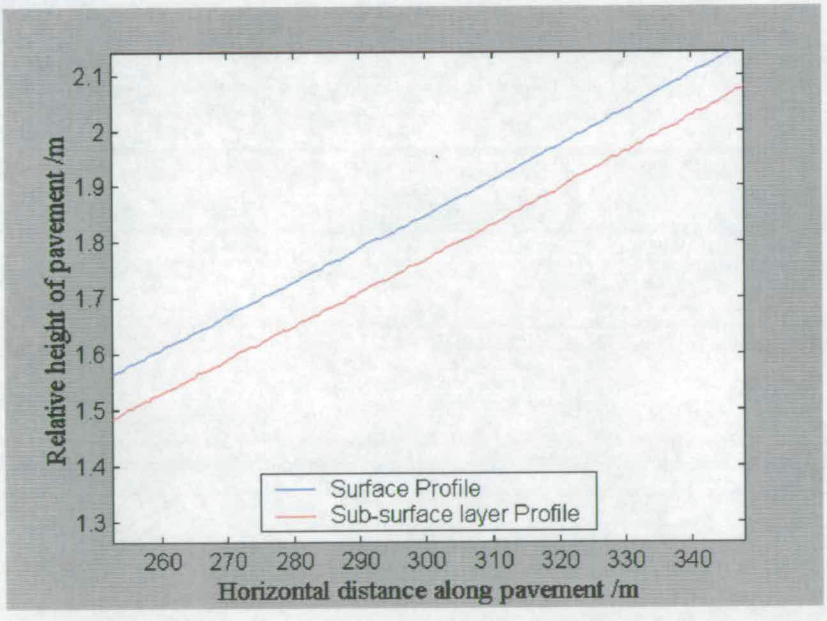

Figure 7.11: Showing a magnified section of Figure 7.10(b))

These results have shown that increasing the number of samples in the windowing function does not make the plot smoother. The information is clearer when using 128 samples compared to 256. Therefore, the 128-window size will be used instead of the 256 samples in subsequent analysis.

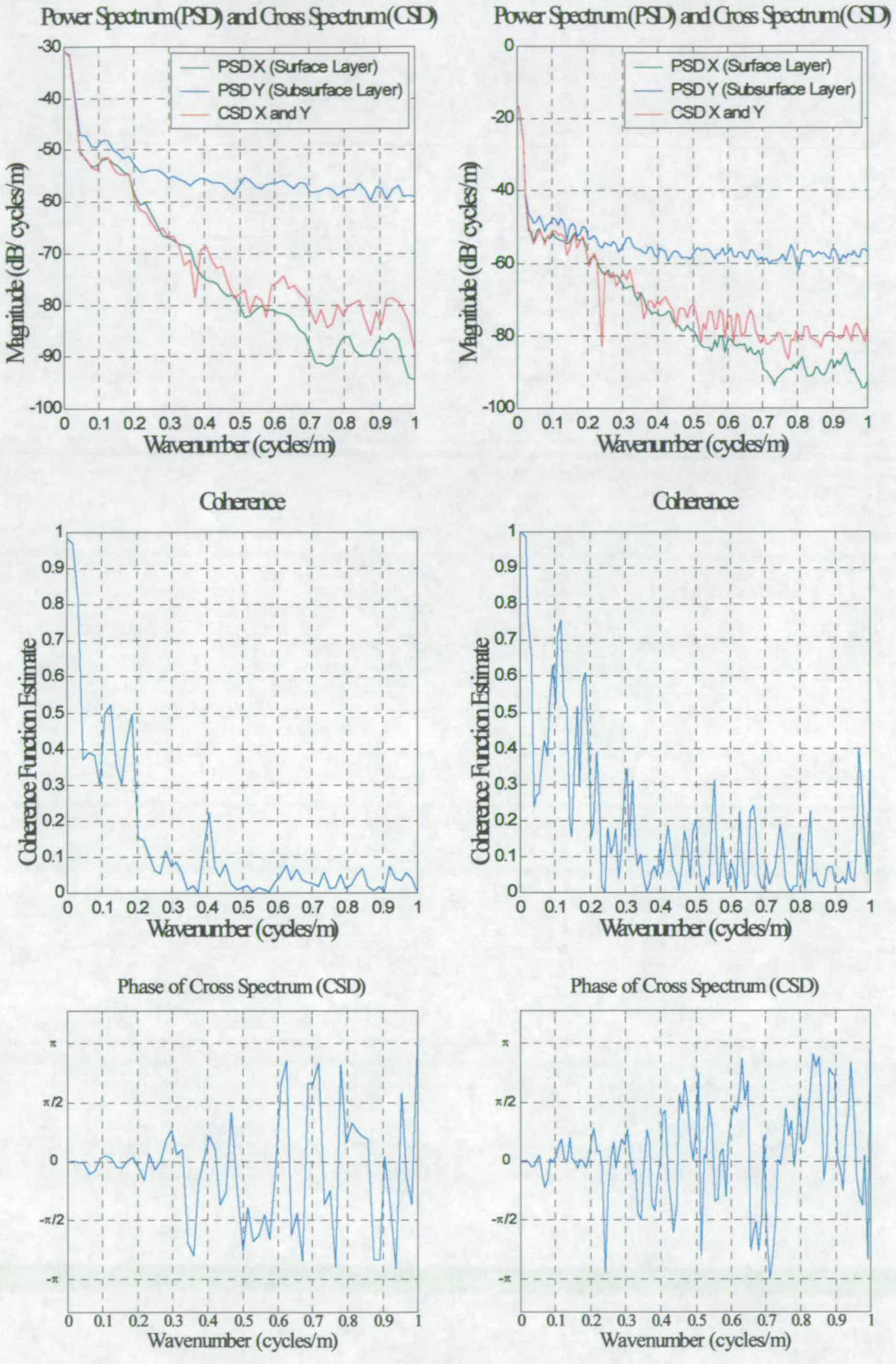

Figure 7.12: Spectral analysis of surface and sub-surface profiles on the M8 using the long wavelength set-up (Window size = 128 samples (left side); 256 samples (right side))

7.3.1.2 Short wavelength analysis

Figure 7.13 represents the radargram produced by the antenna coupled to the pavement surface when measuring short wavelengths along the M8 extension.

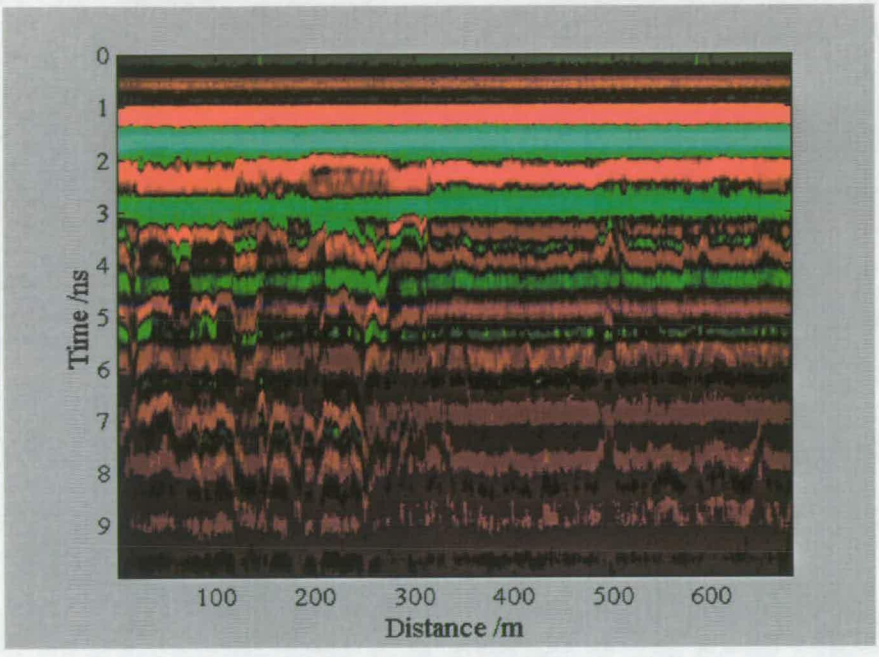

Figure 7.13: Radargram of the M8 pavement layers (short wavelength survey)

The spectral analysis of the data, shown on Figure 7.14, shows that there is a very good correlation for a wavenumber of 0.38cycles/m, i.e. 1.8m wavelengths. The coherence value at this point is 0.85, which represents a good correlation between profiles at these wavelengths. This is to be expected as the M8 extension had been in operation for about four and half years, which is very young in terms of design life. It will therefore not have experienced very much deterioration of the layers. The good correlation reflects good construction with consistent surface thickness.

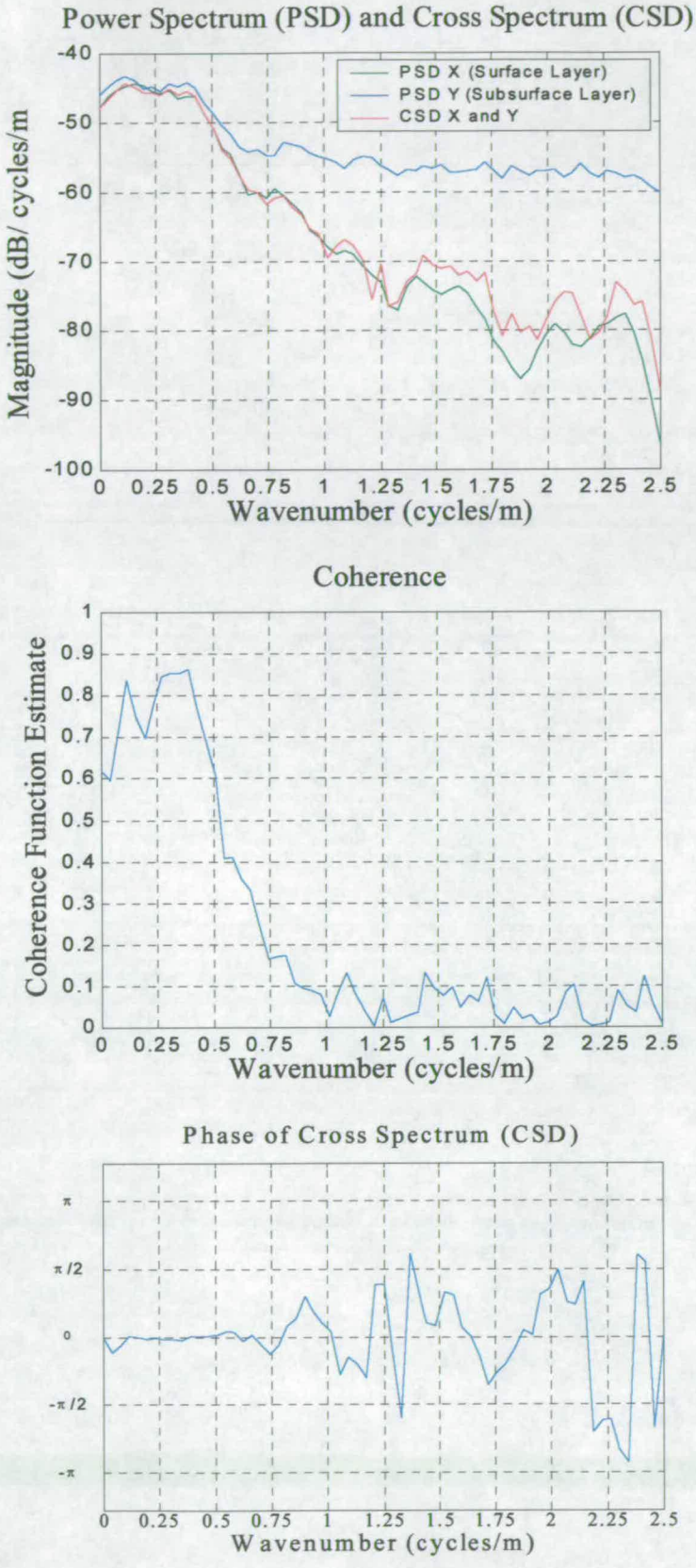

Figure 7.14: Spectral analysis of surface and sub-surface profiles on the M8 using the short wavelength set-up

7.3.2 A720 wavelength analysis

7.3.2.1 Long wavelength analysis

Figure 7.15(a) represents the radargram produced by the antenna coupled to the pavement surface. Reflections are occurring at 2ns and 3ns from the start of the survey up to about 1100m. However, after this point, the 2ns reflections stop (apart from a group around 1600m). This is shown in greater detail in the short wavelength survey (Figure 7.19) where more scans are recorded per meter.

Petroy and Roberts (Petroy and Roberts, 1997) discussed what can cause these shallower depth reflections:

- Differential compaction of the layer when it is constructed,
- A slight change in moisture content due to percolating rain water or a more impermeable zone with the rain water trapped above,
- Diffractions from large gravel pieces,
- Changes in mineral content within parts of a layer (e.g. a lorry load from a different source),
- Delaminations of the layer.

Unfortunately the author was only given the information from two cores along this road (section 7.2.2). Therefore, with the limited information available, it is impossible to explain the causes of the reflections.

It was decided that the information before 1100m should be removed from the analysis as it was impossible to locate the exact position of the bottom of the surface layer (Figure 7.16). This meant that the data in the short wavelength survey (Figure 7.19) could not be used as it only covered the first part.

The layer picking program (section 6.6.2) was then used to calculate the thickness of this layer. The thickness value is then subtracted from the surface profile in order to produce the profile of the sub-surface layer. The surface and sub-surface layer profiles are shown in Figure 7.16(b). A magnified section of this plot is shown on Figure 7.17.

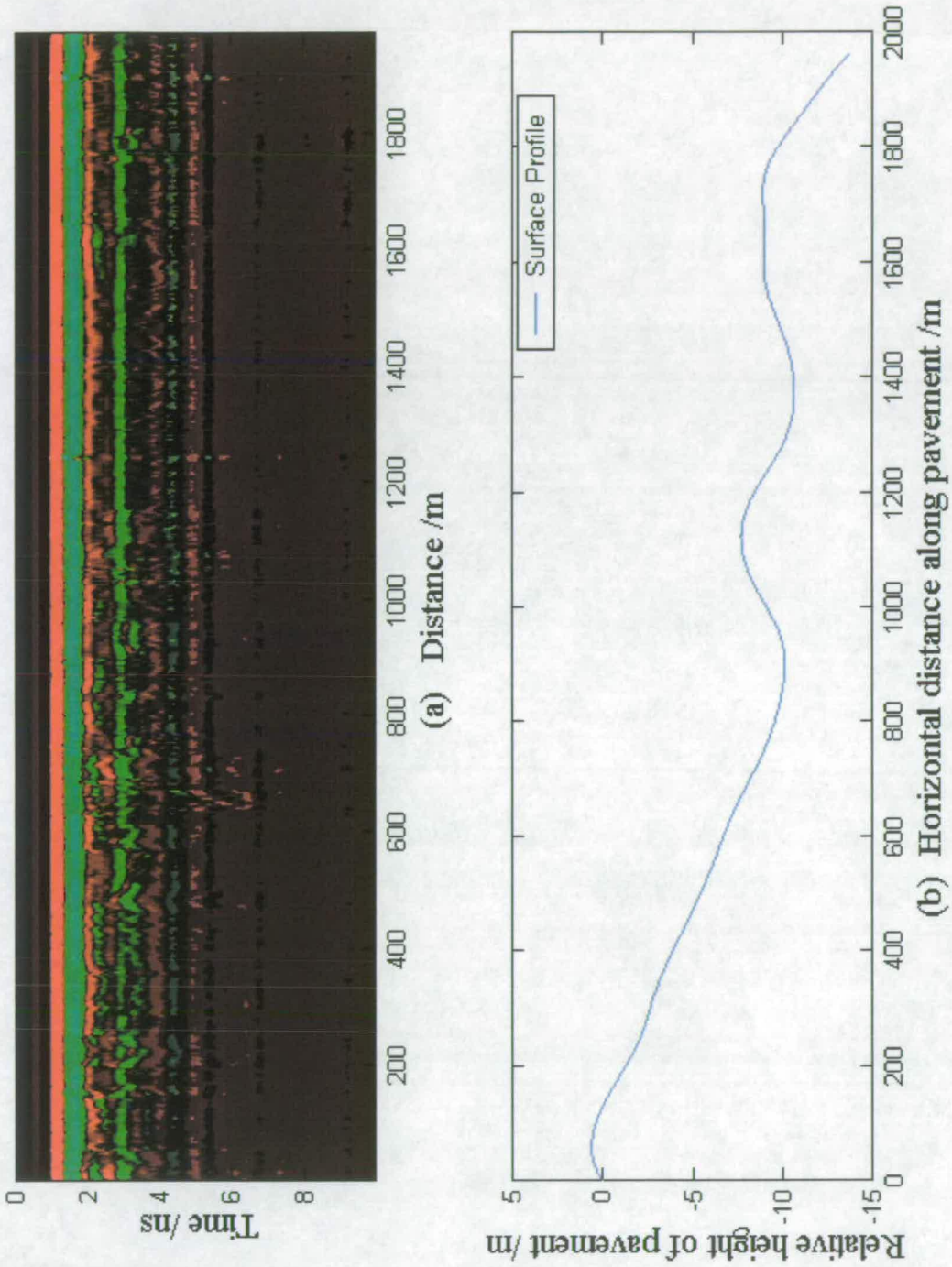

Figure 7.15: (a) Radargram of A720 pavement layers (b) Pavement elevation (Long wavelength survey)

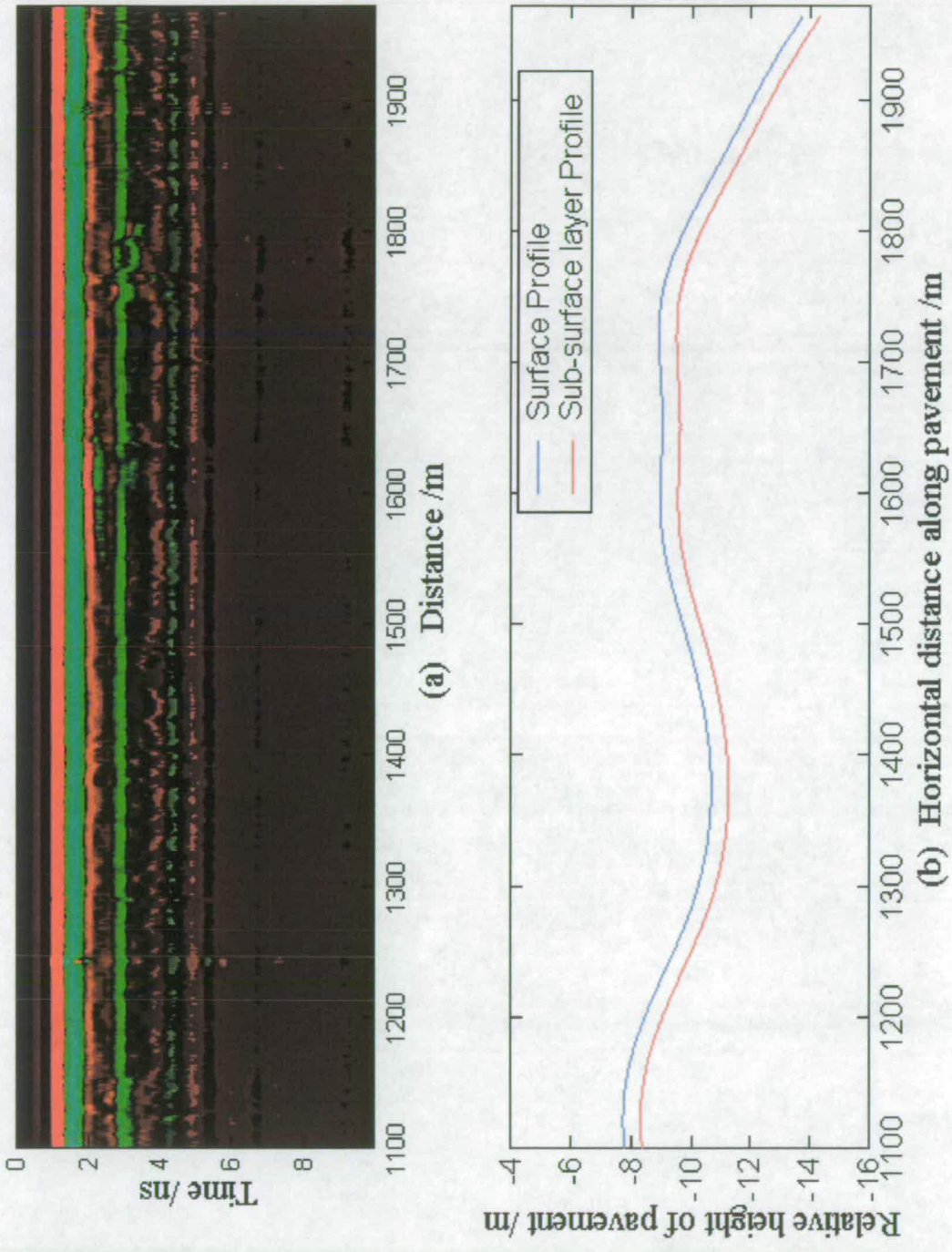

Figure 7.16: Re-adjusted figure showing (a) Radargram of A720 pavement layers (b) Pavement elevation (Long wavelength survey)

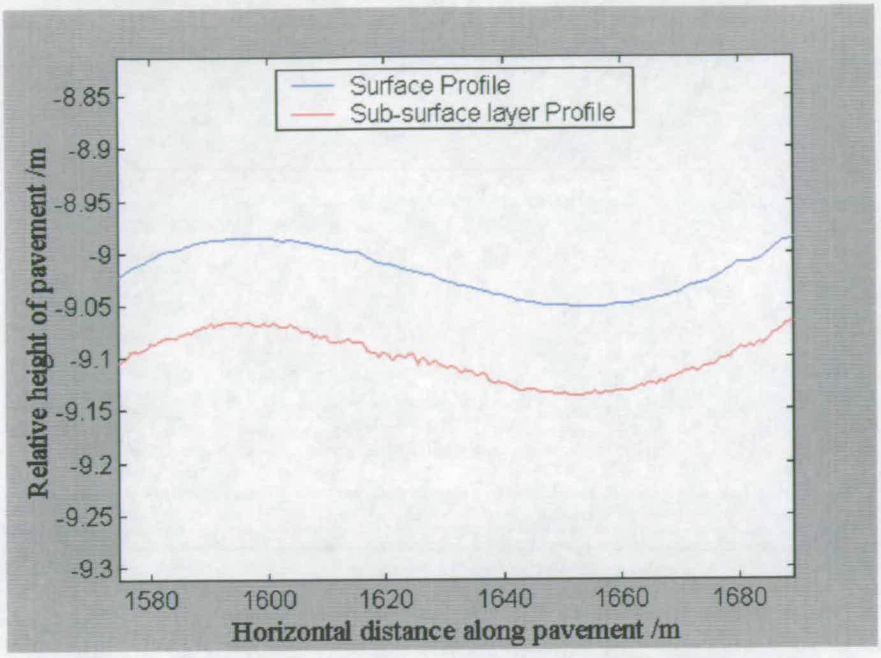

Figure 7.17: A magnified section of Figure 7.16(b))

The spectral analysis of the data, shown on Figure 7.18, shows that two prominent wavenumbers occur at 0.22cycles/m and 0.11cycles/m, corresponding to wavelengths of 4.5m and 9.1m respectively. The coherence values for these wavelengths were 0.54 and 0.56 respectively. These values indicate that a medium correlation is present between these wavelengths being present in either profile.

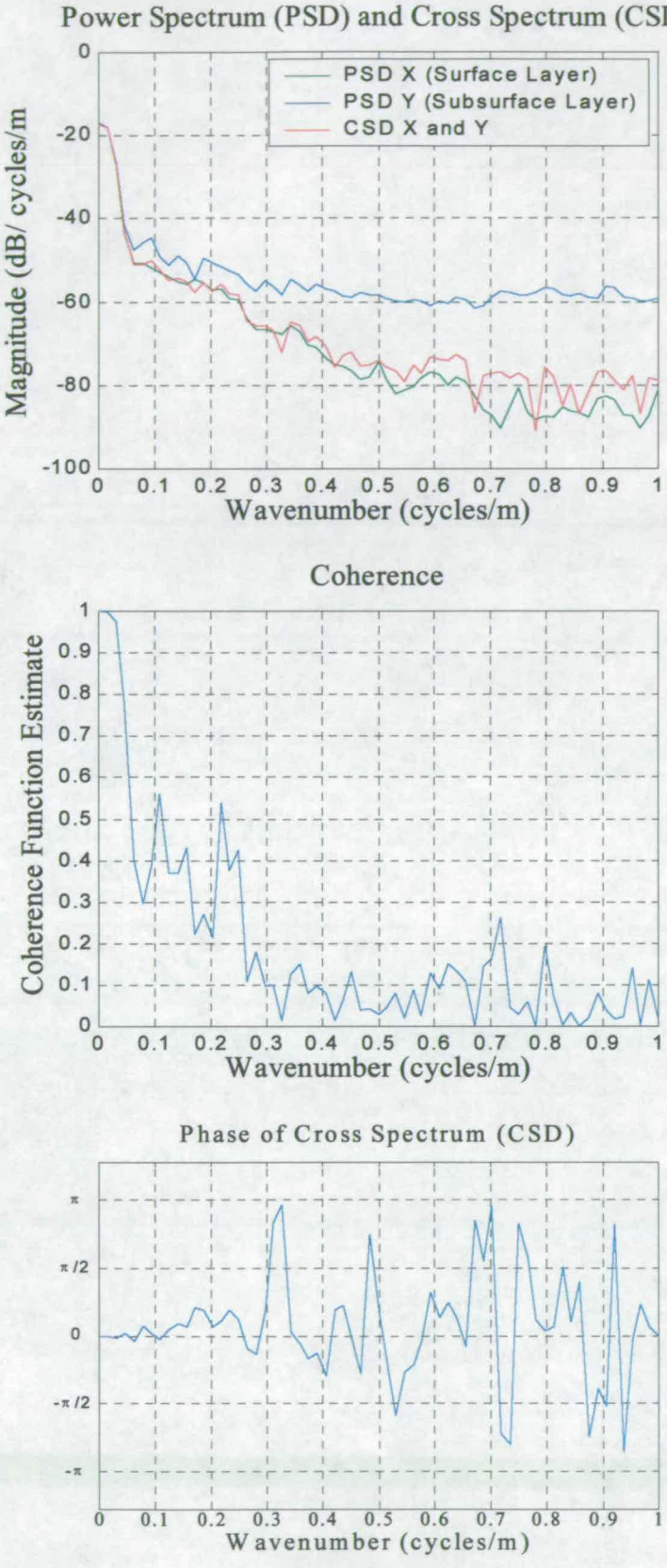

Figure 7.18: Spectral analysis of surface and sub-surface profiles on the A720 using the long wavelength set-up

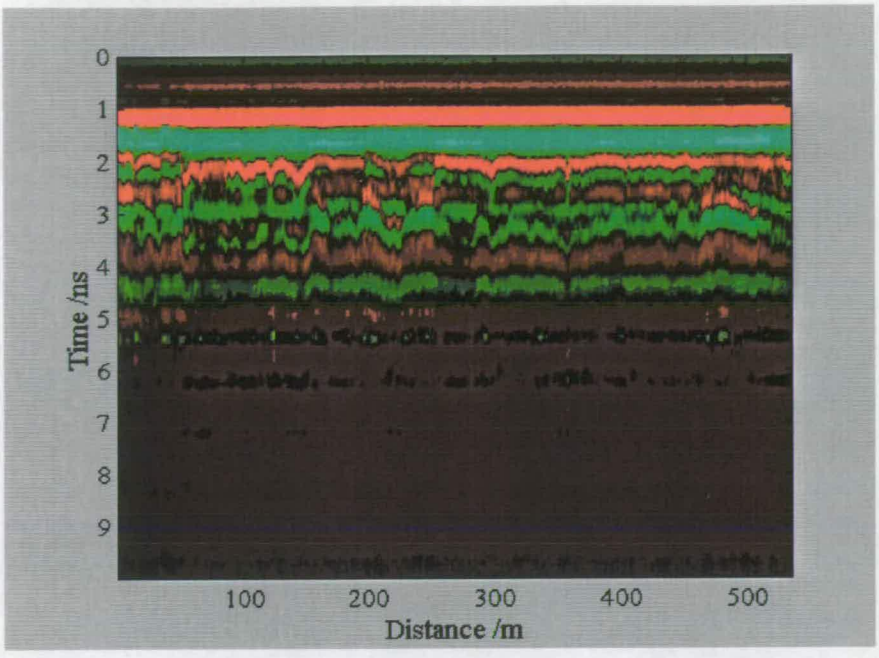

Figure 7.19: Radargram of the A720 pavement layers (short wavelength survey)

7.3.3 A199 wavelength analysis

7.3.3.1 Long wavelength analysis

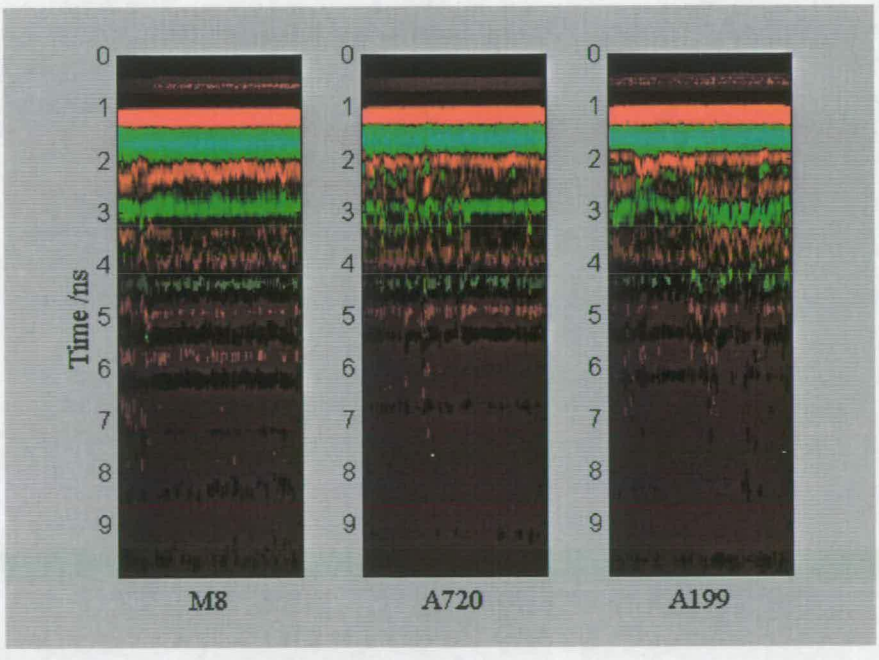

Figure 7.20: Compressed plots showing the radargrams recorded at each road

Figure 7.20 shows a compressed view of the radargrams recorded at each road when using the long wavelength set-up. This helps determine the position of the bottom of the surface layer as no core records could be obtained for this road. Each road will have a 40mm top layer. The bottom of this layer can be seen at approximately 3ns in the M8 and A720 radargram. Therefore, it is more than likely that the wavy line centred around 3ns on the A199 radargram, is the bottom of the surface layer.

There is also a faint reflection occurring at about 2ns on the A199 road, which may be due to delaminations of the surface layer or an overlay used to increase the life of the road.

A section of the A199 has been reconstructed to incorporate a flyover, enabling the road to go over the A1, this can be seen between 200m and 800m on Figure 7.21. The radar response from the bridge can be seen around 600m, which was subsequently removed and the total length of the survey readjusted (Figure 7.22(a)). The long wavelength analysis was therefore carried out from about 700m onwards. The re-adjusted radargram is shown on Figure 7.23. A magnified section of this plot is shown on Figure 7.24.

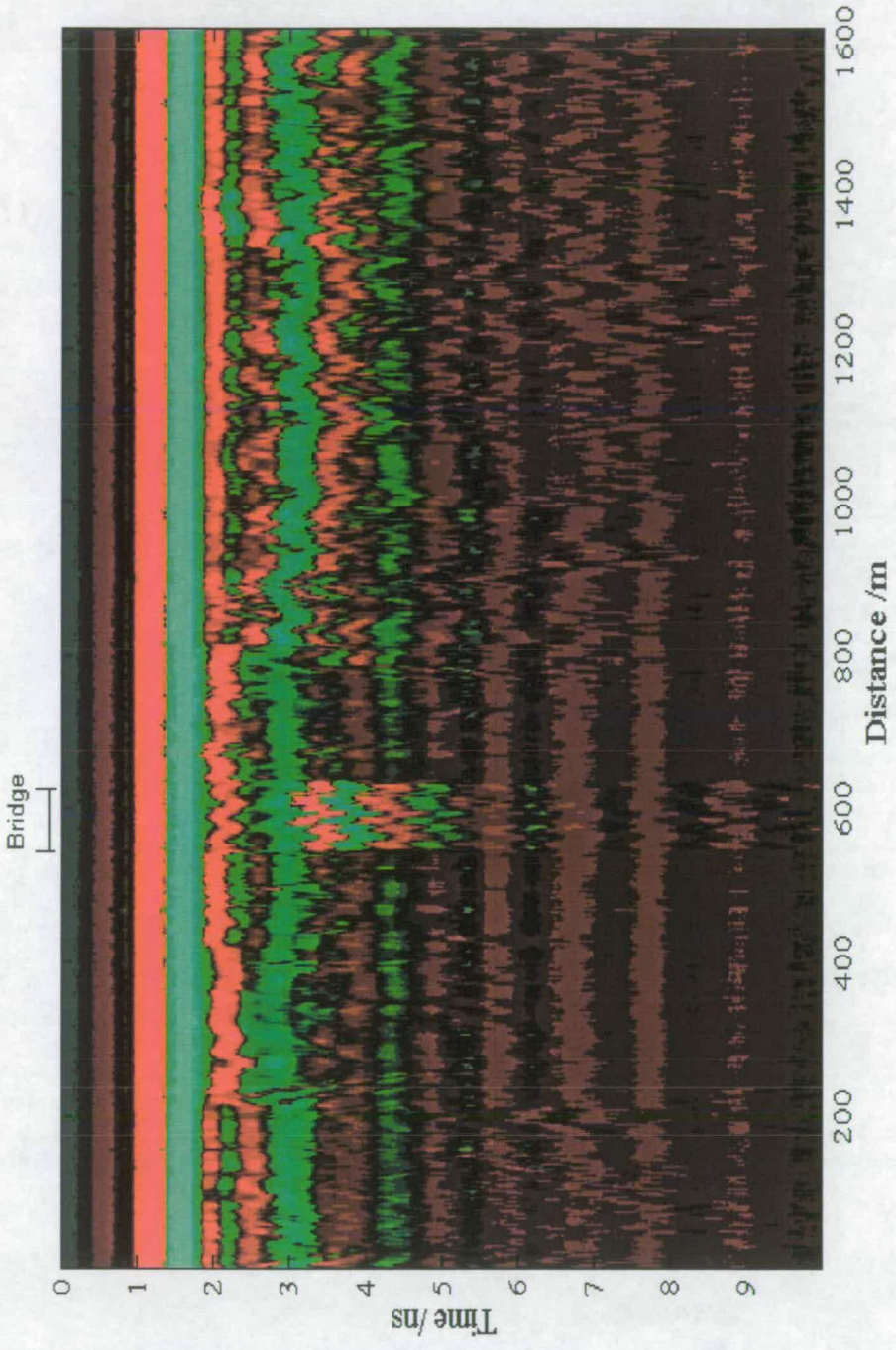

Figure 7.21: Radargram of A199 pavement layers showing the position of the bridge

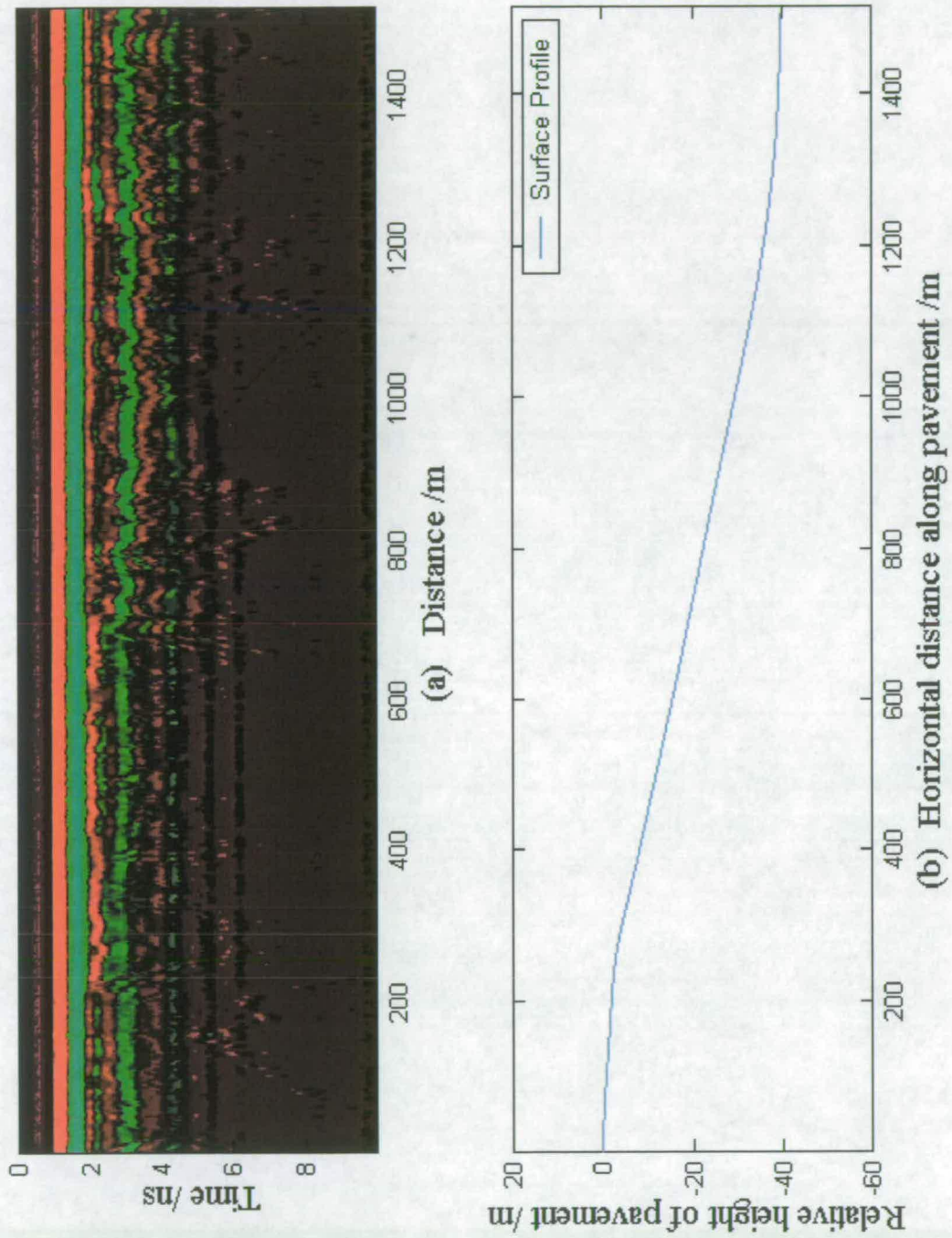

Figure 7.22: (a) Radargram of A199 pavement layers (b) Pavement elevation (Long wavelength survey)

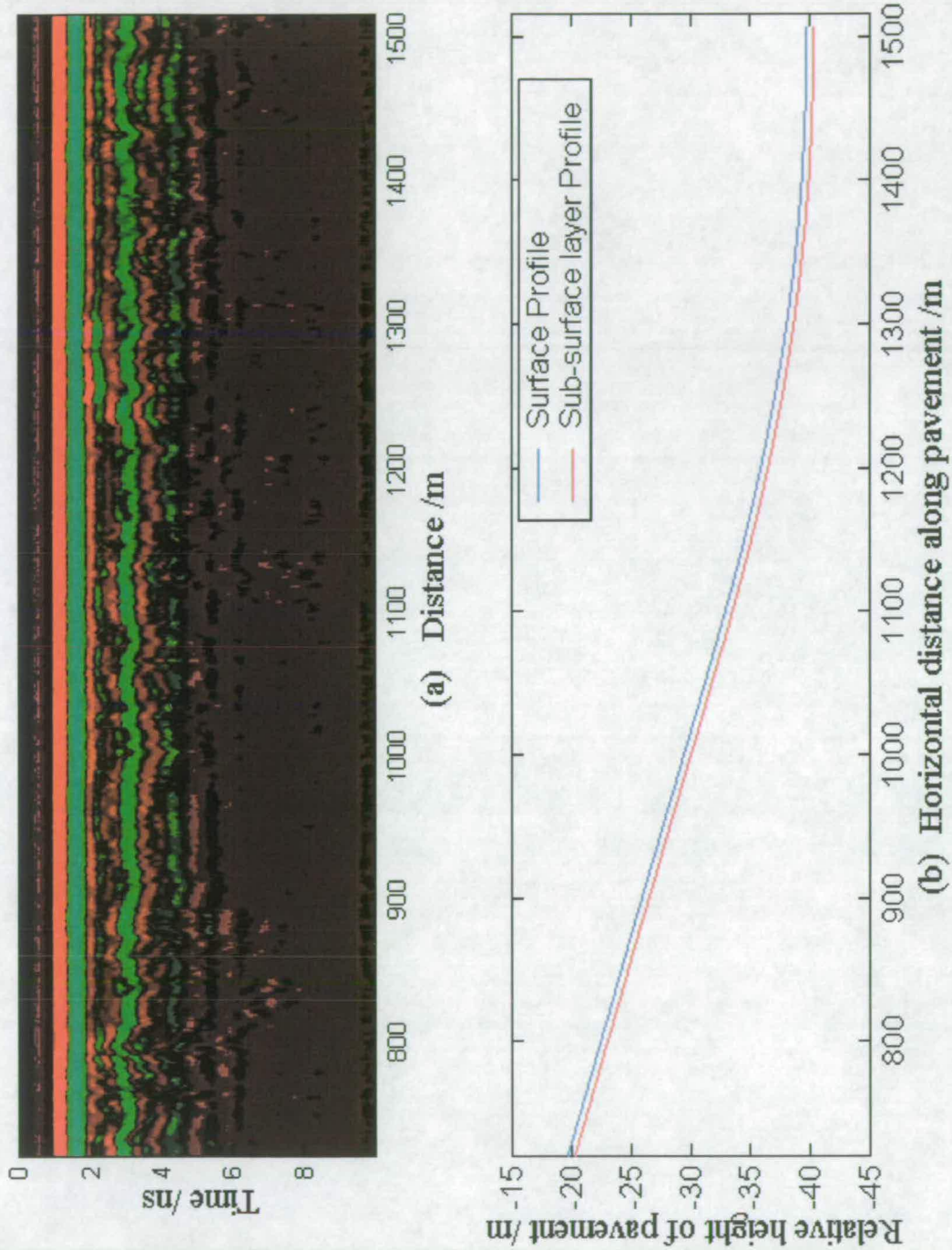

Figure 7.23: Re-adjusted figure showing (a) Radargram of A199 pavement layers (b) Pavement elevation (Long wavelength survey)

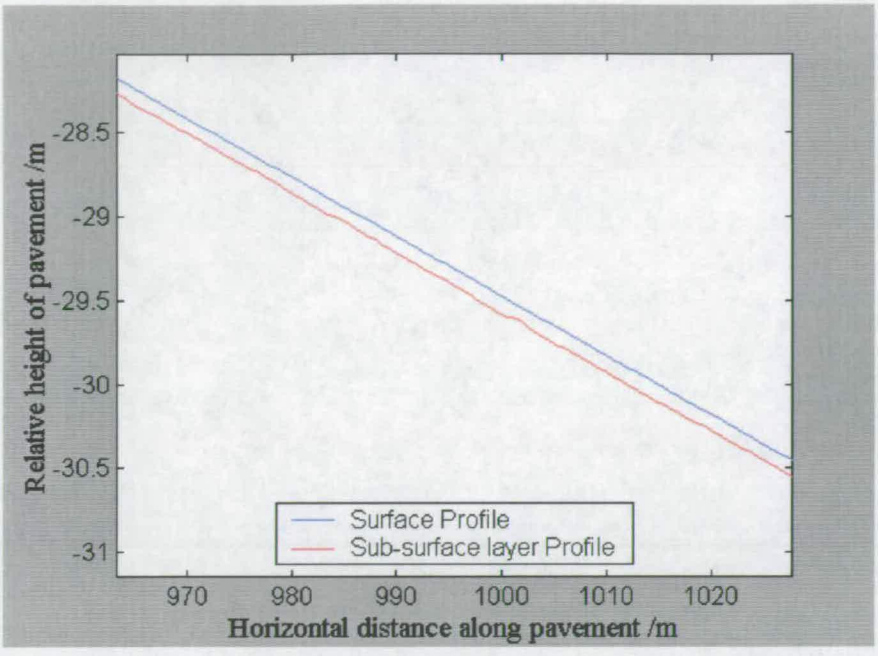

Figure 7.24: A magnified section of Figure 7.23(b))

Two different spectral analyses were carried out on the A199. The first one analysed the main reflection centred at 3ns (**A**), the second one analysed the reflection centred at 2ns (**B**).

The spectral analysis of the long wavelength survey (**A**), shown on Figure 7.25, shows that two prominent wavenumbers occur at 0.24cycles/m and 0.49cycles/m, corresponding to wavelengths of 4.2m and 2.0m. The coherence values at these points was 0.51 and 0.45 respectively. The spectral analysis of the long wavelength survey (**B**), shown on Figure 7.26, shows that the main correlation occurs at a wavenumber of 0.12cycles/m, corresponding to a wavelength of 8.3m. The coherence value for this wavelength was 0.4. The coherence values in both surveys show that there is medium to weak correlation between long wavelengths in either layer. This may be due to this road being at the end of its design life, resulting in failure of the layers to such an extent that there is no correlation between wavelengths. However, it could also be caused by inaccuracy in the sub-surface mapping as this road had a rough surface profile with some major cracks along it. The rough surface causes the antenna coupled to the ground to bump as it moves along the surface. The cracks enable any surface water to penetrate more easily into the under lying structures. This will result in the velocity of the radar wave varying along the road, as water reduces the velocity of the radar pulse. Therefore, the assumption that the velocity in layer is the same along the pavement will be incorrect and lead to errors in mapping the sub-surface layer

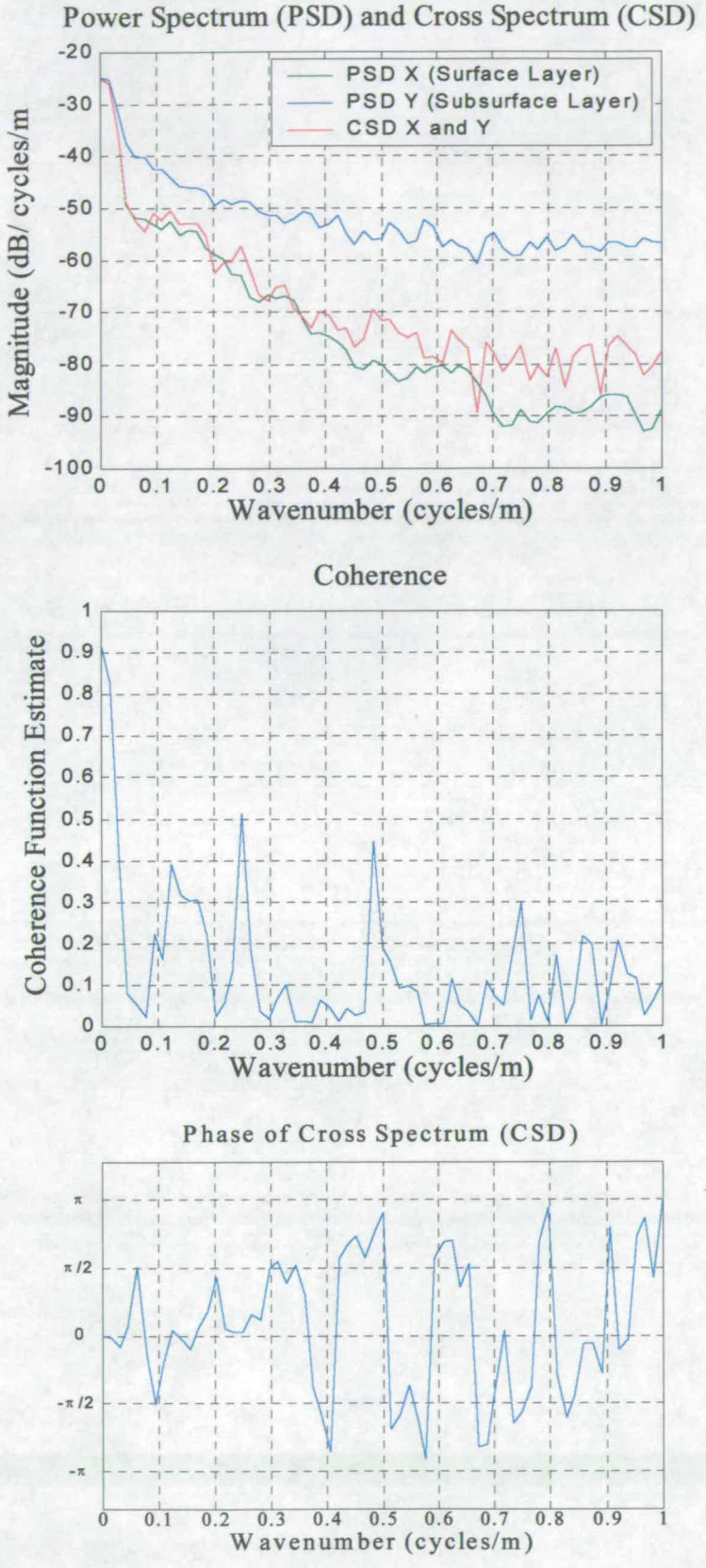

Figure 7.25: Spectral analysis of surface and sub-surface profiles on the A199 using the long wavelength set-up (**A**)

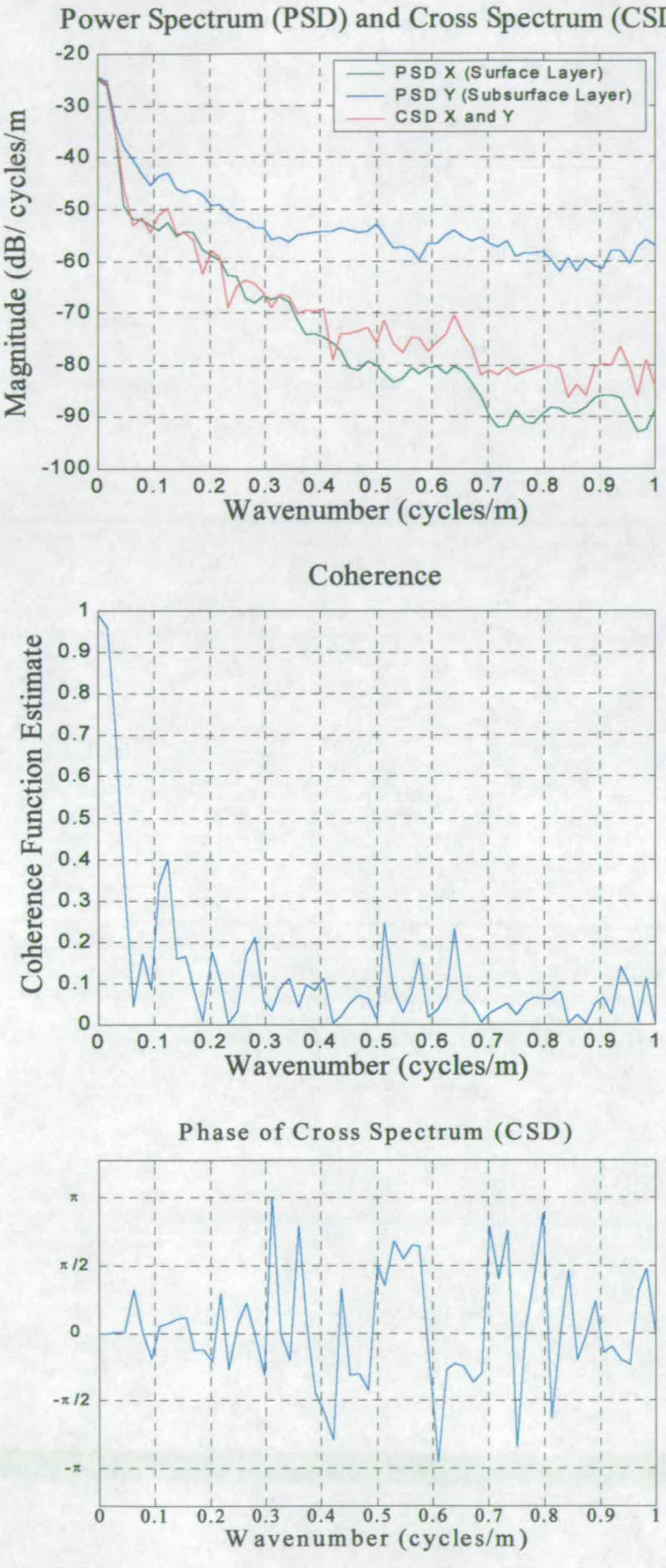

Figure 7.26: Spectral analysis of surface and sub-surface profiles on the A199 using the long wavelength set-up (**B**)

7.3.3.2 Short wavelength analysis

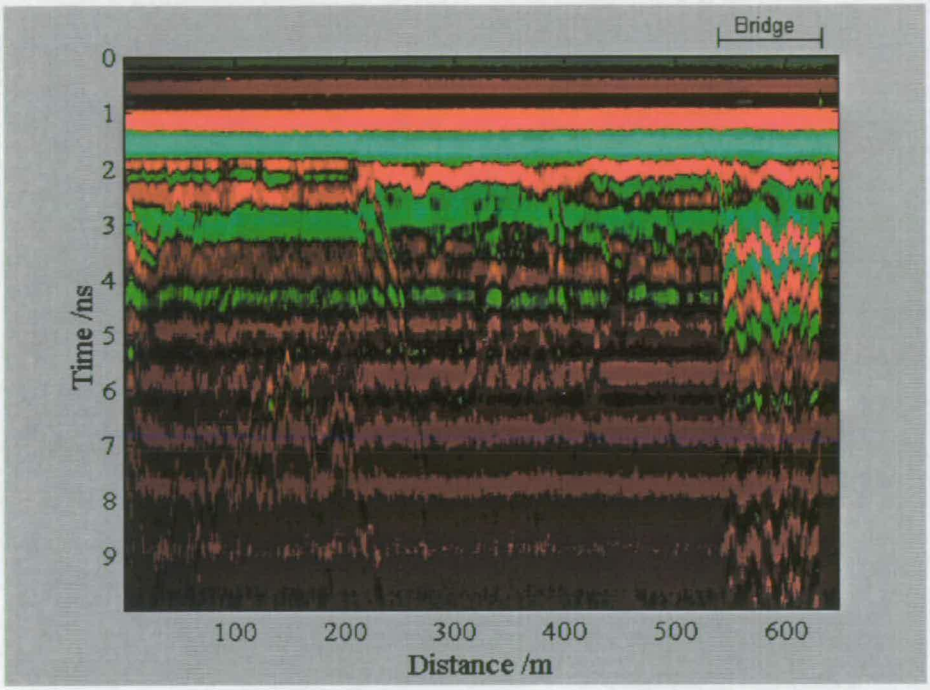

Figure 7.27: Radargram of the A199 pavement layers (Short wavelength survey)

Figure 7.27 shows the radargram produced by the surface mounted antenna. The information after 200m was removed as this is the reconstructed part of the road which incorporates the flyover. The readjusted radargram is shown in Figure 7.28(a). The sub-surface profiling program was used to map two profiles, one centred at 2ns and the other at 3ns. Figure 7.28(b) shows the sub-surface profiles of the 3ns reflection and the surface profile. Figure 7.29 shows a magnified section of Figure 7.28(b).

The spectral analysis compared each of these reflections to the surface layer. The main reflection (centred around 3ns) is denoted by **A** and the 2ns reflection is denoted by **B**. It should be noted that the analysis has been carried out on a different section of the A199 to the long wavelength survey. This was not intended as the long and short wavelength surveys were started at the same position.

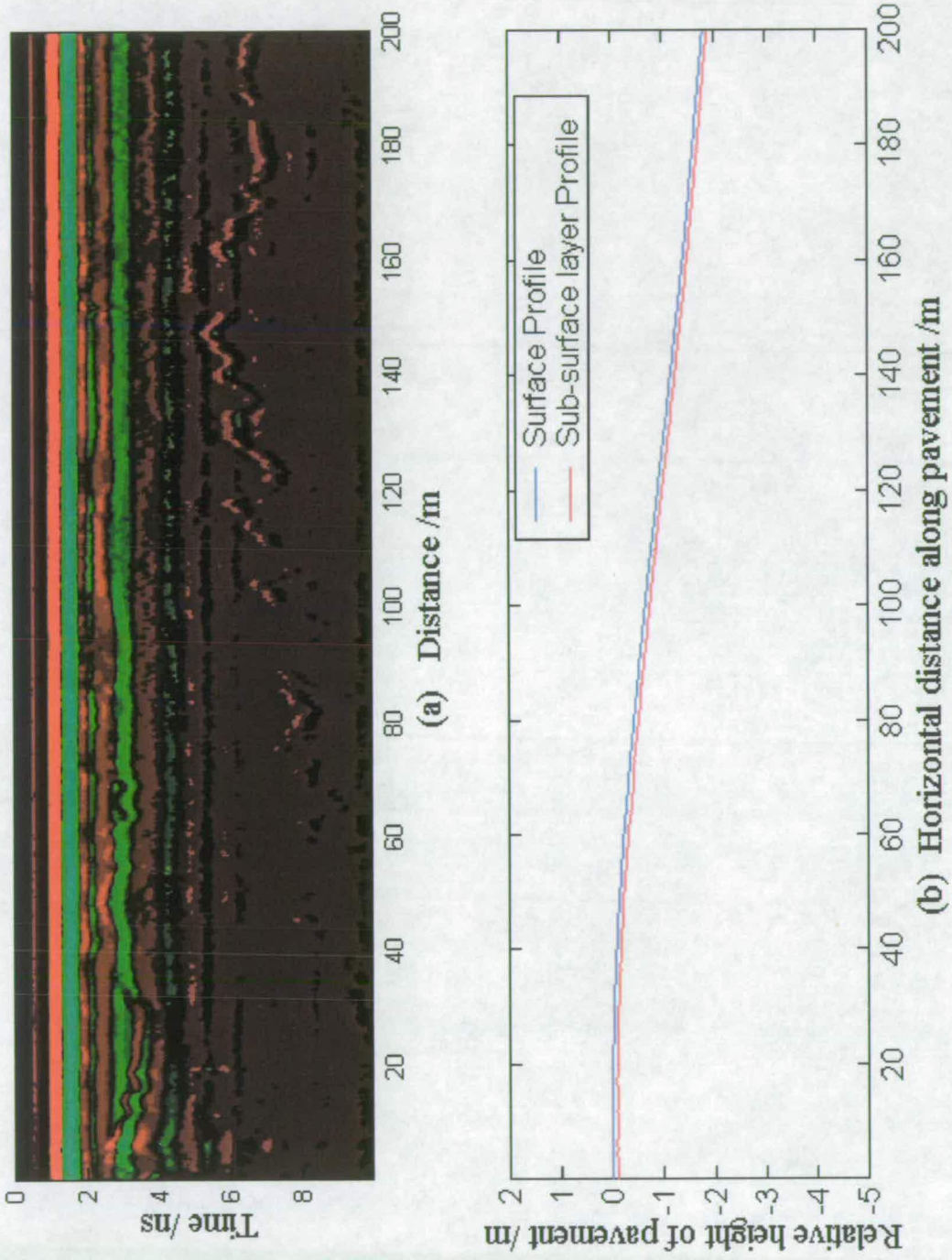

Figure 7.28: Re-adjusted figure showing (a) Radargram of A199 pavement layers (b) Pavement elevation (Short wavelength survey) (sub-surface **A**)

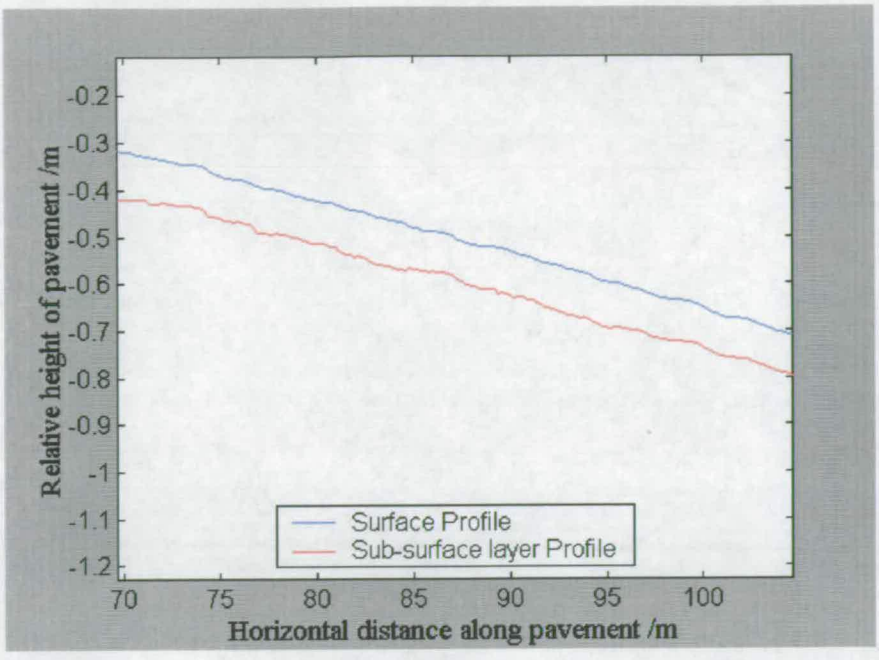

Figure 7.29: A magnified section of Figure 7.28(b)

The spectral analysis of the short wavelength survey (**A**), shown on Figure 7.30, shows that one prominent wavenumber produced some correlation, i.e. 0.5cycles/m, corresponding to a wavelength of 2.0m. The coherence for this wavelength was 0.55. This results indicates that there is a reasonable correlation between the 2m wavelengths occurring in each profile.

The spectral analysis of the short wavelength survey (**B**), shown on Figure 7.31, shows that there is a very good correlation for wavenumbers of 0.55cycles/m, i.e. 1.8m wavelengths. The coherence value at this point is approximately 0.9. This shows that there is a very good correlation between these wavelengths on the road. Unfortunately, the short and long wavelength survey can not be compared as they are from different sections along the road.

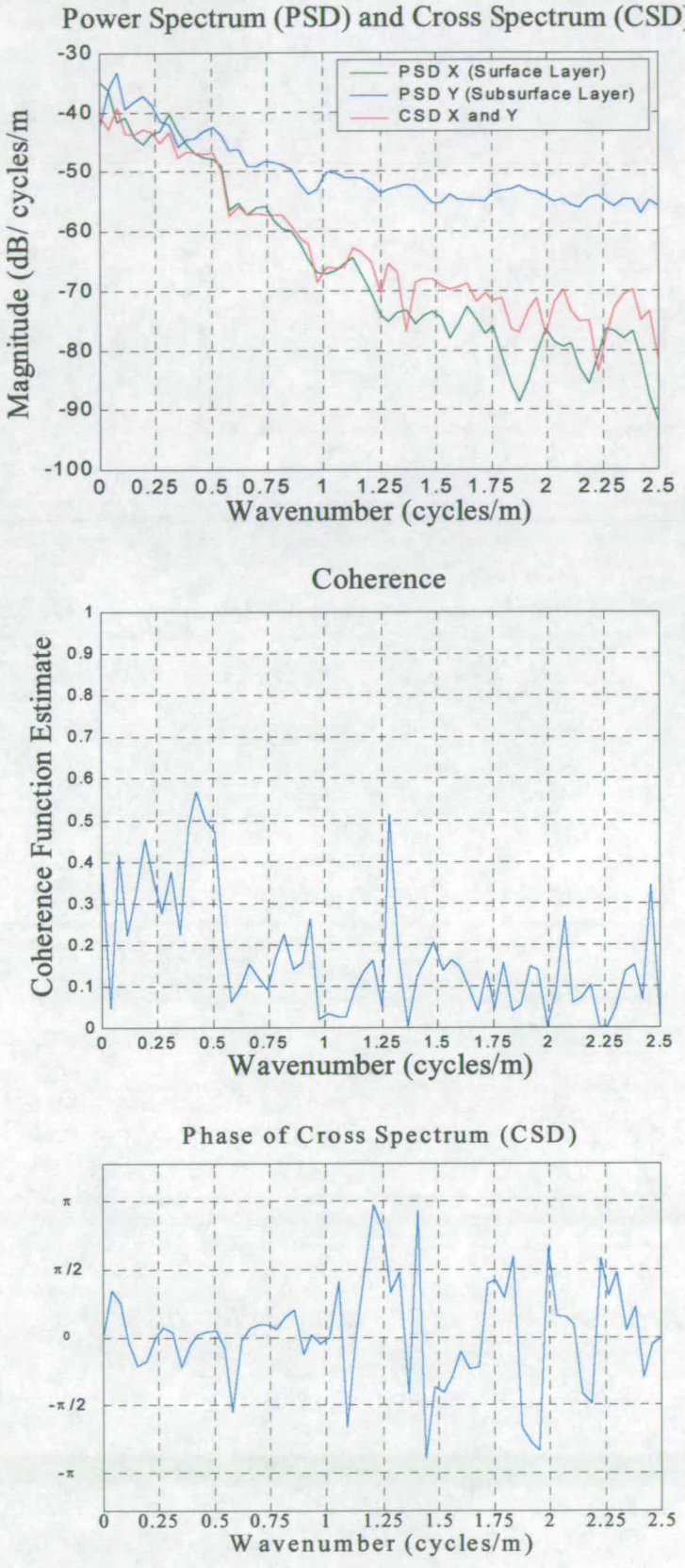

Figure 7.30: Spectral analysis of surface and sub-surface profiles on the A199 using the short wavelength set-up (**A**)

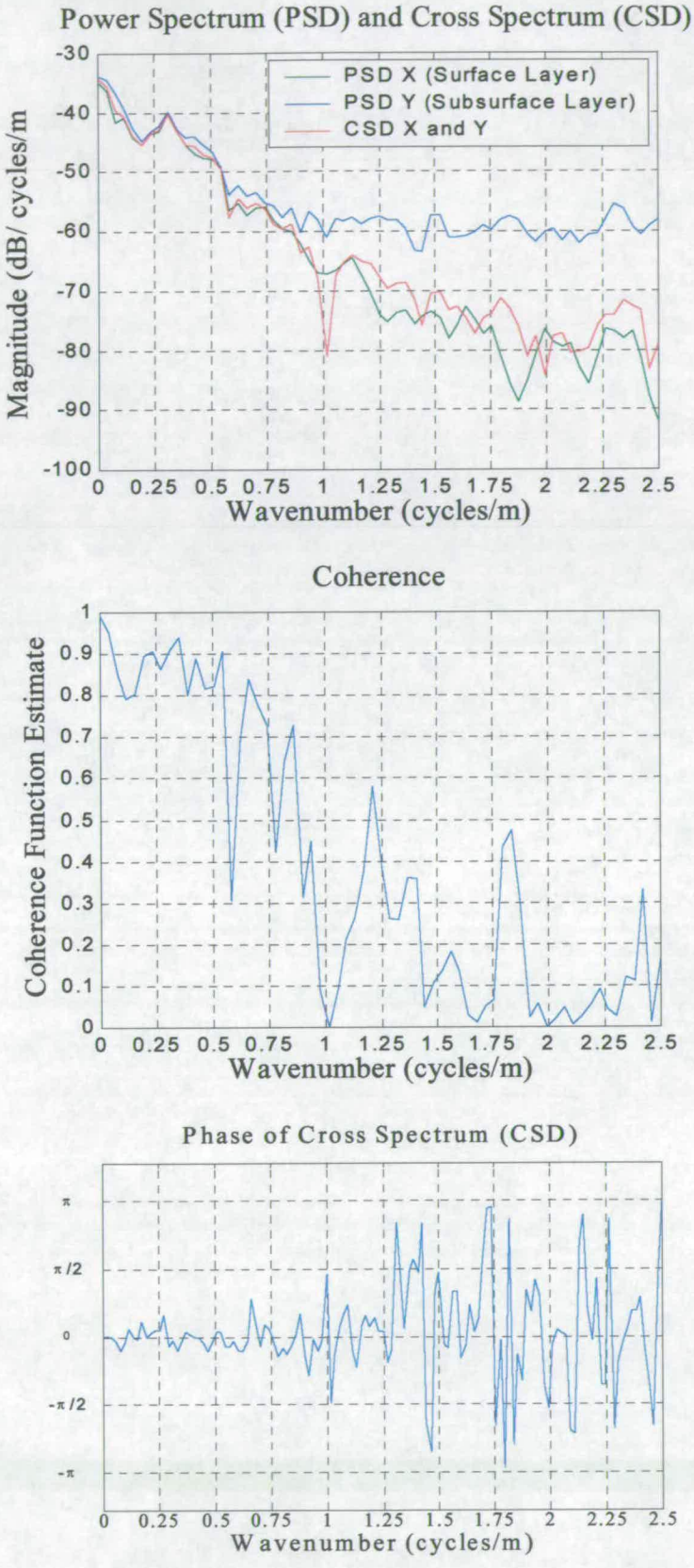

Figure 7.31: Spectral analysis of surface and sub-surface profiles on the A199 using the short wavelength set-up (**B**)

7.4 Conclusions

- The 1.5GHz antenna was the most appropriate antenna to use for detecting thin layers (0.1m >) as its minimum vertical resolution is 0.035m (assuming a velocity of 0.1m/ns), whereas the 400MHz and 500MHz antennas have minimum vertical resolutions of 0.125m and 0.1m respectively.

- The reflection coefficient method was used to calculate the radar velocity in the surface layer.

- The profile of the bottom of the surface layer will only be found due to inaccuracies in the reflection coefficient method to determine velocities in multiple layers.

The main experiments compared the surface and sub-surface profiles from actual road data. This data was obtained from a motorway (M8 extension), 'A' road (A720 bypass) and minor road (A199). The results from the main road experiment are summarised in Table 7.6. The following conclusion were made:

- The M8 showed a good correlation between wavelengths on the surface and sub-surface layer. This is due to the young age of the road, resulting in less deterioration of layers, therefore reflecting good construction with consistent surface thickness.

- The short wavelengths could not be analysed in the A720 survey due to difficulties in determining the exact position of the bottom of the surface layer. The long wavelength analysis showed that there was a medium correlation at 4.5m and 9m wavelengths.

- Two different spectral analyses were carried out on the A199. The first one analysed the main reflection centred at 3ns (**A**), the second one analysed the reflection centred at 2ns (**B**). This was done for both the long and short wavelength surveys. The coherence values, in both long wavelength surveys, showed that there was medium to weak correlation between long wavelengths. The short wavelength analysis showed that there is a very good correlation between wavelengths in each layer. Unfortunately, the short and long wavelength surveys cannot be compared as they were carried out on different sections along the road.

	M8 (40-50mph)		A720 (50-60mph)		A199 (40-50mph)		
					Survey A		Survey B
Long wavelengths (m)	8.3	5.3	9.1	4.5	4.2	2.0	8.3
Coherence	0.5	0.5	0.56	0.54	0.5	0.45	0.4
Vehicle frequency (Hz)	2.1-2.7	3.4-4.2	2.4-2.9	4.9-5.9	4.2-5.3	8.9-11.1	2.1-2.7
Short wavelengths (m)	2.6		No results		2.0		1.8
Coherence	0.85				0.55		0.9
Vehicle frequency (Hz)	6.8-8.5				8.9-11.1		9.9-12.3

Table 7.6: Summary of results also showing vehicle frequencies for typical speeds along the different roads

Note: Coherence values close to 1 show good correlation between wavelengths on the surface and sub-surface, whereas, poor correlation will have a value close to 0.

The vehicle speeds between 40 and 50mph were chosen for the M8 extension because the surveyed section was 80m after a major roundabout, which would reduce the speed of the HGVs. Vehicle speeds between 50 and 60mph (maximum speed of HGVs) were used in the A720 analysis because of the layout of the road. The typical speeds of HGVs would probably be between 40 and 50mph on the A199 because the road was much steeper and at the bottom of the surveyed section was a roundabout.

The correlated frequencies along different roads can either be built-in or generated by the vehicles. The only way to determine if they are built-in is to survey the road immediately after it is laid. Subsequent surveys along the same stretch of road over the years will enable the effects of the vehicle loads to be analysed.

If they are due to the vehicle then Cole (Cole, 1990) showed that two different frequency ranges can be identified:

- 1.5-4 Hz: Sprung mass rigid body vibration (Vibration of main vehicle body).
- 8-15 Hz: Unsprung mass rigid body vibration (Vibration of the axles and wheels, sometimes referred to as "wheel hop").

The results from the M8 and A720 (Table 7.6), for long and short wavelengths, show that the main vehicle body frequencies are causing damage. However, the results from the A199 indicate that the long wavelengths are due to the main body frequencies, whereas the short wavelengths are mainly due to the frequencies produced by the axles and wheels.

These experiments have shown a varied response in the correlation of wavelengths for different types of roads. In general, the short wavelengths correlate better with each other than the long wavelengths. However, more experiments would need to be carried out on different road constructions and different types of roads to establish if any trends occur. Deeper layer profiles should also be correlated with the surface profile to examine if any correlation is present in these layers. This could not be carried out on these experiments as only one antenna was used to map the sub-surface profile.

Chapter 8

Conclusions and recommendations for future work

8.1 Summary of main conclusions

8.1.1 Preliminary non-destructive testing experiments on thin flexible pavements (Chapter 4)

- The GPR responses of thin pavements can be impossible to directly interpret due to the confusion of initial pulse reflections from the bottom of the thin layers (whether the bottom of the bituminous layers of the pavement or interfaces between different bituminous materials).

- The effect of the material beneath the thin layer (and hence the thickness of the layer itself) has no effect on the initial response from the surface and this can therefore be eliminated since this is shown to reveal the response from the bottom of the layer.

- A good correlation was produced with the theoretical values when using a 54kHz ultrasonic transducer on a piece of flexible pavement. In comparison, the 82kHz transducer gave less energy in the important frequency range.

- The sonic technique requires a lot of analysis of the actual material which the waves are propagating through. In the field, this method has many obstacles which must be overcome before it can be successfully applied.

8.1.2 Semi-intrusive determination of radar wave velocity (Chapter 5)

- The chapter reviewed several established techniques used to determine radar wave velocity within various materials. Each technique has its advantages and disadvantages and usage will depend on the accessibility around the object under

investigation, its geometry, the required accuracy, the time and manpower available, and the amount of physical interference with the structure that is acceptable.

- A new semi-intrusive method is proposed here which involves the insertion of a metal bar into the object under investigation. This enables the impulse radar velocity of the material under investigation to be readily interpreted from the radargram. The series of GPR simulations carried out in two and three dimensions using an FDTD GPR model produced results with errors of less than 10%. However, it was noted that these errors could be reduced if more sophisticated methods of regression analysis were used.

- Several experiments were carried out in the laboratory. Initial experiments were carried out to find the optimum insertion angle of the bar and this was found to be between 22° and 26°. Additional experiments investigated how accurately the radar velocities could be determined when two and three-layer models were used. It was found that there was a good correlation between the velocities determined using the transmission method and those using the new method.

- This method was tested in the field to detect layers of sand on a beach. A metal bar was inserted into the sand and it could be seen from the radargram that there were two distinct velocities. The top layer had a velocity of 0.23m/ns, indicating a very dry layer of sand, and the bottom layer was 0.11m/ns, indicating damp sand.

8.1.3 Design and testing of a radar trailer (Chapter 6)

- A method for comparing the longitudinal profiles of the surface and subsurface layers on pavements using GPR is proposed. Three radar antennas were used to detect the surface profile, with a fourth one detecting the sub-surface layers on pavements.

- The optimum height to position the antennas to detect the surface profile was found to be between 25 and 30cm.

- Wavelengths of interest were found to be between 1m and 15m

- In order to map the long wavelengths it was calculated that the three surface antennas needed to be 3m apart. However, due to the position of the axle and limits on the maximum size that a trailer can be by law, the spacing between each antennas was 1.4m and 3m respectively.

- The smallest spacing between the antennas was 0.5m due to the interference from the cables. It was found that with this spacing, the smallest wavelengths that could be measured were 1.8m.

- A preliminary experiment was carried out on the profile mapping of the pavement surface. The results showed that the antennas operated well except with large changes in the road's gradient. It was, however, felt that this road did not simulate the conditions of a motorway. A second set of experiments showed that using spot heights or level information improves the ability of the program to recreate the actual profile.

8.1.4 Wavelength analysis of road layers (Chapter 7)

- The M8 showed a good correlation between wavelengths on the surface and sub-surface layer. This is due to the young age of the road, resulting in less deterioration of the layers, therefore reflecting good construction with consistent surface thickness. The vehicle frequencies along this section were shown to vary between 2.1 Hz and 8.5Hz, depending on the wavelengths.

- The short wavelengths could not be analysed in the A720 survey due to difficulties in determining the exact position of the bottom of the surface layer. The long wavelength analysis showed that there was a medium correlation at 9.1m and 4.5m wavelengths. The vehicle frequencies varied between 2.4 Hz and 5.9Hz, depending on the wavelengths.

- The coherence values in the A199 surveys showed that there was a medium to weak correlation between long wavelengths in either layer. The short wavelength analysis showed that there is a very good correlation between wavelengths on each layer. The vehicle frequencies varied between 2.1Hz and 12.3Hz, depending on the wavelengths.

- The results show that main vehicle body frequencies cause damage on the M8, A720 and long wavelengths on the A199, whereas the short wavelengths on the A199 are due to the frequencies produced by the axles and wheels. However, it is difficult to say whether these frequencies are generated by the vehicle or built-in when the pavement was laid. Built-in frequencies can only be ruled out if a survey is carried out immediately after the pavement is laid and before any traffic is allowed on it.

- These experiments have shown a varied response in the correlation of wavelengths for different types of roads. In general, the short wavelengths correlate better with each other than the long wavelengths.

8.1.5 Recommendations for further work

The tests on the new semi-intrusive technique for determining radar wave velocities were only carried out using a 1.5GHz antenna. This antenna only enables strata in shallow depths to be analysed. Experiments should be performed to analyse the accuracy of the method using lower frequency antennas (greater penetration depths). Further tests should also be carried out on different types of pavements to investigate its effectiveness in pavement analysis.

The experiments using the radar trailer to map the surface and sub-surface profiles have shown a varied response in the correlation of wavelengths for different types of roads. More experiments would need to be carried out on different road construction and different types of roads on order to establish if any trends occur.

The replacement of the radar antennas to map the surface profile with a laser profilometer will remove the need to use spot heights along the road. New improvements in the accuracy of Global Positioning Systems (GPS) will enable the exact position of the trailer along the road to be known. This may eventually replace the need for laser profilometers to map the surface profile.

Multiple sub-surface layer profiles could be measured if three antennas are coupled to the ground instead of using one antenna. This removes the need to use the reflection coefficient method to measure the relative permittivities of each layer. This technique was developed by Mesher *et al.* (Mesher *et al*, 1995) and has shown good results for mapping sub-surface layers. Correlation could therefore be obtained between the surface and deeper layer profiles.

References

Adcock, A. D., Dass, W. C., and Rish, J. W. I., (1995) Ground penetrating radar for airfield pavement evaluations, In *SPIE-The International Society for Optical Engineering, Advanced Microwave and Millimeter-Wave Detectors*, Oakland, CA, pp. 373-384.

Annan, A. P., (1997) *Ground penetrating radar: Workshop notes*, Sensors & Software Inc, Canada.

Anon, (1962A) The AASHO road test, Special Report 73, *Highway Research Board.*

Anon, (1962B) The AASHO road test: Report 7: Summary Report, Special Report 61G, *Highway Research Board.*

Anon, (1987) *Department of Transport: Regulation of heavy lorries*, National Audit Office, HMSO, London.

Anon, (1992A) *Design guide for road surface dressing*, Road note 39, TRL.

Anon, (1992B) *Bituminous mixes and flexible pavements: An Introduction*, BACMI, London.

Anon, (1994) Use and limitations of ground-penetrating radar for pavement assessment, in Design Manual for Roads and Bridges, HMSO.

Anon, (1997A) *Department of the Environment, Transport and the Regions: Lorry weights-A consultation document*, DETR.

Anon, (1997B) *The complete towing guide for trailer and caravan owners nationwide*, 9th Edition, Indespension Ltd.

Anon, (1999A) Paving the way: A consultation paper, Highways Agency.

Anon, (1999B) Data collection and reduction with portable seismic pavement analyser (PSPA), Short course notes, Centre for highway materials research, The University of Texas at El Paso.

Armitage, R. J., (1989) A structural evaluation method for concrete pavements, *Highways*, May, pp. 9-21.

Atkinson, K. (editor), (1997) *Highway maintenance handbook*, 2nd Edition, Thomas Telford Ltd, London.

Attoh-Okine, N. O., (1996) Using ground penetrating radar in pavement thickness measurements - a cost comparison with the traditional coring method, *Proceedings of the Institution of Civil Engineers: Municipal Engineers*, **115**, pp. 86-89.

B.S. 4987, (1993) Coated macadam for roads and other paved areas: Part 1 Specification for constituent materials and for mixtures, BSI, London.

B.S. 4987, (1993) Coated macadam for roads and other paved areas: Part 2 Specification for transport, laying and compaction, BSI, London.

B.S. 594, (1992) Hot rolled asphalt for roads and other paved areas: Part 1 Specification for constituent materials and asphalt mixtures, BSI, London.

B.S. 594, (1992) Hot rolled asphalt for roads and other paved areas: Part 2 Specification for transport, laying and compaction of rolled asphalt, BSI, London.

B.S. 598, Part 107, (1990) Method of test for the determination of the composition of design wearing course rolled asphalt, BSI, London, (Amended, May 1996).

B.S. 6100, (1992) Sub section 2.4.1, Glossary of building and civil engineering terms, BSI, London.

B.S. 76, (1986) Specification for tars for road purposes, London, BSI.

Ballard, G. S., (1993) Non-destructive assessment of pavement design and new build quality, In *International Conference on Non-Destructive Testing in Civil Engineering*, The British Institution of NDT, Liverpool, Vol. 1, April , pp. 391-404.

Brademeyer B., Delatte, N., and Markow, M., (1986) Analysis of dynamic loads on highway pavements: Part II – Pavement Response, In *Proceedings of the 1st International Symposium on Heavy Vehicle Weights and Dimensions*, Kelowna, British Columbia, June.

Brademeyer B., (1988) Mechanistic vehicle-pavement interactions, In *Load Equivalency Workshop*, McLean, Virginia, September.

Brook, D., and Wynne, R. J., (1988) *Signal processing: Principles and applications*, Edward Arnold, London.

Brown, S. J., (1998) Developments in pavement structural design and maintenance, *Proceedings of the Institution of Civil Engineers: Transportation*,**129**, pp. 201-206.

Brown, S. J., (1996) Soil mechanics in pavement engineering, *Géotechnique*, **46**(3), pp. 383-426.

Brunton. J., Brown, S. F., and Armitage, R. J., (1989) Use of the Falling Weight Deflectometer for the evaluation of pavements with cement treated bases, In *Proceedings of the 5th Conference on asphalt pavements for Southern Africa*, Swaziland, June.

Bungey, J. H., and Millard, S. G., (1993) Radar inspection of structures, *Proceedings of the Institution of Civil Engineers: Structures & Building*, **99**, pp. 173-186.

Cebon, D., and Newland, D. E., (1983) The artificial generation of road surface topography by the inverse FFT method, In *Proceedings of the 8th IAVSD Symposium on the dynamics of vehicles on roads and on railway tracks*, Cambridge, MA, pp. 29-42.

Cebon, D., (1985) *The dynamic interaction between vehicles and road surfaces*, PhD Thesis, University of Cambridge, Engineering Department.

Chan, W. K. E., and Evans, A. R., (1994) Assessing concrete pavements with the falling weight deflectometer, *Concrete*, **28**(6), pp. 14-16.

Cole, D. J., (1990) *Measurement and analysis of dynamic tyre forces generated by lorries*, PhD Thesis, University of Cambridge, Engineering Department.

Colla, C., Forde, M.C., McCann, D.M., Das, P.C. & Batchelor, A.J., (1997) "Radar tomography of masonry arch bridges", In *Proceedings of the Seventh International conference on Structural Faults and Repair*, Edinburgh, Scotland, Vol. 1, pp. 143-151.

Collins, H. J., and Hart, C. A., (1936) *Principles of road engineering*, Edward Arnold & Co., London.

Collop, A. C., (1994) *Effects of traffic and temperature on flexible pavement wear*, PhD thesis, University of Cambridge, Engineering Department.

Daniels, D. J., (1996A) Surface-penetrating radar, *Electronics & Communication Engineering Journal*, **18**(4), pp. 165-182.

Daniels, D. J., (1996B) *Surface-penetrating radar*, The Institution of Electrical Engineers, London, 1996.

Davidson, N. C. and Forde, M. C., (1996) A laboratory appraisal of ground-penetrating radar over water, *Nondestructive Testing and Evaluation*, **12**(4), pp. 219-242.

Dickerson, R.S., and Mace, D.G.W., (1976) High speed road profilometers preliminary description, TRRL Supplementary Report 182, TRRL.

Djordjevic, B. B. and Green, R. E., (1994) Non-contact ultrasonic techniques for process control of composite fabrication, In *Conference on NDE applied to Composite Fabrication*, NTIAC and McDonnell Douglas Aerospace, St. Louis, Missouri, Oct.

Dodds, C. J. and Robson, J. D., (1973) The description of road surface roughness, *Journal of Sound and Vibration*, **31**(2), pp. 175-183.

Edwards, I., Gros, X. E., Strachan, P., and Lowden, D. W., (1993) Fusion of NDT data, *British Journal of NDT*, **35**(12), pp. 710-713.

Elton, J. D., and Harr, M. E., (1988) New non-destructive pavement evaluation method, *Journal of Transportation Engineering*, **114**(1), pp. 76-92.

Fink, D. G., and Beaty, H. W. (eds), (1993) *Standard handbook for electrical engineers*, 13th Edition, McGraw-Hill Inc., London.

Fraleigh, J. B., (1985) *Calculus with analytic geometry*, 2nd Edition, Addison-Wesley Publishing Company, USA.

Giannopoulos, A, (1997) "The investigation of transmission-line matrix and finite-difference time-domain methods for the forward problem of ground probing radar", D.Phil thesis, University of York, UK.

Gordon, M.O., Hardy, M.S.A. & Broughton, K.J., (1998) "The assessment of the value of GPR imaging of flexible pavements", *NDT & E International*, **31**(6), pp. 429-438.

Gros, X. E., (1997) *NDT data fusion*, Arnold, London.

Gros, X. E., Strachan, P., and Lowden, D. W., (1995A) A bayesian approach to NDT data fusion, *INSIGHT*, **37**(5), pp. 363-367.

Gros, X. E., Strachan, P., and Lowden, D. W., (1995B) Theory and Implementation of NDT Data Fusion, *Research in Nondestructive Evaluation*, **6**, pp. 227-236.

Gros, X. E., Strachan, P., Lowden, D., and Edwards, I., (1994) NDT data fusion, In *6th European Conference on NDT*, Nice, France, pp. 355-359.

GSSI, (1996) Sir System 10A+ User's manual.

GSSI, (1998) Sir System 10H User's manual.

Halabe, U. B., Sotoodehnia, A., Maser, K. R., and Kausel, E. A., (1993) Modelling the electromagnetic properties of concrete, *ACI Materials Journal*, **90**(6), pp. 552-563.

Heiler, M., McNeil, S., and Garrett, J. J., (1995) Ground-penetrating radar for highway and bridge deck condition assessment and inventory, In *SPIE-The International Society for Optical Engineering, Nondestructive evaluation of aging bridges and highways*, Oakland, CA, Vol. 2456, 6-7 June, pp. 195-206.

Hobbs, C. P., Temple, J.A.G., Hillier, M.J., Silk, H.G. and Tattersall, M.G., (1993) Radar inspection of civil engineering structures, In *International Conference on Non-Destructive Testing in Civil Engineering*, The British Institution of NDT, Liverpool, April, Vol. 1, pp. 79-96.

Huang, G. H., Tillotson, H., and Snaith, M., (1998) Massively parallel computing techniques might improve highway maintenance, *IEEE Concurrency*, pp. 58-67.

Hugenschmidt, J., Partl, M. N., and De Witte, H., (1998) GPR inspection of a mountain motorway in Switzerland, *Journal of Applied Geophysics*, **40**, pp. 95-1054.

Hulsenbeck, (1926) & Co. German patent 489 434.

Johansson, E. M. and Mast, J. E., (1994) Three-dimensional ground penetrating radar imaging using synthetic aperture time-domain focusing, In *SPIE-The International Society for Optical Engineering: Advanced Microwave and Millimeter-Wave Detectors*, San Diego, CA, Vol. 2275, 25-26 July, pp. 205-214.

Jordan, P. G., and Cooper D. R. C., (1989) Road profile deterioration as an indicator of structural condition, *Transport and Road Research Laboratory*, Report 706.

Koehler, B., Hentges, G., and Mueller, W., (1997) A novel technique for advanced ultrasonic testing of concrete by using signal conditioning methods and a scanning laser vibrometer, In *International Conference on Non-Destructive Testing in Civil Engineering*, The British Institution of NDT, Liverpool, Vol. 1, 8-11 April, pp. 123-134.

Kraus, J. D., (1991) *Electromagnetics*, 4th Edition, McGraw-Hill, London.

Langman, A. and Inggs, M. R., (1994) Improving the resolution of a stepped frequency CW ground pentrating radar, In *SPIE-The International Society for Optical Engineering,: Advanced Microwave and Millimeter-Wave Detectors*, San Diego, CA, Vol. 2275, 25-26 July, pp. 146-155.

Laurent, J., Talbot, M., and Doucet M., (1997) Road surface inspection using laser scanners adapted for the high precision 3D measurements of large flat surfaces, In *Proceedings of the International Conference on recent advances in 3D digital image and modelling*, Piscataway, NJ, pp. 303-310.

Lide, D. R., (Chief Editor) (1999), *Handbook of Chemistry and Physics*, 79th Edition.

Lister N. W., (1972) Deflection criteria for flexible pavements, DoE/DTp, TRRL, *Laboratory Report 375.*

Maser, K. R., (1986) Detection of progressive deterioration in bridge decks using ground-penetrating radar, *ASCE Convention*, Boston, MA, pp. 42-57.

Maser, K. R. and Roddis, W. M. K., (1990) Principles of thermography and radar for bridge deck assessment, *ASCE Journal of Transporation Engineering*, **116**(5), pp. 583-601.

Maser, K. R., (1991) Bridge deck evaluation utilizing high speed radar, Infrasense Inc, Cambridge MA.

Maser, K. R., (1993) Highway speed radar for pavement and bridge deck evaluation', In *International Conference on Non-Destructive Testing in Civil Engineering*, The British Institution of NDT, Liverpool, Vol. 1, April, pp. 187-209.

Maser, K. R., (1994) Highway speed radar for pavement and bridge deck evaluation, In *Structural Materials Technology* Technomic Publishing Co. Inc., Atlantic City, NJ, Feburary, pp. 136-140.

Maser, K. R., Kristiansen, J., Schellenberger, W. and Fippinger, F., (1995) Evaluation of pavement thickness using ground penetrating radar, In *International Symposium on Non-Destructive Testing in Civil Engineering (NDT-CE)* DGZfP, Berlin, Vol. 1, 26-28 Sept., pp. 655-662.

Maser, K. R., (1996) Condition assessment of transportation infrastructure using ground-penetrating radar, *Journal of Infrastructure Systems*, **2,** pp. 94-101.

Maser, K. R. and Sande, I., (1999) Application of ground penetrating radar for evaluation of the sub-surface airfield conditions in Denmark and Norway, In *7th International Conference on Structural Faults and Repair,* Engineering Technics Press, Edinburgh, July.

Mast, J. E. and Johansson, E. M., (1994) Three-dimensional ground penetrating radar imaging using multi-frequency diffraction tomography, In *SPIE-The International Society for Optical Engineering: Advanced Microwave and Millimeter-Wave Detectors* San Diego, CA, Vol. 2275, 25-26 July, pp. 196-204.

Mesher, D. E., Dawley, C.B., Davis, J.L. and Rossiter, J.R., (1995) Evaluation of new ground-penetrating radar technology to quantify pavement structure, *Transportation Research Record*, Part 1505, pp. 17-26.

Nelson, S. D., (1994) Electromagnetic modelling for ground-penetrating imaging radar (GPIR) using 3-D finite difference time-domain (FDTD) modelling codes, In *SPIE-The International Society for Optical Engineering: Advanced Microwave and Millimeter-Wave Detectors*, San Diego, CA, Vol. 2275, 25-26 July, pp. 186-195.

Newland, D. E., (1993) *An introduction to random vibration, spectral & wavelet analysis*, Third ed, Longman.

Noss, P. M., (1990) The Noss Roughness meter: A Norwegian road-roughness measurement system, *Surface Characteristics of roadways: International research and technologies*, ASTM STP 1031, Meyer, W. E. and Reichert, J. Eds., American Society for testing and materials, Philidelphia, pp. 237-244.

Oppenheim, A. V., (1978) Editor, *Application of digital signal processing,* Signal Processing Series, Prentice-Hall Inc..

Papagiannakis, A., Hass, R., Woodrooffe, and Leblanc, P., (1998) Impact of roughness-induced dynamic load on flexible pavement performance, In *Proceedings of the 1st International Symposium on surface characteristics*, Pennsylvania State College, June.

Patterson, W. D. O., (1986) Prediction of road deterioration and maintenance effects. Theory and quantification, Highway Design and Maintenance Study, Vol. 3, World Bank, Washington D.C..

Paul, C. R. and Nasar, S. A., (1987) *Introduction to electromagnetic fields*, 2nd Edition, Mc-Graw Hill, London.

Perera, R. W., Kohn, S. D., and Behanian, S., (1996) Comparison of road profilers, *Transportation Research Record*, Part 1536, pp. 117-124.

Petroy, D., and Roberts, R., (1997) Spatial sampling for GPR road evaluations, In *7th International Conference on Structural Faults and Repair*, Engineering Technics Press, Vol 3, July, pp. 119-131.

Popovics, S., and Popovics, J. S., (1998) NDT methods for the in-situ evaluation of pavements in the USA - a review, *Insight*, **40**(7), pp.496-500.

Ramirez, R. W., (1985) *The FFT, fundamentals and concepts*, Prentice-Hall Inc..

Robson, J. D., (1979) Road surface description and vehicle response, *International Journal of vehicle design*, **1**(1), pp. 25-35.

Roesset, J. M., Stokoe, K. H., and Seng, C-R, (1995) Determination of depth to bedrock from falling weight deflectometer test data, *Transportation Research Record*, Part 1504, pp. 68-78.

Rose, J. G., Hutchinson, J. W., and Gallaway, B. M., (1973) Summary and attributes of methods of surface texture measurements, *ASTM Special Technical Publication 530*, ASTM, Philadelphia.

Salter, R. J., (1988) *Highway design and construction*, 2nd Edition, Macmillan Education Ltd.

Sansalone, M. and Carino, N. J., (1989) Detecting delaminations in reinforced concrete slabs with and without asphalt concrete overlays using the impact-echo method, *ACI Materials Journal*, **86**(2), pp. 175-184.

Sansalone, M. and Carino, N. J., (1988) Impact-echo method: detecting honeycombing, the depth of surface-opening cracks, and ungrouted ducts, *Concrete International*, **10**(4), pp. 38-46.

Sansalone, M., (1997) Impact-echo story, *ACI Material Journal*, **94**(6), pp.777-86.

Sayers, M. W., Gillespie, T. D., and Paterson, D. O., (1986A) Guidelines and Calibrating road roughness measurements, *World Bank technical Paper No. 46*, The World Bank, Washington DC.

Sayers, M. W., Gillespie, T. D., and Queiroz, C. A. V., (1986B) The International road roughness experiment: A basis for establishing a standard scale for road roughness measurements, *Transportation Research Record*, Part 1084, pp. 76-85.

Sayers, M. W., (1995) On the calculation of international roughness index from longitudinal road profile, *Transportation research record*, Part 1501, pp. 1-12.

Sellmann, P. V., Delaney, A. J., and Arcone, S. A., (1993) Observations of radar performance for bottom and sub-bottom information in fresh water, *Second Government Workshop on GPR, Advanced Ground-Penetrating Radar: Technologies and Applications*, Ohio State University, 26-28 Oct., pp 59-70.

Smith H. R., and Jones C. R., (1998) Bituminous surfacings for heavily trafficked roads in tropical climates, *Proceedings of the Institution of Civil Engineers: Transportation*,**129**, pp. 28-33.

Snaith, M. S., and Kerali, H. R., (1986) Highway maintenance management systems for the UK, *Institution of British asphalt and coated macadam: Annual Conference*, Quarry Products Association, London.

Spangler, E. B., and Kelly, W. J., (1964) GMR Road Profilometer, A method for measuring road profile, *Research Publication GMR-452*, General Motors Corp., Michigan.

Still, P., and Jordan, P. G., (1980) Evaluation of the TRRL high speed profilometer, *TRRL Laboratory Report 922*, TRRL, Crowthorne.

Uddin, W. and Hudson, W. R., (1994) Evaluation of NDT equipment for measuring voids under concrete pavements, ASTM Special Technical Publication, In *Proceedings of the Symposium on Nondestructive Testing of Pavements and Backcalculation of Moduli*, Atlanta, GA, Vol. 1198, 23-24 June, pp 488-502.

Ullidtz, P., and Larsen, B., (1983) Mathematical model for predicting pavement performance, *Transportation research record*, Part 949, pp. 1-12.

Warhus, J. P., Mast, J.E., Johansson, E.M. and Nelson, S.D., (1994) Advanced ground-penetrating radar, In *SPIE-The International Society for Optical Engineering: Advanced Microwave and Millimeter-Wave Detectors,* San Diego, CA, Vol. 2275, 25-26 July, pp. 177-185.

Watson, J., (1994) Highway construction and maintenance, 2nd Edition, Longman Scientific & Technical, Essex, UK.

Weedon, W. H., Chew, W. C., and Ruwe, C. A., (1994) Step-frequency radar imaging for NDE and GPR applications, In *SPIE-The International Society for Optical Engineering: Advanced Microwave and Millimeter-Wave Detectors,* San Diego, CA, Vol. 2275, 25-26 July, pp. 156-167.

Weil, G. J., (1991) Infrared thermographic techniques, Handbook on non-destructive testing of concrete, CRC Press, Boston, pp. 305-316.

Weil, G. J., (1992A) Non-destructive testing of bridge, highway and airport pavements, In *Nondestructive Evaluation of Civil Structures and Materials,* Boulder, Colorado, May, pp. 385-394.

Weil, G. J., (1992B) Non-destructive testing of bridge, highway and airport pavements, In *No trenches in town proceedings of international conference,* Paris, France, 12-14 Oct., pp. 243-246.

Weil, G. J., (1993A) Non-destructive testing of bridge, highway and airport pavements, In *5th International Conference on Structural Faults and Repair,* Engineering Technics Press, Edinburgh, Vol. 2, July, pp. 71-80.

Weil, G. J., (1993B) Non-destructive testing of bridge, highway and airport pavements, In *International conference on NDT of concrete in the infrastructure,* Dearbon, Michigan, 9-11 June, pp. 93-105.

Weil, G. J., (1995) Non-destructive testing of bridge, highway and airport pavements, In *International Symposium on Non-Destructive Testing in Civil Engineering (NDT-CE)* DGZfP, Berlin, Vol. 1, 26-28 Sept., pp. 467-474.

Yoder, E. J., and Witczak, M. W., (1975) *Principles of pavement design*, 2nd Edition, John Wiley and Sons, New York, N.Y..

Yoder, E. J., (1973) Pavement evaluation using roadmeters, *Highway Research Board Special Report*, Highway Research Board, National Research Council, Washington D.C..

Yuan, D., Nazarian, S., and Baker, M. R., (1997) Use of seismic pavement analyser for NDT of roads, *International Conference on Non-Destructive Testing in Civil Engineering*, The British Institution of NDT, Liverpool, Vol. 2, 8-11April, pp. 713-727.

Yuan, D., Nazarian, S., Chen, D-H., and Hugo, F., (1998) Use of Seismic Pavement Analyzer to monitor degradation of flexible pavements under Texas mobile load simulator, *Transportation Research Record*, Part 1615, pp. 3-10.

Zhu, J. J., Zhu, W., Smailus, T., and Martinez, M., (1996) Evaluation and implementation of automated profilogram reduction system: APPARE, *Transportation research record*, Part 1545, pp. 16-25.

Appendix A

Propagation velocity of a radar wave

The velocity of propagation of an EM wave through a low loss dielectric material is:

$$v = \frac{1}{\sqrt{\mu\varepsilon}} \text{ m/ns} \tag{A.1}$$

Velocity of light in free space:

$$c = \frac{1}{\sqrt{\mu_0\varepsilon_0}} \approx 0.3 \text{ m/ns} \tag{A.2}$$

where: μ_0 = permeability of a vacuum $4\pi \times 10^{-7}$ H/m

ε_0 = permittivity in a vacuum (8.85×10^{-12} Farads/m)

Relative magnetic permeability of a medium is:

$$\mu_r = \frac{\mu}{\mu_0} \tag{A.3}$$

Relative permittivity of a medium is:

$$\varepsilon_r = \frac{\varepsilon}{\varepsilon_0} \tag{A.4}$$

where: ε = permittivity of a medium

It should be noted that the material permittivity is complex: $\varepsilon = \varepsilon' - j\varepsilon''$

where:

ε' = real part of the permittivity
ε'' = imaginary part of the permittivity

However, ε'' is essentially related to the signal losses and is small compared to ε' in low loss materials.

$$\therefore \varepsilon_r = \frac{\varepsilon'}{\varepsilon_0}$$

Subsitute (A.3) and (A.4) into (A.1)

$$c = \frac{1}{\sqrt{\mu_0 \varepsilon_0}} = \frac{1}{\sqrt{\frac{\mu\varepsilon}{\mu_r \varepsilon_r}}} = v\sqrt{\mu_r \varepsilon}$$

$$v = \frac{c}{\sqrt{\varepsilon_r}} \qquad \text{(A.5)}$$

($\mu_r \approx 1$ for common geological materials)

Appendix B

FFT theory

Fourier series

The fourier series of a periodic signal is the decompositon of a signal into a infinite number of sinusoidal components at discrete frequencies.

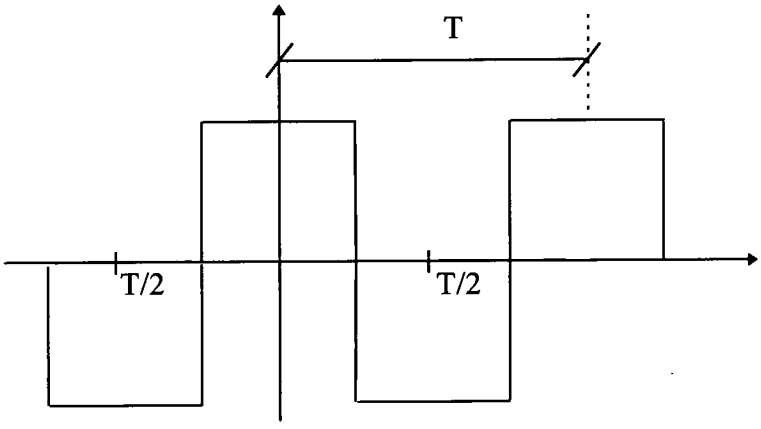

Figure B.1: Square wave

Trignometric form

$$x(t) = \frac{A_0}{2} + \sum_{n=1}^{\infty}\left(A_n \cos n\omega_0 t + B_n \sin n\omega_0 t\right)$$

where $\omega_0 = 2\pi f_0$

$$A_0 = \frac{2}{T}\int_{-T/2}^{T/2} x(t)dt$$

$$A_n = \frac{2}{T}\int_{-T/2}^{T/2} x(t)\cos n\omega_0 t dt$$

$$B_n = \frac{2}{T}\int_{-T/2}^{T/2} x(t)\sin n\omega_0 t dt$$

Exponential form

$$Cos(n\omega_0 t) = \frac{e^{jn\omega_0 t} + e^{-jn\omega_0 t}}{2}$$

$$Sin(n\omega_0 t) = \frac{e^{jn\omega_0 t} - e^{-jn\omega_0 t}}{2j}$$

$$\therefore x(t) = \sum_{n=-\infty}^{\infty} c_n e^{jn\omega_0 t}$$

where $c_n = \frac{1}{T}\int_{-T/2}^{T/2} x(t)e^{-jn\omega_0 t} dt$

note: A_0 is the DC (direct current) or steady component of the signal, i.e. mean value

Obtaining the fourier series of a periodic waveform enables the magnitude and phase of the frequency components to be calculated. However, non-periodic or aperiodic signals cannot be analysed using the fourier series. The Fourier transform is required to explain the frequency characteristics of these types of signal.

Fourier Transform

$$x(t) = \sum_{n=-\infty}^{\infty} c_n e^{jn\omega_0 t}$$

Each harmonic is separated by $\Delta = \frac{1}{T}$

As $T \to \infty$

$$x(t) = \lim_{T\to\infty} \frac{1}{T} \sum_{n=-\infty}^{\infty} X(n\omega_0) e^{jn\omega_0 t}$$

Since $\Delta f = \frac{1}{T}$

$$x(t) = \lim_{\Delta f\to 0} \frac{1}{T} \sum_{n=-\infty}^{\infty} X(n\omega_0) e^{jn\omega_0 t}$$

$\Delta f \to 0$ causes the summation to become an integral

$$\left.\begin{aligned} x(t) &= \int_{-\infty}^{\infty} X(w) e^{j\omega t} d\omega \text{ Inverse fourier transform (IFT)} \\ X(\omega) &= \int_{-\infty}^{\infty} x(t) e^{-j\omega t} dt \text{ Fourier Transform} \end{aligned}\right\} \text{Fourier Transform Pair}$$

Discrete Fourier Transform

The discrete Fourier transform (DFT) is the discrete equivalent of Fourier transform which enables analogue signals to be sampled.

$$X_k = \sum_{n=0}^{N} x(n) e^{\frac{-j2\pi nk}{N}} \text{ (DFT)} \qquad \text{(B.1)}$$

$$x(n) = \frac{1}{N} \sum_{n=0}^{N-1} X_K e^{\frac{j2\pi nk}{N}} \text{ (Inverse DFT)} \qquad \text{(B.2)}$$

note :The $\left(\frac{1}{N}\right)$ value in x(n) can be included in either expression not both.

The Fast Fourier Transform (FFT) is a more efficient algorithm for evaluating the DFT. Its ability to eliminate most of the repetition in the calculation allows the computation to be carried out more rapidly.

Power Spectral Density Function

The power spectral density (PSD) is a measure of the power per unit bandwidth of a signal, Brook and Wynne (Brook and Wynne, 1988).

$$P_{XX} = \frac{1}{N} X.conj(X) \tag{B.3}$$

where: P_{XX} = Power spectral density

N = Number of samples in signal(x)

conj(X) = Conjugate of X

Cross Spectral Density Function

The cross spectral density (CSD):

$$P_{XY} = \frac{1}{N} X.conj(Y) \tag{B.4}$$

where: P_{XY} = Cross spectral density

N = Number of samples in signal(x)

conj(Y) = Conjugate of Y

Coherence Function

The coherence function is the quotient of the magnitude squared of the CSD and the product of the PSD. The values obtained from this function will vary between 0 and 1, indicating the measure of correlation between the signals, i.e. a good correlation will have a value close to 1 and poor correlation will have a value close to 0.

The magnitude squared coherence between two signal x(n) and y(n) is:

$$C_{xy}(\omega) = \frac{\left|P_{xy}(\omega)\right|^2}{P_{xx}(\omega)P_{yy}(\omega)} \tag{B.5}$$

Transfer function

The transfer function is the function of frequency which is the ratio of a phasor output to a phasor input in a linear system, Fink and Beaty (Fink and Beaty (eds), 1993).

$$T_{XY}(\omega) = \frac{P_{XY}(\omega)}{Pxx(\omega)} \tag{B.6}$$

Appendix C

Curvature calculations

The calculations below prove why the curvature values using the radar trailer are smaller than the total station values. (All heights on diagrams are in metres)

Taking the value perpendicular to the radar antennas which is the value the total station will measure:

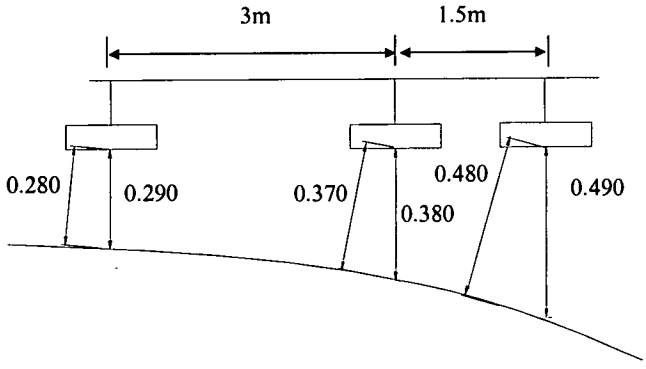

$$\text{Curvature} = \frac{d_i L_1 + d_i L_2 - d_{i-1} L_2 - d_{i+1} L_1}{\frac{1}{2}\left(L_1 L_2 (L_1 + L_2) + d_i{}^2 L_1 + d_i{}^2 L_2 - d_{i+1}{}^2 L_1 - d_{i-1}{}^2 L_2\right)}$$

$$= \frac{(3 \times 0.380) + (1.5 \times 0.380) - (1.5 \times 0.290) - (3 \times 0.490)}{\frac{1}{2}\left((3 \times 1.5)(3 + 1.5) + (0.380^2 \times 3) + (0.380^2 \times 1.5) - (0.490^2 \times 3) - (0.290^2 \times 1.5)\right)}$$

$$= -0.019\ \text{m}^{-1}$$

Taking the point on the road which is closest to the antennas:

$$\text{Curvature} = \frac{(3 \times 0.370) + (1.5 \times 0.370) - (1.5 \times 0.280) - (3 \times 0.480)}{\frac{1}{2}\left((3 \times 1.5)(3 + 1.5) + (0.370^2 \times 3) + (0.370^2 \times 1.5) - (0.480^2 \times 3) - (0.280^2 \times 1.5)\right)}$$

$$= -0.016\ \text{m}^{-1}$$

Taking the value perpendicular to the radar antennas which is the value the total station will measure:

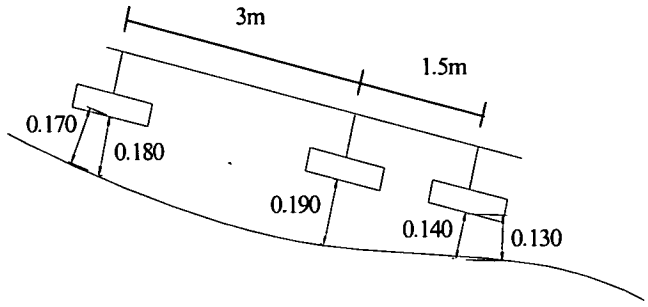

$$\text{Curvature} = \frac{(3\times 0.190)+(1.5\times 0.190)-(1.5\times 0.180)-(3\times 0.140)}{\frac{1}{2}\left((3\times 1.5)(3+1.5)+(0.190^2\times 3)+(0.190^2\times 1.5)-(0.180^2\times 3)-(0.140^2\times 1.5)\right)}$$

$$= 0.020\,\text{m}^{-1}$$

Taking the point on the road which is closest to the antennas:

$$\text{Curvature} = \frac{(3\times 0.170)+(1.5\times 0.190)-(1.5\times 0.170)-(3\times 0.130)}{\frac{1}{2}\left((3\times 1.5)(3+1.5)+(0.190^2\times 3)+(0.190^2\times 1.5)-(0.170^2\times 3)-(0.130^2\times 1.5)\right)}$$

$$= 0.010\,\text{m}^{-1}$$

Appendix D

Empirical calculations showing the influence of water content on the relative permittivity of different pavement layers

Wearing course

The following information is based upon construction information for the M8 extension.

40mm of HRA was used in the top layer.

Nominal content of coarse aggregate (% by mass of total mix) = 30% (14mm sized aggregate) (BS598 Part 107: 1990 (Amended, May 1996))

	Nominal content %	***Assume content %**
COARSE	30	32
FINE	49.4	52.5
FILLER	8.82	9
BINDER	6.5	6.5

Table D.1: Content of materials in HRA (based on BS594 Part1: 1992 (table 3))

*Note: The total amount in the first column added up to 94.7%, however, these are only nominal values, so they are therefore adjusted in the second column to add up to 100%.

Roadbase layer

The second layer used in the M8 extension was a roadbase layer made of HDM (Heavy Duty Macadam).

	Nominal content %	*Assume content %
COARSE	30	32
FINE	49.4	52.5
FILLER	8.82	9

Table D.2: Content of materials in HDM (based on BS4987 Part1: 1993 (table 1))

The binder content= 4% by mass of total mixture

Mass content of HDM = COARSE + FINE + FILLER + BINDER + WATER

Void content ≈ 6% of total volume

Total mass of HDM = M

Note: There will be a certain content of air voids with the HDM layer (no mass)

$$\frac{61}{M}+\frac{32}{M}+\frac{8}{M}+0.04+watercontent=1$$

Assume 10% of air voids are filled with water

$$\therefore \frac{61}{M}+\frac{32}{M}+\frac{8}{M}+0.04+\frac{0.006}{M}=1$$

$$M=105.21$$

	DENSITY (kg/m^3)	% BY MASS
COARSE: Granite	2700	58
FINE: Sand	1600	30
FILLER: Hydrated lime	2200	8
BINDER: Road tar	1130	4
WATER	1000	5×10^{-3}

Table D.3: Shows density of material (Lide, 1999) and their percentage by mass

	Wearing course: HRA	**Roadbase: HDM**	***Relative permittivity***
	% by vol	**% by vol**	
COARSE: Granite	20.4	42.6	6
FINE: Sand	56.6	37.2	4
FILLER: Hydrated lime	7.1	7.2	7
BINDER: Road tar	9.9	7	4
AIR	6	6	1
WATER	0-100% Sat.	0-100% Sat.	81

Table D.4: Percentage volume of materials and their permittivity properties

$$Vol = Vol_{COARSE} + Vol_{FINE} + Vol_{FILLER} + Vol_{BINDER} + Vol_{AIR} + Vol_{WATER}$$

$$Volume = \frac{Mass}{Density}$$

The overall relative permittivity of HDM and HRA was found by using a *Complex Refractive Index Method* (CRIM), used in modelling the electromagnetic properties of concrete (Halabe, 1993). This is a volumetric model in which only the volume fraction of the constituents is considered.

$$\varepsilon_{MATERIAL} = \varepsilon_C Vol_C + \varepsilon_F Vol_F + \varepsilon_{FR} Vol_{FR} + \varepsilon_B Vol_B + \varepsilon_A Vol_A + \varepsilon_W Vol_W$$

ε_{HRA}	4.441
ε_{HDM}	4.888

$$R = \frac{\sqrt{\varepsilon_1} - \sqrt{\varepsilon_2}}{\sqrt{\varepsilon_1} + \sqrt{\varepsilon_2}} = \frac{\sqrt{4.441} - \sqrt{4.888}}{\sqrt{4.441} + \sqrt{4.888}} = -0.02 = -34dB$$

However, these values are obtained by assuming that the materials are completely dry. The following table shows how the overall relative dielectric property of the layers change when the moisture content is varied from 0 to 100% saturation.

Saturation Ratio (%)	Relative permittivity	
	ε_{HRA}	ε_{HDM}
0	4.441	4.888
10	4.921	5.368
20	5.401	5.848
30	5.881	6.328
40	6.361	6.808
50	6.841	7.288
60	7.321	7.768
70	7.801	8.248
80	8.281	8.728
90	8.761	9.208
100	9.241	9.688

Table D.5: The effect of varying the saturation ratio on the relative permittivity

	S. R. (%)	0	10	20	30	40	50	60	70	80	90	100
	ε_{HDM}	4.888	5.368	5.848	6.328	6.808	7.288	7.768	8.248	8.728	9.208	9.688
S. R. (%)	ε_{HRA}											
0	4.441	-0.02	-0.05	-0.07	-0.09	-0.11	-0.12	-0.14	-0.15	-0.17	-0.18	-0.19
10	4.921	0.00	-0.02	-0.04	-0.06	-0.08	-0.10	-0.11	-0.13	-0.14	-0.16	-0.17
20	5.401	0.02	0.00	-0.02	-0.04	-0.06	-0.07	-0.09	-0.11	-0.12	-0.13	-0.15
30	5.881	0.05	0.02	0.00	-0.02	-0.04	-0.05	-0.07	-0.08	-0.10	-0.11	-0.12
40	6.361	0.07	0.04	0.02	0.00	-0.02	-0.03	-0.05	-0.06	-0.08	-0.09	-0.10
50	6.841	0.08	0.06	0.04	0.02	0.00	-0.02	-0.03	-0.05	-0.06	-0.07	-0.09
60	7.321	0.10	0.08	0.06	0.04	0.02	0.00	-0.01	-0.03	-0.04	-0.06	-0.07
70	7.801	0.12	0.09	0.07	0.05	0.03	0.02	0.00	-0.01	-0.03	-0.04	-0.05
80	8.281	0.13	0.11	0.09	0.07	0.05	0.03	0.02	0.00	-0.01	-0.03	-0.04
90	8.761	0.14	0.12	0.10	0.08	0.06	0.05	0.03	0.02	0.00	-0.01	-0.03
100	9.241	0.16	0.13	0.11	0.09	0.08	0.06	0.04	0.03	0.01	0.00	-0.01

Table D.6: The relationship between the saturation ratio (S. R.) and the reflection coefficient

Using the reflection coefficient method it was found that the value obtained for the M8 extension was 5.4. It had been raining very heavily a few days before the survey; however, it did not rain on the day of the survey. Therefore, assume that most of the water travelled into the HDM layer, leaving only 20% water saturation in the HRA and about 80% saturation in the HDM layer. Putting these values into the reflection coefficient equation will give you a value of –18.5dB, which will result in the generation of a reflection wave.

Appendix E

Published journal and conference papers

Journal Papers

Gordon, M. O., Hardy, M. S. A., and Broughton, K. J., The assessment of the value of GPR imaging of flexible pavements, *NDT & E International*, **31**, 1998, pp. 429-438.

Gordon, M. O., Giannopoulos, A., Hardy, M. S. A., Semi-intrusive determination of ground penetrating radar wave velocity, *NDT & E International*, Elsevier, (accepted for publication in 2000)

Conference Papers

Gordon, M. O. and Hardy, M. S. A., Back analysis of GPR images of flexible pavements, In *Proceedings of the 7th International Conference on Structural faults and Repair*, Vol. 3, July 1997, pp133-144.

Gordon, M. O. and Hardy, M. S. A., Advanced NDT of flexible pavements, In *5th Heavy Vehicle Weights and Dimensions Symposium*, Australia, March 1998.

Gordon, M. O. and Hardy, M. S. A., Longitudinal surface profiling of highway pavements using GPR, In P*roceedings of the 8th International Conference on Structural faults and Repair*, 13-15 July, 1999.

Journal Papers

ELSEVIER

PII: S0963-8695(98)00041-3

NDT&E International, Vol. 31, No. 6, pp. 429–438, 1998

Printed in Great Britain
0963-8695/98 $19.00+0.00

The assessment of the value of GPR imaging of flexible pavements

M.O. Gordon*, K. Broughton, M.S.A. Hardy

NDT Group, Department of Civil and Environmental Engineering,
The University of Edinburgh, Crew Building, King's Buildings, Edinburgh EH9 3JN, UK

A survey of the different applications of ground penetrating radar (GPR) for highway pavement investigation is presented with a critical appraisal of the success with which it was applied. The problems associated with this technique are also discussed. These include discussions of the accuracy of the technique and the difficulties in trying to interpret the recorded signals. Suggestions for the future direction of the research in this field to enhance the data collection and interpretation are made. The remainder of this paper investigates the advances that can be made in the use of existing GPR technology in the field of thin pavements investigation. © 1998 Elsevier Science Ltd. All rights reserved.

Keywords: GPR, pavements, ndt

Ground penetrating radar (GPR) is a non-destructive technique for investigating objects hidden by optically opaque barriers. It detects changes in the electromagnetic properties of materials, principally the permittivity, and is capable of producing cross-sectional representations of what is beneath surfaces. This paper presents an introduction to the technique and a review of its application to the investigation of highway pavements. It then looks forward to the developments currently underway in the field and what might be possible in the near future with advances in hardware and signal processing capability.

General principles

The basic principle underlying GPR is that electromagnetic signals transmitted into the medium of interest are partially reflected on encountering a change in the electrical properties. The reflected signal is recorded at a receiver while the transmitted part continues through the new material. This process is continued when further electrically different media are met by the transmitted signal. The series of reflections recorded at the receiver allow an image of the interior structure to be built up. An explanation of GPR is also provided in the HMSO document[1] which concerns the technique's usage for the investigation of pavement defects. The depth of a layer of material is determined from the time it takes the reflected wave to be detected at the receiver. Knowing the velocity of the wave through the relevant media the depth is calculated as:

$$d = v\left(\frac{1}{2}\right) \tag{1}$$

where: d, thickness of layer; v, velocity of electromagnetic wave through the layer; and t, time between reflections.

In the determination of layer thicknesses the previous equation is employed using the time between the observed reflections and the relevant velocity, this can be estimated from Table 1.

Material properties

The electrical properties that govern the propagation of electromagnetic waves through materials are electrical conductivity and the dielectric constant.

These properties and corresponding radar velocities are presented in Table 1 for the materials of interest in a pavement survey. In general the conductivity determines how far through a material the signal penetrates while contrasts in the dielectric constant govern the proportion of energy transmitted and reflected at material boundaries.

The velocity of the electromagnetic wave decreases with an increase in the dielectric constant. The speed of electromagnetic waves through low-loss nonmagnetic materials such as water or soils is approximately:

$$v = \frac{c}{\sqrt{\epsilon_r}} \tag{2}$$

* Corresponding author

Table 1 Electrical properties of water and pavement materials

Material	Relative dielectric constant	Velocity (m ns^{-1})[a]
Fresh water	81	0.033
Saturated clays	5–40	0.05–0.13
Saturated silts	5–30	0.06–0.13
Saturated sand	20–30	0.06–0.07
Wet bedrock	5–20	0.05–0.13
Dry asphalt	2–4	0.15–0.21
Wet asphalt	6–12	0.07–0.21
Dry concrete	4–10	0.09–0.15
Wet concrete	10–20	0.07–0.091

[a]For GPR data nanoseconds (ns), i.e. 10^{-9} s, is an appropriate unit of time.

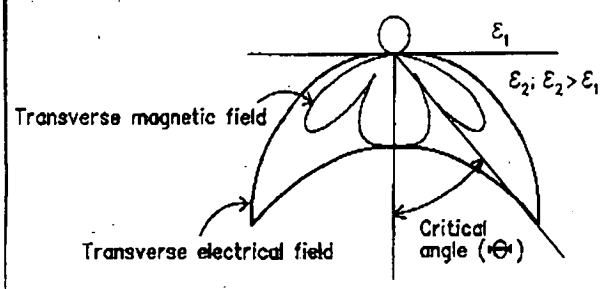

Figure 1 The radiation pattern of a dipole antenna when placed on the ground

where: v, signal velocity; c, velocity of light (0.3 m ns^{-1}); and ϵ_r, relative dielectric constant.

The electrical conductivity has the greatest bearing on the degree of signal attenuation, i.e. on the extent to which the signals penetrate. The higher the conductivity the greater the attenuation and lesser the depth of penetration. Conductivities of paving materials can vary greatly caused by the presence of salt in any water that is present in the pores. The attenuation also increases with the frequency of the wave that is propagating through the medium so high frequency surveys will not be able to penetrate wet materials that have salt dissolved in them.

The power of emitted radiation is also a factor and as the lower frequency antennas produce the more powerful signals they therefore allow greater depths to be probed. However, there is a trade off, as the lower the frequency the poorer the resolution.

Radar antenna

This paper considers the response of two types of ground probing radar antenna generally identified as 'bowtie' and 'horn' antenna. The horn antenna produces a more focused beam though the general pattern of radiation. These types of antenna are typical of those found in most commercial GPR systems, they are preferred because of their linear phase response over a wide frequency range and convenient size.

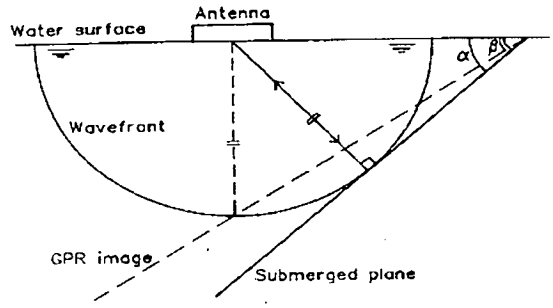

Figure 2 Ground-penetrating radar image of a sloping plane[3]

On placing an antenna on a surface the frequency content of the emitted pulse changes relative to that emitted in air. The antenna is said to be coupled or loaded to the surface. The peak frequency of the radiated signal generally becomes lower on coupling[2].

Ground-penetrating radar antennas produce signals which emerge in quite a complex pattern as is shown in Figure 1. The diagram indicates the form of radiation emitted by a dipole antenna when placed on the ground of a uniform dielectric constant. Estimation of the beam width for different frequency antennas over water is provided by Davidson and Forde[3] which indicates the generalized response for sub-surface interfaces in homogenous layered materials.

The dispersed radar beam also leads to some geometrical distortion of the sub-surface layer profiles. On passing over an inclined layer the signal returned to the receiver is that from the point on the sub-surface interface perpendicular to the emerging signals rather than the point directly below the antenna. Figure 2 illustrates this principal for the use of GPR to locate river beds. This causes a shift in the depth and angle of inclination which is significant beyond slope angles of 25°. Such angles are only encountered in pavements where there are significant changes in the structure.

A further factor to consider is the influence of signals 'ringing' back and forth between two good reflectors. This is apparent when GPR is used over water as the interface is shown repeatedly in time down the profile. These reflections are known as 'multiples' and should not be confused with reflections from true structure.

Review of recent investigations on highway pavements

Weil[4–9], reports on experience of using infrared thermography (IRT) and GPR to assess highway and airport pavements. IRT uses an infrared camera to detect changes in surface temperature that can be related to the presence of voids beneath the pavement, or delaminations within the pavement itself. IRT is limited insofar as that whilst large areas can be covered quickly, it is not possible to gain

accurate pictures of the depths or exact extents of voiding beneath, or cracking within, pavements. Whilst GPR is a slower technique to apply, as pavements must be scanned in many parallel lines, Weil does recognise its value in pinpointing problems and finding the true depth of voiding.

Weil recommends that IRT is used to direct the GPR surveys to particular areas where it can be used more efficiently to get a detailed picture of damaged areas.

Adcock *et al.*[10] report the use of GPR by the USA air force to detect significant variations in pavement thickness, voiding and water ingress as well as the thicknesses of surfaces on airfield pavements of both Portland cement concrete (PCC) and asphalt concrete (AC).

They developed a sophisticated vehicle with GSSI 2.5 GHz horn antennas mounted at the front and 900 MHz bowtie antennas at the rear. The aim was to use the 2.5 GHz antennas to give accurate information about the dielectric constant of the surface material. This was calculated by measuring the amplitude of the reflected pulse from the pavement and comparing it with the amplitude of the pulse reflected from a steel plate. As the reflected field strength is related to the incident strength by the reflection coefficient

$$r = \frac{\sqrt{\epsilon_2} - \sqrt{\epsilon_1}}{\sqrt{\epsilon_2} + \sqrt{\epsilon_1}} \qquad (3)$$

where ϵ_1 is the permittivity of the medium through which the pulse is travelling when it meets an interface with a material of permittivity ϵ_2.

The high frequency pulse was not suitable for penetrating through the PCC or AC top layer so the 900 MHz antennas are used to measure the time for the reflection from the bottom of these layers. The knowledge of the permittivity of the material from the reflection coefficient allows the travel times for the 900 MHz pulse to be translated back into a layer depth. The system that they developed was intended to be fully automated, but they found it difficult to ensure that an automated system could find all the GPR imaging of correct peaks in the signals for the data analysis and, therefore, some manual intervention was required. However, with this intervention, layer depths could be found with accuracies of $\pm 5\%$.

Heiler *et al.*[11] have tackled the problem of automatic detection of asphalt thickness and depth to reinforcement in composite pavements using neural networks. The networks were trained to recognise the quality of the data presented to them and to locate the reflections from the three features required. Different networks were used for the quality testing and the location, but the location network has 124 input points and three analogue outputs, one per feature required.

The results were quite promising with the networks identifying the rogue data sets, but also identifying between 5% and 20% of the correct data sets as defective. It is pointed out by the authors that this conservatism by the networks is at least on the safe side.

For good data sets the location of the features were very accurate. It is clear that huge amounts of accurate data are required to train the networks before they can be of any use and that accurate and good quality radar data is required if there are to be consistent, good results.

The use of neural networks in this context is quite encouraging if characteristic responses within the radar signal are easily identifiable. Unfortunately, what is being looked for in the radar trace is often quite difficult to predict in advance of seeing it and there is a long way to go before such networks can replace the eye of an experienced operator.

Daniels' book, '*Surface Penetrating Radar*'[12] contains many case studies including reports from Wilkinson, of Durham County Council, UK and Caiou, Côte and Derobert of the Laboratoires des Ponts et Chausées (LPC) in France on the applicition of GPR to pavement investigation.

Wilkinson reports that GPR can be used to determine thicknesses of bituminous or concrete pavements, spacing and location of reinforcement and dowels, cracking and if there is not too much reinforcement in concrete pavements, the position of cracks and voids beneath the pavements. This can be carried out more efficiently than by the traditional methods of coring. Surveys can even be carried out at highway speed with sufficient accuracy. Wilkinson does report that a survey of operators in the UK were not able to agree on the materials of construction of older roads where the pavement had been developed in a piecemeal fashion. As perhaps 80% of the UK's roads fall into this category, this is one area where there may be room for development.

The team from the LPC report on their experience of using a 700 MHz centre-frequency system and confirm that it can only resolve layers of 5 cm or greater, and that the accuracy is approximately 8%. This work was carried out in the 1980s and since then they have investigated the use of synthetic-pulse radar. They are encouraged by their initial findings and suggest that it can penetrate further into the road than the amplitude modulated pulse system by a factor of 1.5 or more.

Mesher *et al.*[13] have developed the road radar with the specific objective of identifying and quantifying pavement layer thicknesses. Rather than use the amplitude of reflected waves to determine the permittivity of layers they use a multiple antenna array to evaluate it. This is because the amplitude of a pulse reflected by a material interface is prone to changes in its amplitude caused by other factors apart from the reflectivity of the interface. These factors include the height of the antenna above the road, which is difficult to maintain constant at high speed and the rough surface of the pavement scatters the incident pulse rather than reflecting it neatly. The set-up of their multiple antenna array is shown in Figure 3.

The change in the travel time as the pulse travels along different path lengths can be used to determine the layer thicknesses.

Along with this system, they have developed sophisticated

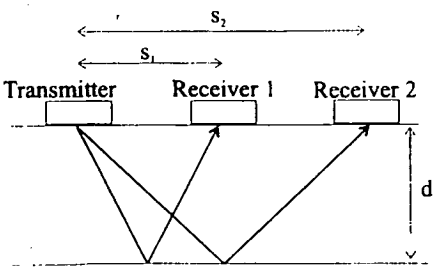

Figure 3 Multiple receiver bistatic antenna array

software incorporating artificial intelligence, time-domain signal processing, neural networks and pattern recognition techniques. The software will still defer to the operator if it encounters changes in construction which it is not happy to analyse. Once the operator has intervened the software can take over once more.

They present several field studies and the results are very encouraging for resolving layer thicknesses from 50 mm to 2 m. They suggest, however, that the precise determination of the velocity in the material might be strongly correlated to the pavement density or water content.

As the water content is probably the most influential factor influencing the wave speed through the material it is likely that this might be determined from the velocity. The dielectric constant of water is 81 and for most dry material, it is less than 10. The effective dielectric constant of a wet material is considerably higher than in its dry state, even when the water content is only a small percentage by volume.

The velocities measured on three pavements varied between 120 and 148 mm ns^{-1} although the average values at the three pavements were 126, 129 and 130 mm ns^{-1}. These velocities match those in Table 1 well, but the spread of velocities at each site was 120–143, 125–133 and 121–148 mm ns^{-1} which indicates that using a single core at a site as a calibration for the radar survey is likely to lead to errors of the order of 10% or so.

Maser[14] presents a review of the use of GPR for evaluation of pavements, bridge decks, bridge piers and geotechnical applications. He compares contact bowtie antenna technology and non-contact horn antennas. Maser suggests that the amplitude of the reflection of the pulse can be used to determine the permittivity and, hence, wave-speed of each layer in a pavement and that it is possible to make suitable measurements at highway speed. Asphalt layers as thin as 5 cm can be detected with a 1 GHz horn antenna. The accuracy achieved for asphalt layer thicknesses was ±7.5% and for the base layers is ±12%. Success with concrete pavements has not been so good caused by the poor penetration of the pulse through the concrete because:

- Similar dielectric properties of concrete with the granular base material it is placed on makes it more difficult to pick up the reflection from the concrete–base layer interface.
- The water and dissolved salts content of the concrete cause more electromagnetic attenuation compared with asphalt.

A hybrid horn–coupled antenna system is suggested to improve the penetration whilst maintaining the calculation of the wave speed by examination of the reflection of the pulse from the concrete surface.

Maser[15–20] presents the field studies from New Hampshire, Germany, Texas and Kansas on which he bases his paper above.

Ballard has investigated some experimental sections of road that were cored for comparison[21]. He identifies significant variations in pavement thickness along the length of each pavement investigated (up to 30 mm or 10% of the pavement thickness) and suggests that these might have a significant effect on the life of the pavements involved. As the pavement stiffness is, to a first order according to simple plate bending theory, proportional to the thickness to the third power he is undoubtedly correct. GPR provides a much better tool for investigating the quality of new pavements or overlays than other methods as it can give spatial resolution along the road much more precisely than even the most extensive and, hence, destructive coring surveys.

Hobbs *et al.*[22] review the advantages of the GPR technique for surveying structures in general and the specific costs of maintaining the highway infrastructure in the UK and USA. They cite the difficult-to-interpret nature of GPR traces as one reason why GPR is not more widely used and suggest the techniques used for ultrasonic signal analysis might be useful for reduction of GPR images. It is also shown by illustration that GPR images can be more amenable than their ultrasonic counterparts in certain circumstances. Ultrasonic testing of road pavements has not met with much success as the short wavelengths involved are diffracted by all the small inhomogeneities of the materials involved. This leads to rapid attenuation of the travelling wave and significant 'clutter' of the received signal.

Uddin and Hudson[23] are interested in detecting voids beneath concrete pavements. They state that half of these can be found by visual inspection looking for pumped material. Deflection measurements were tried but are not reliable indicators because of variable slab-to-slab joint conditions and lifting of slab edges caused by temperature effects.

They report use of two different GPR systems. RODAR is a vehicle mounted, non-contact system that can carry out surveys at 10 mph. Donahue's remote sensing van uses a combination of IRT and GPR. High frequency transducers are used to give good resolution although the paper does not give much detail of the systems involved.

Several case studies are taken from the literature and it is concluded that GPR is a promising tool for this purpose, but that improvements need to be made to the analysis of the results and presentation to the end user.

Attoh-Okine[24] compares the cost of a GPR survey from a vehicle in the traffic stream with a traditional coring survey,

with cores at either 20 per mile or 2 per mile depending on the purpose of the survey. He developed a cost model for each method and then compared them. This study showed that the GPR survey would be between 2 and 3.5 times cheaper than coring although there is very little data to back these figures up.

This brief survey of recent literature highlights the possible benefits of using GPR for pavement thickness evaluation, such as rapid and cheap surveys with more detail than is possible by other methods, but also reveals the engineers frustration at the amount of manual intervention that is required to analyse the masses of data that can be collected. The use of advanced processing systems has not yet alleviated this problem.

Two methods for determining the permittivity of the pavement materials are found. Either the amplitude of the reflected pulse can be used or a multiple antenna bistatic array can be used. Both methods appear to were successful.

Current and future developments

Maser[14] looks at future developments including the stepped frequency and synthetic aperture radar.

Stepped freqnency radar can be explained by examining the Fourier decomposition of the desired pulse that is transmitted by the antenna. As the pulse is sent repeatedly, at a pulse repetition rate, T, then the pulse can be synthesized by the summation of a set of scaled and appropriately phased sine waves with frequencies i/T Hz, where $i = 1,2,3....$ If each of these component sine waves is transmitted in turn the response to the pulse can be detemined by the inverse Fourier transform of the scaled and phase-corrected responses.

This method gives great control over the effective shape of the transmitted pulse and an increase in the power that can be transmitted, hence, improving the penetration. The cost of this is that the signals take longer to transmit as many frequencies that must be transmitted and the results must be recombined before a picture is produced.

The synthetic aperture radar involves use of an array of antennas (or a single moving one) that can together provide data that resolves the shape and depth of targets with much greater accuracy than a single antenna can on its own. Again, there is a cost in the data processing associated with this method.

Both of these methods are explained in more detail by Daniels[12,25]. Further signal processing developments are also discussed including the possibility Wavelet analysis has to enhance images.

Weedon *et al.*[26] explain the development of a stepped frequency radar (SFR) system with a switched antenna array designed specifically to resolve images at a range of 40 cm. A two-dimensional finite difference time domain simulation is used to try to reconstruct the true image from the radar image by iteratively modifying the simulation model until its output matches the measured image. They meet with some success, but are limited to locating two-dimensional images such as straight bars and only attempted the procedure with the bars in the optimum position for the antenna array. These limitations mean that this technique cannot be applied directly to highway pavements, but the extension to three-dimensional and the use of planar, rather than focused arrays would not seem to be insurmountable extensions to this work.

Langman *et al.*[27] describe the theory and development of a stepped frequency radar system and describe the extended prony method as an alternative to the IFT for getting enhanced spatial resolution. The results are convincing both in simulation and experiment but there is no mention of the processing time cost which would appear to be considerable.

Warhus *et al.*[28] describe in detail the design requirements for a GPR system with a single transmitter but an array of receivers spanning the pavement surface particularly for RC bridge decks. Images of the deck are reconstructed using the techniques for synthetic aperture radar processing as described by Daniels[12].

Mast and Johansson[29] explain their three-dimensional reconstruction of a test specimen of reinforced concrete using a synthesised aperture technique. Their antenna had a bandwidth from 0.5–3.5 GHz and the three-dimensional rendered image is very impressive. The downside of this is the quantity of data that has to be collected to produce the images, but with the cost of the hardware reducing all the time it may well be possible to produce a similar technique for scanning highways in the future using arrays of antennas in parallel, or maybe as described by Warhus *et al.*[28]

Johansson and Mast[30] present an alternative method for producing three-dimensional images. The data acquisition required is the same but the analysis procedure is very different and is more akin to a deconvolution and migration of the data in three-dimensions. Whilst the results of this analysis do not look as good as those from the previous technique[29], the authors point out that the computational effort is much reduced and that this method will become more attractive as the number of strata involved in the analysis increase.

Nelson[31] reports on the three-dimensional modelling efforts for simulating GPR with finite difference time domain simulation at the Lawrence Livermore National Laboratory.

The concrete is modelled as a two-phase random mixture with the aggregate having different electromagnetic properties to the cement matrix. The simulations are compared with real measurements under fairly ideal conditions in an anechoic laboratory. These prove to be a good match. The conclusions are that the precise modelling of the aggregate–cement mix is important if the simulation is to work as the scattering, diffracting and shadowing effects of the particles are significant.

Gros, Edwards, Strachan *et al.*[32–36] have brought the concept of data fusion into NDT. Data fusion is the

simultaneous analysis of the results of different sensors, not necessarily even the same type of sensor, to give an improved image of the object under investigation. A simple example is the fusion of many readings of a GPR record by averaging in order to reduce background noise effects and improve the image. More sophisticated techniques are illustrated by different sensors that detect aircraft by scanning the skies in a crude and rough way, a second set of sensors can identify the aircraft, and a third set will give its speed and direction.

There are several mathematical techniques available for bringing together the information from different sensors, such as IRT and GPR data with different antenrra. These include statistical ensemble averaging, Baysian inference methods, the Dempster–Shafer theory of evidence, fuzzy logic and neural networks.

Gros[35] implements Baysian and Dempster–Shafer fusion theory to bring together eddy current surveys (which give a surface profile of defects), ultrasonic surveys (which give cross-sectional profiles of defects), and X-ray radiographic surveys (giving through depth images) of weld cracks. He concludes that the Dempster–Shafer extension of the Baysian theory gives better answers.

Current state of the art

The range of techniques available to highway engineers for the assessment of pavement condition are many and varied. The simultaneous analysis of the information from different systems would greatly enhance the reliability of the interpretation, and even extend interpretation into areas not yet envisaged.

New developments in radar hardware include, stepped-frequency radar, improved horn and array antennas, and synthetic aperture techniques. Accurate three-dimensional simulation requires improved understanding and training of neural networks and the techniques of data fusion to bring together many sources of information in a rational and quantifiable way.

Many of the developments discussed earlier are at a theoretical or laboratory stage and are not yet suitable for engineers to take out into the field. The remainder of this paper investigates the advances that can be made in the use of existing GPR technology in the field of thin pavements investigation.

Impulse radar of thin pavements

These pavements (thicknesses < 200 mm) create particular problems for GPR as the wavelength of a 1 GHz radar pulse is in the range 90–21 mm according to the velocity information given in Table 1. In the radar image, the response from the underside of the pavement can not be seen clearly. This is caused by it not being easy to resolve the individual constituents of the radar signal, which can include the response from the initial impulse, the direct transmission from the transmision to the receiver and the reflections from the pavement surface itself. This is illustrated in Figure 4 which shows a GPR survey over a section of road pavement. The pavement thickness was only 100 mm and this was removed over the central section of the scan. The antenna itself was moved over the top of a thin sheet of timber so that it had a flat surface to run along and also so that an air-gap appeared beneath the antenna where the surface had been removed. It was hoped that the radar scan would pick up the sudden change in the road surface, but it is not clear at all from the scans shown in Figure 4. If the data from Table 1 is used, the reflection of the bottom of the pavement appears after a period of between 0.10 and 0.22 ns from the start of the transmit pulse. It is clear from Figure 4 that this time range is within the initial surface reflection–direct transmission time of this antenna. It is possible to use higher frequency antennas but these were not available to the researchers at the time and a higher frequency antenna would run into exactly the same problems if it was applied to thinner pavements.

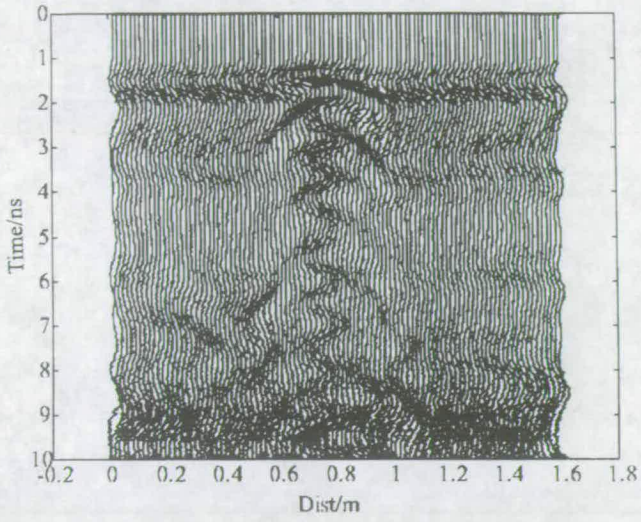

Figure 4 900 MHz GPR scans over a thin pavement with surface slab removed at the middle section

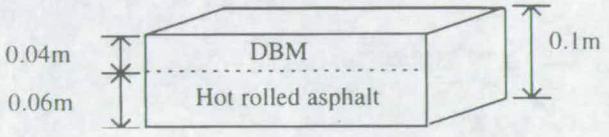

Figure 5 Thickness detail of the pavement slab

GPR investigation of thin asphalt slabs

The surface slab that had been removed from the road scanned in Figure 4 was removed to the laboratory for further investigation. Details of the slab geometry are shown in Figure 5.

An initial investigation was carried out to find the precise speed of the radar pulse through the slab. The pavement slab was placed on its side and passed between two 900 MHz antennas, which were also on their sides. The antennas were a distance of 0.105 m apart, in order for the piece of pavement to fit between them. The velocity of the radar pulse through the slab is given by Equation (2) above, where ϵ_r is the relative permittivity of the slab material. Pulses were transmitted from one antenna to the other with the slab in position, and also with the slab removed so that the pulse only travelled through the air. The received pulses are shown in Figure 6(a).

The transmit time between antennas is extended because of the slower speed through the slab. Closer inspection shows that this time increase is 0.40 ns. Let T_s be:

(1) Travel time from the transmitting antenna (some distance inside the box in which it is mounted) through to the front of the box.
(2) Through the small air gap between the antenna and the slab,
(3) Through the slab and out of the other side,
(4) Through the clearance gap and into the box of the receiving antenna.

Before being picked up by the receiver. Let T_a be the travel time when the slab is replaced by an air gap. Then:

$$T_s = \frac{d}{v_s} + T_0 \text{ and } T_a = \frac{d}{v_a} + T_0 \quad (4)$$

where d is the thickness of the slab, v_s is the speed through the slab, v_a is the speed through air and T_0 is the time to travel through everything except the slab or the air that has replaced it.

Simply taking the difference of these gives the observed delay, Δ as:

$$\Delta = T_s - T_a = \frac{d}{v_s} - \frac{d}{v_a} = \frac{d}{c}(\sqrt{\epsilon_r} - 1) \quad (5)$$

as Δ, d and c are known, it is easy to find the relative dielectric constant of the slab material and, hence, the velocity through the slab (it is assumed that the velocity through the air is 0.3 m ns^{-1}). It turns out that the velocity of the radar pulse through the slab is 0.14 m ns^{-1} giving a relative permittivity of 4.8. this value is low in the range and indicates a dry material which is consistent with the slab having been kept indoors for several days after removal from the road.

Testing of slab on artificial sub-base

Figure 6(b) shows three scans with the transmit and receive antennas on the top surface of the slab as it rests on a bed of course 'concrete' sand. The reflection from the bottom of the slab is expected at 1.4 ns after the initial pulse and is therefore confused with the initial pulse as expected. The large reflections between 12 and 16 ns are from the bottom of the sand bed. This figure shows the repeatability of the radar scans, and it is this property that will be used to try to distinguish the slab thickness from the initial pulse.

As well as using a coarse 'concrete' sand as a sub-base material a single-graded silica sand and a gravel with stone sizes up to 10 mm were also used. The results from the radar scans with these three different sub-bases are shown in Figure 6(c). It is clear from this figure that the direct transmission and reflection from the asphalt slab surface are not changed by the sub-base material. However, by 6 ns the pulses are diverging as the reflections from the bottom of the slab are now being received and these will be modified by the different materials with which the slab is in contact. The pulses diverge at approximately 1.5 ns after the initial pulse is received which is consistent with this observation.

Figure 7(a)–(c) are the responses when the height of the slab is raised above the sub-base. The introduction of this air gap between the top of the sub-base and the slab is observed to change the reflection from the bottom of the slab in each case only when the initial clearance of 0.1 m is introduced. After this clearance the reflection from the bottom of the slab does not change but there is an additional reflection from the surface of the sub-base material. The expected delay after the reflection off the slab base is 0.667 ns for every 0.1 m that the slab is raised. This is consistent with the observation.

In order to emphasize this effect Figure 7(d)–(f) show the same results but the response of the slab in contact with the sub-base (zero height) was subtracted off all the other responses. The original response with the slab not raised is also included so that the time delay between the slab surface and base reflections can be identified

It is clear that the initial received pulse is very repeatable and the procedure adopted allows for the slab surface and base responses to be identified individually. It is difficult to distinguish the responses from the increasing gap between the slab base and the sub-base material, although the deviations from the zero height response do appear to be the same up to approximately 0.7 ns as expected. It is possible that averaging together of many scans would reduce the noise levels sufficiently for these to be identified with more accuracy.

When this technique was tried to remove the initial pulse from the scan on the actual road it did not meet with any success. This is thought to be caused by the fact that the slab had dried between its existence in the field and testing in the laboratory. The effect of moisture in pavement materials has a great effect on their testing with GPR caused by the high permittivity of water.

Conclusion

The range of techniques available to highway engineers for the assessment of pavement condition are many and varied.

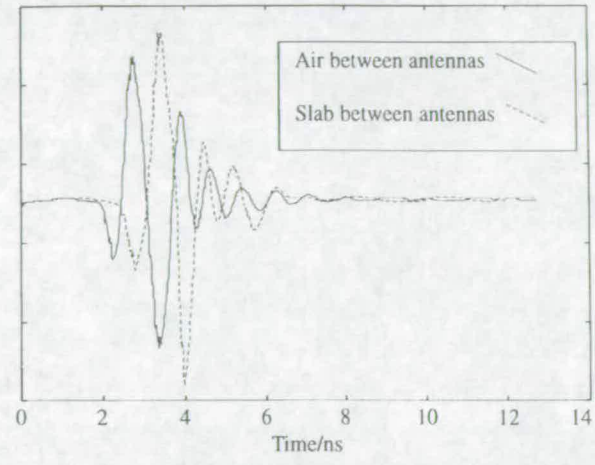

(a)

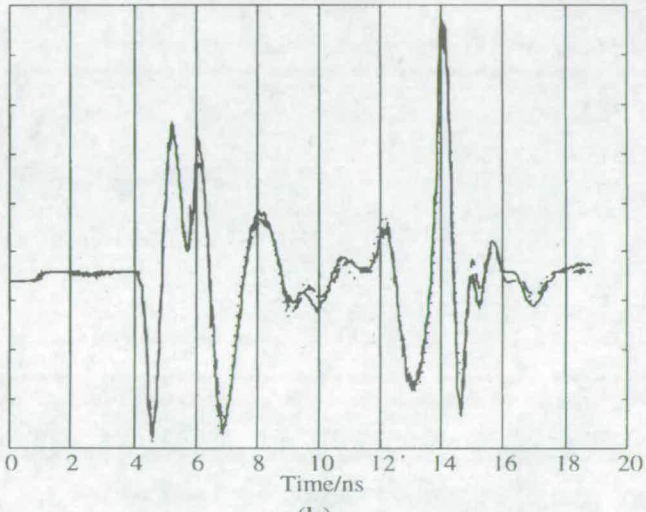

(b)

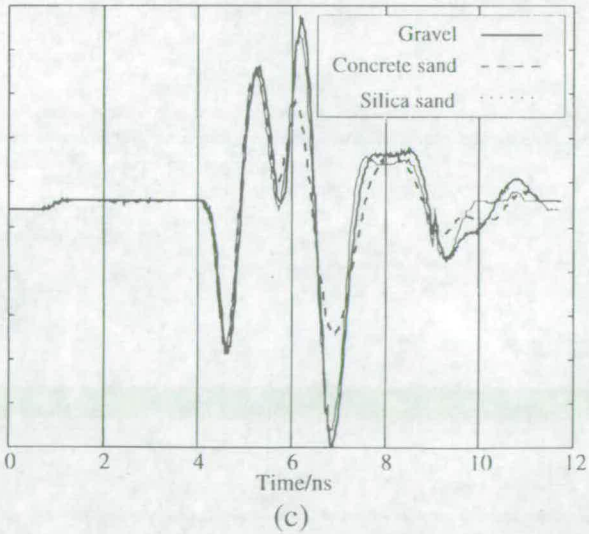

(c)

Figure 6 (a) Delay of radar pulse through the slab; (b) Repeatability of the radar scans; (c) Scans with different sub-base materials

The simultaneous analysis of the information from different systems would greatly enhance the reliability of the interpretation, and even extend interpretation into areas not yet envisaged.

The developments of new radar hardware such as stepped-frequency radar, improved horn and array antennas, signal processing techniques such as synthetic aperture radar, the accurate three-dimensional simulation of these techniques

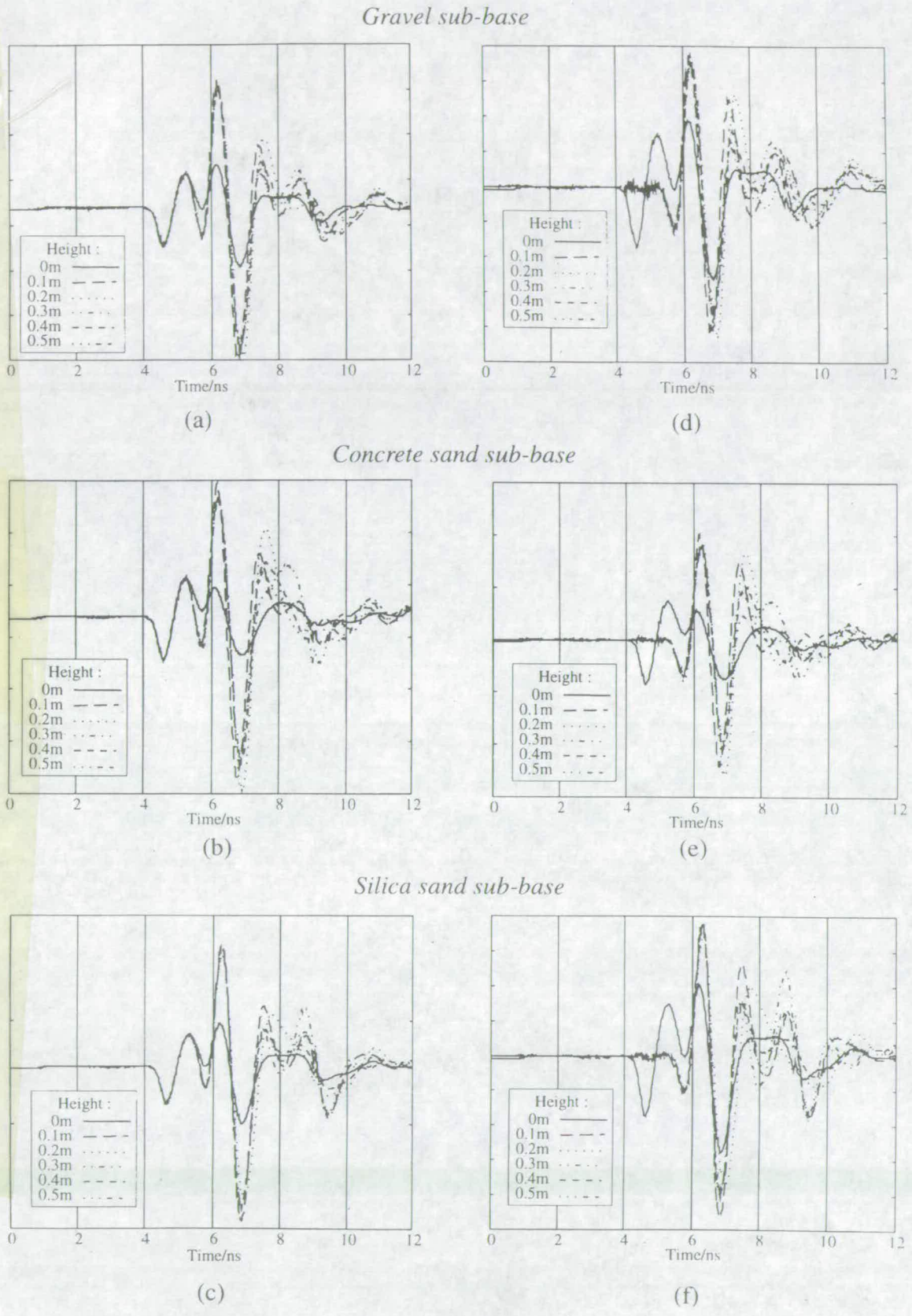

Figure 7 (a)–(c) Effect of lifting slab off different sub-bases; (d)–(f) Deviation as slab is raised off different sub-bases

for improved understanding and training of neural networks, and the techniques of data fusion to bring together many sources of information in a rational and quantifiable way seem to spell an exciting and rapidly developing improvement in the use of GPR in many fields, including highway pavement assessment.

The GPR responses of thin pavements can be impossible to

interpret directly caused by confusion of initial pulses reflections from the bottom of the thin layers (whether the bottom of the bituminous layers of the pavement or interfaces between different bituminous materials).

The effect of the material beneath the thin layer and, hence, the thickness of the layer itself, has no effect on the initial response from the surface and this can, therefore, be eliminated as shown to reveal the response from the bottom of the layer.

References

1 **Anon.** Use and limitations of ground-penetrating radar for pavement assessment. In *Design Manual for Roads and Bridges*, HMSO, London, 1994.

2 **Sellmann, P. V., Delaney, A. J. and Arcone, S. A.** Observations of radar performance for bottom and sub-bottom information in fresh water, *Second Government Workshop on GPR, Advanced Ground-Penetrating Radar. Technologies and Applications*, Ohio State University, OH, 1993, pp. 59–70.

3 **Davidson, N. C. and Forde, M. C.,** A laboratory appraisal of ground-penetrating radar over water. *Nondestructive Testing and Evaluation*, 1996, **12**(4), 219–242.

4 **Weil, G. J.** Infrared thermographic techniques. In *Handbook on Non-destructive Testing Of Concrete*, CRC Press, Boston, MA, 1991, pp. 305–316.

5 **Weil, G. J.** Non-destructive testing of bridge, highway and airport pavements. Proceedings of the conference on *Nondestructive Evaluation of Civil Structures and Materials*, Boulder, CO, Atkinson-Noland and Associates, Inc, 1992, pp. 385–394.

6 **Weil, G. J.** Non-destructive testing of bridge, highway and airport pavements. *No trenches in town proceedings of international conference*, Paris, France, 1992, pp. 243–246.

7 **Weil, G. J.** Non-destructive testing of bridge, highway and airport pavements. In *5th International Conference on Structural Faults and Repair*, Vol. 2, Engineering Technics Press, Edinburgh, 1993, pp. 71–80.

8 **Weil, G. J.** Non-destructive testing of bridge, highway and airport pavements In *International conference on NDT of concrete in the infrastructure*, Dearbon, MI, 1993, pp. 93–105.

9 **Weil, G.** Non-destructive testing of bridge, highway and airport pavements. In *International Symposium on Non-Destructive Testing in Civil Engineering* (NDT-CE) DGZfP Berlin, Vol. 1, 1995, pp. 467–474.

10 **Adcock, A. D., Dass, W. C., and Rish, J. W. I.** Ground penetrating radar for airfield pavement evaluations. *SPIE-The International Society for Optical Engineering, Advanced Microwave and Millimeter-Wave Detectors*, Oakland, CA, 1995, pp. 373–384.

11 **Heiler, M. S. M., and Garrett, J. J.** Ground-penetrating radar for highway and bridge deck condition assessment and inventory. *SPIE-The International Society for Optical Engineering, Nondestructive evaluation of aging bridges and highways*, Vol. 2456, Oakland, CA, 1995, pp. 195-206.

12 **Daniels, D. J.** *Surface-penetrating radar*, The Institution of Electrical Engineers, London, 1996.

13 **Mesher, D. E., Dawley, C. B., Davis, J. L. and Rossiter, J. R.** Evaluation of new ground-penetrating radar technology to quantify pavement structure. *Transportation Research Record*, Part 1505, 1995, National Research Council, Washington, DC, USA. pp. 17–26.

14 **Maser, K. R.,** Condition assessment of transportation infrastructure using ground-penetrating radar. *Journal of Infrastructure Systems*, 1996, **2**, 94–101.

15 **Maser, K. R.** Detection of progressive deterioration in bridge decks using ground-penetrating radar. *ASCE Convention*, Boston, MA, 1986, pp. 42–57.

16 **Maser, K. R. and Roddis, W. M. K.,** Principles of thermography and radar for bridge deck assessment. *ASCE Journal of Transporation Engineering*, 1990, **116**(5), 583–601.

17 **Maser, K. R.** *Bridge deck evaluation utilizing high speed radar*, Intrasense, Cambridge, MA, 1991.

18 **Maser, K. R.** Highway speed radar for pavement and bridge deck evaluation. In *International Conference on Non-Destructive Testing in Civil Engineering*, Vol. 1, The British Institution of NDT, Liverpool, 1993, pp. 187–209.

19 **Maser, K. R.** *Highway speed radar for pavement and bridge deck evaluation*, Structural Materials Technology Technomic, Atlantic City, NJ, 1994, pp. 136–140.

20 **Maser, K. R., Kristiansen, J., Schefienberger, W. and Fippinger, F.** Evaluation of pavement thickness using ground penetrating radar. In *International Symposium on NonDestructive Testing in Civil Engineering* (NDT-CE) DGZfP, Berlin, Vol. 1, 1995, pp. 655–662.

21 **Ballard, G. S.** Non-destructive assessment of pavement design and new build quality. In *International Conference on Non-Destrucitve Testing in Civil Engineering*, Vol. 1, The British Institution of NDT, Liverpool, 1993, pp. 391–404.

22 **Hobbs, C. P., Temple, J. A. G., Hillier, M. J., Silk, H. G. and Tattersall, M. G.** Radar inspection of civil engineering structures. In *International Conference on Non-Destructive Testing in Civil Engineering*, Vol. 1, The British Institution of NDT, Liverpool, 1993, pp. 79–96.

23 **Uddin, W. and Hudson, W. R.** Evaluation of NDT equipment for measuring voids under concrete pavements, ASTM Special Technical Publication. *Proceedings of the Symposium on Nondestructive Testing of Pavements and Backcalculation of Moduli*, Vol. 1198, Atlanta, GA, 1994, pp. 488–502.

24 **Attoh-Okine, N. O.** Using ground penetrating radar in pavement thickness measurements—a cost comparison with the fraditional coring method. In *Proceedings of the Institute of Civil Engineers, Municipal Engineers*, Thomas Telford Services Ltd., London, 1996, Vol. 115, pp. 86–89.

25 **Daniels, D. J.,** Surface-penetrating radar. *Electronics and Communication Engineering Journal*, 1996, **18**(4), 165–182.

26 **Weedon, W. H., Chew, W. C., and Ruwe, C. A.** Step-frequency radar imaging for NDE and GPR applications. *SPIE-The International Society for Optical Engineering: Advanced Microwave and Millimeter-Wave Detectors*, San Diego, CA, Vol. 2275, 1994, pp. 15.6—167.

27 **Langman, A. and Inggs, M. R.** Improving the resolution of a stepped frequency CW ground pentrating radar. *SPIE-The International Society for Optical Engineering,: Advanced Microwave and Millimeter-Wave Detectors*, San Diego, CA, Vol. 2275, 1994, pp. 146—155.

28 **Warhus, J. P., Mast, J. E., Johansson, E. M. and Nelson, S.D.** Advanced ground-penetrating radar. *SPIE-The International Society for Optical Engineering: Advanced Microwave and Millimeter-Wave Detectors*, San Diego, CA, Vol. 2275, 1994, pp. 177—185.

29 **Mast, J. E. and Johansson, E. M.** Three-dimensional ground penetrating radar imaging using multifrequency diffraction tomography. *SPIE-The International Society for Optical Engineering: Advanced Microwave and Millimeter-Wave Detectors*, San Diego, CA, Vol. 2275, 1994, pp. 196—204.

30 **Johansson, E. M. and Mast, J. E.** Three-dimensional ground penetrating radar imaging using synthetic aperture time-domain focusing. *SPIE-The International Society for Optical Engineering: Advanced Microwave and Millimeter-Wave Detectors*, San Diego, CA, Vol. 2275, 1994, pp. 205—214.

31 **Nelson, S. D.** Electromagnetic modelling for groundpenetrating imaging radar (GPIR) using 3-D finite difference time-domain (FDTD) modeling codes *SPIE-The International Society for Optical Engineering: Advanced Microwave and MillimeterWave Detectors*, San Diego, CA, Vol. 2275, 1994, pp. 186—195.

32 **Gros, X. E., Strachan, P., Lowden, D. and Edwards, I.** NDT data fusion. In *6th European Conference on NDT*, Nice, France, 1994, pp. 355—359.

33 **Gros, X. E., Strachan, P. and Lowden, D. W.,** Theory and implementation of NDT data fusion. *Research in Nondestructive Evaluation*, 1995, **6**, 227–236.

34 **Gros, X. E., Strachan, P. and Lowden, D. W.,** A bayesian approach to NDT data fusion. *INSIGHT*, 1995, **37**(5), 363–367.

35 **Gros, X. E.** *NDT Data Fusion*, Arnold, London, 1997.

36 **Edwards, I., Gros, X. E., Strachan, P. and Lowden, D. W.,** Fusion of NDT data. *British Journal of NDT*, 1993, **35**(12), 710–713.

Semi-intrusive determination of ground penetrating radar wave velocity

M.O. Gordon, M.S.A. Hardy, A. Giannopoulos

School of Civil and Environmental Engineering, The University of Edinburgh, The King's Buildings, Edinburgh, EH9 3JN, Scotland, UK

Abstract

A review of established techniques used to determine radar wave velocities within different materials is presented. A new semi-intrusive method for determining the velocity of impulse radar energy through materials is proposed based on the refraction of electromagnetic waves as they transmit through layers of different materials. Inserting a metal bar into the material and traversing the surface of it enables the impulse radar velocities of the material under investigation to be readily interpreted from the radargram. This new method provides a quick, readily interpreted and practical tool for GPR operators to use.

Introduction

The use of ground penetrating radar (GPR) in civil engineering is becoming increasingly common. GPR is a non-destructive technique for investigating objects hidden by optically opaque barriers. High frequency radio wave pulses are transmitted from an antenna through the host material. Changes in dielectric properties of the material result in partial reflections of the pulses. These are detected by a sensitive receiving antenna. Given the velocities of the impulse radar wave

through the different materials and the time interval between transmission and reception of the radar pulse, the engineer may obtain the distance to the reflecting object or interface. There are several techniques used to find the velocity of propagation. This paper presents a review of established techniques used to determine impulse radar wave velocities within materials and introduces a new, semi-intrusive method developed to determine velocities. This new method provides an additional, quick, readily interpreted, and practical tool for GPR operators to use.

Methods used to determine radar wave velocity

The method chosen to determine radar pulse velocity in practice will depend on the accessibility over/around the object under investigation, its geometry, the required accuracy, the time and manpower available, and the amount of physical interference with the structure that is acceptable. It is well known [3] that the radar pulse velocities depend on the electrical properties of the media under investigation. In this paper all media are assumed to be of low loss and therefore the radar pulse velocity is well approximated as being only a function of the electrical permittivity. Such an assumption is commonly made in GPR fieldwork.

Transmission method

This method can only be used if two sides, either side of a structure or object, are available to the user. By placing a transmitter and a receiver on different sides of the structure, the time taken for the radar wave to travel directly from one antenna, through the structure and into the second antenna can be obtained. The velocity can be calculated by dividing the separation distance of the antennas, d, by the time taken for the signal to travel through the structure, T_1.

$$v = \frac{d}{T_1} \tag{1}$$

Gordon *et al* [1] discussed the experimental set-up of this method in more detail. The method can be very accurate but it only gives an average velocity between the transmitter and receiver. If there are changes in the velocity along the path from transmitter to receiver then the pulse will be refracted, its path length will not be straight (unless the path happens to be perpendicular to the interfaces where the velocity changes), and this will lead to errors in using equation (1) even if the average velocity is required.

This method is the basis for impulse radar tomography which is a sophisticated and time-consuming technique by which the radar pulse velocity can be found at any point in the structure (assuming that sufficient access is available to implement the transmission method many times), [2].

Common-mid Point method (CMP)

The Common mid-point (CMP) or Common depth-point (CDP) can be used to determine the radar pulse velocity when only one side of the structure is accessible. Daniels [3] discusses this method in more detail. A transmitter and receiver are placed next to each other on the same surface of the material and they are then moved in incremental steps away to equal distances from a common point. A series of travel times between the receiver and transmitter are recorded. If the travel times are t_1 and t_2 for antenna separations of x_1 and x_2, then the velocity is given by:

$$v = \sqrt{\frac{x_1^2 - x_2^2}{t_1^2 - t_2^2}} \tag{2}$$

The wide angle reflection and refraction (WARR) method is very similar to the CMP method where one antenna is held fixed while the other one is moved incrementally away along a straight line.

Reflection coefficient method

An antenna is placed at a height from the surface of the material such that a clear reflected signal is observed. Let the reflected signal have an amplitude of A_S. A metal plate is then placed below the antenna which results in 100% reflection of the radar pulse. This fully reflected amplitude is A_P. The radar velocity through the material can be calculated from:

$$v = \left(\frac{A_P - A_S}{A_P + A_S} \right) c \tag{3}$$

where c is the speed of light in free space. A more detailed discussion of the method can be found in Maser [5].

Trenching and coring

Perhaps the most commonly used method for determining the speed of impulse radar through civil engineering materials is to take cores from the object under investigation, or cut a trench through a section of it, in order to determine the target depth, and hence impulse radar velocity.

Summary of existing methods

Each of the existing methods has its place and is favoured by certain practitioners. The main advantage of the transmission and reflection coefficient methods is the simplicity of implementing them. However, the applicability of the transmission method is limited by the need to have access to opposite sides of the structure under investigation. Further, only an average value of the velocity is obtained although more than one layer can be present. The main disadvantage of the reflection coefficient method is the variation in the accuracy of the results. This is a consequence of the underlining assumptions on which this method is based (plane wave reflection) and to what degree they are fulfilled in actual field tests. The CMP method can provide accurate estimations of the GPR velocities. However, post-processing of the data is required which is time consuming. To implement this method, physically separated transmitting and receiving antennas are required, but, in some commercial GPR systems both the transmitter and the receiver are located within the same unit and cannot easily be separated.

A new semi-intrusive method is proposed which is easy to implement using any commercial radar system and the interpretation can be done with relative accuracy in the field. The obvious disadvantage of this method is its intrusive nature.

A new semi-intrusive method

A direct method of GPR pulse velocity determination, which involves less intrusion than coring or trenching, is proposed. The method can be easily employed and used directly in the field investigation of stratified materials producing reasonably accurate results. For example GPR surveys of masonry walls, road pavements and geological sites.

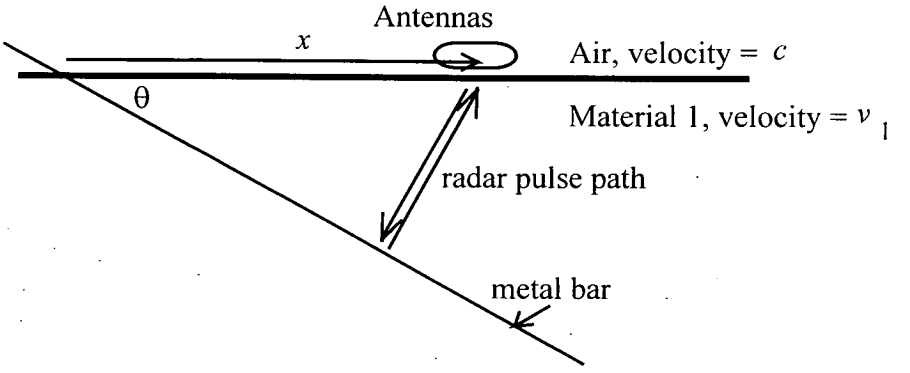

Figure 1: Locating a metal bar with impulse radar

A metal bar is inserted into the object under investigation at a known angle and this is then observed using radar. As a pencil protruding out of a glass of water appears to bend due to the different speeds of light through air and water, so the straight metal bar will appear to bend due to changes in the velocity through different materials. Figure 1 shows an investigation of a metal bar at an angle θ to the ground. When the antenna is at a distance x from the point of insertion of the bar, then the path length for a reflection from the bar is:

$$l_1 = 2x\sin\theta \tag{4}$$

and the time taken to travel this distance in this material is:

$$T = \frac{l_1}{v_1} = \frac{2x\sin\theta}{v_1} \tag{5}$$

Therefore, if a graph is plotted of T against x, a straight line with gradient $2\sin\theta/v_1$ will result. If material 1 comprises a layer of thickness H_1 over the top of a different material, which has a radar pulse velocity of v_2, then the path followed by the pulse to the bar and back is complicated by refraction at the layer interface as shown in Figure 2. Snell's law gives us:

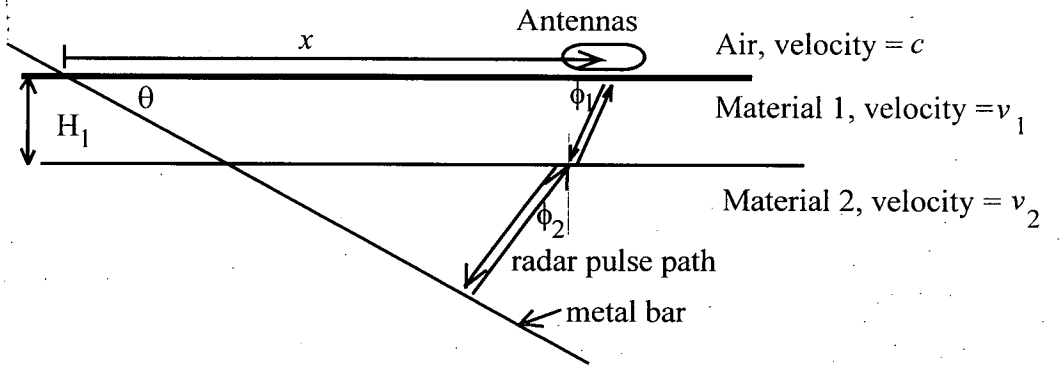

Figure 2: Locating a metal bar through an overlying layer

$$\frac{\sin\phi_1}{\sin\phi_2} = \frac{v_1}{v_2} \tag{6}$$

and because the first reflection from the bar is at right angles to it:

$$\phi_2 = \theta \Rightarrow \sin\phi_1 = \frac{v_1}{v_2}\sin\theta$$

$$\Rightarrow \cos\phi_1 = \sqrt{1 - \left(\frac{v_1}{v_2}\right)^2 \sin^2\theta}$$

$$\Rightarrow \tan\phi_1 = \frac{\frac{v_1}{v_2}\sin\theta}{\sqrt{1 - \left(\frac{v_1}{v_2}\right)^2 \sin^2\theta}}$$

Therefore the total time for the pulse to travel from the transmitting antenna to the bar and back to the receiver is now:

$$T_2 = 2\left(\frac{H_1}{v_1\cos\phi_1} + \left\{x - \frac{H_1}{\tan\theta} - H_1\tan\phi_1\right\}\frac{\sin\theta}{v_2}\right)$$
$$= 2H_1\left\{\frac{v_2^2 - v_1^2\sin^2\theta}{v_1 v_2^2\sqrt{1-\left(\frac{v_1}{v_2}\right)^2\sin^2\theta}} - \frac{\cos\theta}{v_2}\right\} + \frac{2\sin\theta}{v_2}x \qquad (7)$$

Therefore, if a graph is plotted of T against x, a straight line with gradient $2\sin\theta/v_2$ will again result. Therefore the speed of radar signals at any point on the radar trace is most easily estimated by measuring the gradient and using:

$$v = 2\sin\theta\frac{\Delta x}{\Delta T} \qquad (8)$$

where $\frac{\Delta x}{\Delta T}$ is the best estimate for the rate of change of x with T (reciprocal of the slope determined above) at the required position. In fact the gradient of the line will always be $2\sin\theta/v$ no matter how many layers are passed through. The change in velocity with depth can therefore be reconstructed by the investigation of the tangent to the T against x curve.

Computer simulation

In order to test the effectiveness of this technique a series of GPR simulations were carried out in two and three dimensions using a finite-difference time-domain (FDTD) based GPR developed by one of the authors [5]. Figure 3 shows the result of a two

dimensional simulation of a three-layer system. The top layer has an impulse radar velocity of 0.130m/ns, the middle layer a velocity of 0.110m/ns, and the underlying layer has a velocity of 0.075m/ns. A metal bar is penetrating the layers at an angle of 26 degrees to the horizontal. The reflection from this bar can be clearly seen, as can the reflections from each layer interface. When equation (8) is used to determine the velocity in each layer they are recalculated as 0.140m/ns, 0.107m/ns and 0.082m/ns. The errors in these estimations are less than 10%. The expected error is directly attributable to the accuracy with which the slopes can be determined from the graph. In this case measurements were made using pencil and ruler, as they might be if used out in the field. More sophisticated methods of regression analysis are available for more accurate velocity determination, although they have not been used in this investigation.

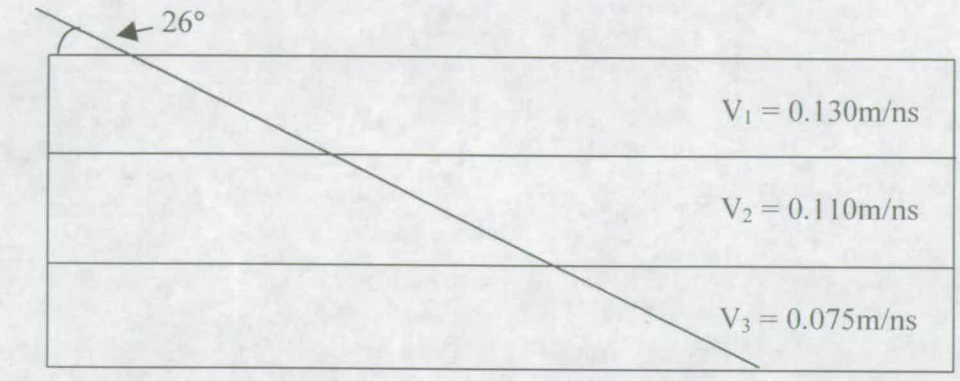

(a)

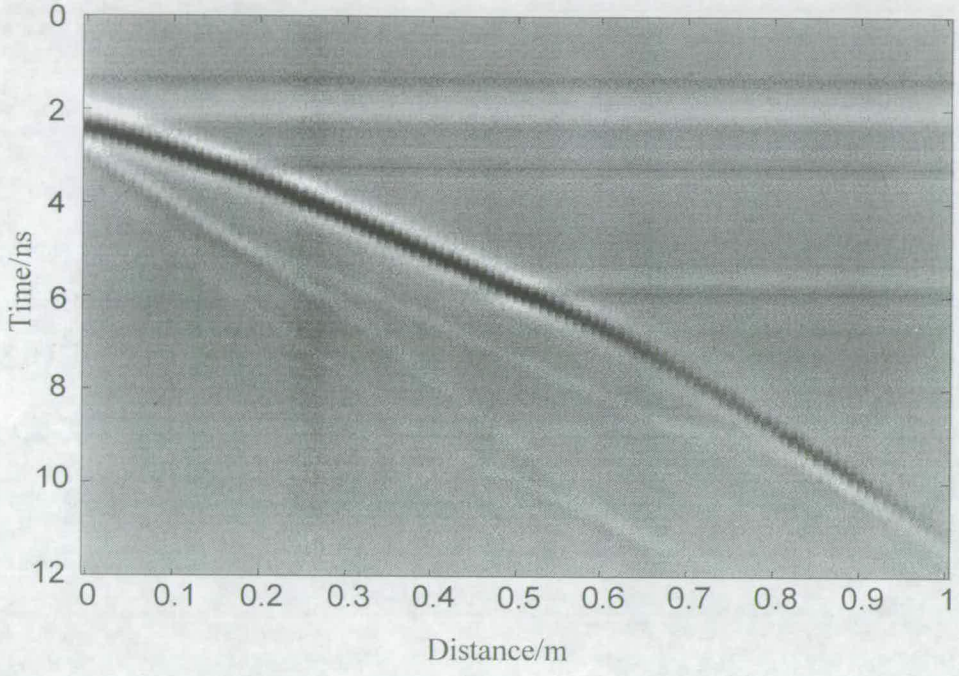

(b)

Figure 3. (a) Schematic drawing showing the three distinct layers used in the two dimensional simulation (b) Simulated radar data

Figure 4 shows the simulation of a similar system, but with the radar pulse velocity of the middle layer varying linearly with depth, ranging between the velocity values of the top and bottom layers. The effect of a layer like this is to greatly reduce the reflections from any interface which could lead to a wrongful assumption that there are no layers present and therefore that the bottom (third) layer has the same

properties as the top layer. With this configuration, the metal bar is observed to bend gradually through the depth of the second layer.

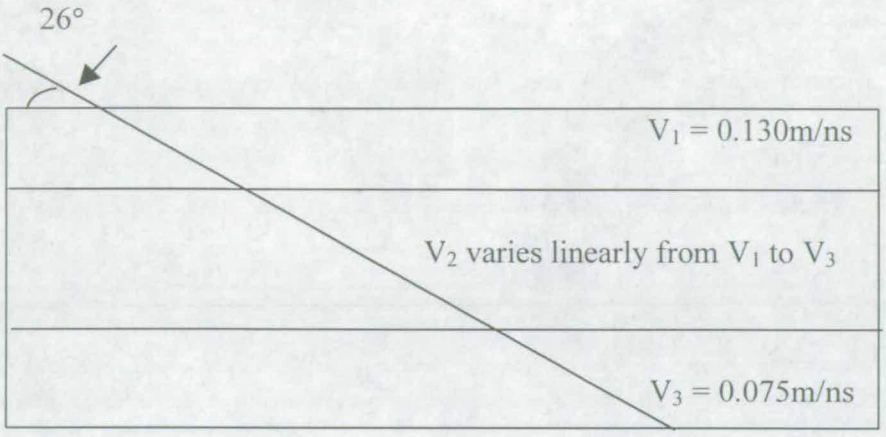

(a)

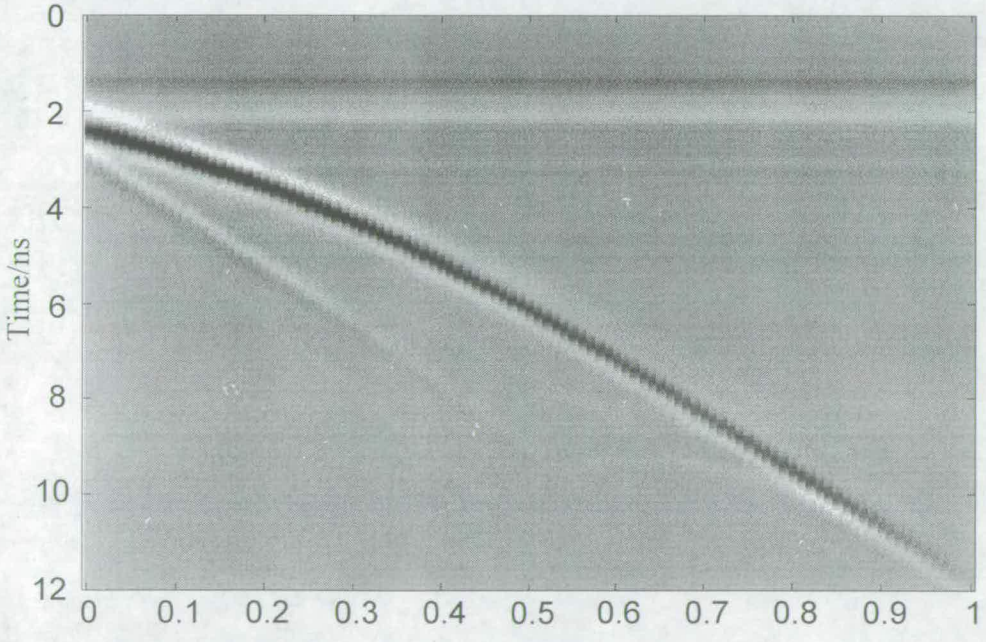

(b)

Figure 4. (a) Schematic drawing showing the gradated layers used in the two dimensional simulation (b) Simulated radar data

Equation (8) can be used to determine the radar speed at any point on this radargram. None of the conventional means of determining radar velocity could have determined this gradual change in material properties.

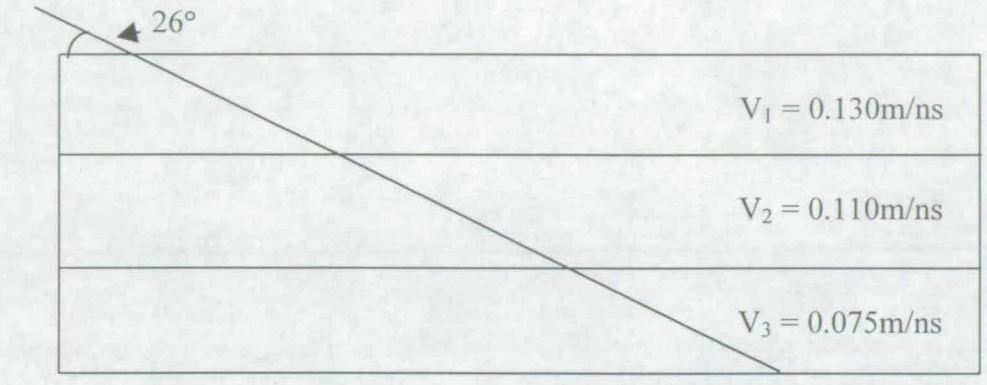

(a)

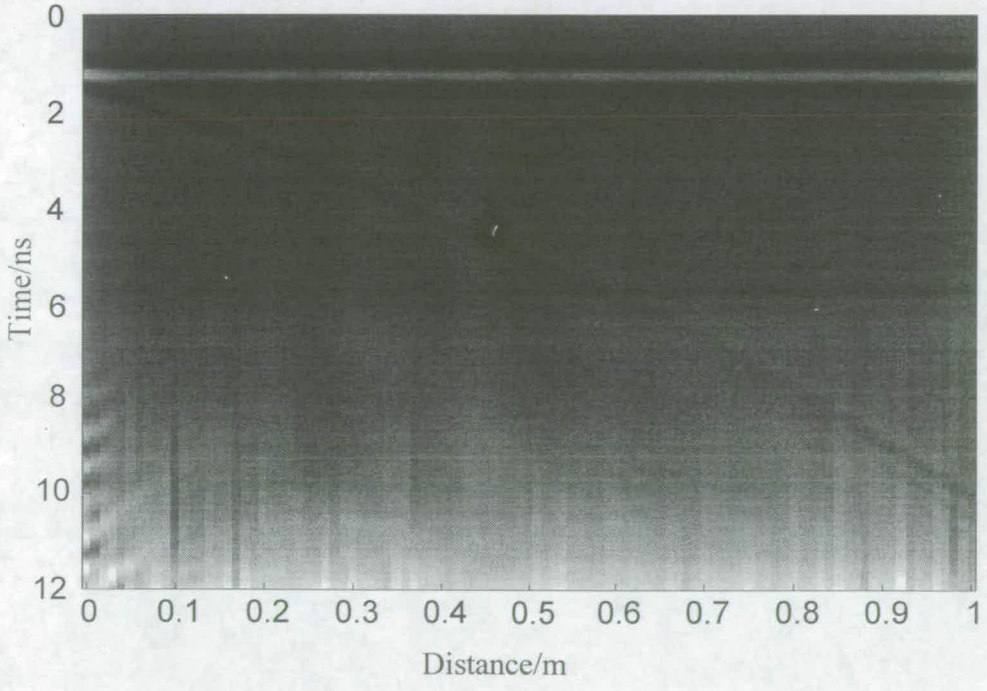

(b)

Figure 5. (a) Schematic drawing showing the three distinct layers used in the three dimensional simulation (b) Simulated radar data

Finally, in Figure 5 a three dimensional simulation of the first experiment is presented. The reflections from the bar are now not as strong due to the increased geometric attenuation of the radar pulse. This was expected because contrary to the two dimensional models, where the simulated GPR source produces a cylindrical propagating wave, in the three dimensional ones the GPR pulse is simulated as a propagating spherical wave [5]. However, the reflections from the bar are still clearly visible and equation (8) can still be used to determine the impulse radar velocities. The derived velocities are identical to those for the two-dimensional simulation.

Laboratory experiments

Before implementing the technique in the field some initial experiments were carried out in the laboratory. A plastic tank was filled with layers of saturated sand (100% moisture content), damp gravel (2.2% moisture content), and saturated gravel.

The transmission method, described earlier, was used to determine the velocities through these materials. The velocities were 0.07, 0.16, 0.05 m/ns for the saturated sand, damp gravel and saturated gravel respectively.

Initial experiments were carried out to determine the optimum angle for inserting the metal bar. Angles greater than 30° gave weak reflections because the main energy in the radar is directed downward into the soil and the energy radiated at angles greater than 30° are small. Angles less than 20° gave good reflections, but require large horizontal distances if significant depth penetration into the ground is required. Therefore shallow angles should be avoided. In practice angles between 22° and 26° were used, as these gave a good compromise between the requirements.

Two typical results are shown in Figures 6 and 7. These show radargram plots of the time against the horizontal distance along which the antenna has been moved. Figure 6 shows a layer of saturated sand over saturated gravel.

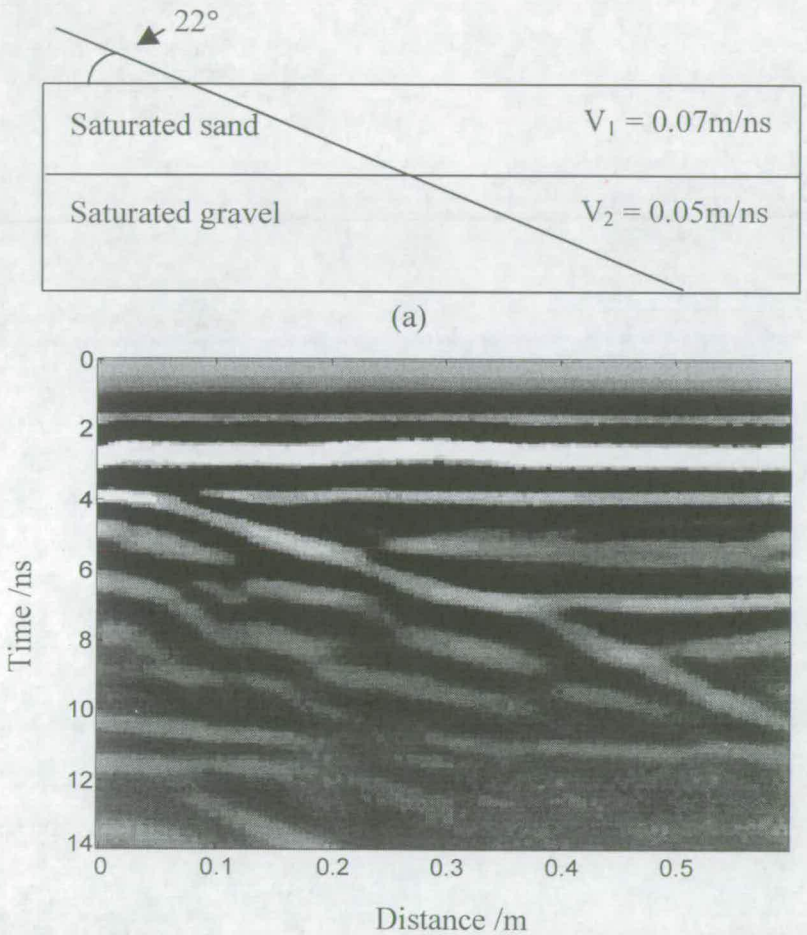

Figure 6. (a) Cross sectional view of the saturated sand over saturated gravel (b) Results from the ground penetrating radar survey

The top layer has the faster velocity and the velocities were determined using equation (8) as 0.07m/ns and 0.05m/ns which correlated with the values determined using the transmission method. In Figure 7 a three-layer example with layers of damp gravel, saturated sand and saturated gravel is presented. The slopes of the graph give

velocities of 0.13m/ns, 0.07m/ns and 0.06 m/ns respectively. These laboratory experiments proved that the method could be used to determine impulse radar velocities through different strata

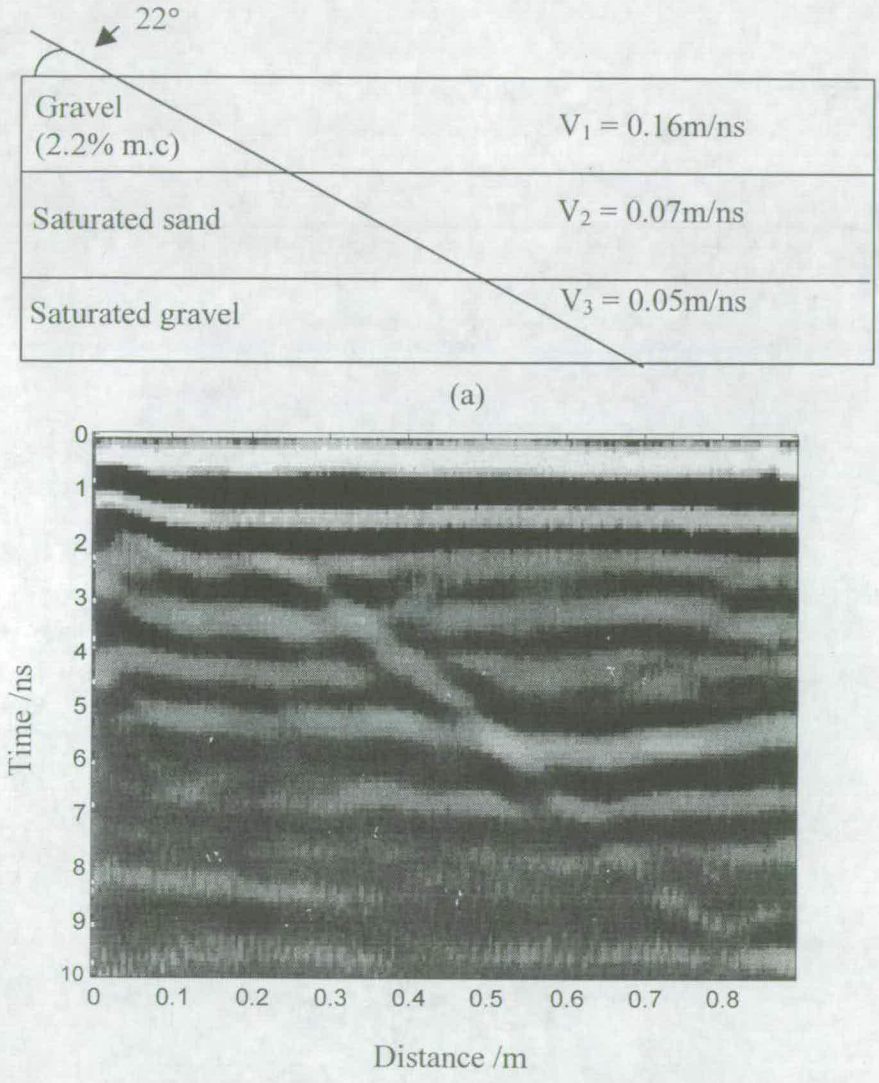

Figure 7. (a) Cross sectional view of the gravel (2.2%m.c) over saturated sand over saturated gravel (b) Results from the ground penetrating radar survey

Field Trial

A radar survey of the beach at Gullane in East Lothian, Scotland as shown in Figure 8, was carried out to determine how many different layers of sand can be identified using this method. A metal bar was inserted into the sand and a radar survey was carried out above it.

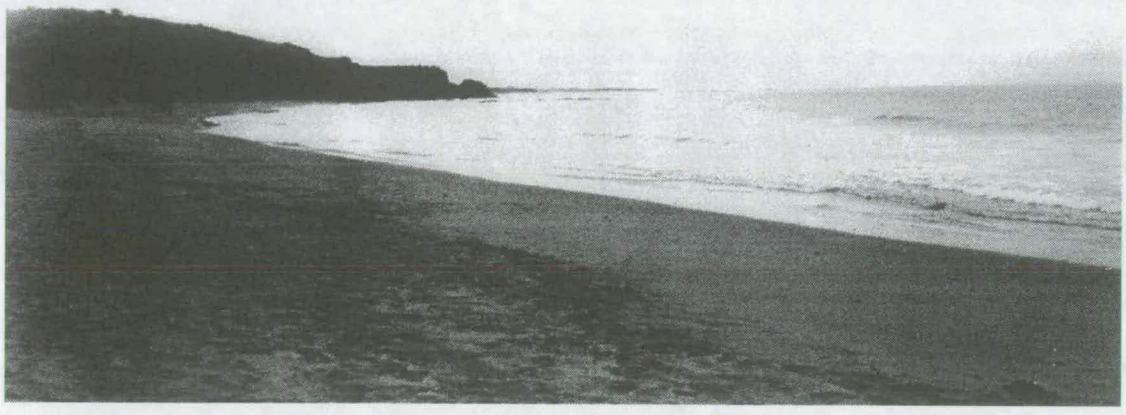

Figure 8. The beach at Gullane in East Lothian, Scotland where the field trial was carried out.

The result can be seen in Figure 9. This radargram clearly shows two different layers each with a distinct velocity. The top layer of sand has an impulse radar velocity of 0.23 m/ns as determined by equation (8). The next layer, which is the least distinct due to the steep angle, has a velocity of 0.11m/ns. As one would expect, the top layer velocity indicates that the sand layer is very dry and the bottom layer velocity shows that this sand layer is damp.

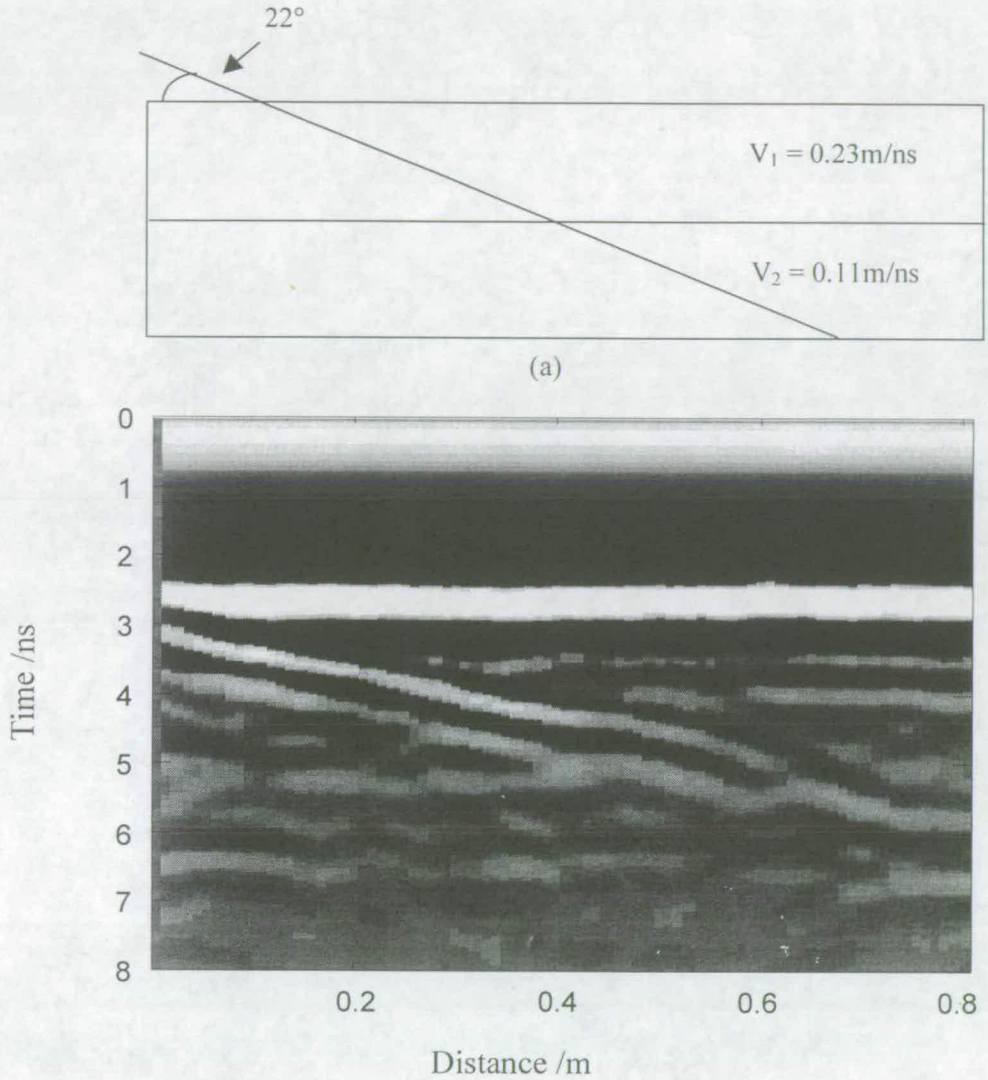

Figure 9. (a) Derived velocities from the radargram (b) Results from the ground penetrating radar survey carried out on the beach

Conclusions

The paper reviewed several established techniques used to determine radar wave velocity within various materials. Each technique has its advantages and disadvantages and usage will depend on the accessibility around the object under

investigation, its geometry, the required accuracy, the time and manpower available, and the amount of physical interference with the structure that is acceptable.

A new semi-intrusive method is proposed which involves the insertion of a metal bar into the object under investigation, thus enabling the impulse radar velocity of the material under investigation to be readily interpreted from the radargram. The series of GPR simulations carried out in two and three dimensions using an FDTD GPR model produced results with errors of less than 10%. However, it was noted that these errors could be reduced if more sophisticated methods of regression analysis were used.

Several experiments were carried out in the laboratory. Initial experiments were carried out to find the optimum insertion angle of the bar this was found to be between 22° and 26°. Additional experiments investigated how accurately the radar velocities could be determined when two and three-layer models were used. It was found that there is a good correlation between the velocities determined using the transmission method and those using the new method.

Finally, the new method was tested in a field. The aim was to determine how many different layers of sand could be identified. A metal bar was inserted into the sand and it could be seen from the radargram that there were two distinct velocities. The top layer had a velocity of 0.23m/ns, indicating a very dry layer of sand, and the bottom layer was 0.11m/ns, indicating damp sand.

This new method provides a quick, readily interpreted and practical tool for GPR operators to use. However, it is confined to shallow depths due to the limited depth of penetration of the metal bar.

References

[1]. Gordon MO, Hardy MSA, Broughton KJ. The assessment of the value of GPR imaging of flexible pavements. NDT & E International 1998;31(5):429-438.

[2]. Colla C, Forde MC, McCann, DM, Das PC, Batchelor A.J., Radar tomography of masonry arch bridges, In: Forde MC, editor. Proceedings of the Seventh International conference on Structural Faults and Repair, Edinburgh, UK, Vol. 1, July 1997. p. 143-151.

[3]. Daniels DJ. Surface-penetrating radar. London: The Institution of Electrical Engineers, 1996.

[4]. Maser KR. Highway speed radar for pavement and bridge deck evaluation. In Bungey JH, editor. International Conference on Non-Destructive Testing in Civil Engineering. Vol. 1, The British Institution of NDT, Liverpool, 1993. p. 187-209.

[5]. Giannopoulos A. The investigation of transmission-line matrix and finite-difference time-domain methods for the forward problem of ground probing radar. University of York, UK, D.Phil thesis, 1997.

Conference Papers

BACK ANALYSIS OF GPR IMAGES OF FLEXIBLE PAVEMENTS

Dr M.S.A. Hardy ,
Lecturer,
University of Edinburgh,
Crew Building, King's Buildings,
Edinburgh EH9 3JN,
Scotland.

M.O. Gordon,
Postgraduate Student,
University of Edinburgh,
Crew Building, King's Buildings,
Edinburgh EH9 3JN,
Scotland.

KEYWORDS: GPR, PAVEMENTS, NDT

ABSTRACT

Surface penetrating radar was developed to investigate the thickness of glacial flows. From this application it spread rapidly into more general use in geophysical investigations and has recently been further developed for use in Civil Engineering Non-Destructive Testing/Evaluation.

The principal is that a pulse of electro-magnetic radiation with frequency components in the range 30MHz to 2GHz is transmitted into the medium under investigation. This pulse is partially reflected when it encounters a change in electromagnetic impedance. The reflections are recorded and these give an indication of the material interfaces that can be found beneath the surface.

The problems associated with this technique that are pertinent to highway pavement investigation are discussed. These include discussions of the accuracy of the technique and the difficulties in trying to interpret the recorded signals. There are inevitable compromises that must be made and these are discussed and appropriate methods of compromise suggested.

A survey of the different applications of this technique for highway pavement investigation is presented with a critical appraisal of the success with which it has been applied. Suggestions for the future direction of the research in this field to enhance the data collection and interpretation are made. The remainder of this paper investigates the advances that can be made in the use of existing GPR technology in the field of thin pavements investigation.

INTRODUCTION

Ground Penetrating Radar (GPR) is a non-destructive technique for investigating objects hidden by optically opaque barriers. It detects changes in the electro-magnetic properties of materials, principally the permittivity, and is capable of producing cross-sectional representations of what is beneath surfaces. This paper presents an introduction to the technique and a review of its application to the investigation of highway pavements. It then looks forward to the developments currently underway in the field and what might be possible in the near future with advances in hardware and signal processing capability. Finally it investigates the advances that can be made in the use of existing GPR technology in the field of thin pavements investigation.

Table 1. Electrical properties of water and pavement materials

Material	Relative dielectric constant	Velocity (m/ns)*
Fresh water	81	0.033
Saturated clays	5 - 40	0.05 - 0.13
Saturated silts	5 - 30	0.06 - 0.13
Saturated sand	20 - 30	0.06 - 0.07
Wet bedrock	5 - 20	0.05 - 0.13
Dry asphalt	2 - 4	0.15 - 0.21
Wet asphalt	6 - 12	0.07 - 0.21
Dry concrete	4 - 10	0.09 - 0.15
Wet concrete	10 - 20	0.07 - 0.09

*For GPR data nanoseconds (ns), i.e. 10^{-9} seconds, is an appropriate unit of time.

[1] The literature review of this paper was presented at "Non-destructive testing of highway pavements" at the Institution of Electrical Engineers, London, 30 January 1997

General principles

The basic principle underlying GPR is that electromagnetic signals transmitted into the medium of interest are partially reflected on encountering a change in the electrical properties. The reflected signal is recorded at a receiver while the transmitted part continues through the new material. This process is continued when further electrically different media are met by the transmitted signal. The series of reflections recorded at the receiver allow an image of the interior structure to be built up. An explanation of GPR is also provided (HA 72/94, HMSO) concerns the technique's usage for the investigation of pavement defects.

The depth of the a layer of material is determined from the time it takes the reflected wave to be detected at the receiver. Knowing the velocity of the wave through the relevant media the depth is calculated as:

$$d = v\left(\frac{t}{2}\right) \tag{1}$$

where: d = thickness of layer
v = velocity of electromagnetic wave through the layer
t = time between reflections.

The time is divided by two as the signals are recorded after travelling down to the layer boundary and back up to the receiver, i.e. a 'two-way travel time' is given. In the determination of sediment thicknesses the above equation is employed using the time between the observed reflections and the relevant velocity can be estimated from Table 1.

Material properties

The electrical properties that govern the propagation of electromagnetic waves through materials are electrical conductivity and dielectric constant. These properties and corresponding radar velocities are presented in Table 1 for the materials of interest in a pavement survey. In general the conductivity determines how far through a material the signal penetrates while contrasts in dielectric constant govern the proportion of energy transmitted and reflected at material boundaries.

The velocity of the electromagnetic wave decreases with an increase in dielectric constant as the speed of electromagnetic waves through non-magnetic materials such as water or soils is approximately, for low-loss materials:

$$v = \frac{c}{\sqrt{\varepsilon_r}} \tag{2}$$

where: v = sign a velocity, c = velocity of light in free space (0.300 m/ns), ε_r = relative dielectric constant.

The electrical conductivity has the greatest bearing on the degree of signal attenuation, i.e. on the extent to which the signals penetrate. The higher the conductivity the greater the attenuation and less the depth of penetration. Conductivities of paving materials can vary greatly due to the presence of salt in any water that is present in the pores. The attenuation also increases with the frequency of the wave that is propagating through the medium so high frequency surveys will not be able to penetrate wet materials that have salt dissolved in them.

The power of emitted radiation is also a factor and as the lower frequency antennas produce the more powerful signals they therefore allow greater depths to be probed. However, there is a trade off, as the lower the frequency the poorer the resolution.

Radar antennas

On placing an antenna on a surface the frequency content of the emitted pulse changes relative to that emitted in air. The antenna is said to be coupled or loaded to the water. The peak frequency of the radiated signal generally becomes lower on coupling (Sellmann *et al.*, 1993).

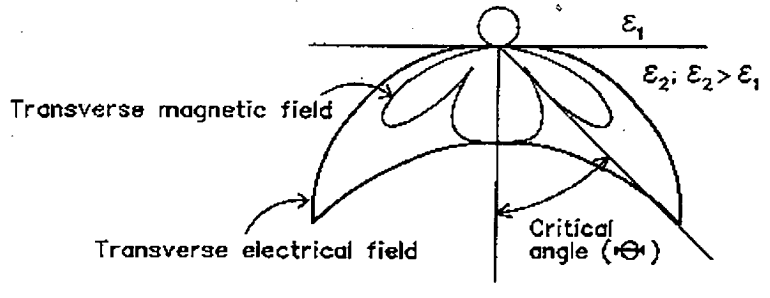

Figure 1: The radiation pattern of a dipole antenna when placed on the ground.

Ground-penetrating radar antennas produce signals which emerge in quite a complex pattern as is shown in Figure 1. The diagram indicates the form of radiation emitted by a dipole antenna when placed on ground of uniform dielectric constant. Estimation of the beam width for different frequency antennas over water is provided by Davidson and Forde (Davidson & Forde, 1996). There is a further type of

antenna, a horn antenna, which produces a more focused beam though the general pattern of radiation is similar.

The dispersed radar beam also leads to some geometrical distortion of the river bed shape. On passing over inclined layer the signal returned to the receiver is that from the point on the bed perpendicular to the emerging signals rather than the point directly below the antenna. Figure 2 illustrates this principal for the use of GPR to locate river beds. This causes a shift in the depth and angle of inclination which is significant beyond slope angles of 25°. Such angles are only encountered in pavements where there are significant changes in the structure.

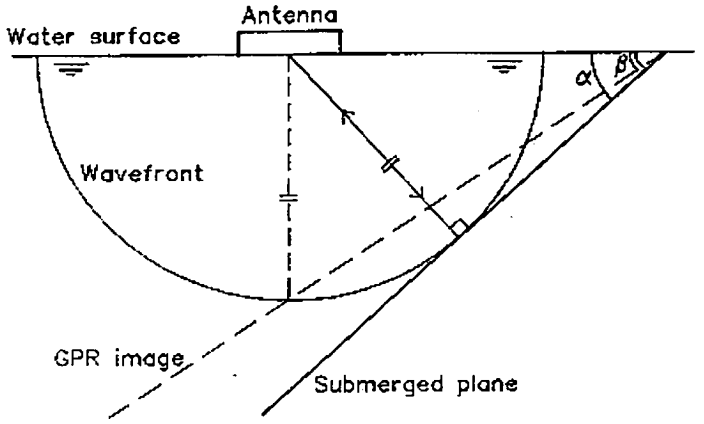

Figure 2: Ground-penetrating radar image of a sloping plane.

A further factor to consider is the influence of signals 'ringing' back and forth between two good reflectors. This is apparent when GPR is used over water as the bed surface is shown repeatedly in time down the profile. These reflections are known as 'multiples' and should not be confused with reflections from true structure.

Review of recent investigations on highway pavements

Weil (Weil, 1991; 1992A; 1992B; 1993A; 1993B; 1995), reports on experience of using Infrared Thermography (IRT) and GPR to assess highway and airport pavements. IRT uses a infrared camera to detect changes in surface temperature that can be related to the presence of voids beneath the pavement, or delaminations within the pavement itself. The limitations of IRT are that whilst large areas can be covered quickly, it is not possible to gain accurate pictures of the depths or exact extents of voiding beneath or cracking within pavements. Whilst GPR is a slower technique to apply, as pavements must be scanned in many parallel lines, he does recognise its value in pinpointing problems and finding the true depth of voiding.

Weil recommends that IRT is used to direct the GPR surveys to particular areas where it can be used more efficiently to get a detailed picture of damaged areas.

Adcock *et al.* (Adcock *et al.*, 1995) report the use of GPR by the USA Air Force to detect significant variations in pavement thickness, voiding and water ingress as well as the thicknesses of surfaces on airfield pavements of both Portland Cement Concrete (PCC) and Asphalt Concrete (AC).

They developed a sophisticated vehicle with GSSI 2.5 GHz horn antennas mounted at the front and 900MHz bowtie antennas at the rear. The aim was to use the 2.5GHz antennas to give accurate information about the dielectric constant of the surface material. This was calculated by measuring the amplitude of the reflected pulse from the pavement and comparing with the amplitude of the pulse reflected from a steel plate. As the reflected field strength is related to the incident strength by the reflection coefficient

$$r = \frac{\sqrt{\varepsilon_2} - \sqrt{\varepsilon_1}}{\sqrt{\varepsilon_2} + \sqrt{\varepsilon_1}} \qquad (3)$$

where ε_1 is the permittivity of the medium through which the pulse is travelling when it meets an interface with a material of permittivity ε_2.

The high frequency pulse was not suitable for penetrating through the PCC or AC top layer so the 900MHz antennas are used to measure the time for the reflection from the bottom of these layers. The knowledge of the permittivity of the material from the reflection coefficient allows the travel times for the 900MHz pulse to be translated back into a layer depth. The system that they developed was intended to be fully automated, but they found it difficult to ensure that an automated system could find all the correct peaks in the signals for the data analysis and therefore some manual intervention was required. However, with this intervention, layer depths could be found with accuracies of ±5%.

Heiler *et al.* (Heiler *et al.*, 1995) have tackled the problem of automatic detection of asphalt thickness and depth to reinforcement in composite pavements using neural networks. The networks were trained to recognise the quality and of the data presented to them and to locate the reflections from the three features required. Different networks were used for the quality testing and the location, but the location network has 124 input points and 3 analogue outputs, one per feature required.

The results were quite promising with the networks identifying the rogue data sets, but also identifying between 5 and 20% of the correct data sets as defective. It is pointed out by the authors that this conservatism by the networks is at least on the safe side.

For good data sets the location of the features was very accurate. It is clear that huge amounts of accurate data are required to train the networks before they can be of any use and that accurate and good quality radar data is required if there are to be consistent, good results.

The use of neural networks in this context is quite encouraging if the precise features that are under investigation can be easily identified. Unfortunately, what is being looked for in the radar trace is often quite difficult to predict in advance of seeing it and there is a long way to go before such networks can replace the eye of an experienced operator.

Daniels' book, Surface Penetrating Radar (Daniels, 1996), contains many case studies including reports from Wilkinson, of Durham County Council, UK and Caiou, Côte and Derobert of the Laboratoires des Ponts et Chausées (LPC) in France on the application of GPR to pavement investigation.

Wilkinson reports that GPR can be used to determine thicknesses of bituminous or concrete pavements, spacing and location of reinforcement and dowels, cracking and, if there is not too much reinforcement in concrete pavements, the position of cracks and voids beneath the pavements. This can be carried out more efficiently than by the tradition methods of coring. Surveys can even be carried out at highway speed with sufficient accuracy. He does report that a survey of operators in the UK were not able to agree on the materials of construction of older roads where the pavement had been developed in a piecemeal fashion. As perhaps 80% of the UK's roads fall into this category this is one area where there may be room for development.

The team from the LPC report on their experience of using a 700MHz centre-frequency system and confirm that it can only resolve layers of 5cm or greater, and that the accuracy is approximately 8%. This work was carried out in the '80s and since then they have investigated the use of synthetic-pulse radar. They are encouraged by their initial findings and suggest that it can penetrate further in to the road than the amplitude modulated pulse system by a factor of 1.5 or more.

Mesher *et al.* (Mesher *et al.*, 1995) have developed the Road Radar with the specific objective of identifying and quantifying pavement layer thicknesses. Rather than use the amplitude of reflected waves to determine the permittivity of layers they use a multiple antenna array to evaluate it. This is because the amplitude of a pulse reflected by a material interface is prone to changes in its amplitude due to other factors apart from the reflectivity of the interface. These factors include the height of the antenna above the road, which is difficult to maintain constant at high speed, and the rough surface of the pavement scatters the incident pulse rather than reflecting it neatly. The set-up of their multiple antenna array is shown in figure 3.

The change in the travel time as the pulse travels along different path lengths can be used to determine the layer thicknesses.

Along with this system, they have developed sophisticated software incorporating artificial intelligence, time-domain signal processing, neural networks and pattern recognition techniques. The software will still defer to the operator if it encounters changes in construction which it is not happy to analyse. Once the operator has intervened the software can take over once more.

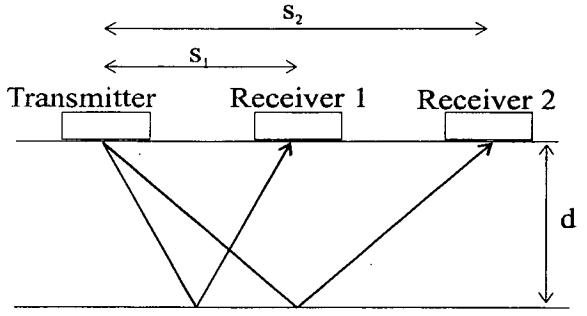

Figure 3: Multiple receiver bistatic antenna array

They present several field studies and the results are very encouraging for resolving layer thicknesses from 50mm to 2m. They suggest, however, that the precise determination of the velocity in the material might be strongly correlated to the material properties of interest to the pavement engineers.

As the water content is probably the most influential factor influencing the wave speed through the material it is likely that this might be determined from the velocity, but they suggest that it might be possible to determine compaction (which is related to the volume of air voids and density) and the volumetric ratios of the other constituents.

The velocities measured on three pavements varied between 120 and 148 mm/ns although the average values at the three pavements were 126, 129 and 130 mm/ns. These velocities match those in Table 1 well, but the spread of velocities at each site was 120-143, 125-133 and 121-148 mm/ns which indicates that using a single core at a site as a calibration for the radar survey is likely to lead to errors of the order of 10% or so.

Maser (Maser, 1996) presents a review of the use of GPR for evaluation of pavements, bridge decks, bridge piers and geotechnical applications. He compares contact bowtie antenna technology and non-contact horn antennas. He also suggests that the amplitude of the reflection of the pulse can be used to determine the permittivity, and hence wave-speed, of each layer in a pavement and that it is possible to make suitable measurements at highway speed. Asphalt layers as thin as 5cm

can be detected with a 1GHz horn antenna. The accuracy achieved for asphalt layer thicknesses has been ±7.5% and for the base layers is ±12%. Success with concrete pavements has not been so good due to the poor penetration of the pulse through the concrete. A hybrid horn/coupled antenna system is suggested to improve the penetration whilst maintaining the calculation of the wave speed by examination of the reflection of the pulse from the concrete surface.

Maser (Maser, 1986; Maser, 1990; Maser, 1991; Maser, 1993; Maser, 1994; Maser, 1995), presents the field studies from New Hampshire, Germany, Texas and Kansas on which he bases his paper above.

Ballard has investigated some experimental sections of road that have been cored for comparison (Ballard, 1993). He identifies significant variations in pavement thickness along the length of each pavement investigated (up to 30mm or 10% of the pavement thickness) and suggests that these might have a significant effect on the life of the pavements involved. As the pavement stiffness is, to a first order according to simple bending plate theory, proportional to the thickness to the third power he is undoubtedly correct. GPR provides a much better tool for investigating the quality of new pavements or overlays than other methods as it can give spatial resolution along the road much more precisely than even the most extensive, and hence destructive, coring surveys.

Hobbs *et al.* (Hobbs *et al.*, 1993) review the advantages of the GPR technique for surveying structures in general and the specific costs of maintaining the highway infrastructure in the UK and USA. They cite the difficult-to-interpret nature of GPR traces as one reason why GPR is not more widely used and suggest the techniques used for ultrasonic signal analysis might be useful for reduction of GPR images. It is also shown by illustration that GPR images can be more amenable than their ultrasonic counterparts in certain circumstances. Ultrasonic testing of road pavements has not met with much success as the short wavelengths involved are diffracted by all the small inhomogeneities of the materials involved. This leads to rapid attenuation of the travelling wave and significant "clutter" of the received signal.

Uddin and Hudson (Uddin & Hudson, 1994) are interested in detecting voids beneath concrete pavements. They state that half of these can be found by visual inspection looking for pumped material. Deflection measurements have been tried but are not reliable indicators because of variable slab-to-slab joint conditions and lifting of slab edges due to temperature effects.

They report use of two different GPR systems. RODAR is a vehicle mounted, non-contact system that can carry out surveys at 10mph. Donahue's Remote Sensing Van uses a combination of IRT and GPR. High frequency transducers are used to give good resolution although the paper does not give much detail of the systems involved.

Several case studies are taken from the literature and it is concluded that GPR is a promising tool for this purpose, but that improvements need to be made to the analysis of the results and presentation to the end user.

Attoh-Okine (Attoh-Okine, 1996) compares the cost of a GPR survey from a vehicle in the traffic stream with a traditional coring survey, with cores at either 20/mile or 2/mile depending on the purpose of the survey. He developed a cost model for each method and then compared them. This study showed that the GPR survey would be between 2 and 3.5 times cheaper than coring although there is very little data to back these figures up.

This brief survey of recent literature highlights the possible benefits of using GPR for pavement thickness evaluation, such as rapid and cheap surveys with more detail than is possible by other methods, but also reveals the engineer's frustration at the amount of manual intervention that is required to analyse the masses of data that can be collected. The use of advanced processing systems has not yet alleviated this problem.

Two methods for determining the permittivity of the pavement materials are found. Either the amplitude of the reflected pulse can be used or a multiple antenna bistatic array can be used. Both methods appear to have been successful.

Current and future developments

Maser (Maser, 1996) looks at future developments including the stepped frequency and synthetic aperture radar.

Stepped frequency radar can be explained by examining the Fourier decomposition of the desired pulse that is transmitted by the antenna. As the pulse is sent repeatedly, at a pulse repetition rate, T, then the pulse can be synthesised by the summation of a set of scaled and appropriately phased sine waves with frequencies i/T Hz. If each of these component sine waves is translated in turn the response to the pulse can be determined by the inverse Fourier transform of the scaled and phase-corrected responses.

This method gives great control over the shape of the transmitted pulse and an increase in the power that can be transmitted, hence improving the penetration. The cost of this is that the signals take longer to transmit as many frequencies must be transmitted and the results must be recombined before a picture is produced.

The synthetic aperture radar involves use of an array of antennas (or a single moving one) that can together provide data that resolves the shape and depth of targets with much greater accuracy than a single antenna can on its own. Again, there is a cost in the data processing associated with this method.

Both of these methods are explained in more detail by Daniels (Daniels, 1996A). Further signal processing developments are also discussed including the possibility Wavelet analysis to enhance images, see also (Daniels, 1996B).

Weedon *et al.* (Weedon *et al.*, 1994) explain the development of a stepped frequency radar (SFR) system with a switched antenna array designed specifically to resolve images at a range of 40cm. A 2D Finite Difference Time Domain simulation is used to try to reconstruct the true image from the radar image by iteratively modifying the simulation model until its output matches the measured image. They meet with some success, but are limited to locating 2D images such as straight bars and only attempted the procedure with the bars in the optimum position for the antenna array. These limitations mean that this technique cannot be applied directly to highway pavements, but the extension to 3D and the use of planar, rather than focused arrays would not seem to be insurmountable extensions to this work.

Langman *et al.* (Langman *et al.*, 1994) describe the theory and development of a stepped frequency radar system and describe the Extended Prony Method as an alternative to the IFT for getting enhanced spatial resolution. The results are convincing both in simulation and experiment but there is no mention of the processing time cost which would appear to be considerable.

Warhus *et al.* (Warhus *et al.*, 1993; Warhus *et al.* 1994) describe in detail the design requirements for a GPR system with a single transmitter but an array of receivers spanning the pavement surface particularly for RC bridge decks. Images of the deck are reconstructed using the techniques for synthetic aperture radar processing as described by Daniels [12].

Mast and Johansson (Mast & Johansson, 1994) explain their 3-dimensional reconstruction of a test specimen of reinforced concrete using a synthesised aperture technique. Their antenna had a bandwidth from 0.5-3.5GHz and the 3D rendered image is very impressive. The downside of this is the quantity of data that has to be collected to produce the images but with the cost of the hardware reducing all the time it may well be possible to produce a similar technique for scanning highways in the future using arrays of antennas in parallel, or maybe as described by Warhus *et al.* (Warhus *et al.*, 1993A; Warhus *et al.* 1994).

Johansson and Mast (Johansson & Mast, 1994) present an alternative method for producing 3D images. The data acquisition required is the same but the analysis procedure is very different and is more akin to a deconvolution and migration of the data in three dimensions. Whilst the results of this analysis do not look as good as those from the previous technique [30], the authors point out that the computational effort is much reduced and that this method will become more attractive as the number of strata involved in the analysis increase.

Nelson (Nelson, 1994) reports on the 3D modelling efforts for simulating GPR with Finite Difference Time Domain simulation at the Lawrence Livermore National Laboratory.

The concrete is modelled as a 2-phase random mixture with the aggregate having different electromagnetic properties to the cement matrix. The simulations are compared with real measurements under fairly ideal conditions in an anechoic laboratory. These prove to be a good match. The conclusions are that the precise modelling of the aggregate-cement mix is important if the simulation is to work as the scattering, diffracting and shadowing effects of the particles are significant.

Gros, Edwards, Strachan *et al.* (Gros *et al.*, 1994; Gros *et al.*, 1995A; Gros *et al.*, 1995B; Gros, 1997; Gros *et al.*, 1993) have brought the concept of data fusion into NDT. Data fusion is the simultaneous analysis of the results of different sensors, not necessarily even the same type of sensor, to give an improved image of the object under investigation. A simple example is the fusion of many readings of a GPR record by averaging in order to reduce background noise effects and improve the image. More sophisticated techniques are illustrated by different sensors that detect aircraft by scanning the skies in a crude and rough way, a second set of sensors can identify the aircraft, and a third set will give its speed and direction.

There are several mathematical techniques available for bringing together the information from different sensors, such as IRT and GPR data with different antenna. These include statistical ensemble averaging, Baysian inference methods, the Dempster-Shafer theory of evidence, fuzzy logic and neural networks.

Gros (Gros, 1997) implements Baysian and Dempster-Shafer fusion theory to bring together eddy current surveys (which give a surface profile of defects), ultrasonic surveys (which give cross-sectional profiles of defects), and X-ray radiographic surveys (giving through depth images) of weld cracks. He concludes that the Dempster-Shafer extension of the Baysian theory gives better answers.

Current State of the art

The range of techniques available to highway engineers for the assessment of pavement condition are many and varied. The simultaneous analysis of the information from different systems would greatly enhance the reliability of the interpretation, and even extend interpretation into areas not yet envisaged.

The developments of new radar hardware such as stepped-frequency radar, improved horn and array antennas, signal processing techniques such as synthetic aperture radar, the accurate three-dimensional simulation of these techniques for improved understanding and training of neural networks, and the techniques of data fusion to bring together many sources of

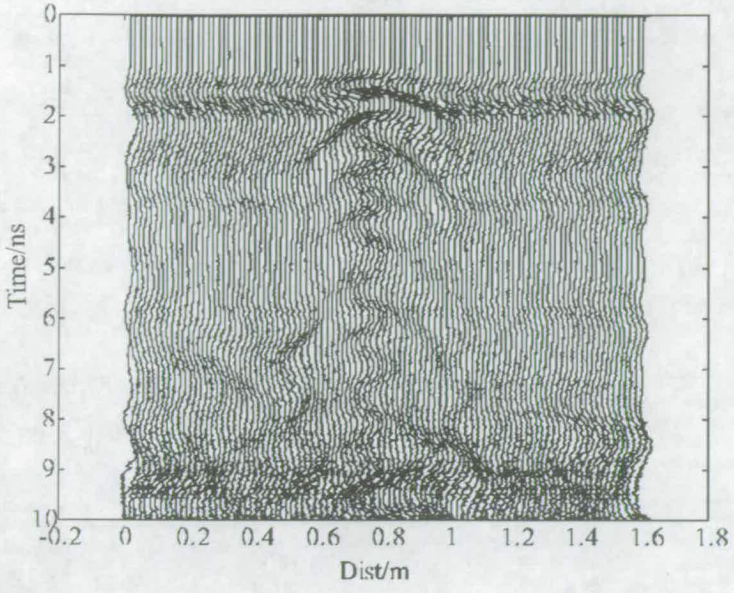

Figure 4: 900MHz GPR scans over a thin pavement with surface slab removed at the middle section.

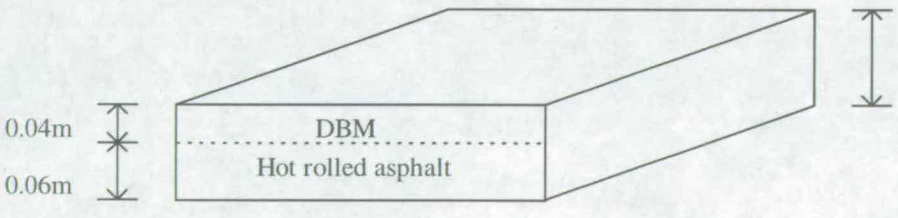

Figure 5: Thickness detail of the pavement slab

information in a rational and quantifiable way seem to spell an exciting and rapidly developing improvement in the use of GPR in many fields, including highway pavement assessment.

Many of the developments discussed above are at a theoretical or laboratory stage and are not yet suitable for engineers to take out into the field. The remainder of this paper investigates the advances that can be made in the use of existing GPR technology in the field of thin pavements investigation.

IMPULSE RADAR OF THIN PAVEMENTS

These pavements (thicknesses < 200mm) create particular problems for GPR as the wavelength of a 1GHz radar pulse is in the range 90-210mm according to the velocity information given in Table 1. The response from the underside of the pavement is therefore likely to be confused in the radar image with the response from the initial impulse either by direct transmission from the transmitter to the receiver, from reflections from the pavement surface itself, or most likely, both. This is illustrated in figure 4 which shows a GPR survey over a section of road pavement. The pavement thickness was only 100mm and this was removed over the central section of the scan. The antenna itself was moved over the top of a thin sheet of timber so that it had a flat surface to run along and also so that an air-gap appeared beneath the antenna where the surface had been removed. It might have been hoped that the radar scan would pick up the sudden change in the road surface, but it is not clear at all from the scans shown in figure 4 because the reflection of the bottom of the pavement appears at a time of between 0.22 and 0.10 ns if the data from table 1 is used. It is clear from figure 4 that this time range is within the initial surface reflection/direct transmission time of this antenna. It is possible to use higher frequency antennas but these were not available to the researchers at the time and a higher frequency antenna would run into exactly the same problems if it was applied to thinner pavements.

GPR INVESTIGATION OF THIN ASPHALT SLABS

The surface slab that had been removed from the road scanned in figure 4 was removed to the laboratory for further investigation. Details of the slab geometry are shown in figure 5.

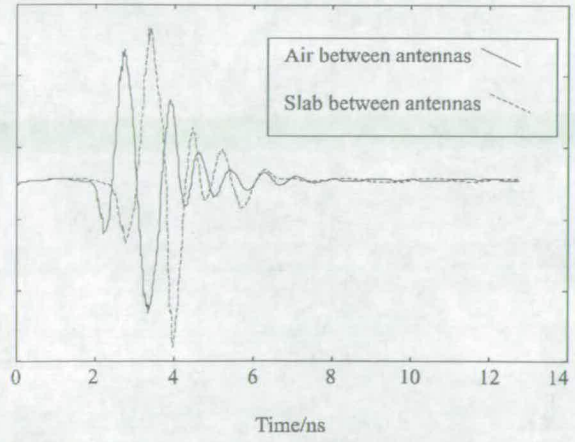

Figure 6: Delay of radar pulse through the slab

Speed of radar pulses through the asphalt slab

An initial investigation was carried out to find the precise speed of the radar pulse through the slab. The pavement slab was placed on its side and passed between two 900 MHz antennas, which were also on their sides. The antennas were at a distance of 0.105m apart, in order for the piece of pavement to fit between them. The velocity of the radar pulse through the slab is given by equation 2 above, where ε_r is the relative permittivity of the slab material. Pulses were transmitted from one antenna to the other with the slab in position, and also with the slab removed so that the pulse only travelled through the air. The received pulses are shown in figure 6. It is clear that the slower pulse speed through the slab causes the pulse to be delayed. Closer inspection shows that this delay is 0.40ns. If the time it

takes for the pulse to travel from the transmitting antenna (some distance inside the box in which it is mounted) through to the front of the box, through the small air gap between the antenna and the slab, through the slab and out of the other side. Then through the clearance gap and into the box of the receiving antenna, before being picked up is T_s and the similar travel time without the slab being present is T_a then we can write that:

$$T_s = \frac{d}{v_s} + T_0$$

$$\text{and } T_a = \frac{d}{v_a} + T_0 \tag{4}$$

where d is the thickness of the slab, v_s is the speed through the slab, v_a is the speed through air and T_0 is the time to travel through everything except the slab or the air that has replaced it.

Simply taking the difference of these gives the observed delay, Δ as:

$$\Delta = T_s - T_a = \frac{d}{v_s} - \frac{d}{v_a} = \frac{d}{c}\left(\sqrt{\varepsilon_r} - 1\right) \tag{5}$$

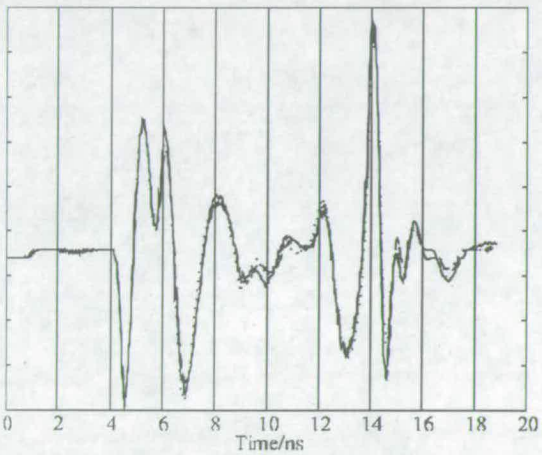

Figure 7: Repeatability of the radar scans

as Δ, d and c are known it is simple to find the relative dielectric constant of the slab material and hence the velocity through the slab (it is assumed that the velocity through the air is c). It turns out that the velocity of the radar pulse through the slab is 0.14m/ns giving a relative permittivity of 4.8. this value is low in the range and indicates a dry material which is consistent with the slab having been kept indoors for several days after removal from the road.

Testing of slab on artificial sub-base.

Figure 7 shows three scans with the transmit and receive antennas on the top surface of the slab as it rests on a bed of course "concrete" sand. The reflection from the bottom of the slab is expected at 1.4ns after the initial pulse and is therefore confused with the initial pulse as expected. The large reflections between 12 and 16ns are from the bottom of the sand bed. This figure shows the repeatability of the radar scans, and it is this property that will be used to try to distinguish the slab thickness from the initial pulse.

As well as using a coarse "concrete" sand as a sub-base material a single-graded silica sand and a gravel with stone sizes up to 10mm were also used. The results from the radar scans with these three different sub-bases are shown in figure 8. It is clear from this figure that the direct transmission and reflection from the asphalt slab surface are not changed by the sub-base material. However, by 6ns the pulses are diverging as the reflections from the bottom of the slab are now being received and these will be modified by the different materials with which the slab is in contact. The pulses diverge at approximately 1.5ns after the initial pulse is received which is consistent with this observation.

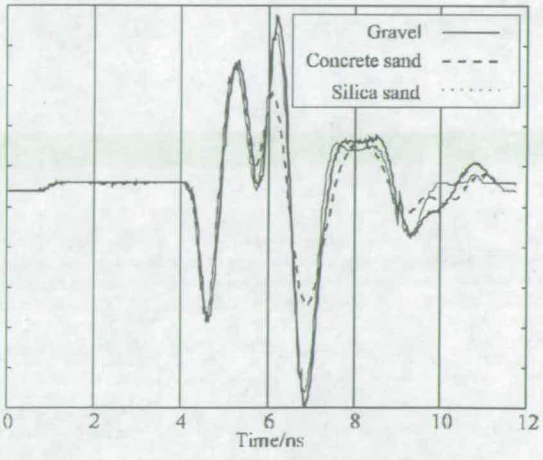

Figure 8: Scans with different sub-base materials

Figures 9, 10 and 11 are the responses when the height of the slab is raised above the sub-base. The introduction of this air gap between the bottom of the sub-base and the slab is observed to change the reflection from the bottom of the slab in each case only when the initial clearance of 0.1m is introduced. After this clearance the reflection from the bottom of the slab does not change but there is an additional reflection from the surface of the sub-base material. The expected delay after the reflection off the slab base is 0.667ns for every 0.1m that the slab is raised. This is consistent with the observation.

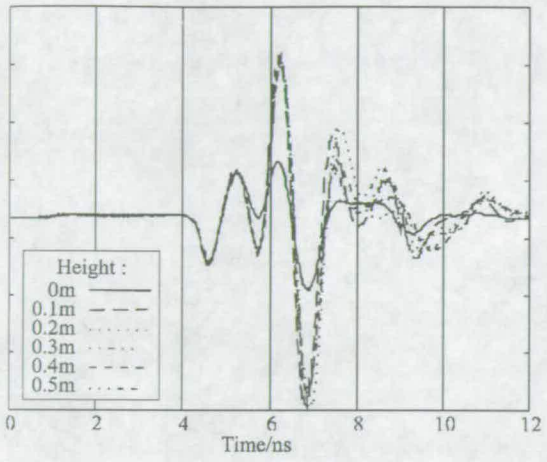

Figure 9: Effect of lifting slab off the gravel sub-base

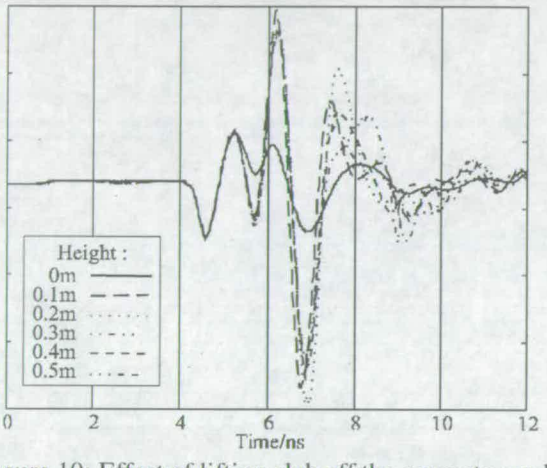

Figure 10: Effect of lifting slab off the concrete sand sub-base

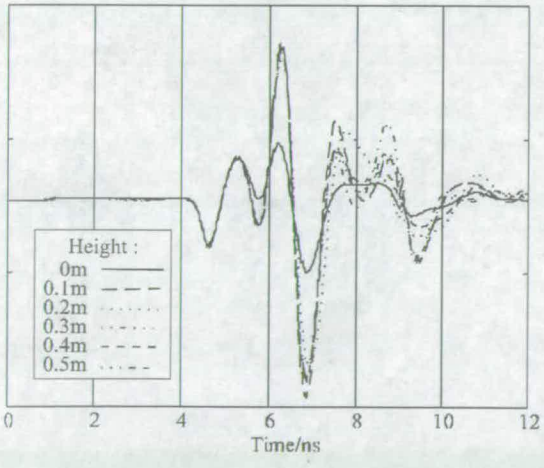

Figure 11: Effect of lifting slab off the silica sand sub-base

In order to emphasise this effect figures 12, 13 and 14 show the same results but the response of the slab in contact with the sub-base (zero height) has been subtracted off all the other responses. The original response with the slab not raised is also included so that the time delay between the slab surface and base reflections can be identified.

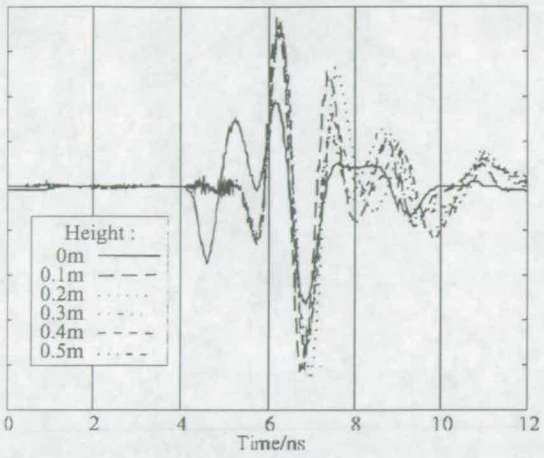

Figure 12: Deviation as slab is raised off the gravel sub-base

same up to approximately 0.7ns as expected. It is possible that averaging together of many scans would reduce the noise levels sufficiently for these to be identified with more accuracy.

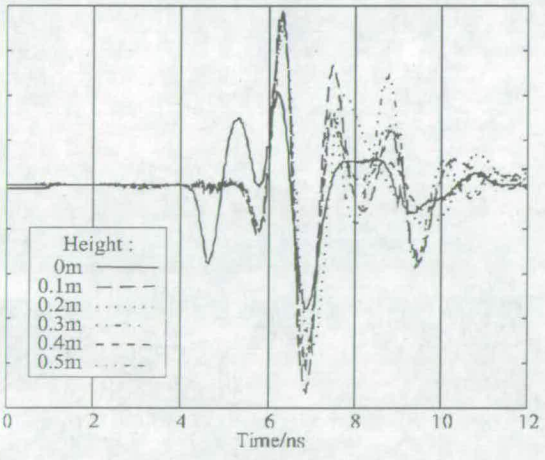

Figure 14: Deviation as slab is raised off the silica sand sub-base

It is clear that the initial received pulse is very repeatable and the procedure adopted allows for the slab surface and base responses to be identified individually. It is difficult to distinguish the responses from the increasing gap between the slab base and the sub-base material, although the deviations from the zero height response do appear to be the

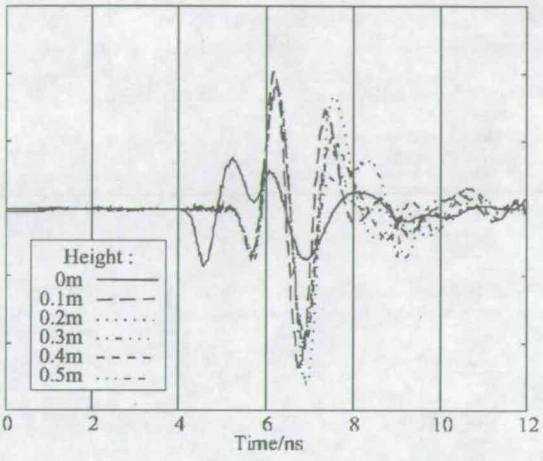

Figure 13: Deviation as slab is raised off the concrete sand sub-base

When this technique was tried to remove the initial pulse from the scan on the actual road it did not meet with any success. This is thought to be due to the fact that the slab had dried between its existence in the field and testing in the laboratory. The effect of moisture in pavement materials has a great effect on their testing with GPR due to the high permittivity of water.

CONCLUSION

The range of techniques available to highway engineers for the assessment of pavement condition are many and varied. The simultaneous analysis of the information from different systems would greatly enhance the reliability of the interpretation, and even extend interpretation into areas not yet envisaged.

The developments of new radar hardware such as stepped-frequency radar, improved horn and array antennas, signal processing techniques such as synthetic aperture radar, the accurate three-dimensional simulation of these techniques for improved understanding and training of neural networks, and the techniques of data fusion to bring together many sources of information in a rational and quantifiable way seem to spell an exciting and rapidly developing improvement in the use of GPR in many fields, including highway pavement assessment.

The GPR responses of thin pavements can be impossible to interpret directly due to confusion of initial pulses reflections from the bottom of the thin layers (whether the bottom of the bituminous layers of the pavement or interfaces between different bituminous materials).

The effect of the material beneath the thin layer (and hence the thickness of the layer itself) has no effect on the initial response from the surface and this can therefore be eliminated as shown to reveal the response from the bottom of the layer.

ACKNOWLEDGEMENT

The authors would like to thank Kevin Broughton for his assistance in the experimental part of theis project.

REFERENCES

"Use and limitations of ground-penetrating radar for pavement assessment," in *Design Manual for Roads and Bridges*, vol. 7 of Pavement Design and Maintenance, HA 72/94, HMSO

Adcock, A.D., Dass, W.C., and Rish, J.W.I. "Ground penetrating radar for airfield pavement evaluations," presented at SPIE-The International Society for Optical Engineering, Advanced Microwave and Millimeter-Wave Detectors, Oakland, CA, USA, 1995.

Attoh-Okine, N.O. "Using ground penetrating radar in pavement thickness measurements - a cost comparison with the traditional coring method," *Proc. Inst. Civ. Engnrs. Mun. Engnr.*, vol. 115, pp. 86-89, 1996.

Ballard, G.S. "Non-destructive assessment of pavement design and new build quality," presented at Int. Conf. on Non-Destructive Testing in Civil Engineering, Liverpool, 1993.

Daniels, D.J. *Surface-penetrating radar.* London: Institution of Electrical Engineers, 1996.

Daniels, D.J. "Surface-penetrating radar," *Electronics & Communication Engineering Journal*, pp. 165-182, 1996.

Davidson, N.C., and Forde, M.C. "A laboratory appraisal of ground-penetrating radar over water," *Nondestructive Testing and Evaluation*, vol. 12, pp. 219-242, 1996.

Edwards, I., Gros, X.E., Lowden, D.W,, and Strachan, P. "Fusion of NDT data," *British Journal of NDT*, vol. 35, pp. 710-713, 1993.

Gros, X.E., Strachan, P., Lowden, D., and Edwards, I. "NDT data fusion," presented at 6th European Conference on NDT, Nice, France, 1994.

Gros, X.E., Strachan, P., and Lowden, D. "Theory and Implementation of NDT Data Fusion," *Research in Nondestructive Evaluation*, vol. 6, pp. 227-236, 1995.

Gros, X.E., Strachan, P., and Lowden, D. "A bayesian approach to NDT data fusion," *INSIGHT*, vol. 37, pp. 363-367, 1995.

Gros, X.E. *NDT data fusion*, First ed: Arnold, 1997.

Heiler, M., and Garrett, J.J. "Ground-penetrating radar for highway and bridge deck condition assessment and inventory," presented at SPIE-The International Society for Optical Engineering, Nondestructive evaluation of ageing bridges and highways, Oakland, CA, USA, 1995.

Hobbs, C.P., Temple, J.A.G., Hillier, M.J., Silk, H.G., Tattersall, M.G. "Radar inspection of civil engineering structures," presented at Int. Conf. on Non-Destructive Testing in Civil Engineering, Liverpool, 1993.

Johansson, E.M., and Mast J.E. "Three-dimensional ground penetrating radar imaging using synthetic aperture time-domain focusing," presented at SPIE-The International Society for Optical Engineering, Advanced Microwave and Millimeter-Wave Detectors, 1994.

Langman, A., and Inggs, M.R. "Improving the resolution of a stepped frequency CW ground penetrating radar," presented at SPIE-The International Society for Optical Engineering, Advanced Microwave and Millimeter-Wave Detectors, San Diego, CA, USA, 1994.

Maser, K.R. "Condition assessment of transportation infrastructure using ground-penetrating radar," *Journal of Infrastructure Systems*, vol. 2, pp. 94-101, 1996.

Maser, K.R."Detection of progressive deterioration in bridge decks using ground-penetrating radar," presented at ASCE Convention, Boston, MA, 1986.

Maser, K.R. and. Roddis, W.M.K. "Principles of thermography and radar for bridge deck assessment," *ASCE Journal of Transportation Engineering*, 1990.

Maser, K.R., "Bridge deck evaluation utilizing high speed radar," Intrasense Inc., Cambridge Mass, USA 1991.

Maser, K.R., "Highway speed radar for pavement and bridge deck evaluation," presented at Int. Conf. on Non-Destructive Testing in Civil Engineering, Liverpool, 1993.

Maser, K.R., "Highway speed radar for pavement and bridge deck evaluation," presented at Structural Materials Technology, Atlantic City, NJ, USA, 1994.

Maser, K.R., Kristiansen, J., Schellenberger, W., and Fippinger, F. "Evaluation of pavement thickness using ground penetrating radar," presented at Int.. Symp. on Non-Destructive Testing in Civil Engineering (NDT-CE), Berlin, 1995.

Mesher, D.E., Dawley, C.B., Davis, J.L., and. Rossiter, J.R. "Evaluation of new ground-penetrating radar technology to quantify pavement structure," *Transportation Research Record*, pp. 17-26, 1995.

Mast J.E., and Johansson, E.M. "Three-dimensional ground penetrating radar imaging using multi-frequency diffraction tomography," presented at SPIE-The International Society for Optical Engineering, Advanced Microwave and Millimeter-Wave Detectors, 1994.

Nelson, S.D. "Electromagnetic modelling for ground-penetrating imaging radar (GPIR) using 3-D finite difference time-domain (FDTD) modeling codes," presented at SPIE-The International Society for Optical Engineering, Advanced Microwave and Millimeter-Wave Detectors, San Diego, CA, USA, 1994.

Sellmann, P.V., Delaney, A.J., and Arcone, S.A. "Observations of radar performance for bottom and sub-bottom information in fresh water," presented at Second Government Workshop on GPR, Advanced Ground-Penetrating Radar: Technologies and Applications, Ohio State University, 1993.

Uddin, W., and Hudson, W.R. "Evaluation of NDT equipment for measuring voids under concrete pavements," presented at ASTM Special Technical Publication, Proceedings of the Symposium on Nondestructive Testing of Pavements and Backcalculation of Moduli, Atlanta, GA, USA, 1994.

Warhus, J.P., Scott, D.N., Jeffrey, E.M., and Johansson, E.M. "Advanced ground-penetrating, imaging radar for bridge inspection," . Livermore, California: Engineering Research, Development and Technology, Lawrence Livermore National Laboratory, 1993.

Warhus, J.P., Mast, J.E., Johansson, E.M., and Nelson, S.D. "Advanced ground-penetrating radar," presented at SPIE-The International Society for Optical Engineering, Advanced Microwave and Millimeter-Wave Detectors, San Diego, CA, USA, 1994.

Weedon, W.H., Chew, W.C., and Ruwe, C.A. "Step-frequency radar imaging for NDE and GPR applications," presented at SPIE-The International Society for Optical Engineering, Advanced Microwave and Millimeter-Wave Detectors, San Diego, CA, USA, 1994.

Weil, G.J, "Infrared thermographic techniques," in *Handbook on non-destructive testing of concrete*, M. V. Malhotra and N. J. Carino, Eds. Boston: CRC Press, 1991, pp. 305-316.

Weil, G.J, "Non-destructive testing of bridge, highway and airport pavements," presented at Nondestructive Evaluation of Civil Structures and Materials, Boulder, Colorado, 1992.

Weil, G.J, "Non-destructive testing of bridge, highway and airport pavements," presented at No trenches in town proceedings of international conference, Paris,France, 1992.

Weil, G.J, "Non-destructive testing of bridge, highway and airport pavements," presented at 5th Intern. Conference on Structural Faults and Repair, Edinburgh, 1993.

Weil, G.J, "Non-destructive testing of bridge, highway and airport pavements," presented at International conference on NDT of concrete in the infrastructure, Dearbon, Michigan, USA, 1993.

Weil, G.J, "Non-destructive testing of bridge, highway and airport pavements," presented at Int. Symp. on Non-Destructive Testing in Civil Engineering (NDT-CE), Berlin, 1995.

ADVANCED NDT OF FLEXIBLE PAVEMENTS

M. O. Gordon & M. S. A. Hardy, Department of Civil & Environmental Engineering, The University of Edinburgh, King's Buildings, Edinburgh, EH9 3JN, Scotland, UK.

ABSTRACT

A survey of the different applications of Ground Penetrating Radar (GPR) for highway pavement investigation is presented with a critical appraisal of the success with which it has been applied. The problems associated with this technique are also discussed. These include discussions of the accuracy of the technique and the difficulties in trying to interpret the recorded signals. Suggestions for the future direction of the research in this field to enhance the data collection and interpretation are made.

The remainder of the paper investigates the advances that can be made in the use of existing GPR technology in the field of thin pavements investigation. A second method for identifying pavement thicknesses is also investigated. This is the "impulse echo" method which uses sonic rather than electromagnetic waves to detect the interfaces of materials.

INTRODUCTION

Ground Penetrating Radar (GPR) is a non-destructive technique for investigating objects hidden by optically opaque barriers. It detects changes in the electromagnetic properties of materials, principally the permittivity, and is capable of producing cross-sectional representations of what is beneath surfaces. This paper presents an introduction to the technique and a review of its application to the investigation of highway pavements. It then looks forward to the developments currently underway in the field and what might be possible in the near future with advances in hardware and signal processing capability.

Material	*Relative dielectric constant*	*Velocity(m/ns)**
Fresh water	81	0.033
Saturated clays	5 - 40	0.05 - 0.13
Saturated silts	5 - 30	0.06 - 0.13
Saturated sand	20 - 30	0.06 - 0.07
Wet bedrock	5 - 20	0.05 - 0.13
Dry asphalt	2 - 4	0.15 - 0.21
Wet asphalt	6 - 12	0.07 - 0.21
Dry concrete	4 - 10	0.09 - 0.15

Table 1. Electrical properties of water and pavement materials

*For GPR data nanoseconds (ns), i.e. 10^{-9} seconds, is an appropriate unit of time.

GENERAL PRINCIPLES

The basic principle underlying GPR is that electromagnetic signals transmitted into the medium of interest are partially reflected on encountering a change in the electrical properties. The reflected signal is recorded at a receiver while the transmitted part continues through the new material. This process is continued when further electrically different media are met by the transmitted signal. The series of reflections recorded at the receiver allow an image of the interior structure to be built up. An explanation of GPR is also provided (HA72/94 HMSO), it concerns the technique's usage for the investigation of pavement defects. The depth of a layer of material is determined from the time it takes the reflected wave to be detected at the receiver. Knowing the velocity of the wave through the relevant media the depth is calculated as:

$$d = v\left(\frac{t}{2}\right) \qquad (1)$$

where: d = thickness of layer,
v = velocity of electromagnetic wave through the layer,
t = time between reflections.

In the determination of layer thicknesses the above equation is employed using the time between the observed reflections and the relevant velocity can be estimated from Table 1.

MATERIAL PROPERTIES

The electrical properties that govern the propagation of electromagnetic waves through materials are electrical conductivity and dielectric constant. These properties and corresponding radar velocities are presented in Table 1 for the materials of interest in a pavement survey. In general the conductivity determines how far through a material the signal penetrates while contrasts in dielectric constant govern the proportion of energy transmitted and reflected at material boundaries.

The velocity of the electromagnetic wave decreases with an increase in dielectric constant as the speed of electromagnetic waves through non-magnetic materials such as water or soils is approximately, for low-loss materials:

$$v = \frac{c}{\sqrt{\varepsilon_r}} \qquad (2)$$

where: v = signal velocity,
c = velocity of light (0.3 m/ns),
ε_r = relative dielectric constant.

The electrical conductivity has the greatest bearing on the degree of signal attenuation, i.e. on the extent to which the signals penetrate. The higher the conductivity the greater the attenuation and less the depth of penetration. Conductivities of paving materials can vary greatly due to the presence of salt in any water that is present in the pores. The attenuation also increases with the frequency of the wave that is propagating through the medium so high frequency surveys will not be able to penetrate wet materials that have salt dissolved in them.

The power of emitted radiation is also a factor and as the lower frequency antennas produce the more powerful signals they therefore allow greater depths to be probed. However, there is a trade off, as the lower the frequency the poorer the resolution.

RADAR ANTENNAS

On placing an antenna on a surface the frequency content of the emitted pulse changes relative to that emitted in air. The antenna is said to be coupled or loaded to the water. The peak frequency of the radiated signal generally becomes lower on coupling (Sellmann *et al.*, 1993).

Ground-penetrating radar antennas produce signals which emerge in quite a complex pattern as is shown in figure 1. The diagram indicates the form of radiation emitted by a dipole antenna when placed on ground of uniform dielectric constant. Estimation of the beam width for different frequency antennas over water is provided by Davidson and Forde (Davidson & Forde, 1996) There is a further type of antenna, a horn antenna, which produces a more focused beam though the general pattern of radiation is similar.

The dispersed radar beam also leads to some geometrical distortion of the river bed shape. On passing over an inclined layer the signal returned to the receiver is that from the point on the bed perpendicular to the emerging signals rather than the point directly below the antenna. Figure 2 illustrates this principal for the use of GPR to locate river beds. This causes a shift in the depth and angle of inclination which is significant beyond slope angles of 25°. Such angles are only encountered in pavements where there are significant changes in the structure.

A further factor to consider is the influence of signals 'ringing' back and forth between two

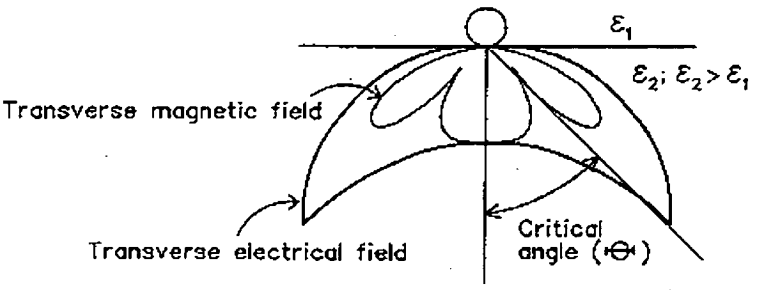

Figure 1: The radiation pattern of a dipole antenna when placed on the ground.

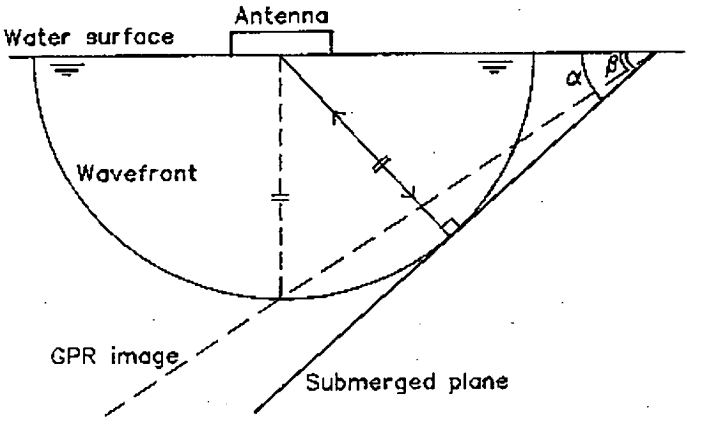

Figure 2: Ground-penetrating radar image of a sloping plane

good reflectors. This is apparent when GPR is used over water as the bed surface is shown repeatedly in time down the profile. These reflections are known as 'multiples' and should not be confused with reflections from true structure.

CURRENT AND FUTURE DEVELOPMENTS

Maser (Maser, 1996) looks at future developments including the stepped frequency and synthetic aperture radar.

Stepped frequency radar can be explained by examining the Fourier decomposition of the desired pulse that is transmitted by the antenna. As the pulse is sent repeatedly, at a pulse repetition rate, T, then the pulse can be synthesised by the summation of a set of scaled and appropriately phased sine waves with frequencies i/T Hz, where i=1,2,3... . If each of these component sine waves is transmitted in turn the response to the pulse can be determined by the inverse Fourier transform of the scaled and phase-corrected responses.

This method gives great control over the effective shape of the transmitted pulse and an increase in the power that can be transmitted, hence improving the penetration. The cost of this is that the signals take longer to transmit as many frequencies must be transmitted and the results must be recombined before a picture is produced.

The synthetic aperture radar involves use of an array of antennas (or a single moving one) that can together provide data that resolves the shape and depth of targets with much greater accuracy than a single antenna can on its own. Again, there is a cost in the data processing associated with this method.

Both of these methods are explained in more detail by Daniels (Daniels, 1996A Further signal processing developments are also discussed including the possibility Wavelet analysis to enhance images, see also (Daniels, 1996B).

Weedon *et al.* (Weedon *et al.*, 1994) explain the development of a stepped frequency radar (SFR) system with a switched antenna array designed specifically to resolve images at a range of 40cm. A 2D Finite Difference Time Domain simulation is used to try to reconstruct the true image from the radar image by iteratively modifying the simulation model until its output matches the measured image. They meet with some success, but are limited to locating 2D images such as straight bars and only attempted the procedure with the bars in the optimum position for the antenna array. These limitations mean that this technique cannot be applied directly to highway pavements, but the extension to 3D and the use of planar, rather than focused arrays would not seem to be insurmountable extensions to this work.

Langman *et al.* (Langman *et al.*, 1994) describe the theory and development of a stepped frequency radar system and describe the Extended Prony Method as an alternative to the IFT for getting enhanced spatial resolution. The results are convincing both in simulation and experiment but there is no mention of the processing time cost which would appear to be considerable.

Warhus *et al.* (Warhus *et al.*, 1993; Warhus *et al.* 1994) describe in detail the design requirements for a GPR system with a single transmitter but an array of receivers spanning the pavement surface particularly for RC bridge decks. Images of the deck are reconstructed using the techniques for synthetic aperture radar processing as described by Daniels (Daniels, 1996).

Mast and Johansson (Mast & Johansson, 1994) explain their 3-dimensional reconstruction of a test specimen of reinforced concrete using a synthesised aperture technique. Their antenna had a bandwidth from 0.5-3.5GHz and the 3D rendered image is very impressive. The downside of this is the quantity of data that has to be collected to produce the images, but with the cost of the hardware reducing all the time it may well be possible to produce a similar technique for scanning highways in the future using arrays of antennas in parallel, or maybe as described by Warhus *et al.* (Warhus *et al.*, 1993A; Warhus *et al.* 1994).

Johansson and Mast (Johansson & Mast, 1994) present an alternative method for producing 3D images. The data acquisition required is the same but the analysis procedure is very different and is more akin to a deconvolution and migration of the data in three dimensions. Whilst the results of this analysis do not look as good as those from the previous technique (Mast & Johansson, 1994), the authors point out that the computational effort is much reduced and that this method will become more attractive as the number of strata involved in the analysis increase.

Nelson (Nelson, 1994) reports on the 3D modelling efforts for simulating GPR with Finite Difference Time Domain simulation at the Lawrence Livermore National Laboratory.

The concrete is modelled as a 2-phase random mixture with the aggregate having different electromagnetic properties to the cement matrix. The simulations are compared with real measurements under fairly ideal conditions in an anechoic laboratory. These prove to be a good match. The conclusions are that the precise modelling of the aggregate-cement mix is important if the simulation is to work as the scattering, diffracting and shadowing effects of the particles are significant.

Gros, Edwards, Strachan *et al.* (Gros *et al.*, 1994; Gros *et al.*, 1995A; Gros *et al.*, 1995B; Gros, 1997; Gros *et al.*, 1993) have brought the concept of data fusion into NDT. Data fusion is the simultaneous analysis of the results of different sensors, not necessarily even the same type of sensor, to give an improved image of the object under investigation. A simple example is the fusion of many readings of a GPR record by averaging in order to reduce background noise effects and improve the image. More sophisticated techniques are illustrated by different sensors that detect aircraft by scanning the skies in a crude and rough way, a second set of sensors can identify the aircraft, and a third set will give its speed and direction.

There are several mathematical techniques available for bringing together the information from different sensors, such as IRT and GPR data with different antenna. These include statistical ensemble averaging, Baysian inference methods, the Dempster-Shafer theory of evidence, fuzzy logic and neural networks.

Gros (Gros, 1997) implements Baysian and Dempster-Shafer fusion theory to bring together eddy current surveys (which give a surface profile of defects), ultrasonic surveys (which give cross-sectional profiles of defects), and X-ray radiographic surveys (giving through depth images) of weld cracks. He concludes that the Dempster-Shafer extension of the Baysian theory gives better answers.

CURRENT STATE OF THE ART

The range of techniques available to highway engineers for the assessment of pavement condition are many and varied. The simultaneous analysis of the information from different systems would greatly enhance the reliability of the interpretation, and even extend interpretation into areas not yet envisaged.

The developments of new radar hardware such as stepped-frequency radar, improved horn and array antennas, signal processing techniques such as synthetic aperture radar, the accurate three-dimensional simulation of these techniques for improved understanding and training of neural networks, and the techniques of data fusion to bring together many sources of information in a rational and quantifiable way seem to spell an exciting and rapidly developing improvement in the use of GPR in many fields, including highway pavement assessment.

Many of the developments discussed above are at a theoretical or laboratory stage and are not yet suitable for engineers to take out into the field. The remainder of this paper investigates the advances that can be made in the use of existing GPR technology and sonics in the field of thin pavements investigation.

IMPULSE RADAR OF THIN PAVEMENTS

These pavements (thicknesses < 200mm) create particular problems for GPR as the wavelength of a 1GHz radar pulse is in the range 90-210mm according to the velocity information given in Table 1. The response from the underside of the pavement is therefore likely to be confused in the radar image with the response from the initial impulse either by direct transmission from the transmitter to the receiver, from reflections from the pavement surface itself, or most likely, both. This is illustrated in figure 3 which shows a GPR survey over a section of road pavement. The pavement thickness was only 100mm and this was removed over the central section of the scan. The antenna itself was moved over the top of a thin sheet of timber so that it had a flat surface to run along and also so that an air-gap appeared beneath the antenna where the surface had been removed. It might have been hoped that the radar scan would pick up the sudden change in the road surface, but it is not clear at all from the scans shown in figure 3 because the reflection of the bottom of the pavement appears at a time of between 0.10 and 0.22 ns if the data from table 1 is used. It is clear from figure 3 that this time range is within the initial surface reflection/direct transmission time of this antenna. It is possible to use higher frequency antennas but these were not available to the researchers at the time and a higher frequency antenna would run into exactly the same problems if it was applied to thinner pavements.

GPR INVESTIGATION OF THIN ASPHALT SLABS

The surface slab that had been removed from the road scanned in figure 3 was removed to the laboratory for further investigation. Details of the slab geometry are shown in figure 4.

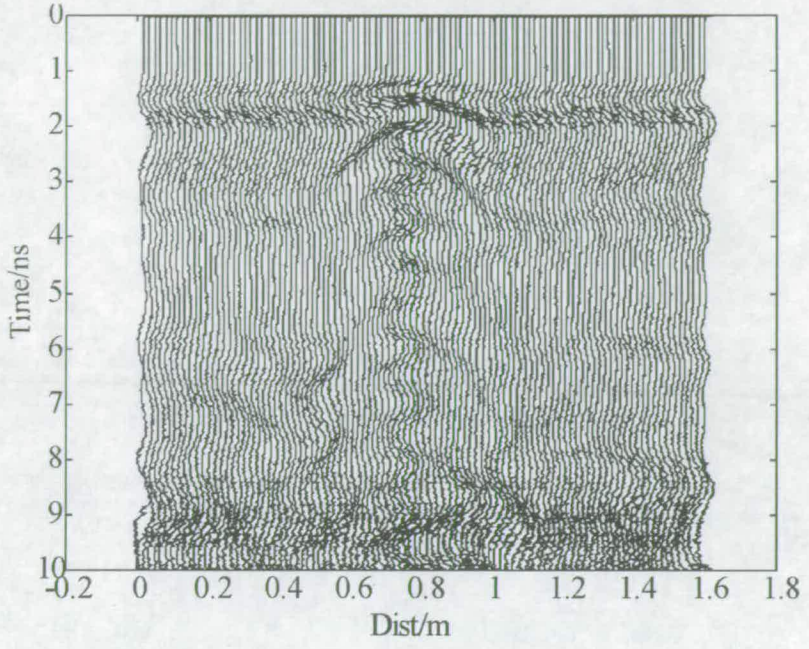

Figure 3: 900MHz GPR scans over a thin pavement with surface slab removed at the middle section.

Speed of radar pulses through the asphalt

An initial investigation was carried out to find the precise speed of the radar pulse through the slab. The pavement slab was placed on its side and passed between two 900 MHz antennas, which were also on their sides. The antennas were at a distance of 0.105m apart, in order for the piece of pavement to fit between them. The velocity of the radar pulse through the slab is

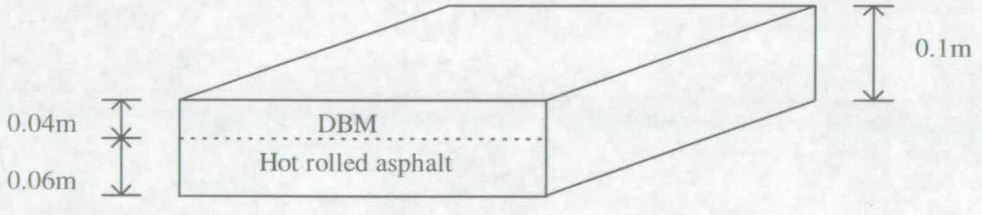

Figure 4: Thickness detail of the pavement slab

given by equation 2 above, where ε_r is the relative permittivity of the slab material. Pulses were transmitted from one antenna to the other with the slab in position, and also with the slab removed so that the pulse only travelled through the air. The received pulses are shown in figure 5.

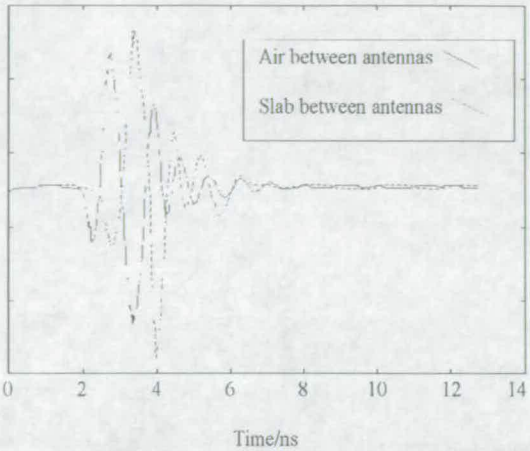

Figure 5: Delay of radar pulse through the slab

It is clear that the slower pulse speed through the slab causes the pulse to be delayed. Closer inspection shows that this delay is 0.40ns. If the time it takes for the pulse to travel from the transmitting antenna (some distance inside the box in which it is mounted) through to the front of the box, through the small air gap between the antenna and the slab, through the slab and out of the other side, then through the clearance gap and into the box of the receiving antenna, before being picked up is T_s and the similar travel time without the slab being present is T_a then we can write that:

$$T_s = \frac{d}{v_s} + T_0$$
$$\text{and } T_a = \frac{d}{v_a} + T_0 \qquad (4)$$

where d is the thickness of the slab, v_s is the speed through the slab, v_a is the speed through air and T_0 is the time to travel through everything except the slab or the air that has replaced it. Simply taking the difference of these gives the observed delay, Δ as:

$$\Delta = T_s - T_a = \frac{d}{v_s} - \frac{d}{v_a} = \frac{d}{c}\left(\sqrt{\varepsilon_r} - 1\right) \qquad (5)$$

as Δ, d and c are known it is simple to find the relative dielectric constant of the slab material and hence the velocity through the slab (it is assumed that the velocity through the air is 0.3m/ns). It turns out that the velocity of the radar pulse through the slab is 0.14m/ns giving a relative permittivity of 4.8. This value is low in the range and indicates a dry material which is consistent with the slab having been kept indoors for several days after removal from the road.

The next part of the experiment was to set the 900 MHz antenna on top of the pavement block which was positioned on its side, as shown in figure 6..

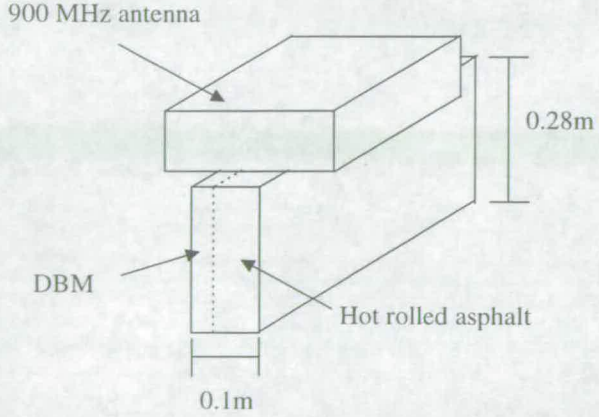

Figure 6: Setup used to detect the bottom of the pavement layer

The response from the pavement block was recorded by the radar equipment. The block with the antenna still on top was placed on a metal plate. This would show clearly where on the response the bottom of the pavement block was, as metal has a reflection coefficient of -1.0 which would produce a large amplitude on the response. This can be seen on figure 6. The two-way travel time of the reflection from the metal plate was found to be 3.8ns.

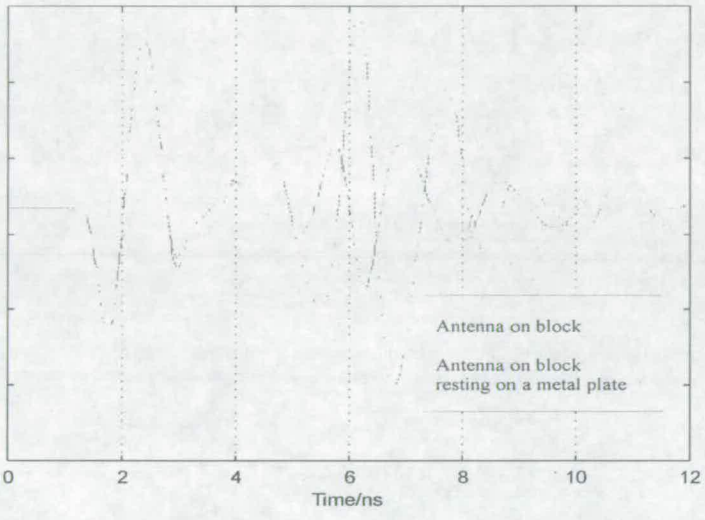

Figure 7: Effect of placing antenna on top of the slab

Using the velocity of 0.14m/ns, which was calculated earlier, and putting this value into equation 1, it was found that the theoretical value of the two-way travel time was 4ns. There is, therefore, a good correlation between the experimental values and the theoretical value.

TESTING OF SLAB ON ARTIFICIAL SUB-BASE.

Figure 8 shows three scans with the transmit and receive antennas on the top surface of the slab as it rests on a bed of course "concrete" sand. The reflection from the bottom of the slab is expected at 1.4ns after the initial pulse and is therefore confused with the initial pulse as expected. The large reflections between 12 and 16ns are from the bottom of the sand bed. This figure shows the repeatability of the radar scans, and it is this property that will be used to try to distinguish the slab thickness from the initial pulse.

As well as using a coarse "concrete" sand as a sub-base material a single-graded silica sand and

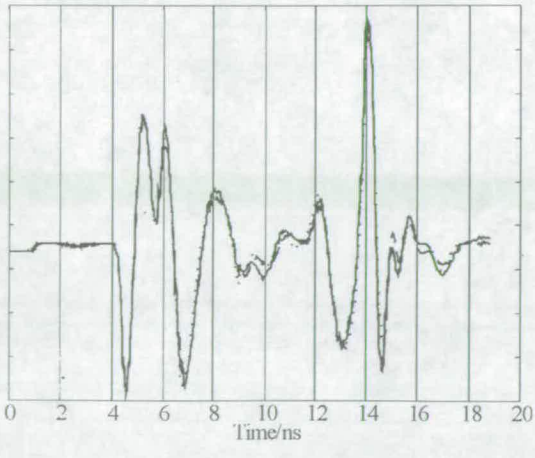

Figure 8: Repeatability of the radar scans

a gravel with stone sizes up to 10mm were also used. The results from the radar scans with these three different sub-bases are shown in figure 9. It is clear from this figure that the direct transmission and reflection from the asphalt slab surface are not changed by the sub-base material. However, by 6ns the pulses are diverging as the reflections from the bottom of the slab are now being received and these will be modified by the different materials with which the slab is in contact. The pulses diverge at approximately 1.5ns after the initial pulse is received which is consistent with this observation.

Figure 10, 11 and 12 are the responses when the height of the slab is raised above the sub-base. The introduction of this air gap between the bottom of the sub-base and the slab is observed to change the reflection from the bottom of the slab in each case only when the initial clearance of 0.1m is introduced. After this clearance the reflection from the bottom of the slab does not

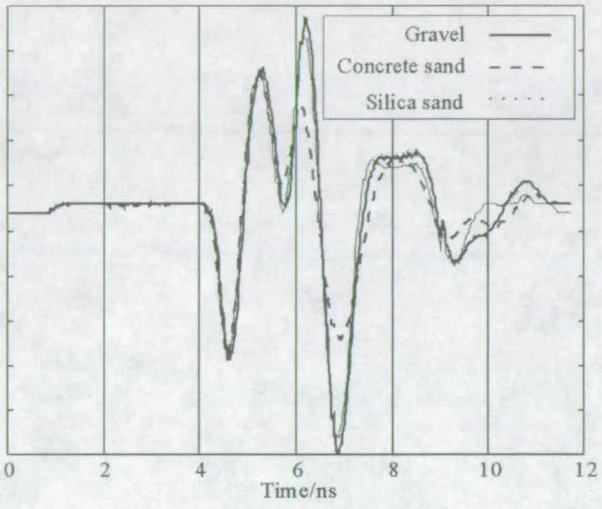

Figure 9: Scans with different sub-base materials

change but there is an additional reflection from the surface of the sub-base material. The expected delay after the reflection off the slab base is 0.667ns for every 0.1m that the slab is raised. This is consistent with the observation.

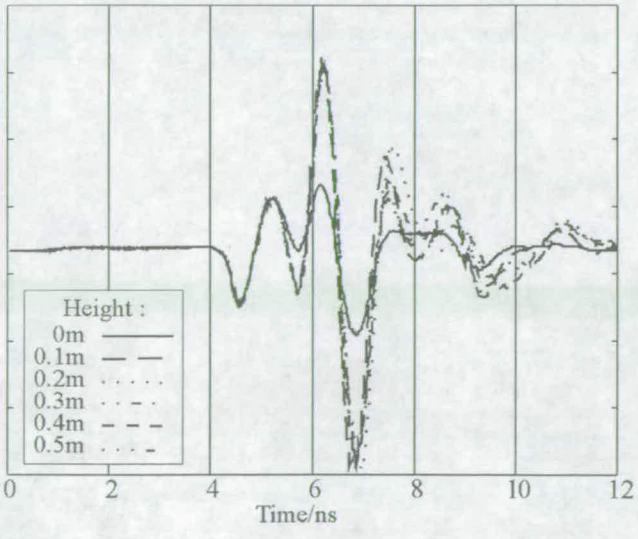

Figure 10: Effect of lifting slab off the gravel sub-base

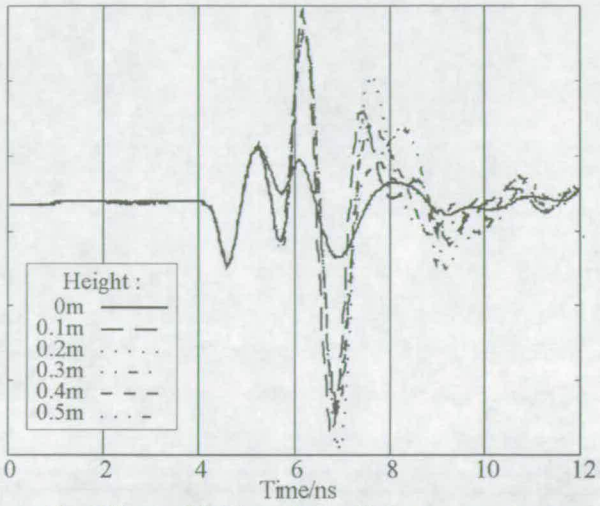

Figure 11: Effect of lifting slab off the concrete sand sub-base

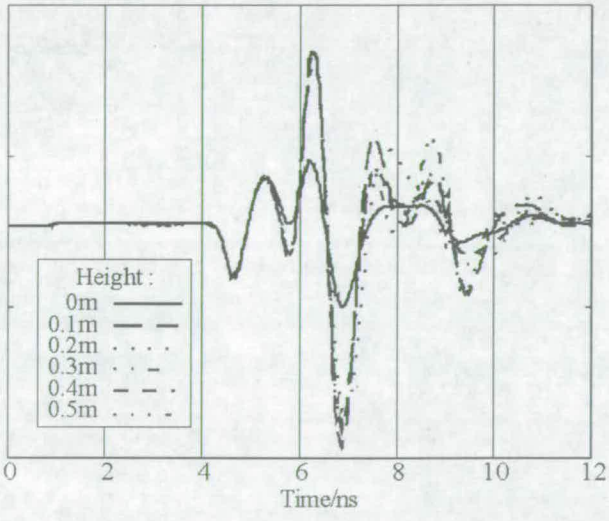

Figure 12: Effect of lifting slab off the silica sand sub-base

This can be seen more clearly on figure 13, which shows the response of the slab in contact with the "concrete" sand sub-base, the response of the slab in contact with the sub-base (zero height) is subtracted off all the other responses, with the lines separated to increase the clarity. The bottom of the pavement slab is shown in the figure. The 0.4/0.3m reposes lines, shown in the upper diagram, are exactly the same up to 0.3m. However the 0.4m line represents the pavement block being lifted a further 0.1m, therefore the lines will separate at the 0.3m marking. This same observation is found when looking at the 0.1/0.2m response lines, shown in the lower diagram.

It is clear that the initial received pulse is very repeatable and the procedure adopted allows for the slab surface and base responses to be identified individually. It is difficult to distinguish the responses from the increasing gap between the slab base and the sub-base material, although the deviations from the zero height response do appear to be the same up to approximately 0.7ns as expected. It is possible that averaging together of many scans would reduce the noise levels sufficiently for these to be identified with more accuracy.

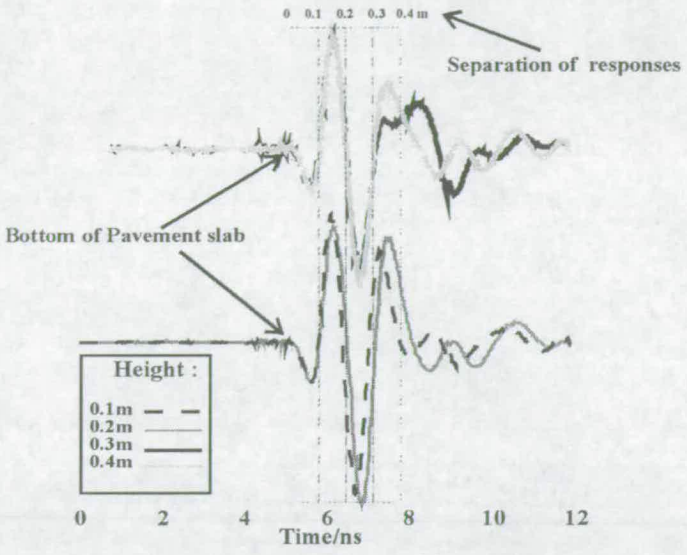

Figure 13: Shows the separation of the responses when the concrete sand sub-base is tested

When this technique was tried to remove the initial pulse from the scan on the actual road it did not meet with any success. This is thought to be due to the fact that the slab had dried between its existence in the field and testing in the laboratory. The effect of moisture in pavement materials has a great effect on their testing with GPR due to the high permittivity of water.

IMPACT ECHO APPLIED TO THIN PAVEMENTS

Impact echo is an acoustic, nondestructive method used to evaluate the conditions of a wide range of structures. It is used to detect structural damage like delaminations, voids and cracks within many different types of materials.

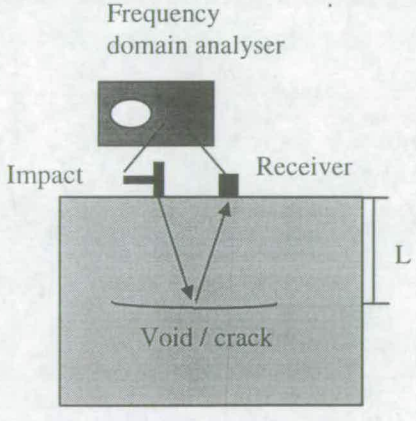

Figure 14: Impact echo test method

When a piece of material like a pavement is tapped with a hammer or impactor, a compressive wave is produced which propagates through the medium (figure 14). Reflections of these waves will occur at the bottom of the material or at a crack within the material, i.e. where there is a sudden change in acoustic properties. When the reflected wave reaches the surface it will experience a major acoustic change due to the air/pavement medium thus the wave will reflect back into the material. This will occur several times until all the energy has been dissipated. These oscillations will produce displacements at the top of the surface which will be detected by a receiver (accelerometer) several centimetres away from the impact point. A major

advantage of this non-destructive test method is that only one surface needs to be accessible for the hammer impact and receiver attachment.

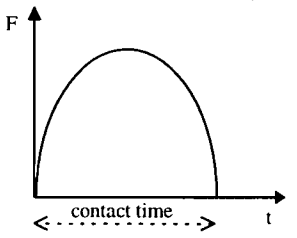

Figure 15: Force-time graph showing the contact time of the impact

The impact on the surface of the material is approximated to a half sine wave as shown on the force vs. time diagram in figure 15. The duration of this wave is known as the *contact time*. Reducing this time means that smaller defects can be detected, however the energy and therefore the penetration capability of the wave are reduced. Therefore the selection of the impact source is very important when carrying out Impact- echo testing.

When the stress wave encounters an interface at depth L it is reflected and gives rise to surface excitation at frequency:

$$f = \frac{V_P}{2L} \qquad (6)$$

where V_p is the velocity of the wave.

The travel path is the thickness of the material or the distance to the anomaly, as shown in figure 14.

SONIC TESTING OF THIN ASPHALT PAVEMENTS

The compressive velocity of the pavement block was found by using two ultrasonic transducers and a Pundit ultrasonic non-destructive digital indicating tester, produced by C.N.S Instruments Ltd.

The transmitter was placed on one end of the pavement block and the receiver on the other end (figure 16). This setup enabled the transmit time through the pavement slab to be accurately measured. Knowing the distance the pulses travel in the material will enable the velocity to be determined from the equation below:

$$\text{Pulse velocity} = \frac{\text{Path length}}{\text{Transmit time}} \qquad (7)$$

It is stated in the Pundit manual (Pundit Manual) that the transmit time and path length should be measured to an accuracy of about (+/-)1%.

The following results where obtained when measuring the velocity through the two layers of the pavement block.

Fine Layer
Transmit time =99μs,
Path length = 0.28m,
∴velocity = 2828m/s,

Course layer
Transmit time = 97μs,
Path length = 0.28m
∴velocity=2887m/s

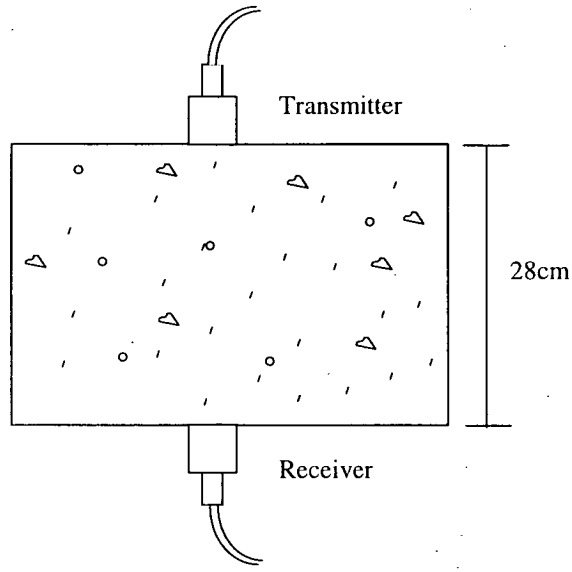

Figure 16: Direct transmission setup used to propagate ultrasonic pulses through the pavement block

Theoretical values of frequency

when L=0.1m (Block is flat)
f =14kHz

when L=0.28m (Block is on its side)
f =5kHz

The slab was then placed flat on the work bench and a NBS conical reference transducer, produced by the National Institute of Standards and Technology (N.I.S.T.), was used to receive the reflected waves. The transducer, which was connected to a frequency analyser, was placed on the surface of the pavement slab. The N.I.S.T. transducer has a larger frequency range, 0 to 1Mhz, and good coupling with the surface. A PCB type 086 C80 hammer was used to apply impacts to the surface of the slab.

The impact point was initially 2cm away from the receiving transducer. This distance was increased in steps of 2cm up to and including 6cm. A total of five different impacts were recorded by the frequency analyser so that the background noise could be reduced when the responses were averaged.

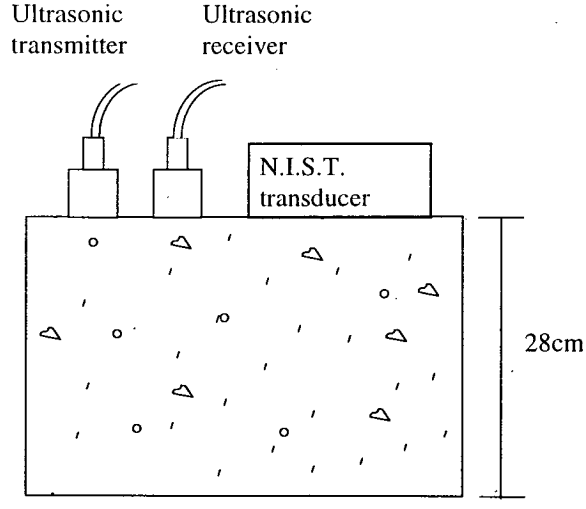

Figure 17: Setup used to analyse the pavement block using the ultrasonic transducers

The next part of the experiment was to use two sets of ultrasonic transducers (U.Ts.), a 54kHz and 82kHz, in place of the PCB hammer (figure 17). One of the transducers was connected to the Pundit the other one was connected to the frequency analyser. The main problem with the U.Ts. was that the actual input waveform was not known. Even though one of them was connected to the analyser, its waveform was not the correct input wave as it had travelled through the pavement prior to being recorded. In order to overcome this obstacle a 26μs reference bar, with an accelerometer at one end and one of the U.Ts. at the other end, was used. The response through the bar was recorded and from this it was possible to find the input waveform as the force is proportional to the displacement. The input response for the 54kHz and 82kHz transducers were calculated. The U.Ts. were positioned at different distances from the N.I.S.T. transducer and measurements were taken. The position of the ultrasonic transmitter and receiver were reversed and the experiment was repeated. The transmitter was initially 7cm from the N.I.S.T. and moved to the positions of 9 and 11cm away. A total of ten responses were recorded and the average of the absolute value of the Fourier transform was found.

These experiments with the PCB hammer and the U.Ts. were repeated with the slab on its edge. The D.B.M layer was analysed when the block was on its side.

ANALYSIS OF IMPACT ECHO RESPONSES

The frequency range of interest, calculated from the velocity, were found earlier to be 5-14kHz. With the PCB hammer it was found that the input frequency range was too small, this can be seen in figure 18. The pavement response when using the 82kHz transducer is shown on figure 19. Whilst it is not clear on initial inspection of these figures comparison with the responses from the 54kHz transducer reveal that the 82kHz transducer gave less energy in the important frequency range.

Calculating the transfer function between the input and output of the 54kHz responses produced good correlation with the theoretical values. Figure 20 & 21 show the responses when the 54kHz transducer is used. It was noted that when the side of the pavement block was being analysed the N.I.S.T. transducer picked up a lot of high frequency responses between 3 and 5cm, however, as you get further away the high frequency responses disappear. The reason for this is due to the transmitter being so close to the N.I.S.T. transducer and the surface area is very small so the surface vibrations will be concentrated in a small area thus causing the receiver to respond to the input 54kHz pulse directly. This effect did not occur when the pavement block was flat due to the larger surface area being analysed so dissipating the vibrations.

The 82kHz responses show that a frequency of 7.5kHz is being continually picked up as the highest frequency. This frequency is also evident to a lesser extent when the 54kHz transducer is used. It can be concluded that this is either a spurious resonance of the measurement system, or a resonance of the specimen that is not connected with the thickness that was being examined. In the field, such resonances would not occur and it is therefore not considered important here.

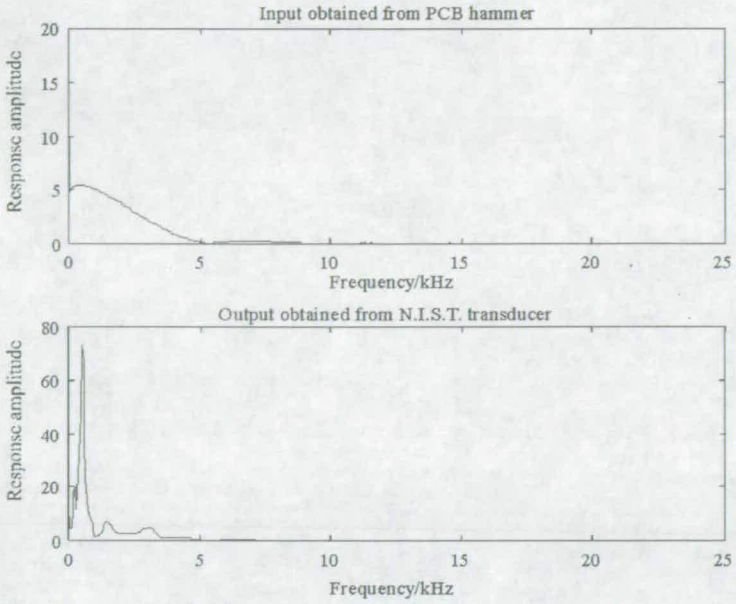

Figure 18: Response obtained from N.I.S.T. transducer when using the PCB hammer

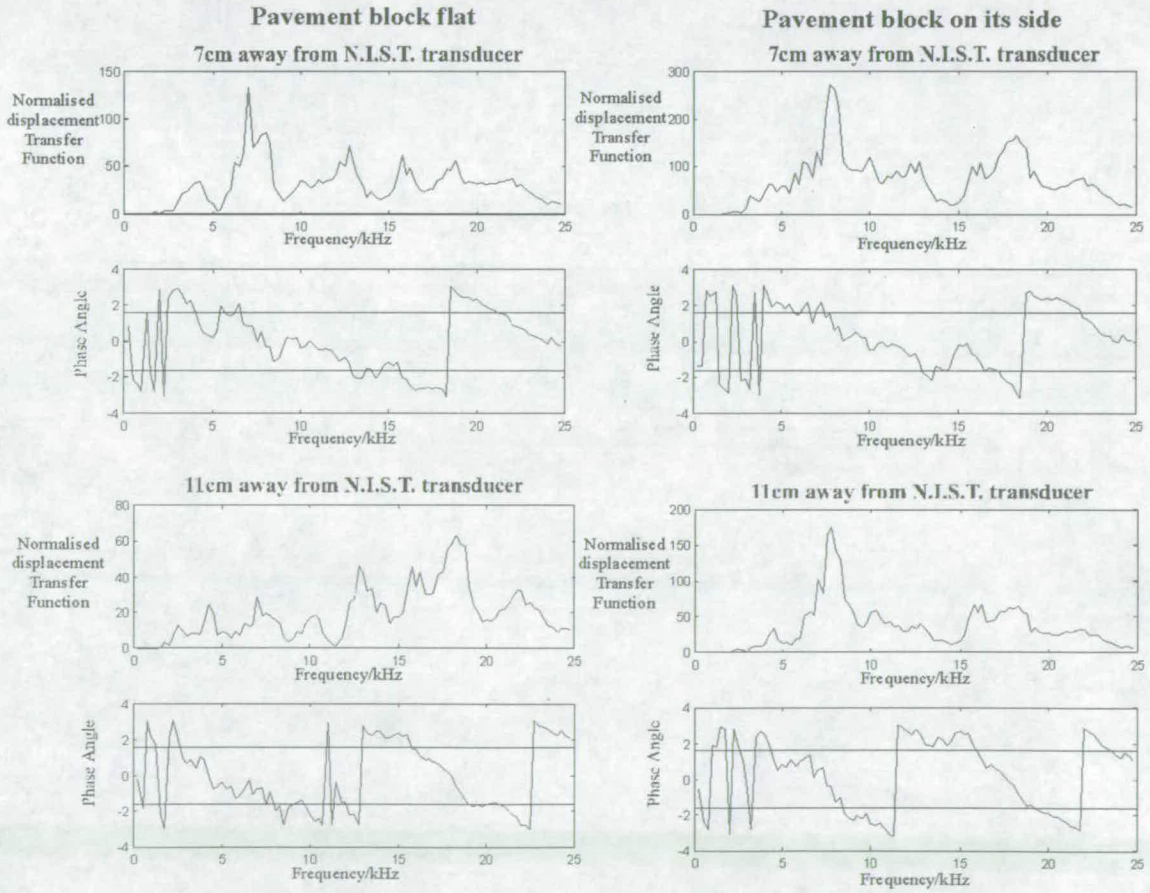

Figure 19: Responses obtained when using the 82kHz transducer

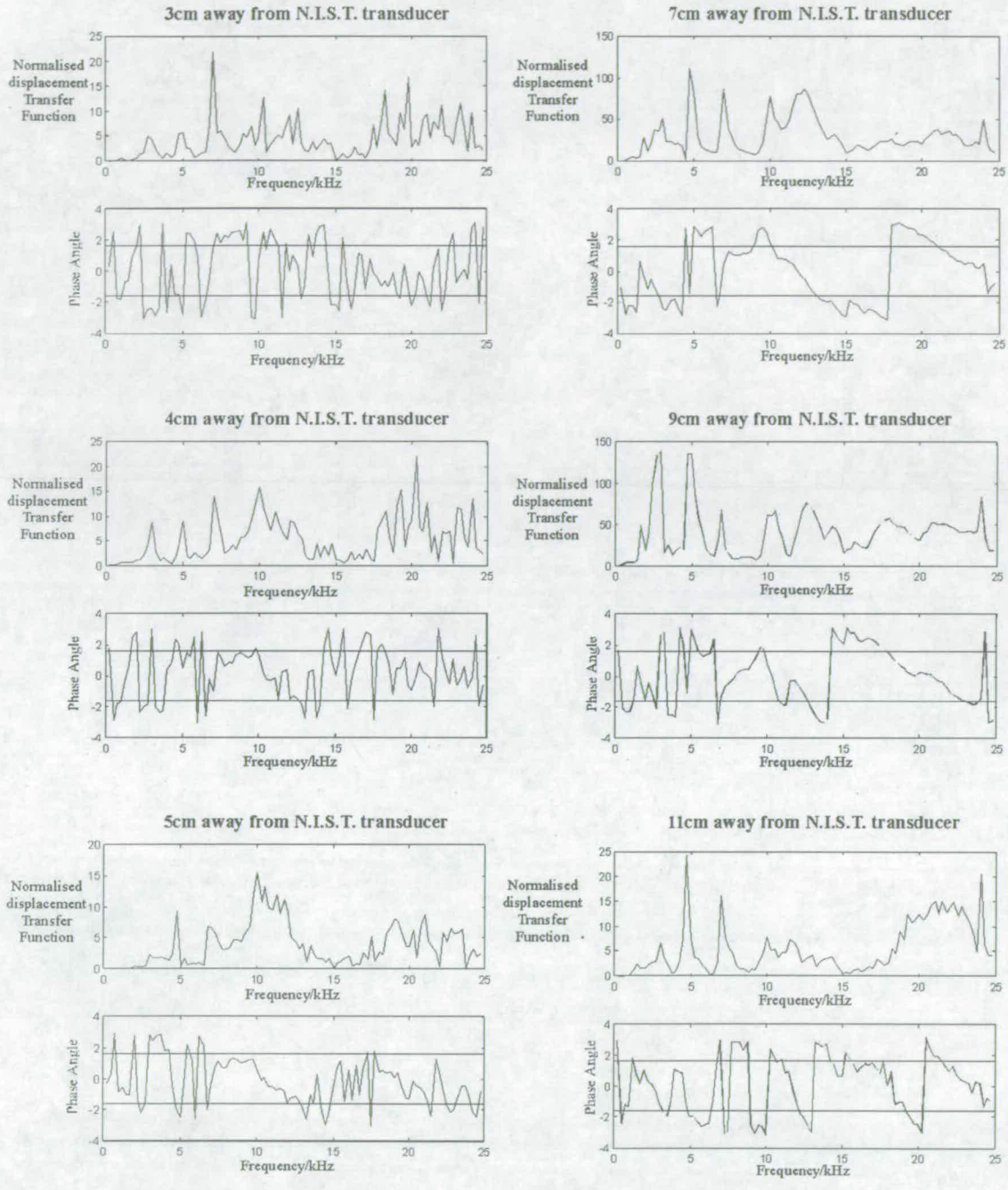

Figure 20: Responses obtained from 54kHz transducer when the pavement block is flat

Theoretical value of the frequency = 5kHz(side)

Theoretical value of the frequency = 14kHz (flat)

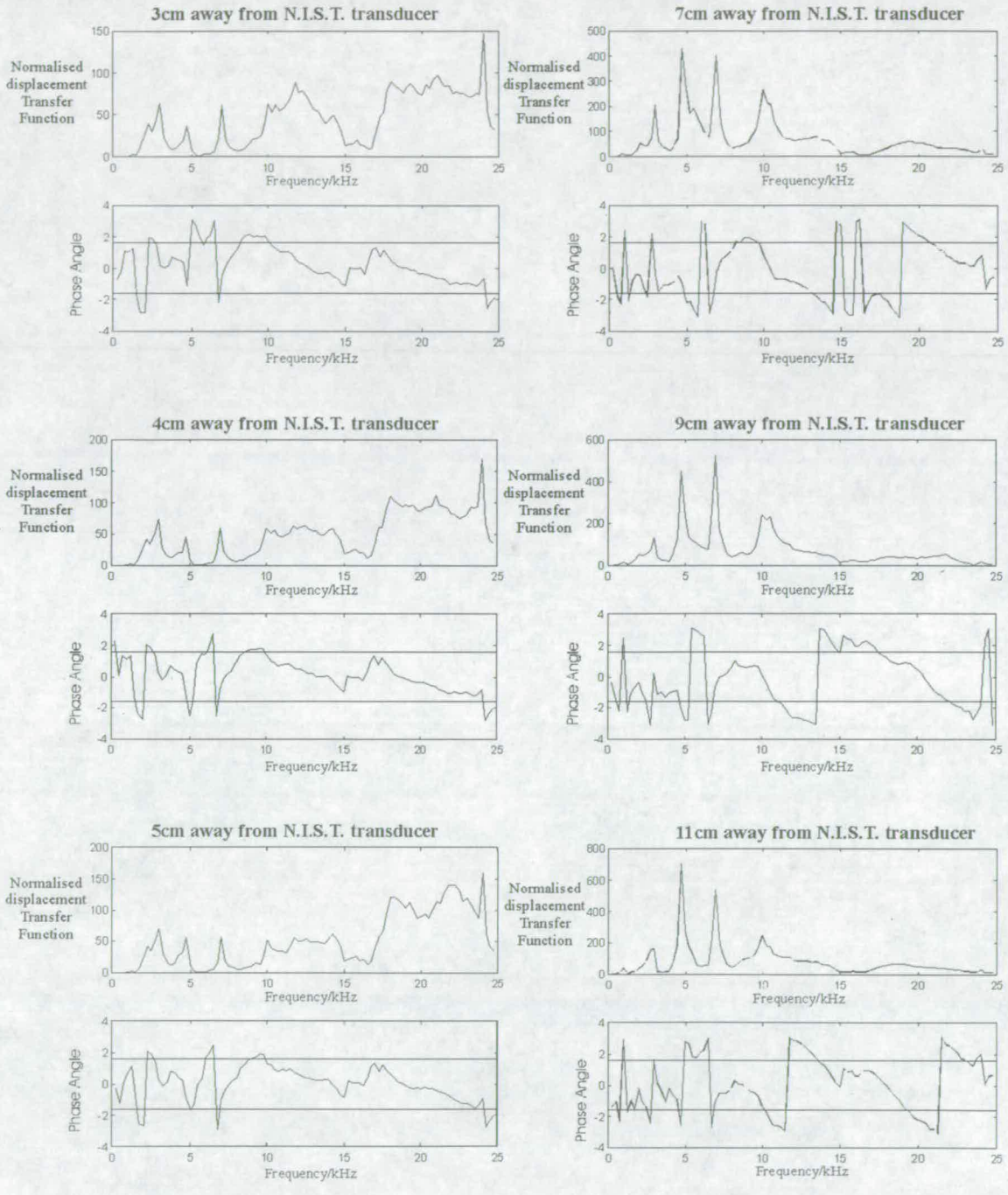

Figure 21: Responses obtained from 54kHz transducer when the pavement block is side

Theoretical value of the frequency = 5kHz (side)

Theoretical value of the frequency = 14kHz (flat)

CONCLUSION

The range of techniques available to highway engineers for the assessment of pavement condition are many and varied. The simultaneous analysis of the information from different systems would greatly enhance the reliability of the interpretation, and even extend interpretation into areas not yet envisaged.

The developments of new radar hardware such as stepped-frequency radar, improved horn and array antennas, signal processing techniques such as synthetic aperture radar, the accurate three-dimensional simulation of these techniques for improved understanding and training of neural networks, and the techniques of data fusion to bring together many sources of information in a rational and quantifiable way seem to spell an exciting and rapidly developing improvement in the use of GPR in many fields, including highway pavement assessment.

The GPR responses of thin pavements can be impossible to interpret directly due to confusion of initial pulses reflections from the bottom of the thin layers (whether the bottom of the bituminous layers of the pavement or interfaces between different bituminous materials).

The effect of the material beneath the thin layer (and hence the thickness of the layer itself) has no effect on the initial response from the surface and this can therefore be eliminated as shown to reveal the response from the bottom of the layer.

When applying sonics to the pavement slab some interesting results were found. The PCB hammer's input frequency range was too small. A good correlation with the theoretical values was found when using the 54kHz transducer. In comparison the 82kHz transducer gave less energy in the important frequency range. Some of the responses could be explained by the setup of the equipment.

The sonic technique requires a lot of analysis of the actual material which the waves are propagating through. In the field this method has a lot of obstacles which must be overcome before it can be successfully applied.

ACKNOWLEDGEMENT

The authors would like to thank Kevin Broughton for his assistance in the experimental part of this project.

REFERENCES

"Use and limitations of ground-penetrating radar for pavement assessment," in *Design Manual for Roads and Bridges*, vol. 7 of Pavement Design and Maintenance, HA 72/94, HMSO

Daniels, D.J. *Surface-penetrating radar*. London: Institution of Electrical Engineers, 1996.

Daniels, D.J. "Surface-penetrating radar," *Electronics & Communication Engineering Journal*, pp. 165-182, 1996

Davidson, N.C., and Forde, M.C. "A laboratory appraisal of ground-penetrating radar over water," *Nondestructive Testing and Evaluation*, vol. 12, pp. 219-242, 1996.

Edwards, I., Gros, X.E., Lowden, D.W,, and Strachan, P. "Fusion of NDT data," *British Journal of NDT*, vol. 35, pp. 710-713, 1993.

Gros, X.E., Strachan, P., Lowden, D., and Edwards, I. "NDT data fusion," presented at 6th European Conference on NDT, Nice, France, 1994.

Gros, X.E., Strachan, P., and Lowden, D. "Theory and Implementation of NDT Data Fusion," *Research in Nondestructive Evaluation*, vol. 6, pp. 227-236, 1995.

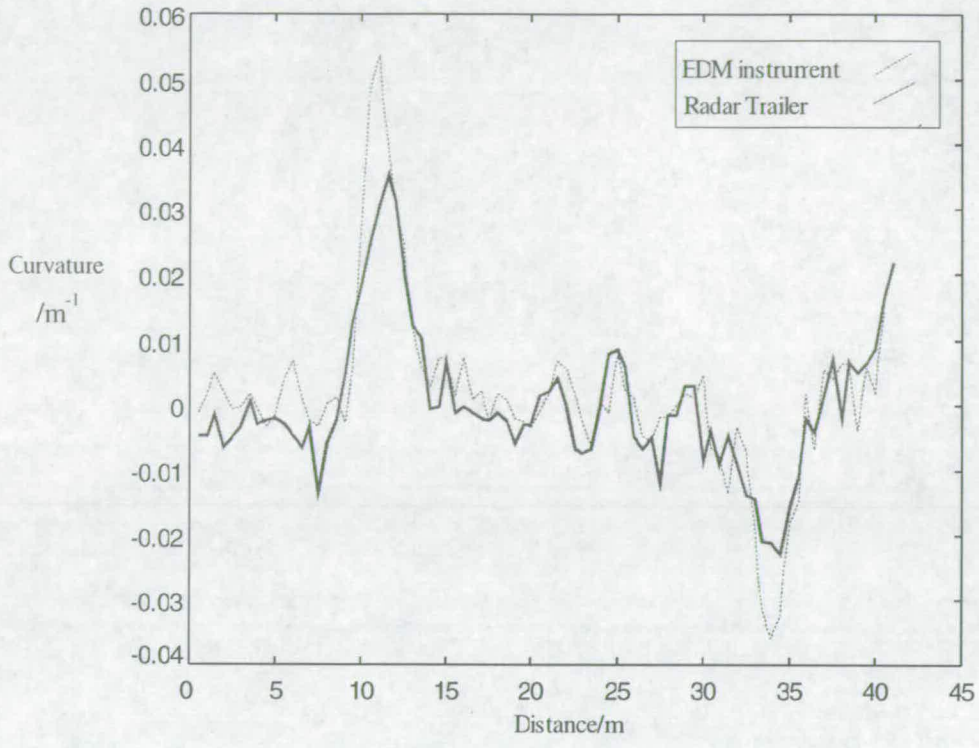

Figure 9: Comparing the EDM and radar trailer curvature values

It was felt that this road was not very representative of a motorway, however, it did highlight a shortcoming of the equipment.

CONCLUSIONS

A method for comparing the longitudinal profiling of the surface and subsurface layers on pavements by using GPR was proposed. Several specifications had to be met in order to achieve these aims.

- Three radar antennas were to be used to detect the surface profile, with a fourth one detecting the sub-surface layers on pavements.
- Wavelengths of interest are between 1m to 16m

Three sets of experiments were carried out:

- Determine how effectively GPR can detect layers within the pavement
- Determine Optimum height range of radar from pavement surface
- Determine the spacing of the antennas.

The optimum height was found to be between 25 and 30cm. A spacing value of 0.5m was calculated to map small wavelengths and 3m for long wavelengths. However, due to the position of the axle and limits on the maximum size that a trailer can be, spacing of 1.5m and 3m were used to map the long wavelengths.

Gros, X.E., Strachan, P., and Lowden, D. "A bayesian approach to NDT data fusion," *INSIGHT*, vol. 37, pp. 363-367, 1995.

Gros, X.E. *NDT data fusion*, First ed: Arnold, 1997.

Johansson, E.M., and Mast J.E. "Three-dimensional ground penetrating radar imaging using synthetic aperture time-domain focusing," presented at SPIE-The International Society for Optical Engineering, Advanced Microwave and Millimeter-Wave Detectors, 1994.

Langman, A., and Inggs, M.R. "Improving the resolution of a stepped frequency CW ground penetrating radar," presented at SPIE-The International Society for Optical Engineering, Advanced Microwave and Millimeter-Wave Detectors, San Diego, CA, USA, 1994.

Maser, K.R. "Condition assessment of transportation infrastructure using ground-penetrating radar," *Journal of Infrastructure Systems*, vol. 2, pp. 94-101, 1996.

Mast J.E., and Johansson, E.M. "Three-dimensional ground penetrating radar imaging using multi-frequency diffraction tomography," presented at SPIE-The International Society for Optical Engineering, Advanced Microwave and Millimeter-Wave Detectors, 1994.

Nelson, S.D. "Electromagnetic modelling for ground-penetrating imaging radar (GPIR) using 3-D finite difference time-domain (FDTD) modeling codes," presented at SPIE-The International Society for Optical Engineering, Advanced Microwave and Millimeter-Wave Detectors, San Diego, CA, USA, 1994.

Sack, D.A., Olson, L.D., "Impact echo scanning of concrete slabs and pipes," presented at CANMET/ACI International Conference in Concrete Technology, Caesars Palace Hotel, Las Vagas, Nevada, 1995

Sellmann, P.V., Delaney, A.J., and Arcone, S.A. "Observations of radar performance for bottom and sub-bottom information in fresh water," presented at Second Government Workshop on GPR, Advanced Ground-Penetrating Radar: Technologies and Applications, Ohio State University, 1993.

Warhus, J.P., Scott, D.N., Jeffrey, E.M., and Johansson, E.M. "Advanced ground-penetrating, imaging radar for bridge inspection," . Livermore, California: Engineering Research, Development and Technology, Lawrence Livermore National Laboratory, 1993.

Warhus, J.P., Mast, J.E., Johansson, E.M., and Nelson, S.D. "Advanced ground-penetrating radar," presented at SPIE-The International Society for Optical Engineering, Advanced Microwave and Millimeter-Wave Detectors, San Diego, CA, USA, 1994.

Weedon, W.H., Chew, W.C., and Ruwe, C.A. "Step-frequency radar imaging for NDE and GPR applications," presented at SPIE-The International Society for Optical Engineering, Advanced Microwave and Millimeter-Wave Detectors, San Diego, CA, USA, 1994.

AUTHOR BIOGRAPHIES

Michael O. Gordon is currently studing for a PhD in Advanced NDT of flexible pavements at the University of Edinburgh. Mr Gordon did his undergraduate studies at the University of Edinburgh.

Dr Mike Hardy is currently a lecture in Civil & Environmental Engineering at the University of Edinburgh. Dr Hardy did his undergraduate and Postgraduate studies at Cambridge University.

LONGITUDINAL SURFACE PROFILING OF HIGHWAY PAVEMENTS USING GPR

M.O. Gordon,
Postgraduate Student,
University of Edinburgh,
Crew Building, King's Buildings,
Edinburgh EH9 3JN,
Scotland.

Dr M.S.A. Hardy,
Lecturer,
University of Edinburgh,
Crew Building, King's Buildings,
Edinburgh EH9 3JN,
Scotland.

KEYWORDS: GPR, Pavements, NDT

ABSTRACT

Ground Penetrating Radar (GPR) has been used to detect moisture, air voids, delaminations and layer thicknesses for pavement evaluations. If used correctly, it can provide accurate information on the condition of a road which can result in major savings in road maintenance.

The longitudinal profile of a pavement is an important measurement which provides information on the ride quality for vehicles and it has also been correlated with structural conditions. There are several techniques available for carrying out this measurement, varying from high-speed vehicle-based profilers, using ultrasonic, laser or optical measuring systems, to a hand-held dipstick. The aim of this project was to use GPR to measure the longitudinal profile of the surface and subsurface layers on pavements. A trailer was designed and built to carry four GPR antennas; three to calculate the surface profile with the fourth to examine the sublayers of the road. Some preliminary tests have been carried out on the surface profile measurements showing some good comparisons to the actual profile.

INTRODUCTION

There are currently over 16 million kilometres of roads in the world of which 365,000 kilometres make up the UK road network. With such a large amount of roads it is important to have a good maintenance programme. Non-destructive investigations of the pavement can play an important role in maintenance. Some of these types of investigations include Falling Weight Deflectometer (FWD), Benkelman beam, video and visual inspection of the road, Rolling Straight Edge (RSE), wave propagation and Ground Penetrating Radar (GPR). The study carried out in this project focused on the use of GPR to inspect the pavement.

GPR has been used to detect layers within the pavement, however, its use in detecting the actual longitudinal surface profile and comparing this to the profile of layers within the pavement has not been documented. The surface profile is usually monitored using a laser profilometer. The aim of this project is to design a trailer to carry out longitudinal profiling of the surface and subsurface layers on pavements by using GPR, which is not possible with laser technology.

INITIAL EXPERIMENTS

Ground Penetrating Radar (GPR) is a non-destructive technique for investigating objects hidden by optically opaque barriers. It detects changes in the electro-magnetic properties of materials, principally the permittivity, and is capable of producing cross-sectional representations of what is beneath surfaces. The use of GPR to detect layer thicknesses has been well documented (Gordon & Hardy, 1998), however, there appears to be no literature on its use in detecting the longitudinal profile of a road.

There are several techniques available for measuring longitudinal profiles, the most sophisticated use lasers. Laser profilers are usually mounted onto the vehicle then measurements of the actual profile of the

roadway in each wheel path are recorded. The profile of the road is obtained by analysing the data supplied by the lasers using a computer inside the vehicle. The measurement of the profile of the pavement gives the highway engineer an idea of how even or uneven the road is. Patterson (Patterson, 1986) found that the unevenness of a pavement was due to four main factors:

- traffic loading
- surface distress
- structural conditions
- climate conditions

The majority of the unevenness found in the UK is due to traffic loads, especially the heavy good vehicles (HGV).

The radar trailer had to meet the following specifications:

- Three radar antennas were used to detect the surface profile, with a fourth one detecting the sub-surface layers on pavements.

- Profile wavelengths of interest are approximately between 1m and 16m, which are calculated as follows:

Vehicle speed = v ;Vehicle bounce frequency = f

Lowest frequency of HGV: $f \approx 2Hz$	*Highest frequency* of HGV: $f \approx 15Hz$
Fastest speed of 70mph = 31.1m/s	Lowest speed of 35mph = 15.6m/s
Longest wavelength $\lambda = 31.1/2 \approx$ **16m**	Smallest wavelength $\lambda = 15.6/15 \approx$ **1m**

Several initial experiments were carried out on pavements GPR:

- Determine how effectively GPR can detect layers within the pavement.

- Determine Optimum height range of radar from pavement surface.

- Determine the spacing of the antennas for optimal measurements of surface profile.

Determination of layer thicknesses

The first experiment was designed to determine how easily the thickness of layers within the pavement could be detected using GPR (Gordon & Hardy, 1998). A GSSI Sir10a was used to carry out the radar analysis. The results from these tests showed that some difficulties are encountered when interpreting the recorded signals. The received signal is made up of several different pulses which must be taken into consideration when interpreting the results. The different signals are:

- the reflected pulse from the surface of the pavement
- the direct transmission from the transmitter to the receiver
- the reflected pulses from the layers within the pavement layer

The higher the central frequency of the antenna the higher the resolution, thus resulting in thinner pavement layers being identified. However, the down side of this was the reduction of the depth of penetration.

Optimum height of radar from pavement surface

The next experiment was designed to determine the optimum height an antenna could be suspended from the pavement in order to receive a clear reflection signal. Figure 1 shows the experimental apparatus used to find this optimum height. A GSSI 900MHz antenna was used to pick up the reflection signals from the pavement surface.

The results on figure 2 show that the two-way travel times in this experiment are less than the theoretical values. The reason for this is that a time constant is added onto the reflection signal to compensate for the time loss caused by the signal traveling through the cables. However, this added value has

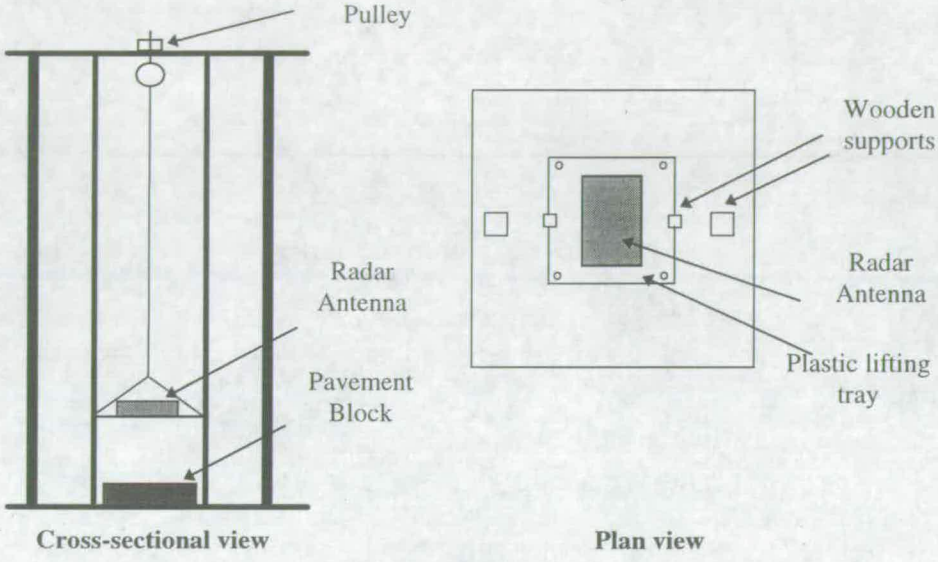

Figure 1: Lifting rig used to determine the optimum height

overcompensated for the loss in time, thus causing the travel time to be less.

The experimental values should be greater than the theoretical values. However, as explained by figure 3, the signal is assumed to travel perpendicular to the antenna, resulting in a shorter travel path. However, in reality the signal travels from within the box making the travel path longer, resulting in a larger two-way travel time compared to the theoretical value. This will result in an offset between the theoretical and experimental values.

The result from this experiment showed that a clear reflection from the surface of the pavement sample could be obtained when the radar antenna was at a height of between 13cm and 38cm. A height between 25 and 30cm gave the best result. Below 13cm, the reflected signal was mixed up with the transmit pulse and the reflected pulse from the layers within the pavement block. Above 38cm, the reflected pulse has a small amplitude, making it difficult to identify. This information was used in the design of a truss which would hold three 900 MHz antennas over the wheel path, on the near side of the road.

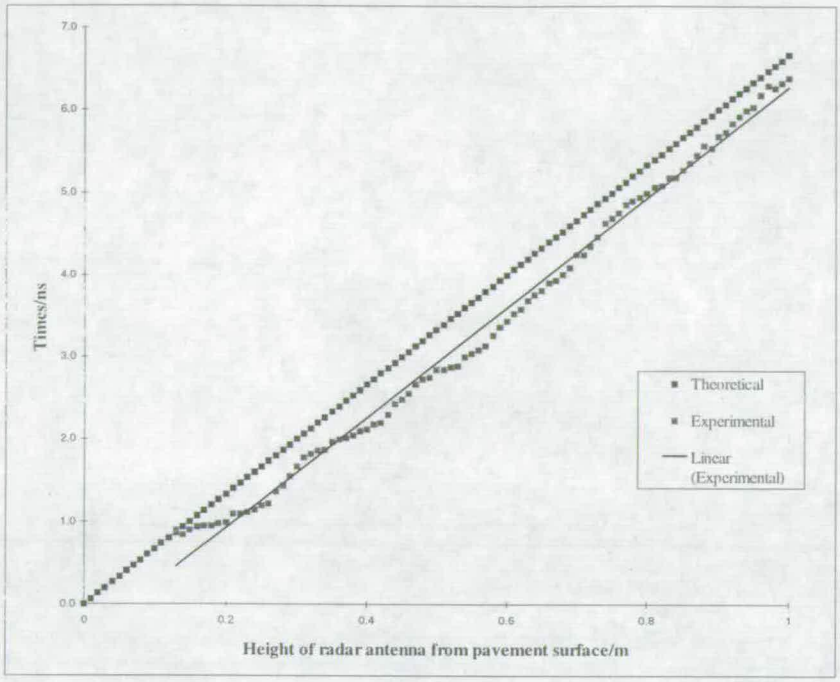

Figure 2: A graph showing the two-way travel time obtained from a 900MHz antenna

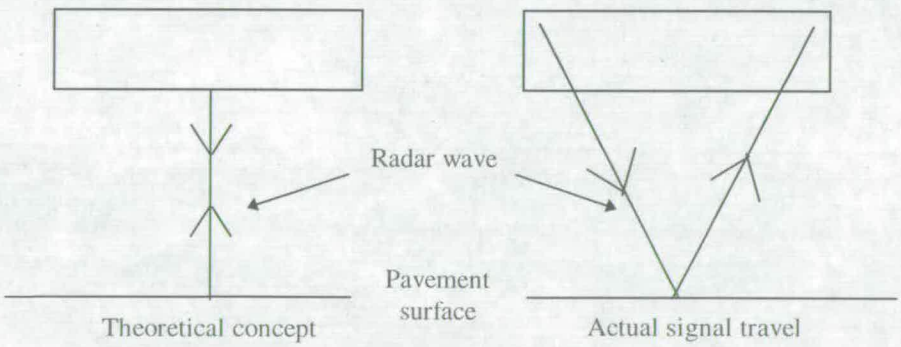

Figure 3: Theoretical and actual path of radar wave from an antenna

Calculating the spacing between each antenna

The height of the antennas from the pavement surface was used to calculate the curvature along the road, as shown below.

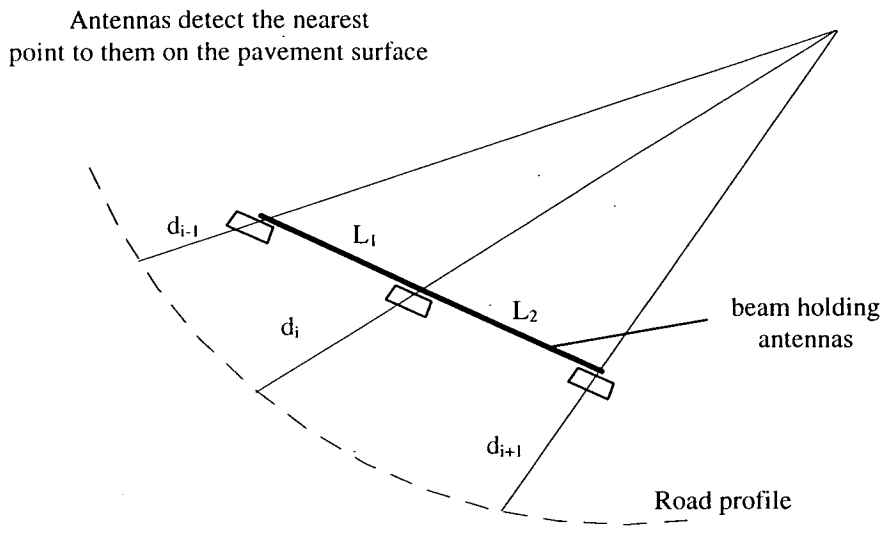

Figure 4: Radius of curvature calculation

From figure 4:

Radius of curvature: $$R = \frac{1}{2}\left(\frac{L_1 L_2 (L_1 + L_2) + d_i{}^2 L_1 + d_i{}^2 L_2 - d_{i+1}{}^2 L_1 - d_{i-1}{}^2 L_2}{d_i L_1 + d_i L_2 - d_{i-1} L_2 - d_{i+1} L_1} \right) \quad (1)$$

$$\therefore \kappa = \frac{d\phi}{ds} = \frac{1}{R_i} = \frac{d^2 y}{dx^2}\bigg|_i$$

$$\phi = \int \frac{1}{R_i} ds + \text{constant}$$

However,

$$\tan \phi_i = \frac{dy}{dx}$$

$$y = \int \tan \phi \, dx$$

The arc length:

$$\text{ds} = \sqrt{1 + \tan^2 \phi} \; dx$$

$$\frac{ds}{dx} = \sqrt{1 + \tan^2 \phi}$$

$$x = \int \frac{1}{\sqrt{1 + \tan^2 \phi}} ds + \text{constant}$$

A graph of y against x can be plotted; this is the radar trailers attempt to plot the surface profile of the pavement.

Mapping the profile of a road using the curvature technique described above requires calculations to be carried out to find which antennas spacing values can most accurately map the profile. The spacing must ensure that wavelengths between 1m and 16m can be mapped. The value of L_1 and L_2 must be determined in order to cover this range of wavelengths.

Noise

In order to find the correct spacing values, several simulations were carried out. The first simulation was to vary the noise ratio on a sine wave and to calculate the curvature for each signal using two methods.

Analytical method

A noise ratio varying from 0 to 1 is applied to the sine wave

$y = \sin(\gamma x) + \text{random noise}$

where: λ = wavenumber (cycles / m)

$$\frac{dy}{dx} = \lambda \cos \lambda x$$

$$\frac{d^2y}{dx^2} = -\lambda^2 \sin \lambda x$$

$$\therefore \text{(From equation 1) } k_1 = \frac{-\lambda^2 \sin \lambda x}{\left[1 + \lambda^2 \cos^2 \lambda x\right]^{\frac{3}{2}}}$$

Computer approximation method

The curvature can also be worked out using the definitions of the first and second derivatives.

s = spacing intervals along the road

$$\frac{dy}{dx} = \frac{y_{i+1} - y_{i-1}}{2s}$$

$$\frac{d^2y}{dx^2} = \frac{\frac{y_{i+1} - y_i}{s} - \frac{y_i - y_{i-1}}{s}}{s}$$

$$\therefore \frac{d^2y}{dx^2} = \frac{y_{i+1} - 2y_i + y_{i-1}}{s^2}$$

$$\text{(From equation 1) } k_2 = \frac{\frac{y_{i+1} - 2y_i + y_{i-1}}{s^2}}{\left[1 + \left(\frac{y_{i+1} - y_{i-1}}{2s}\right)\right]^{\frac{3}{2}}}$$

The percentage error between k_1 and k_2 is calculated using the equation below:

$$\% \text{ error} = \frac{\int (k_1 - k_2)^2}{\int k_1^{\,2}} \times 100 \qquad (2)$$

Figure 5 shows how the percentage error between k_1 and k_2 is effected as the value of s/λ (antenna spacing/wavelength) is increased for different noise ratios. The spacing of the antennas can be found by choosing the minimum value on one of the noise ratio lines on figure 5. The correct line was chosen by calculating the noise ratio for 1 and 16m wavelengths on a simulated "good" road.

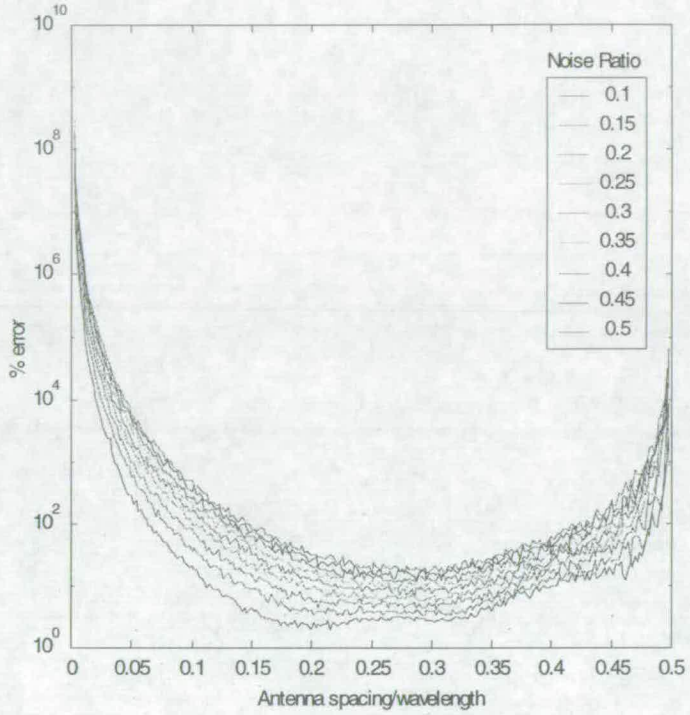

Figure 5: A graph showing how the percentage error varies with increased antenna spacing/wavelength for different noise ratios

A simulated "good" road

The simulation of a one-dimensional random "good" road profile was generated from a series of coefficients derived from spectral density values, (Dodds and Robson, 1977). A set of random phase angles, uniformly distributed between 0 and 2π was applied to the coefficients of the spectral density. In order to obtain the equally spaced spot heights, z_r, along the profile, the inverse discrete Fourier transform of the spectral coefficients must be worked out (Newland, 1993).

$$z_r = \sum_{k=0}^{N-1} \sqrt{s_k} e^{i\left[\theta_k + \frac{2\pi kr}{N}\right]} \quad r = 0,1,2,\ldots,(N-1) \tag{3}$$

where $s_k = \dfrac{2\pi}{N\Delta} S(\gamma_k)$

N = Number of samples

$S(\gamma_k)$ = Desired spectral density

$\gamma_k = \dfrac{k}{N\Delta}$ = the spatial spectral frequency (wavenumber / cycles / m)

Δ = the distance interval between successive ordinates along the surface profile

θ_k = a set of independent random phase angles uniformly distributed between 0 and 2π

$$S(\gamma_k) = S(\gamma_0)\left|\frac{\gamma}{\gamma_0}\right|^{-n_1} \quad \text{for } |\gamma| \le \gamma_0$$

$$S(\gamma_k) = S(\gamma_0)\left|\frac{\gamma}{\gamma_0}\right|^{-n_2} \quad \text{for } |\gamma| \ge \gamma_0$$

$n_1 = 1.0$ (constant)

$n_2 = 2.0$ (constant)

$S(\gamma_0)$: A constant dependent on roughness category

Dodds and Robson gave different road types a different values of $S(\gamma_0)$, shown in table 1. Type (i) or (ii) are generally motorways, (iii) or (iv) are principal roads and (iv) or (v) are minor roads.

	Road Class	$S(\gamma o)$ x10^{-6} m^3/cycle
(i)	Very good	2-8
(ii)	good	8-32
(iii)	average	32-128
(iv)	poor	128-512
(v)	very good	512-2048

Table 1: Values of $S(\gamma o)$ dependent on roughness category

(note: γ_o is $1/2\pi$ cycles/m)

The amplitude for wavelengths between 1 and 16m along the simulated road were found. The ratio of the accuracy of an antenna to the amplitude was found for different wavelengths.

$$\text{Noise ratio} = \frac{\text{Accuracy of antenna}}{\text{Amplitude at a certain wavelength}} \qquad (4)$$

The spacing value for mapping 16m wavelengths ≈ 3m.

However, the antenna spacing values used in the trailer were 1.5m and 3m, figure 6, due to the position of the axle and limits on the maximum size that a trailer can be by law.

The smallest wavelength that could be physically measured, due to the interference of the cables , was found to be 1.5m.

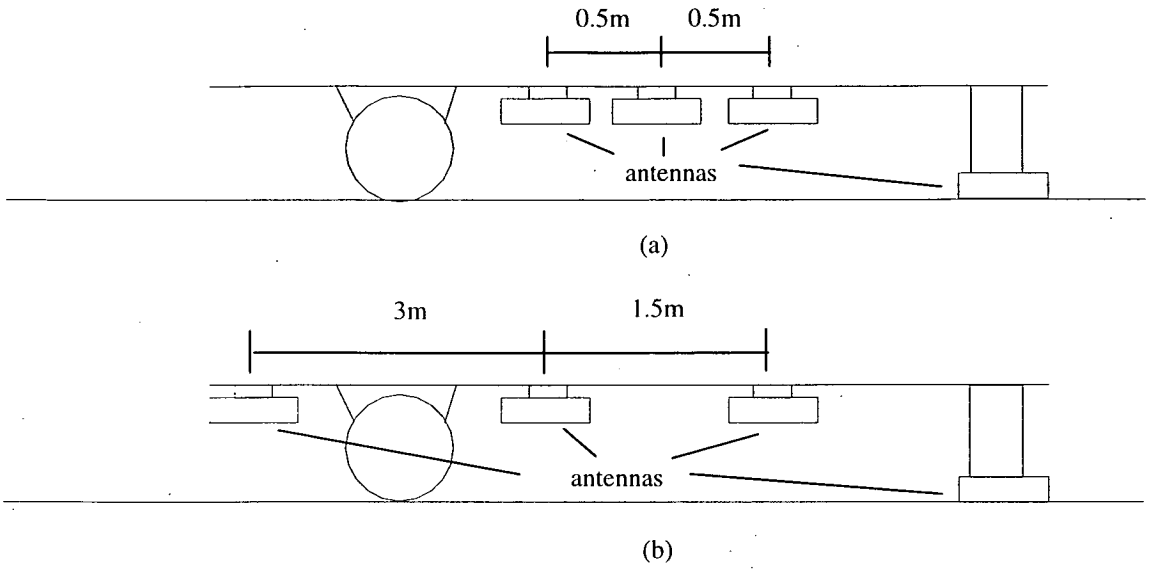

Figure 6: The spacing of the antennas for (a) Short wavelengths (b) Long wavelengths

COMPUTER PROGRAM

The analysis of pavement profiles and thicknesses requires repetitive calculations to be carried out on the radar results. Every scanline, representing a different position along a pavement, would have to be analysed to find out the distance from the pavement to each antenna.

A computer program had to be able to read the output information from four radar antennas, three of them used to produce a profile plot of the surface of the pavement, with the fourth antenna's information used to detect a layer thickness. The surface profile would then be compared to the layer detected within the pavement.

The scanline on figure 7 shows a very clear transmit and reflect pulse, the difference between these is the two-way travel time, which is the time taken for the radar pulse to travel from the antenna to the pavement and back again. The first part of the program had to be able to obtain the two-way travel time from each scanline. The distance traveled is determined from the time it takes the reflected wave to be detected at the receiver. Knowing the velocity of the wave through the relevant media the depth is calculated as:

$$d = v\left(\frac{t}{2}\right) \tag{5}$$

where: d = thickness of layer
v = velocity of electromagnetic wave through the layer
t = time between reflections.

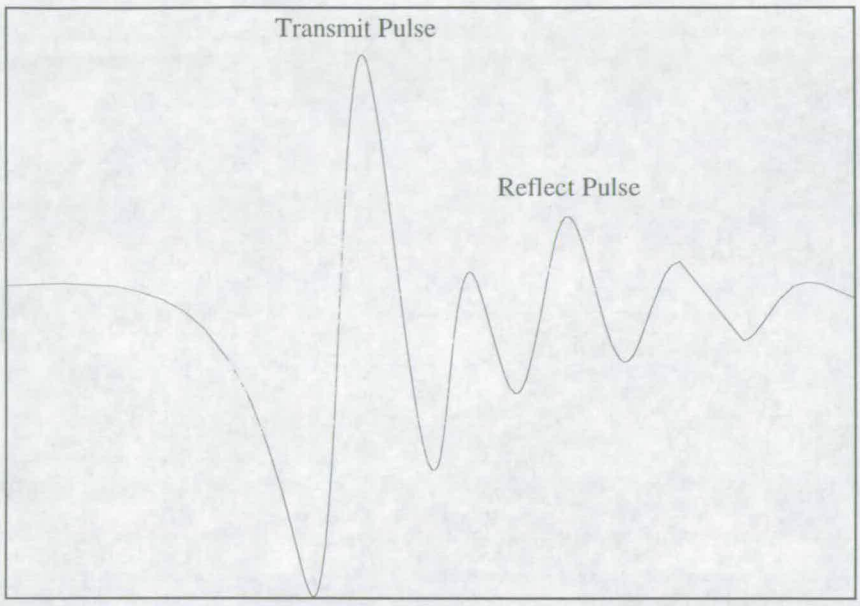

Figure 7: A typical radar scanline

The readings obtained at each metre step along the pavement will be converted into a curvature reading using equation (1), which was discussed earlier.

PRELIMINARY EXPERIMENTS

An experiment was carried out to compare the profile measured using the radar antennas to the actual profile of the road which is determined using an Electromagnetic Distance Wave (EDM). The tested road had an initial gradient of 7 degrees which flattened out to a slope angle of 2 degrees before reverting to 5 degrees. The antenna spacing values for mapping the long wavelengths, i.e. 3m and 1.5m spacing were used in this experiment, the results are shown on figure 8. A graph of the curvature along the road was plotted, shown on figure 9. A good correlation between the radar trailer and the EDM was found, however the antennas had difficulty in mapping large changes in road gradient. This in turn caused the calculated profile plot to be unable to map the profile as accurately. The reason behind this is the same as the reason used to explain the error in figure 2. Calculations to prove this are shown in the appendix.

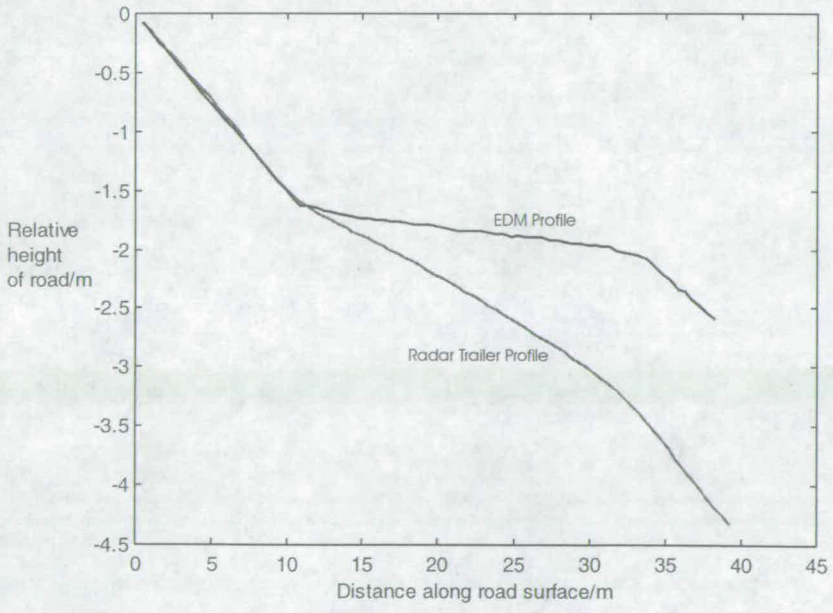

Figure 8: A graph showing the actual road profile and the profile calculated by the radar trailer

A preliminary experiment was carried out on the profile mapping of the pavement surface. The results showed that the antennas operated well except with large changes in the road's gradient. It was, however, felt that this road did not simulate the conditions of a motorway.

REFERENCES

Dodds, C.J., Robson, J.D., "The description of road surface roughness," *Journal of Sound and Vibration*, vol. 31(2), 1973, pp175-183.

Gordon, M.O., Hardy, M.S.A., "The assessment of the value of GPR imaging of flexible pavements," *NDT & E International*, vol. 31, pp. 429-438, 1998.

Newland, D.E., "*An introduction to random vibration, spectral & wavelet analysis*," Third ed, Longman, 1993.

Patterson, W.D.O., "Prediction of road deterioration and maintenance effects. Theory and quantification." Highway Design and Maintenance Study, vol. 3, World Bank, Washington D.C.,1986.

APPENDIX

The calculations below prove why the curvature values using the radar trailer are smaller than the EDM values. (All heights on diagrams are in metres)

Taking the value perpendicular to the radar antennas which is the value the EDM will measure:

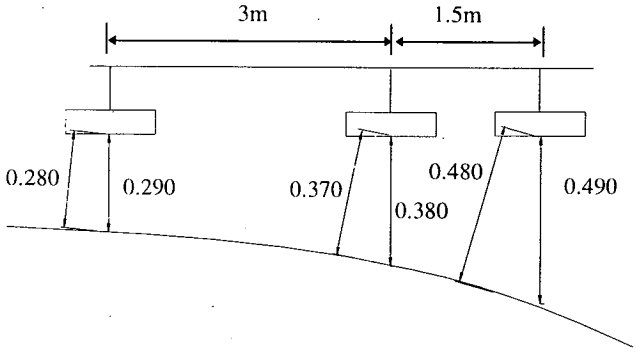

$$\text{Curvature} = \frac{d_i L_1 + d_i L_2 - d_{i-1} L_2 - d_{i+1} L_1}{\frac{1}{2}\left(L_1 L_2 (L_1 + L_2) + d_i^2 L_1 + d_i^2 L_2 - d_{i+1}{}^2 L_1 - d_{i-1}{}^2 L_2\right)}$$

$$= \frac{(3 \times 0.380) + (1.5 \times 0.380) - (1.5 \times 0.290) - (3 \times 0.490)}{\frac{1}{2}\left((3 \times 1.5)(3 + 1.5) + (0.380^2 \times 3) + (0.380^2 \times 1.5) - (0.490^2 \times 3) - (0.290^2 \times 1.5)\right)}$$

$$= -0.019 \text{ m}^{-1}$$

Taking the distance along the road which is closes to the antennas:

$$\text{Curvature} = \frac{(3\times 0.370)+(1.5\times 0.370)-(1.5\times 0.280)-(3\times 0.480)}{\frac{1}{2}\left((3\times 1.5)(3+1.5)+\left(0.370^2\times 3\right)+\left(0.370^2\times 1.5\right)-\left(0.480^2\times 3\right)-\left(0.280^2\times 1.5\right)\right)}$$

$= -0.016\ \text{m}^{-1}$

Taking the value perpendicular to the radar antennas which is the value the EDM will measure:

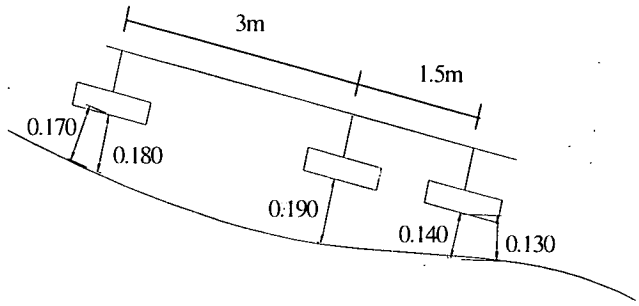

$$\text{Curvature} = \frac{(3\times 0.190)+(1.5\times 0.190)-(1.5\times 0.180)-(3\times 0.140)}{\frac{1}{2}\left((3\times 1.5)(3+1.5)+\left(0.190^2\times 3\right)+\left(0.190^2\times 1.5\right)-\left(0.180^2\times 3\right)-\left(0.140^2\times 1.5\right)\right)}$$

$= 0.020\ \text{m}^{-1}$

Taking the distance along the road which is closes to the antennas:

$$\text{Curvature} = \frac{(3\times 0.170)+(1.5\times 0.190)-(1.5\times 0.170)-(3\times 0.130)}{\frac{1}{2}\left((3\times 1.5)(3+1.5)+\left(0.190^2\times 3\right)+\left(0.190^2\times 1.5\right)-\left(0.170^2\times 3\right)-\left(0.130^2\times 1.5\right)\right)}$$

$= 0.010\ \text{m}^{-1}$